THE UNIVERSITY OF CHICAGO

DYNAMICS OF CELLULAR PATTERNS

VOLUME ONE

A DISSERTATION SUBMITTED TO
THE FACULTY OF THE DIVISION OF THE PHYSICAL SCIENCES
IN CANDIDACY FOR THE DEGREE OF
DOCTOR OF PHILOSOPHY

DEPARTMENT OF PHYSICS

BY
JAMES ALEXANDER GLAZIER

CHICAGO, ILLINOIS
AUGUST, 1989

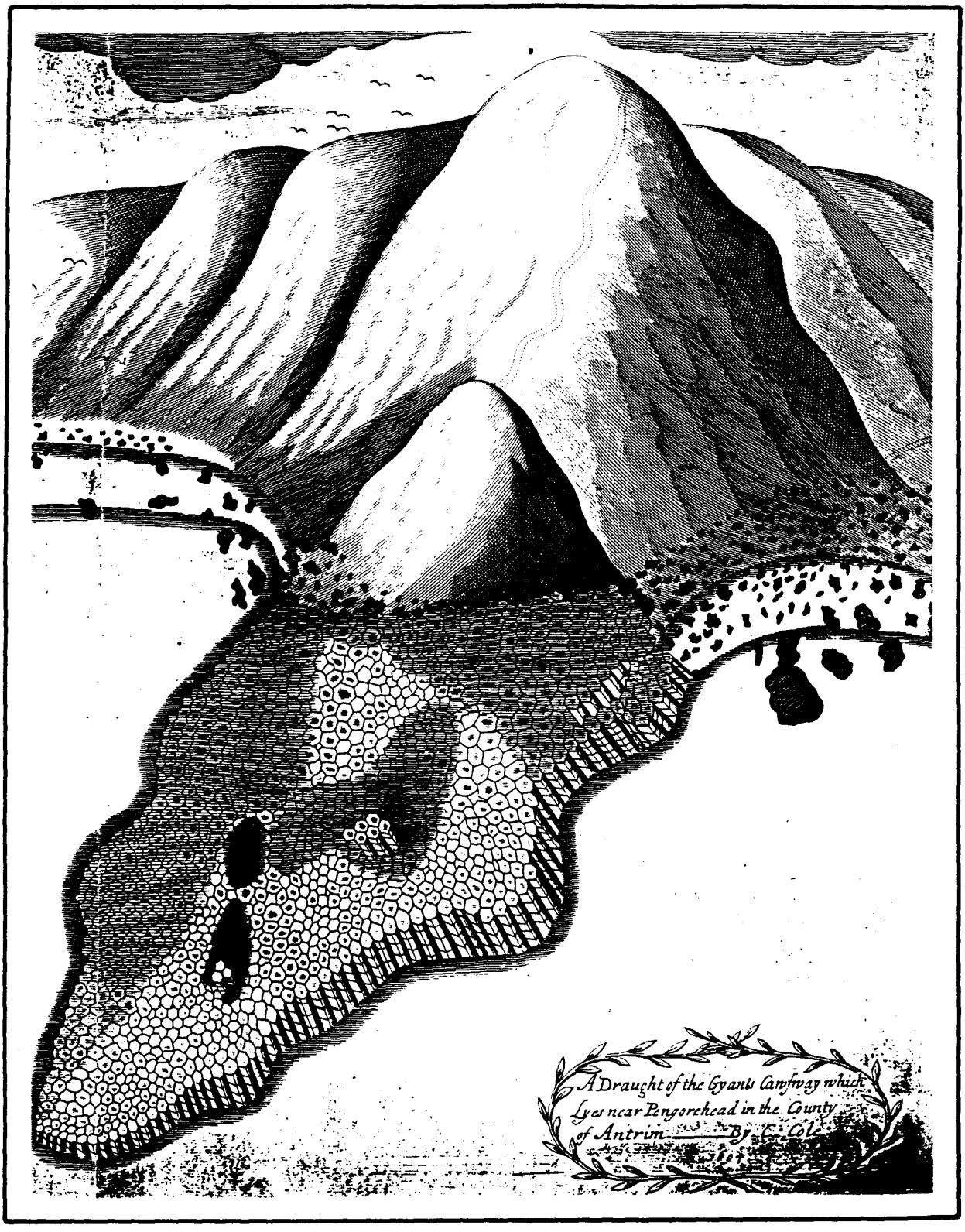
A Draught of the Gyants Cawsway which
Lyes near Pengorehead in the County
of Antrim ——— By C. Cole

Frontispiece: Giant's Causeway. Detail of a copperplate engraving of the Giant's Causeway, Northern Ireland, a basalt fracture pattern (From Sir. R. Bulkley 1693).[40]

Surface tension is of... paramount importance.– Sir D'Arcy Thompson

Like to bubbles that on water swim.– John Dowland

Double double toil and trouble, Fire Burn and Cauldron Bubble.– William Shakespeare

Astra ferar nomenque erat indelibile nostrum.– Ovid

PREFACE

The following discussion of coarsening is an eclectic summary. In most respects it makes no attempt at completeness. The discussion of grain growth in metals, in particular, is cursory and the selection of material arbitrary. The presentation of coarsening models, however, does attempt to present at least a few examples of each of the major types. The basic theme of the whole, for those who get lost among too many examples and too much detail, is how the interaction of diffusion and geometric constraints leads to complex patterns. Depending on context the terms grain, cell and bubble are used more or less interchangeably, as are film, soap film, wall boundary, and grain boundary; froth, pattern, network, array, lattice, and structure; and coarsening and grain growth.

I would like to thank Prof. Albert Libchaber for supervising and supporting this work, cheerfully and completely (even if, as occasionally happened, he disapproved of it). I would also like to thank Prof. Denis Weaire for many ideas, as well as hospitality at Trinity College Dublin, Prof. Nicholas Rivier, and Prof. Brian Kenny for useful criticism and discussions, and Prof. Vladimir Fradkov and Prof. Dmitri Udler for most stimulating correspondence. Dr. Pierre Molho, Dr. Bruno Berge and Marcello Magnasco generously provided data in advance of publication. Much of the work on soap froths discussed herein was done in collaboration with Dr. Joel Stavans, Dr. Gary Grest, Dr. Mike Anderson, Steve Gross and Andrew Belmonte.

Edward Pool did a beautiful job on the figures under tight time pressure. I am happy to acknowledge the support of a Grainger fellowship, which made much of this work possible.

I dedicate this thesis to Prof. Cyril Stanley Smith.

TABLE OF CONTENTS

TABLE OF CONTENTS, *continued*

TABLE OF CONTENTS, *continued*

LIST OF FIGURES

LIST OF FIGURES, *continued*

LIST OF FIGURES, *continued*

LIST OF FIGURES, *continued*

LIST OF TABLES

LIST OF SYMBOLS

Published models and experiments use a great variety of inconsistent notation. While we have tried to reduce our notation to some sort of order, some multiple usage remains. We give definitions of the most important symbols below.

Symbol	Meaning
α	Growth rate exponent. $< a > \propto t^{\alpha}$.
α, β, γ	Angles.
a_0	Initial average bubble area.
$< a >, < A >$	Average bubble area in a pattern.
A	Total area of experimental cell or pattern.
A_{ij}	Contact area between bubbles i and j.
A_n	Area of a single n-sided bubble.
$< a_n >, < A_n >$	Average area of an n-sided bubble.
β	Auxiliary growth exponent. $\alpha = 1/(\beta - 1)$
$c, c_1, c_2, d, \kappa_1, \kappa_2$	Fitting parameters.
δ	Spatial dimension.
$< \delta a >$	Width of area distribution.
ΔP	Pressure difference across bubble walls.
Δt	Time step in simulation.

LIST OF SYMBOLS, *continued*

d_{ij}	Distance between walls of bubble i and bubble j.
D	Diffusion constant for probability, Also the number of disordered bubbles in a pattern.
∂	Disorder parameter.
$< f >$	Average number of faces per polygon.
F	Force on vertex or boundary.
$\mathcal{F}$	Free energy of pattern.
H	Magnetic field.
$\mathcal{H}$	Hamiltonian.
i, j, k	Indices.
$j(r)$	Probability current.
J	Coupling or interaction strength.
κ	Diffusion constant for area. Units vary depending on context.
k	Boltzmann's constant.
λ_n	Relative area of an n-sided bubble $\lambda_n \equiv < a_n > / < a >$.
ℓ	Length of curved bubble wall.
L	Typical length scale.
μ	Boundary or vertex mobility. Units vary depending on context.

LIST OF SYMBOLS, *continued*

μ_2, μ_3, μ_4	Moments of side distribution.
$m(n)$	Average number of sides of neighbors to an n-sided bubble.
M	Magnetization.
n	Number of sides of a bubble.
$< n >$	Average number of sides per bubble.
$\hat{n}$	Local normal to a boundary.
$< n_f >$	Average number of edges per face in three dimensions.
N	Total number of bubbles in a pattern.
N_{edges}, $N_{vertices}$, etc.	Number of edges, vertices, etc.
O	The number of ordered bubbles in a pattern.
ψ	Angle mismatch between spins and lattice.
Q	Number of ground state spins in Potts model.
ρ	Radius of curvature in two dimensions.
ρ_i, ρ_j	Principle radii of curvature in three dimensions.
$\rho(n)$, $\rho(A)$, $\rho(n, A)$	Probability that a bubble has n-sides, area A, n-sides and area A.
$\mathcal{R}$	Ratio between $\rho(5)$ and $\rho(6)$. Also frictional damping force.
$< r_n >$	Average radius of an n-sided bubble.

LIST OF SYMBOLS, *continued*

σ	Surface tension. Units vary depending on context.
$\sigma_{(i,\ j)}$	Spin at lattice site $(i,\ j)$.
S	Entropy.
$\theta(n)$	Average internal angle for an n-sided bubble.
t	Time. Units vary depending on context.
T	Temperature.
$\mathcal{T}$	Topological charge. $\mathcal{T} \equiv n - 6$.
$\vec{v}$	Velocity of vertex or boundary.
W	Width of side distribution.
x, $\vec{x}$	Parameterized positions along bubble walls.

CHAPTER I

INTRODUCTION

I.a Preview

Long before D'Arcy Thompson's *On Growth and Form*,[230] physicists studied the problem of pattern formation, but without much quantitative success. More recently, a great explosion of interest in non-linear dynamics has lead to new attempts to understand complex spatial patterns. In some areas these new techniques have lead to qualitatively new nonlinear approaches, also without too much quantitative success. In others, like those to be discussed here, the reexamination has resulted in a great increase in understanding by applying traditional techniques in new ways. The following pages contain almost no equations that are non-linear in the standard sense. The patterns to be analyzed are not active and dynamic like the reaction-diffusion equations of biological morphogenesis. Instead we find relaxation processes, gradual approaches to statistical equilibria, and almost universally linear equations. It is worth remembering, at a time when nonlinear phenomena receive so much attention, that linear problems involving energy minimization subject to constraints can result in notably complex patterns. Our success modeling and simulating simple large aspect ratio coarsening of this type is welcome given our general lack of understanding of large aspect ratio non-linear systems. Even so, our understanding is far from complete. As we discuss in later sections of this thesis, there are still many unsolved and interesting problems in linear pattern formation.

I.b Overview

The study of the origin and development of granular materials is a large and well developed subject, as anyone who tries to survey the daunting quantity of literature presented in the bibliography will agree. Two schemes of dividing the field seem natural. We can consider the type of material under study, soap froths in one and two dimensions, fracture structures in basalt, grains in pure metals and in alloys (again in two or three dimensions) magnetic bubble systems, biological aggregates like cucumbers or human skin, ceramics, lipid monolayers, droplet condensation, etc., etc.. Alternatively we can characterize by philosophy of approach, mathematical studies of the topological and geometrical properties of random lattices, applied studies of real materials, modeling which attempts to mimic the detailed behavior of coarsening systems, modeling which considers only the basic underlying dynamical laws, engineering studies of practical applications, or philosophical musings on holistic patterns.

We will largely limit ourselves to a study of the coarsening process in cellular materials, paying particular attention to the way in which an initially ordered lattice can evolve into a disordered one. I will try to combine the two strategies mentioned above, to discuss three different systems and also a set of approaches to them. Only the case of the two dimensional soap froth is understood well enough at this point to discuss in detail. Its close cousin, the liquid-gas transition of the lipid monolayer is only now receiving adequate experimental attention. The realm of pattern formation in mag-

netic materials is better known, but the emphasis in the published literature is on device applications and the few studies of the coarsening problem are not notable for their quality.

I.c Current Literature

Anyone trying to acquaint himself with the problems of coarsening and grain growth will want to refer to the many excellent review articles. Preeminence goes to Atkinson's invaluable and up to date "Theories of Normal Grain Growth in Pure Single Phase Systems,"[20] (1988) and to Weaire and Rivier's lively and thorough survey, "Soap, Cells and Statistics–Random patterns in Two Dimensions,"[247] (1984). Both are also notable for their excellent bibliographies. Another recent review is Nagai, Kawasaki and Nakamura, "Dynamics of two dimensional cell patterns,"[178] (1988). Cyril Smith's long series of reviews are older but full of interesting philosophical speculation and contain many helpful guides to the early literature on coarsening (1952-64).[206,207,208,209] Of the older papers on metal grains, the most complete is Beck's, "Annealing of Cold Worked Metals,"[24] (1954). A more recent overview of metallic grain growth may be found in Martin and Doherty's *Stability of Microstructure in Metallic Systems* (1976).[159] Several of the recent papers by Anderson *et al.* also contain reviews of the theory of grain growth.[12,16] Helpful reviews can also be found in several conference proceedings.[192] The popular literature has also given some attention to the coarsening of froths and metals, with a variety of brief summaries in various places.[21,44,91,153,238] Even the artistic world has chipped in.[221]

In the biological literature, the papers of Matzke and Lewis are erudite and contain helpful bibliographies.[140,146,161] For ceramics a good starting point is Brook, *Ceramic Fabrication Processes, Treatise on Materials Science and Technology* (1976).[39] For magnetic bubbles Eschenfelder, *Magnetic Bubble Technology* (1980), is the most useful, though it concentrates on device applications rather than disordered patterns.[63] There is no review available on the coarsening of lipid monolayers. The one published study is by Moore *et al.* (1986).[169]

I.d What is a Two Dimensional Cellular Pattern?

The bulk of this thesis will be devoted to the study of cellular patterns of a particular kind, two dimensional networks with coordination number three, and a dynamics driven by surface tension (or surface energy) forces. A pattern consists of a network of boundaries on a surface which has the property that three boundaries meet at every intersection or vertex. The topology and dynamics are related since the dominance of three-fold vertices results from considerations of structural stability in the presence of surface tension. Four-fold vertices tend to fall apart into pairs of three-fold vertices since the total length of four lines radiating from a single vertex to connect four points is almost always larger than the length of five lines radiating from two vertices (see Fig. 1).[87] The domains outlined by these boundaries

Fig. 1 Length Minimization and Coördination Number. The relative length of sides of four vertices connected by (A) four lines running to a single 90° vertex (length= 2.828) and (B) five lines running to two 120° vertices (length= 2.732). Since surface tension tends to minimize side length, (A) decays into (B).

(A)

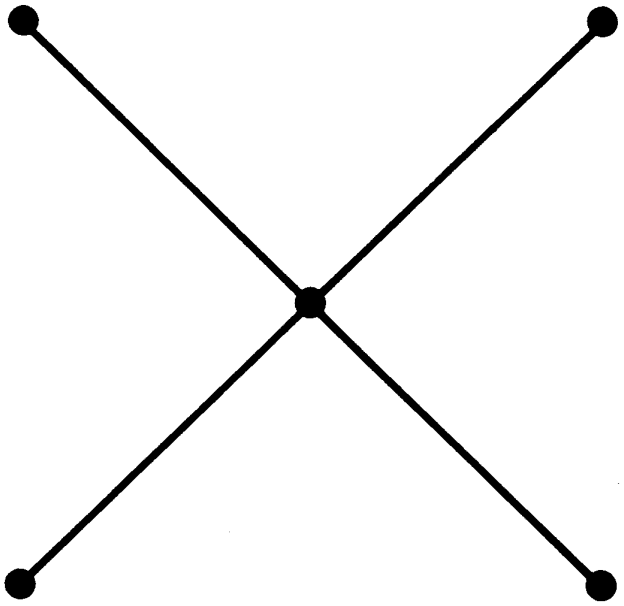

(B)

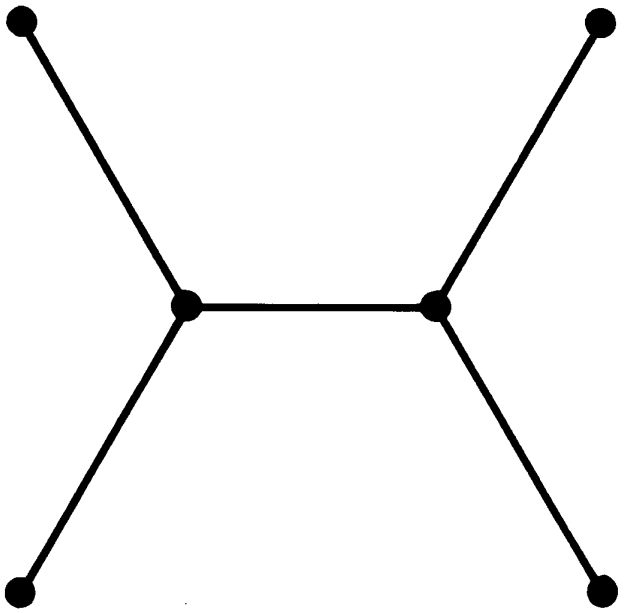

are generally approximately polygonal in shape (though magnetic bubbles present an extreme case where this observation fails), with more or less curved boundaries. Curved walls result in energy differences across walls, and hence diffusion and wall motion.

In soap froths, magnetic bubbles and lipid monolayers, the equilibration time along the boundaries is short compared to the rate at which bubbles grow or shrink, so we may regard the pattern as fully relaxed, or equilibrated. In metal grains, the rates of diffusion along and across grain boundaries are comparable, but we will usually try to get by with assumptions of complete relaxation. We therefore tend to find Plateau's minimal surfaces experimentally, vertices of roughly 120°, walls that are nearly circular arcs, etc.[189,190] Another difference between these two classes of systems is that surface tension in lipids, soap bubbles and some magnetic materials is isotropic, while that in metal grains and other magnetic materials may be significantly anisotropic.

While the basic driving force is simply surface tension, it is the competition between surface minimization and conservation constraints that gives rise to patterns (we will usually neglect wall breakage in froths, grain coalescence in metals and mitosis in cells).

Similar rules hold in three dimensions, but vertices are four-fold connected with 109.47° internal angles, and walls take the form of sections of spheres. We will find however, that some of the geometrical rules that simplify our consideration of two dimensional networks are lost in three dimensions, considerably complicating the problem.

CHAPTER II

HISTORY

The oldest reference to the behavior of a froth that this author has been able to find is in Robert Boyle's *New Experiments.*[35] In a discussion of the effects of a vacuum on a fluid Boyle notes that small bubbles form within the fluid, rise to the top and clump into bubble rafts. Later on he describes the bubbling of human urine under vacuum and notes that the froth coarsens and collapses over time. Doubtless a thorough search in the literature would reveal other studies. Matzke quotes Hooke, and Lewis quotes Leeuwenhoek as the first to have considered froth as a model for aggregates of cells.[108,138,140,161]

II.a Basalts

Geology is a generous source of examples of cellular patterns, as two recent articles in Scientific American pointed out.[128,222] Examples range in scale from millimeters to miles, with a variety of origins, the most common being convective cells and fracture patterns in rock.

The earliest well known investigations of two dimensional cellular patterns are studies not of froths but of the fracture patterns in basalts, in particular the large region of fractured basalt known as the Giant's Causeway in northern Ireland (See Frontispiece and Fig. 4 (C)).[40,55] The most significant of these is Reverend Dr. Samuel Foley's account of 1694.[65] This works contains, among other things, the first distribution function (albeit

a qualitative one) calculated for a two dimensional network of grains: "We found none at all Square, but almost all Pentagonal or Hexagonal; only we observed that a few had seven sides; and many more Pentagons than Hexagons; but they were all irregular, for none that we could observe had their sides of equal breadth."[65] In this short passage, the reverend doctor has already established two of the most important characteristics of equilibrated cellular patterns, that they have more five-sided than six-sided grains and that they are strongly irregular. In particular that they are not merely a poor approximation to an hexagonal array. This basic observation would be neglected for the next few hundred years.

The history of attempts to explain the fracture pattern in basalts is long, and need not detain us, except to note that the study of the origin of these patterns continues to the present.[214] The other point to note is the apparent universality of these patterns. Pieri, in his article on the fracture patterns in the crust of the moon, Europa, presents a helpful summary of the various types of geological patterns, including basalt fracture, large scale straight cracks with coördination number four, and a few models.[191]

II.b Biology

A complete survey of the study of polyhedral structures in biology would take many hundred pages. We can only briefly outline a few of the major ideas and efforts to connect the soap froth to biological tissues, focusing on those that emphasize two dimensional patterns.

Fig. 2 Stages in the Development of a Geranium. Various stages in the development of a geranium embryo showing similarity to a bubble raft (From Souèges 1923).[213]

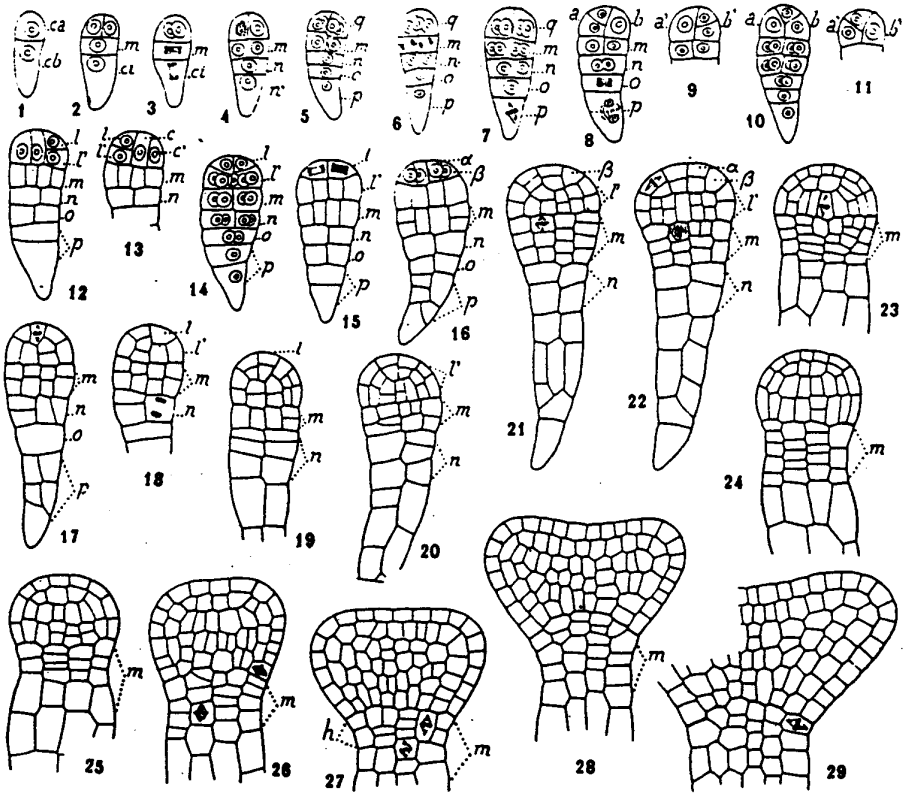

Fig. 3 Grain Growth in Calcium Carbonate. (A) Early stage of grain growth, (B) Developed grains (C) Coarsening. (D) Sample of clam shell showing similar polygonal patterning (Redrawn from D'Arcy Thompson 1942).[230]

(A)

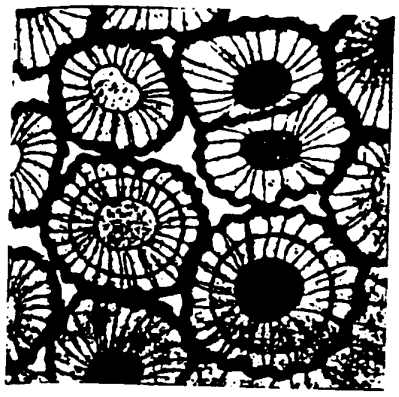

(B)

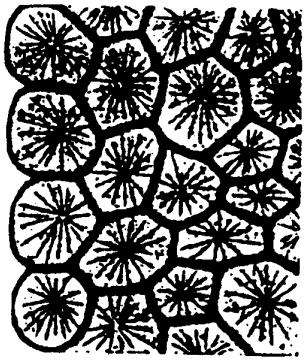

(C)

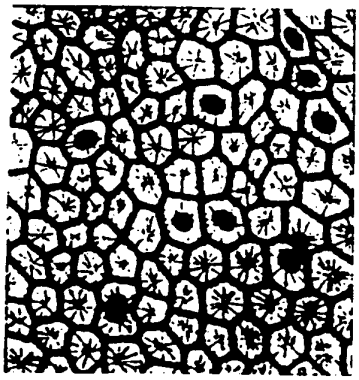

(D)

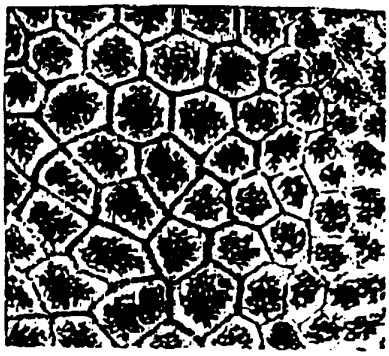

II.b.i D'Arcy Thompson

The obvious similarity in appearance between the cells of a soap froth and the cells in a living organism lead to many attempts to connect the two more formally. The resemblance may, indeed, be striking, as in the development of the geranium (Fig. 2).[213] Sir D'Arcy Thompson expressed the analogy succinctly: "surface tension is of great, and is probably of paramount importance" in the determination of the shapes of simple organisms and cells.[230] He therefore discussed at length the mathematics of minimal surfaces and of surface tension, and catalogued almost every conceivable analogy between bubbles and living forms. He connected the scission of an isolated bubble or floating oil drop to the division of cells,[232,233,234] the pattern of two dimensional soap bubbles to the segmenting egg (p. 601), and honeycomb (p. 494), three dimensional froths to vegetable parenchyma (p. 544), and the tortoise (p. 518). He addressed in particular the analogy between grain growth in molluscan shell and a model system of calcium carbonate crystals growing in albumin (see Fig. 3). The list could be extended to nearly arbitrary length. The fundamental weakness of Thompson's approach, which carries over to later writers as well is an obsession with the crystal, with a regularity and symmetry which he assumed to be the Platonic form for imperfect natural structures. Sir D'Arcy had no room for probability in his ordering of the natural world. For him, disorder was merely a deviation to be characterized and dealt with as an unavoidable inconvenience, but not of interest in itself.

Fig. 4 Sample Two Dimensional Cellular Patterns. (A) Section of the epithelium of a cucumber (From Lewis 1925).[140] (B) Territorial patterns of mouthbreeder fish (From Hasegawa and Tanemura 1976).[105] (C) Detail of the fracture pattern of the Giant's Causeway (From Lewis 1949).[147] (D) Sample of Agfa color film photographic emulsion (From Lewis 1931).[142]

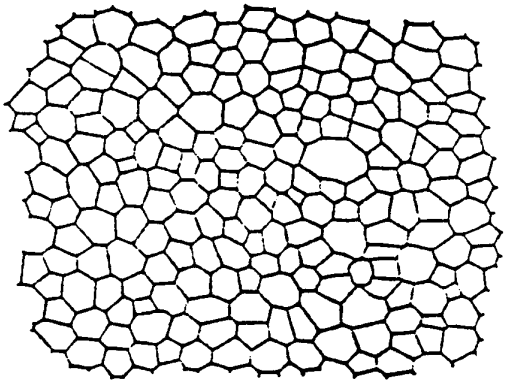

A

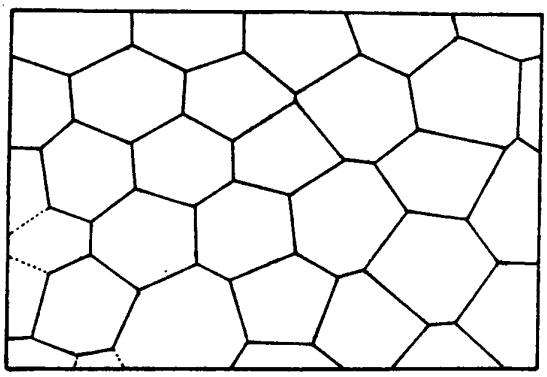

B

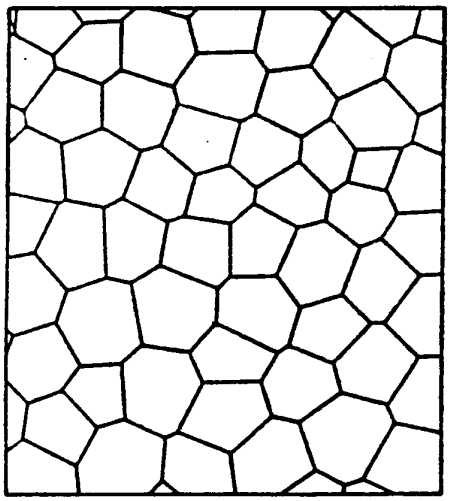

C

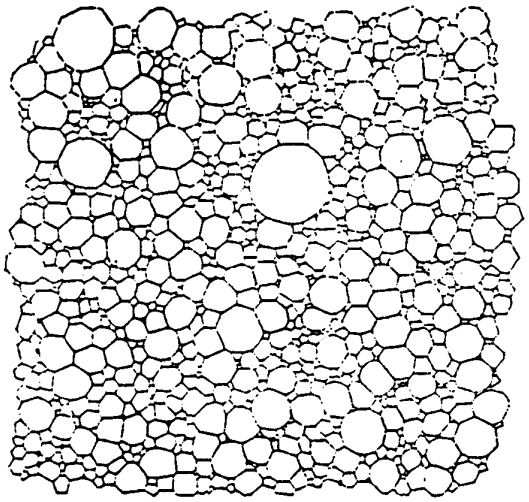

D

TABLE 1

LEWIS' DISTRIBUTION FUNCTIONS[147]

$\rho(n)$	n							
System	4	5	6	7	8	9	10	N
Cucumber Epithelium	0.02	0.251	0.474	0.224	0.03	0.001	–	1000
Wax Convection	0.023	0.357	0.377	0.220	0.023	–	–	300
Giant's Causeway	0.054	0.406	0.464	0.073	0.003	–	–	386
Dividing Cucumber	–	0.016	0.255	0.478	0.224	0.026	0.001	1000.
Eupatorium	0.026	0.265	0.436	0.238	0.034	0.001	–	1000

TABLE 2

LEWIS' LAW[147]

$< a_n >$	n								
System	a_4	a_5	a_6	a_7	a_8	a_9	a_{10}	a_{11}	a_{12}
Cucumber Epithelium	2.0	3.0	4.0	5.1	5.9	6.4	6.7	–	–
Photographic Emulsion	1.3	3.1	6.6	11.1	16.1	23.1	29.7	35.5	42.7
Eupatorium	2.9	5.9	9.0	13.1	18.2	18.8	–	–	–

II.b.ii Lewis and the Cucumber

One of those heavily influenced by Sir D'Arcy's program to attempt physical explanations of biological structure was Frederic T. Lewis, of the Harvard Medical School. His lifetime study was the analogy between living cells and soap froths in both two and three dimensions, by means of which he hoped to demonstrate that surface tension was the chief factor determining the organization of cellular aggregates.[140,141,142,143,144,145,146,147] While much of his writing was devoted to three dimensional structures, he recognized that the two dimensional case was more susceptible to experiment, hence an abiding interest in two dimensional layers of cells, first in the retina, then in human epithelium (surface tissue), a variety of plants and finally in the skin of the cucumber (See Fig. 4 (A)). In approach he followed Sir D'Arcy in positing an ideal regular lattice, either hexagonal in two dimensions or tetrakaidekahedral in three dimensions and regarding all actual observations as imperfect realizations of the ideal. Lewis had a strong distaste for disorder, "Yet, whether certain cells surpass others by accelerated growth or are reduced in size by division, the effect upon the uniform hexagonal mosaic is the same; it becomes a heterogeneous mess."[144] This obsession with order led to an emphasis on the geometry of regular polyhedra and a certain tendency to mysticism, particularly in his later papers. Thus many of his writings are of more historical than scientific interest today. However, Lewis was also a careful observer, and his desire for order never prevented him from recording the real disorder in his samples, nor from attempting to explain the origins

of that disorder. His calculations of the distribution of areas and number of sides of the skin of the cucumber were the first real hard data gathered in the field of cellular patterns, presenting results not only for biological materials but also Bénard-Marangoni convection, photographic emulsion (Fig. 4 (D)) and basalt fracture. Table 1 summarizes his results for cucumber (Fig. 4 (A)), convection in wax, the Giant's Causeway (Fig. 4 (C)), and the *Eupatorium* plant. His studies have inspired many investigators, including Occelli, Guazzelli and Pantaloni who have recently reexamined the cellular patterns present in Bénard-Marangoni convection.[104,185,251]

It is important to notice that in all of these systems, the number of six-sided domains is greater than the number of five-sided domains, and that the cutoff for both many and few-sided domains is very sharp. We will see later how these results for patterns in which there are intrinsic limits placed on the range of areas, e.g. by cell division or wavelength selection in convection, compare to theory and experiment for froths and other unrestricted coarsening.

Lewis is best remembered for his empirical determination of the relation between the number of sides of a cell and its area. We summarize his results in Table 2.

On the basis of this data he concluded that the average area of a cell was a simple linear function of its number of sides, i.e.:

$$< a_n >= c_1 + c_2 * n, \tag{II.1}$$

where a_n is the area of an n-sided cell and c_1 and c_2 are fitting parame-

ters. This relation is known as "Lewis' Law," It has been elevated to the status of a general principle by some later writers,[134,198,201] casting undeserved opprobrium on Lewis, because it seems to be essentially never true for coarsening systems, failing for both soap froths and metal grains, (though it is approximately correct for domains with between five and eight sides). To be fair to Lewis, he proposed it only for the specific case of cucumber epithelium, and noted himself that cells with many sides were smaller than predicted by the linear relation. In this case he was less literal minded than the majority of his followers.

Another relation first proposed by Lewis is the inverse correlation between a cell's number of sides, n, and the number of sides of its neighbors, m(n).[142] In its basic form his conclusion was that

$$m(n) = c + \frac{d}{n}, \tag{II.2}$$

where c and d are constants. Aboav discovered independently a slightly more elaborate version of this harmonic relation in the soap froth, which is usually known as the Aboav-Weaire Law.[9,8]

Studies continue to the present on the significance of cellular patterns in the configurations of animal cells, e.g. in the human retina.[257] Cellular patterns have also attracted interest from population biologists, for example studying the polygonal territories of mouthbreeder fish (see Fig. 4 (C)).[105] Many of the methods we will discuss are also used by sociologists and geographers interested in the distribution and allocation of resources.[89]

II.c Metallurgy

II.c.i The Classical Model of Grain Growth

By far the strongest impetus to the study of soap froths came from the study of metals. The fundamental analogy between the growth of grains in a metal and bubbles in a froth was first recognized by Smith.[206] In this picture each separately oriented grain in the metal was considered analogous to one bubble in the froth and the metal's grain boundaries to correspond to the soap films. The growth or shrinkage of a given bubble corresponded to the growth or shrinkage of the corresponding grain. There are differences, but the basic analogy between the migration of grain boundaries due to surface energy in a metal and the growth of bubbles due to surface tension driven diffusion in a froth is exact (as we discuss in our section on von Neumann's Law), and the comparison between the two systems has proved fruitful as a series of review articles by Smith attest.[207,208,209]

One basic difference between a two phase bubble system, where the walls are made of soap films, and the diffusing material is a gas, and a one phase metal system where the grain boundaries are simply collections of defects, is the rate of grain coalescence. In an ideal froth, walls do not break and there is no grain coalescence. In some metals, on the other hand, if two grains with nearly identical crystalline orientation touch, the boundary between them vanishes. When it occurs, coalescence provides an additional coarsening mechanism that favors the creation of many sided, large and irregularly shaped grains. Other differences between the froth and the metal

Fig. 5 Bubble Rafts. Regular hexagonal free floating bubble raft. Bubbles are 1.41mm in diameter (From Bragg and Nye 1947).[38]

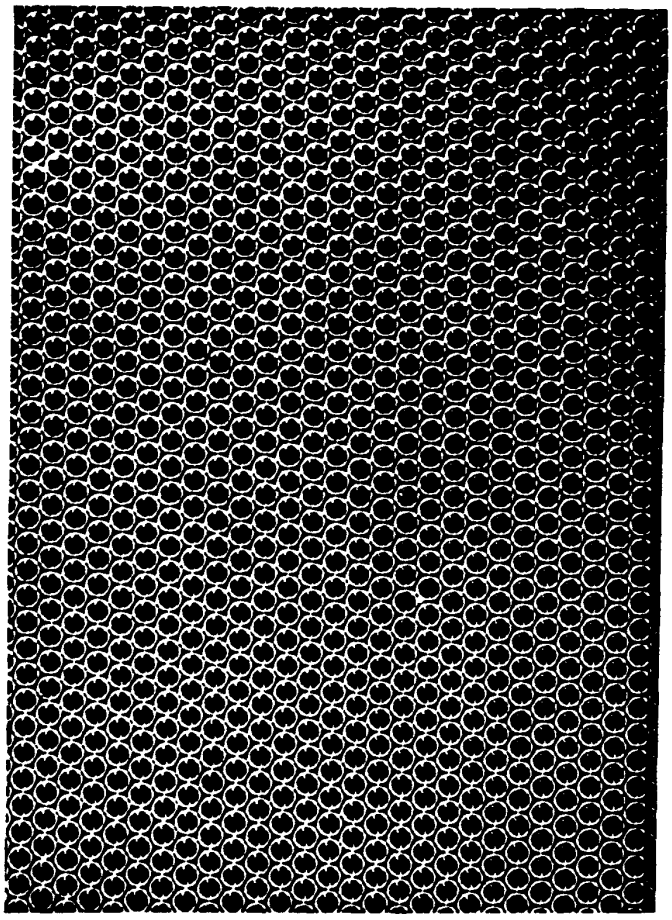

Fig. 6 Recrystallization of a Disordered Bubble Raft. The ordered raft is first shaken to produce a disordered pattern and then allowed to recrystallize. Bubbles are 0.60mm in diameter. (A) $t = 0$ minutes. (B) $t = 2$ minutes. (C) $t = 25$ minutes. Note the irregular shape of the grain boundaries (From Bragg and Nye 1947).[38]

A)

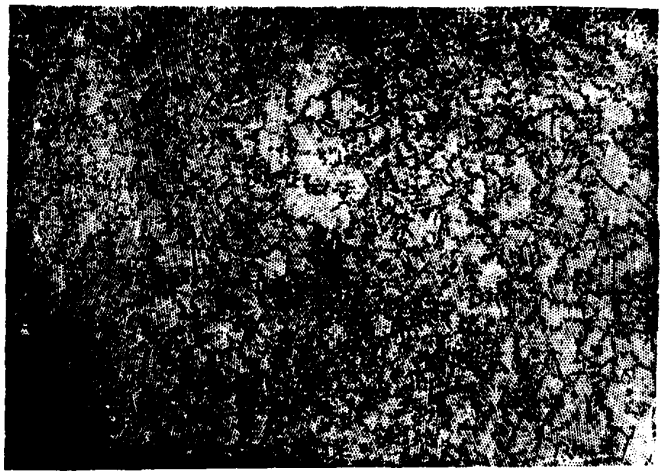

B)

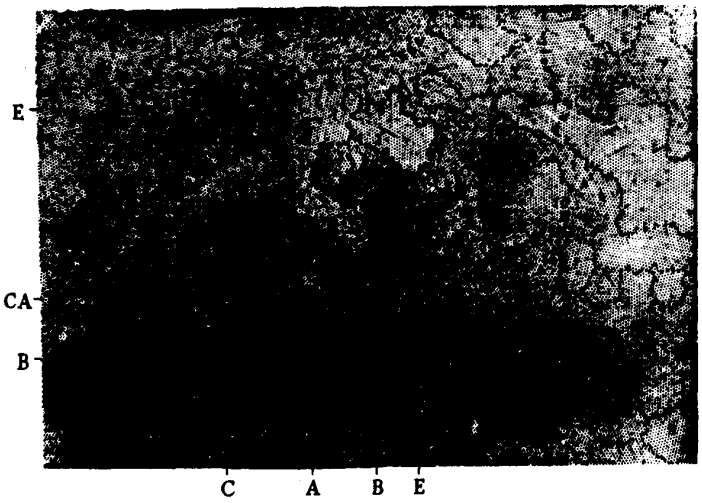

C)

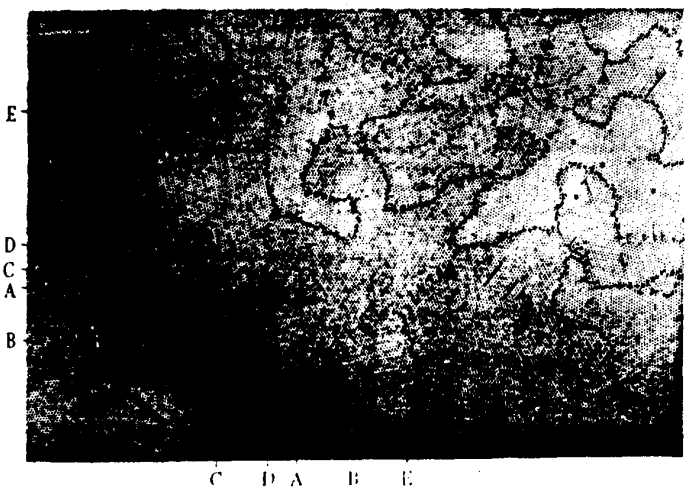

arise from a consideration of time scales. The soap froth's films relax very quickly in comparison to the diffusion time of the gas through the films. The films themselves adjust nearly instantaneously, and even the creep of the films on the walls of their container is fast compared to the diffusion time. Thus soap films always assume their equilibrium shape as minimal surfaces (circular arcs). In a metal this is not the case. The rate at which a grain boundary moves and equilibrates are nearly equal, so grain boundaries can be significantly irregular. Smith's great leap of faith was to assume that when the irregularities of the metal grains were averaged over a sufficiently large population, the differences would average out, and he conducted a series of experiments to show that this averaging did in fact occur.

In both two and three dimensions, the soap froth offers a number of significant advantages over the direct study of metals. The three dimensional structure of a metal is usually determined by serial sectioning, that is, taking a series of thin slices and reconstructing the three dimensional structure from the series of two dimensional images. Attempts at non-destructive measurements have been less successful.[252] Destructive measurements, besides being tedious, prevent the grains from being examined at different stages of growth, making it difficult to measure the basic dynamical laws governing grain coarsening. The three dimensional soap froth can, though with difficulty, be observed in situ.[161] In the case of the two dimensional froth, direct observation is trivial, while the surface preparation required to observe grain growth in metallic thin films or foils, can alter their evolution.

Another barrier to the understanding of metal evolution is the large range of secondary effects, orientational anisotropy, defect pinning, zone refining, vacancy migration, etc., which while interesting in their own right, tend to obscure the underlying dynamics. In the soap froth, such secondary effects are fewer in number, gravity driven thinning in three dimensions, wall breakage, and Plateau border thickening, so they should be easier to control for. Such are the historical motivations for the study of the soap froth as a model system.

II.c.ii Bragg's Model

Bragg put forward an alternative use of bubbles to model two-dimensional grain growth. Instead of looking at the growth or shrinkage of bubbles, Bragg used uniformly sized bubbles, free floating in rafts on water. Individual bubbles in a raft correspond to the atoms in the metal not to entire metallic grains. The orientation of the soap bubble grains corresponds precisely to the crystalline orientation of the corresponding grain. Since floating bubbles attract each other weakly at long range and repel strongly at short range, the analogy is reasonably exact.[18]

A typical experiment consisted of creating a large scale regular hexagonal bubble raft (see Fig. 5), shaking it to destroy the crystalline orientation and then monitoring the regrowth of hexagonal domains (Fig. 6). The observed behavior agreed quite closely with that seen in metals. In particular, the comparable diffusion times along and across grain boundaries resulted in much more irregular grain shapes than observed in soap froths (Fig. 6

(C)). A defect of the model, the absence of a temperature to facilitate the motion of bubbles from one grain to another, can be simulated by applying constant small amplitude shaking. Such shaken systems have been studied by Fukushima and Ookawa, who have also made detailed studies of raft rheology and defect propagation.[66,67,68,69,70,71,177]

The chief disadvantage of such experiments is the difficulty of gathering adequate statistics. To obtain enough grains large compared to the bubble size requires a bubble raft composed of a prohibitively large number of bubbles. Nevertheless this alternative use of bubbles as a microscopic model is very appealing and deserves to be pursued further.

II.d Other Topics

Before we turn to a detailed description of the coarsening of the soap froth, we would like to mention two topics departing from the main focus of this thesis, but which have much intrinsic interest as part of the broader study of bubbles: the properties of soap films and the rheology of foams.

II.d.i The Properties of Soap Films

Early students of soap bubbles were much more interested in the behavior of single films or a few clumped bubbles than in the properties of froths. Newton was the first in a long chain of researchers who studied properties of an isolated soap film.[182] Plateau, the great master of the soap bubble, devoted nearly all of his monumental study of the properties of a weightless fluid to the equilibrium shapes of single films and the interactions

among a few bubbles.[189,190] Even the method of producing a stable soap film was a subject of debate in the days before modern detergents.[36,56] In this century, the microscopic structure of films, and macroscopic properties like film draining, have received particular attention both theoretically and experimentally.[193] The classic guide to this material (including a complete bibliography) is Mysels, Shinoda, and Frankel, *Soap Films: Studies of their Thinning.*[176] We will return to their work when we consider possible explanations for the anomalous behavior observed by Glazier, Gross and Stavans in the long time evolution of two dimensional froths.

The stabilization of foams is a major industrial problem, and there is a large literature of engineering studies of foam stability. Since the chief mechanism for coarsening in three dimensions is gravity induced thinning and breakage, most of these studies focus on the properties of single films. Single soap films have been used for a variety of experimental and diagnostic purposes,[57] including recent studies at University of California, San Diego, on two dimensional shear flows.

We should also not omit to mention the less serious aspects of the 19th century's interest in bubbles. Boys' *Soap Bubbles: Their Colours and the Forces which Mold Them,*[176] in addition to a serious discussion of the properties of single bubbles, includes numerous party tricks, and even *Nature* was not averse to publishing accounts of the wonderful properties of soap bubbles, as observed at aristocratic soirées.[1,91]

II.d.ii Foam Rheology

Another topic of great technological importance is the rheology of foams, the behavior of foams subject to external forces. The best current review is Kraynik's thorough "Foam Flows."[126] Applications where foams are used industrially in conditions of large stress include for transporting of granular and high viscosity materials in pipes, as fire suppressants to smother flames, and in the manufacture of modern nuclear weapons.[21] Elucidating the properties of a true disordered froth subject to stress is difficult. Experimental results are limited and tend to focus on particular engineering applications rather than fundamental properties, though the work of Bragg on bubble rafts is very useful.[38]

Published theoretical studies of the rheology of foams cover almost as many methods of modeling as do those for grain growth. Weaire and collaborators have developed a small scale simulation of a fully disordered two dimensional froth, which shows interesting nonlinear and hysteretic effects.[240,241,243] There are also a number of studies of the principles of defect motion in froths, which can be compared directly to bubble raft and microsphere experiments.[19,171] Finally, Kraynik and his collaborators have developed an elaborate analytic theory for the properties of a perfect honeycomb with soap films described by realistic viscous equations.[125,129,130] Weaire has also examined this model.[239] They have even produced a movie of the stress response for different types of films and different lattice orientation, which exhibits an impressive variety of periodic and quasiperiodic motions.[127]

While we would not expect to find such elegant regularity in a real froth, the potential for complex self organized temporal behavior is an interesting possibility.

II.e Conclusion

The intent of this chapter has not been completeness, but an eclectic sampling of the variety of topics peripheral to our main theme of bubble growth. We hope that it provides some motivation to the study of the two dimensional soap froth (both as an unusually simple example of general grain coarsening and as a material worthy of study in its own right) and to the extension of the ideas developed working with the froth to more complicated systems.

CHAPTER III

THE GEOMETRY OF CELLULAR PATTERNS

Before we turn to the physical processes of two dimensional coarsening we need to discuss a few basic mathematical relations describing general coördination number three networks. We also present the basic evolution equation describing bubble growth, (von Neumann's law), since its derivation is essentially geometrical and will therefore obtain to any purely diffusive surface tension driven system.

III.a Basic Mathematical Relations

The properties of a connected network consisting of vertices, edges, cells (or faces), and polyhedra (in three dimensions) may be briefly encapsulated in the Euler Relation,[51] which states that

$$N_{vertices} - N_{edges} + N_{cells} - N_{polyhedra} = 1. \qquad \text{(III.1)}$$

In two dimensions there are no polyhedra so the Euler Relation reduces to

$$N_{vertices} - N_{edges} + N_{cells} = 1. \qquad \text{(III.2)}$$

Another basic relation, the average number of sides per cell, $< n >$, in an infinite lattice of coordination number 3 may be derived as follows. Each vertex is shared by 3 cells and each cell has $< n >$ vertices on average, so

$$N_{vertices} = \frac{1}{3} < n > N_{cells}. \qquad \text{(III.3)}$$

Each edge is shared by two cells so

$$N_{edges} = \frac{< n >}{2} N_{cells}. \tag{III.4}$$

Applying Euler's Relation we obtain that

$$\frac{1}{3} < n > N_{cells} - \frac{1}{2} < n > N_{cells} + N_{cells} = 1. \tag{III.5}$$

In the limit of a large system,

$$\lim_{N_{cells} \to \infty} \frac{1}{6} < n >= 1. \tag{III.6}$$

So the average number of edges per cell $< n >= 6$.[98] In three dimensions there is an extra degree of freedom, so the equations are underdetermined. If the average number of faces per grain is $< f >$ and the average number of sides per face is $< n_f >$ then for an infinite froth the quantities are related as:

$$< n_f >= 6 - \frac{12}{< f >}. \tag{III.7}$$

III.b Von Neumann's Law

The simplest and most beautiful theoretical result for the dynamics of the soap froth is due to von Neumann, who, in a comment to a presentation by Smith argued that the rate of increase or decrease of a bubble's area should depend only on the bubble's number of sides.[181]

Let us first discuss the driving force behind cell growth and shrinkage, pressure driven diffusion. If a film between two bubbles has a radius of

curvature ρ, and occupies an angle ϕ its length, ℓ is, to lowest order, $\ell = \rho\phi$. For a small change in normal radius, x, $\frac{d\ell}{dx} = \phi$. But $\phi = \arcsin\frac{\ell}{\rho} \sim \frac{1}{\rho}$ to lowest order. So $\frac{d\ell}{dx} \sim \frac{1}{\rho}$. Since the surface tension σ is a force per unit length, the pressure difference required to sustain the curvature is $\Delta P = \sigma\frac{d\ell}{dx} \sim \frac{\sigma}{\rho}$.

The same basic derivation holds for grain growth in polycrystals and for similar reasons. We follow the argument given by Plateau.[189] A curved film has a larger surface energy than a flat film, and a curved grain boundary has a higher surface energy than a flat grain boundary. In a grain there is no surface tension *per se* but there is a surface energy– atoms at the surface of the grain have a higher energy than those in the bulk. An atom sitting in a convex portion of grain surface is more exposed to defects, and hence has a higher energy than an atom sitting across the grain boundary in a concave section of surface. Thus it is energetically favorable for atoms to jump across the grain boundary from convex to concave surfaces. The energy difference is proportional to the surface curvature so the basic result is that energy driven diffusion results in a local boundary velocity, $\vec{v}$, at a point $\vec{x}$, of

$$\vec{v}(\vec{x}) = \mu(\vec{x})\frac{\hat{n}(\vec{x})}{\rho(\vec{x})}, \tag{III.8}$$

where $\mu(\vec{x})$ is the local mobility which may depend strongly on time, temperature (activation energy) and boundary orientation (anisotropy), $\hat{n}(\vec{x})$ is the unit normal to the surface, and $\rho(\vec{x})$ the local curvature.[172] If the temperature is high enough that $kT >>$ orientational anisotropy, and the boundary mobility is constant in time (no zone refining effects), then averaging over a large number of grain orientations reduces the surface energy to an effective

Fig. 7 von Neumann's Law: Explanatory Diagram. A five-sided bubble, where α is the average central angle, β half the average internal angle of a polygonal approximation to the bubble, δ the difference between β and 60°, ℓ the length of the side of the bubble, and ρ the radius of curvature of the side.

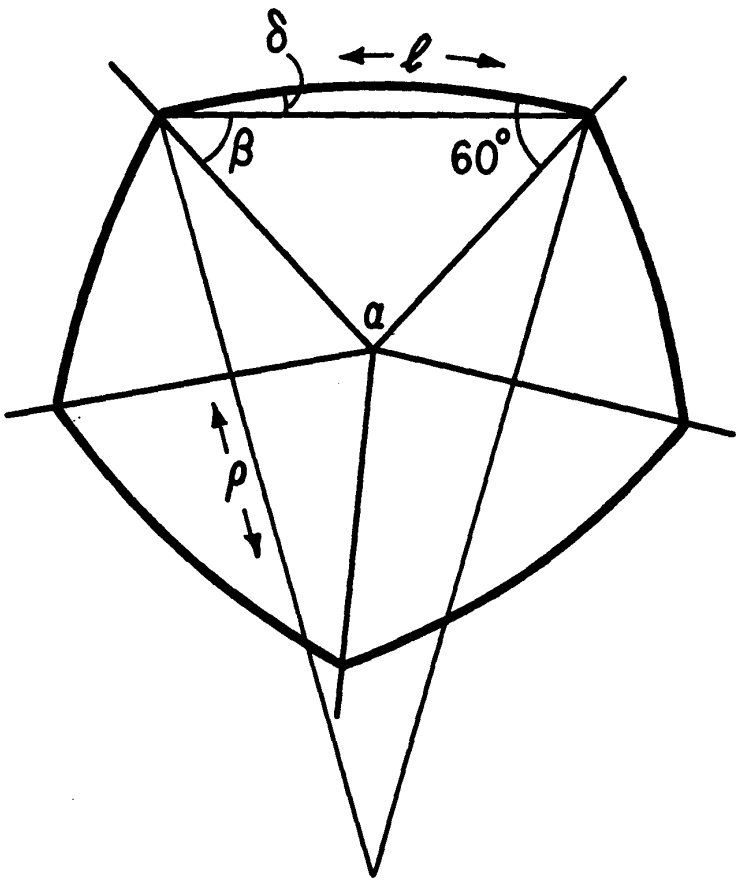
δ
ℓ
β
60°
a
ρ

surface tension and differential pressure, and we can treat grain growth and soap bubble growth as identical. If $kT \approx$ orientational anisotropy, certain grain boundary orientations will be stabilized and grain growth will gradually slow, and may even stop at a finite grain size. If zone refining reduces or enhances the average boundary mobility, cessation of grain growth or explosive anomalous grain growth can result.

The remainder of the argument is purely geometrical and local. Von Neumann's derivation is economical and we follow it closely. We make the following hypotheses. 1) That vertex angles in a froth are 120°. 2) That all walls are sections of circular arcs. 3) That the pressure difference across a wall Δ P is proportional to one over the radius of curvature of the wall. 4) That the rate of gas diffusion across a wall is equal to its length times the pressure difference across it. 5) That pressure differences are small so that diffusion of gas is equivalent to diffusion of area.

We now make the following geometrical observations (See Fig. 7). The average central angle,α of a triangular wedge of an n-sided polygon is $\alpha = 360°/n$ so the average internal angle, β, is

$$\beta = 90°(1 - \frac{2}{n}). \qquad \text{(III.9)}$$

The angle difference between the actual bubble angle and the polygon leaves, by hypothesis 1, an angle deficit to be made up by curvature:

$$\delta = 60° - \beta = 90°(\frac{2}{n} - \frac{1}{3}) \qquad \text{(III.10)}$$

to be made up by curvature, which gives, by hypothesis 2, a radius of curvature,

$$\rho = \frac{\ell}{360°(\frac{2}{n} - 1)}, \tag{III.11}$$

where ℓ is the length of the circular arc over the side of the polygon. If we apply hypothesis 3 we find that

$$\Delta P \propto \frac{180°}{\ell}(\frac{6-n}{3n}). \tag{III.12}$$

Noting that the diffusion of gas is towards the region with lower pressure, and applying hypotheses 4 and 5, we multiply by n sides and the length of each section of circular arc, ℓ, to obtain von Neumann's law, the rate of change of area, A_n of an n-sided bubble,

$$\frac{dA_n}{dt} = \kappa(n-6), \tag{III.13}$$

where κ is a diffusion constant with the units of $\frac{\text{area}}{\text{time}}$.

Note that we have made no assumptions about the regularity of the froth since the lengths of the circular arcs cancel side by side. Thus the law is both exact and local for any pure diffusive system obeying our five hypotheses. If we had assumed an n-dependent typical internal angle, $\theta(n)$, for the froth, the derivation would follow as before to obtain the generalized result:

$$\frac{dA_n}{dt} = \kappa(3n(1 - \frac{\theta(n)}{180°})) - 6). \tag{III.14}$$

If the average internal angle of an n-sided bubble varies from bubble to bubble, this revised law provides a mechanism for a variation of growth rates within the population.

The only patterns that are stable under von Neumann's law are the perfect hexagonal lattice and the empty lattice. Introducing even a single defect pair into a perfect hexagonal lattice results in the collapse and eventual disappearance of all the bubbles in the lattice. Thus we know that the only possible type of equilibrium for the systems is one in which the average length scale grows continuously in time, but the normalized distribution functions ($\rho(n)$, the probability that a given bubble has n sides, $\lambda_n \equiv \frac{<a_n>}{<a>}$, the relative size of n-sided bubbles compared to the total population, etc.) and local correlations (e.g. $m(n)$, the average number of sides of a bubble next to an n-sided bubble), remain constant. We call this equilibrium, if it exists, **a scaling state.**

Von Neumann's law predicts that in a scaling state, i.e., when the functions describing the distribution of areas and number of sides are constant in time, the average area of a bubble, $< a >$ is proportional to the time, t. This result may be argued in several different ways,[94,157,172,173] but we find it simplest to derive as follows. Let A be the area of the entire system, N be the total number of bubbles, $\rho(n)$ and λ_n as above. Then the number of bubbles lost per unit time is the area lost by three-, four-, and five-sided bubbles per unit time divided by their mean areas,

$$\frac{dN}{dt} = -\sum_{n=3,4,5} \frac{\kappa\rho(n)N(n-6)}{\lambda_n < a >}. \qquad \text{(III.15)}$$

Substituting for $< a >$ we obtain

$$\frac{dN}{dt} = -N^2 \sum_{n=3,4,5} \frac{\kappa\rho(n)(n-6)}{\lambda_n A}. \qquad \text{(III.16)}$$

If the distribution functions are time independent, which is what we mean when we say we are in a scaling state, then the sum is a constant and

$$\frac{dN}{dt} \propto -N^2 \Rightarrow N \propto t^{-1} \Rightarrow < a > \propto t. \qquad \text{(III.17)}$$

The modified version of von Neumann's law leads to the same result. Thus by itself, von Neumann's law predicts the asymptotic linear scaling of the froth. Alternative derivation of the growth exponent from the hypothesis of a scaling state have been given by Mullins and Weaire and Kermode.[173,242]

However, von Neumann's law is not a complete description of the dynamics of a froth. It describes only the growth of bubbles with fixed numbers of sides. During the evolution of a froth bubbles typically change their number of sides many times. In particular, whenever a bubble disappears some of its neighbors change their number of sides. Since average bubble area can only increase when bubbles disappear, von Neumann's law cannot provide a complete description of the coarsening process. Any complete description of the evolution of the soap froth must make additional assumptions about how side redistribution takes place. Such information can only come from direct experimental observations of real froths.

CHAPTER IV

BUBBLES–EXPERIMENTAL

IV.a Experimental Procedure

Several groups have collected experimental data on the two dimensional soap froth. Smith made the first studies using low pressure air in a sealed cell circular glass cell and applied vigorous shaking to produce an initially disordered froth with a few hundred bubbles and a bubble diameter of between one and two millimeters. Coarsening from this length scale to the size of the container required approximately two hours.[206] He photographed the cell periodically during coarsening. With this data Smith measured the rate of area growth with time and Aboav the evolving distribution functions of the froth.[8] Fisher and Fullman preformed a similar experiment in a medium pressure sealed container and independently measured the rate of bubble growth.[86] More recently Weaire and Fu studied the evolution of a froth using very small air bubbles in a cell made from microscope slides and photographed under a microscope.[85] Typical coarsening times for their froth were four or five hours. They were particularly interested in experimentally verifying von Neumann's Law. Glazier, Gross and Stavans collected more complete data on the soap froth in a series of experiments which we describe in detail below.[93,94,220]

Glazier, Gross and Stavans used a series of large rectangular experimental cells. These were made of plexiglass and sized to be slightly smaller than either an $8\frac{1}{2}$" x 11" or $8\frac{1}{2}$" x 14" piece of paper. The vertical spacing was

either 1/8" or 1/16". Catheters inserted through holes drilled in the spacer allowed filling and draining. A thick coat of epoxy sealed the joints.

They used a soap solution consisting, of water (approximately 85% by volume), Dawn brand liquid detergent (approximately 10%) and glycerol (approximately 5%). While they did not attempt to control carefully the mixing of the fluid, their results were apparently independent of the exact fluid composition. However, they found that certain solutions (surprisingly those containing a higher percentage of soap and glycerol) had a higher rate of side breakage than others.

In different runs they used bubbles either of helium or air, helium froths evolving roughly five times faster than air froths, but being otherwise similar. In no case did they observe any evidence of leakage of the working gas from the cell.

Since they were interested only in the long term behavior of the forth, neither Smith nor Fullman made any effort to control the uniformity of their initial bubble pattern. Indeed, the method of froth generation they employed always resulted in highly irregular patterns with broad area and side distributions. Glazier, Gross and Stavans, on the other hand were particularly interested in the transition from ordered to disordered patterns. They therefore developed two basic methods to fill the cell with froth. In the first method, which they used to obtain very uniform fills of small bubbles, they completely filled the cell with soap solution, then tipped the cell on its edge and slowly injected gas bubbles at the bottom of the fluid, draining excess

fluid through a catheter at the bottom of the cell. The variation in the size of the injected bubbles determined the initial degree of disorder in the froth. They found that because of the long fill times (approximately ten minutes), the top portion of the froth was significantly more developed than the bottom at the nominal beginning of the experiment, which made early portions of the time series more difficult to interpret. In the second method, they filled the cell only about 10% full and injected the gas through one of the filling catheters just below the surface of the soap solution. This allowed them to control the size and uniformity of the bubbles both by varying the injection pressure and the angle of the cell relative to the vertical. The advantage of this method was that they could fill the cell more quickly, but it was more difficult to obtain very uniform or very small bubbles.

When necessary they "annealed" the froth by injecting excess fluid and gently tipping the cell to remove obvious irregularities, then draining the excess fluid (their failure to measure the volume of fluid remaining in the cell makes it difficult to provide quantitative estimates of the role of Plateau border broadening), injected a small amount of ink and sealed the catheters with corks and vacuum grease. The ink made the **Plateau borders**, the thickened region of fluid between the membranes and the walls (see Fig. 8), easily visible. To make measurements, they placed the prepared cell level on a photocopier and copied periodically at intervals depending on the rate of evolution (intervals of 15 minutes at early times and 12 or 24 hours at long times). The photocopier has several advantages over photographic recording.

Fig. 8 Plateau Border: Top view of the region where three soap films meet. The films' top surfaces are in contact with a flat glass plate. The wetting of the fluid on the glass sucks excess fluid onto the glass, resulting in the broad lines seen. A similar effect thickens the line where the films meet, which seen from above produces the central triangle. The films themselves are thin, and can be seen to be well centered within the Plateau border (Redrawn from Lewis 1949).[147]

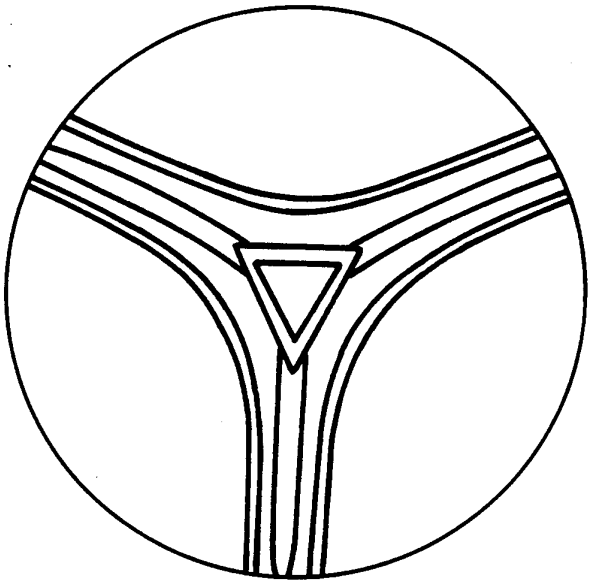

It is simple, much less expensive, and has an intrinsically high contrast ratio. It also produces a large image with correct absolute lengths.

It is important to realize that both photographs and photocopies show the Plateau borders and not the soap membranes themselves. One cannot easily observe the actual position of the soap films nor whether they are curved in the vertical direction. However, examination with a microscope of untinted soap films suggests that the films are both well centered and flat, as seen in Fig. 8.

Glazier, Gross and Stavans used a Xerox model 4000 photocopier which provided relatively low contrast.[94] Stavans and Glazier, and Glazier *et al.* employed a Mita Model DC-1255 photocopier,[93,220] a scanning type which provided much better quality copies, but heated the cell significantly during each copy. While the duration of heating was short, and thus should not have significantly affected the dynamics of the froth, it did result in occasional wall breakage. The total number of walls broken during a run represented less than .1% of the total side redistribution, but nevertheless may have resulted in slightly greater numbers of very many-sided bubble.

IV.b Digitization

Many of the results described for the soap froth were obtained by direct hand counting from photocopies or photographs. Fu, and Glazier Gross and Stavans essentially followed the procedures established by Smith and Aboav, though for area measurements Glazier Gross and Stavans had the

advantage of using a digitizing tablet, a technique also employed by Kreines and Fradkov.[131] Problems with hand digitization include its extreme tedium and large inaccuracies. However, its intrinsic resolution can be very good.

Glazier *et al.* relied on direct digitization of 30% samples of their photocopies using a camera type digitizer with a resolution of 600 x 500 pixels for much of their Potts model and distribution function analysis, editing the digitized images by hand to remove obvious defects in the digitization. Raster images were converted into grains using a standard "worm" technique, each pixel being assigned to a separately numbered grain for analysis. The image quality of their camera digitizer was sufficient that it produced very few spurious bubbles or broken lines (fewer than 2%). The resolution of the digitizer was sufficient to represent a few thousand bubbles with a typical size of 10 x 10 pixels. One advantage of this type of digitization was that the digitized images could serve directly as initial conditions for Potts model simulations, one pixel in the image corresponding to one spin in the model. A disadvantage was that the relatively small image area gave rather poor statistics at long times.

IV.c Basic Experimental Results

IV.c.i Qualitative Description of Coarsening

Let us first look at the qualitative features of the evolution of a soap froth. We distinguish three basic patterns of evolution, that evolving from an initially well ordered state, that evolving from an initially disordered state,

Fig. 9 Evolution of a Soap Froth: Coarsening of a two dimensional soap froth. Illustrations show 15% details of the total area of the experimental cell. (a) The left side shows an initially well ordered run in Helium gas (initial disorder $\partial(0) = 0.17$). Times for the figures: (A) $t = 1$ hour, (B) $t = 2.52$ hours, (C) $t = 4.82$ hours, (D) $t = 8.63$ hours, (E) $t = 19.87$ hours, (F) $t = 52.33$ hours. Letters are keyed to Fig. 16 (d) (b) The right side shows an initially disordered run in air (initial disorder $\partial(0) = 0.85$. Times for the figures: (A') $t = 1.95$ hours, (C') $t = 21.50$ hours, (F') $t = 166.15$ hours. Letters are keyed to Fig. 16 (f). The final states are essentially indistinguishable (From Glazier, Gross and Stavans 1987).[94]

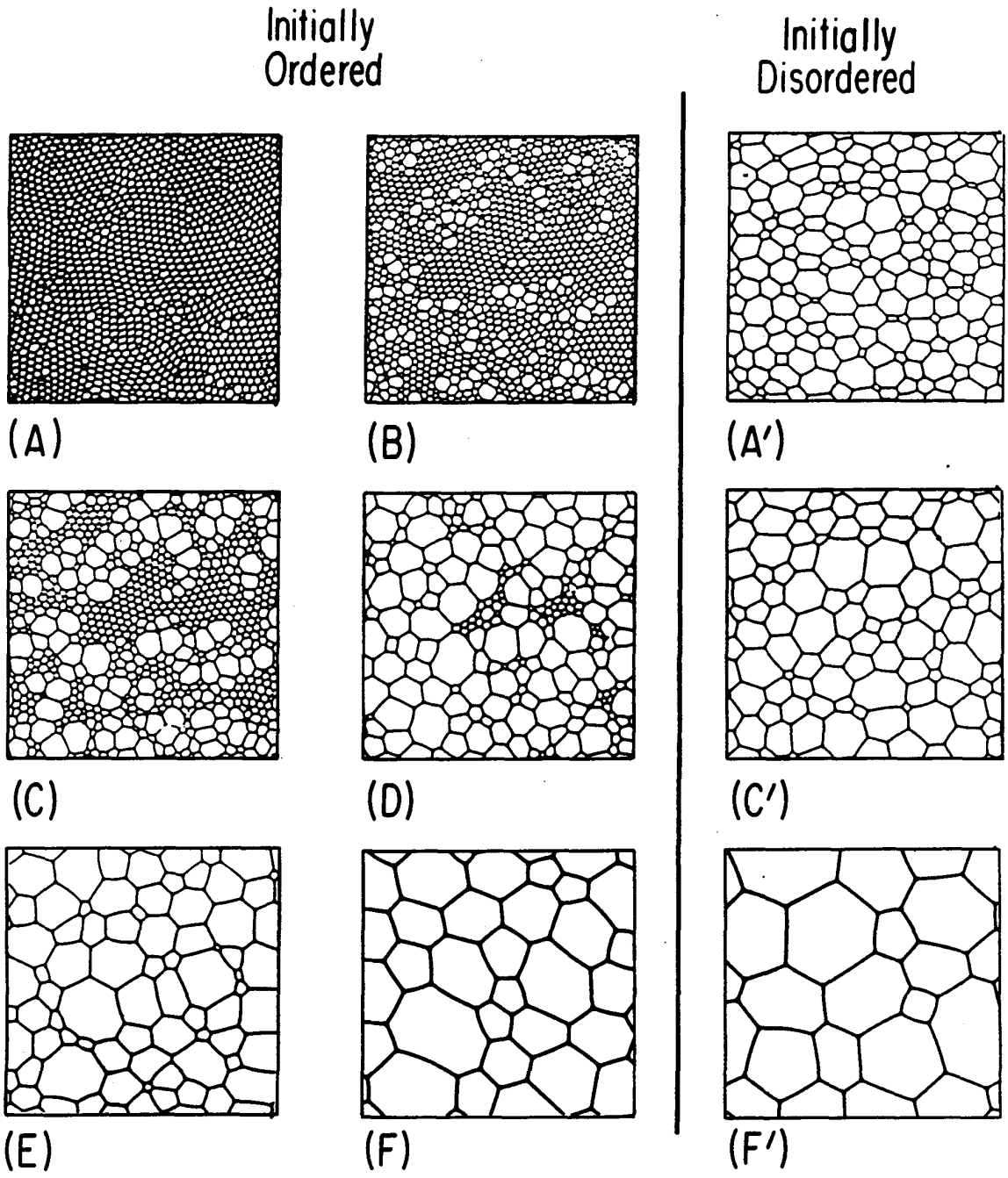
Initially
Ordered
Initially
Disordered
(A)
(B)
(A′)
(C)
(D)
(C′)
(E)
(F)
(F′)
(a)
(b)

Fig. 10 Evolution of a Soap Froth Evolution of an air soap froth with artificially broadened initial distribution functions. Lettered times correspond to regimes in Fig. 16. The illustrated areas represent 5% of the total experimental cell area (From Stavans and Glazier 1989).[220]

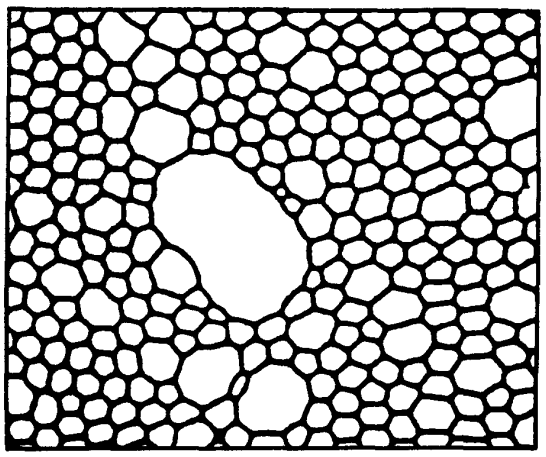

A''

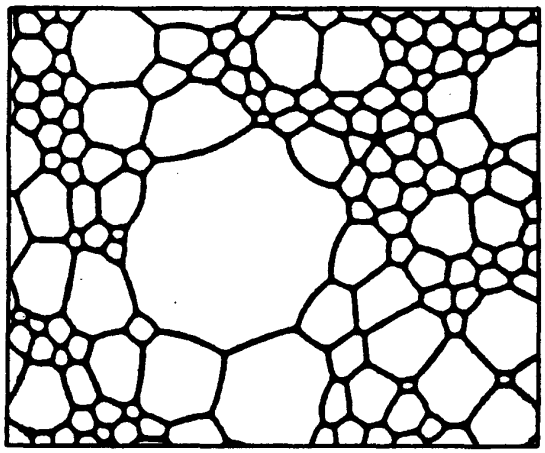

C''

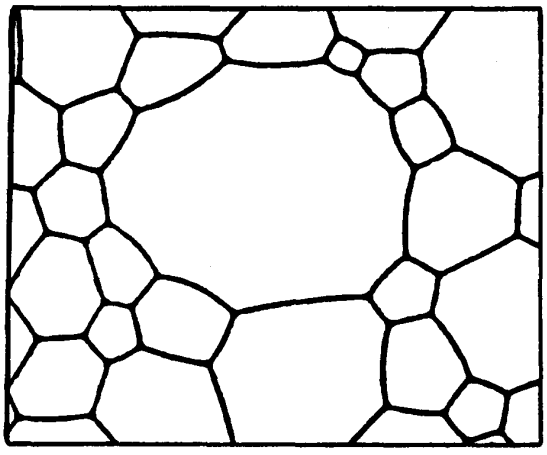

F''

and that evolving from an initial state with an artificially large distribution of initial sizes.

Fig. 9 (a) presents details (corresponding to 15% of total area) of photocopies taken by Glazier, Gross and Stavans of an initially ordered run (with initial disorder to be defined later, $\partial(0) = 0.17$)

We may qualitatively distinguish these figures as follows:

(A) The bubble lattice is essentially ordered, being composed of hexagonal crystal grains with defects consisting of five- and seven-sided bubbles at the grain boundaries. All bubbles are essentially the same size. Most are six-sided. A few are five- or seven-sided. The rate of evolution is slow (See Fig. 16 (d)).

(B) The grain boundaries become visibly marked as five-sided bubbles shrink and seven-sided bubbles grow. However six-sided bubbles do not evolve. The number of bubbles with $n \neq 6$ increases, as does the rate of evolution.

(C) The grain boundaries grow into patches of disorder which eat away at the ordered regions. The ordered and disordered regions occupy essentially equal areas. The normalized width of the area distribution ($\frac{<\delta a>}{<a>}$) is maximal. Many-sided bubbles are common as there is a large probability for a large bubble to be surrounded by much smaller bubbles.

(D) The ordered regions have almost entirely disappeared. The width of the normalized area distribution and the rate of evolution begin to decrease.

The number of many-sided bubbles decreases. The fraction of five-sided bubbles, $\rho(5)$, increases monotonically, while the fraction of six-sided bubbles, $\rho(6)$, decreases. See Fig. 33.

(E), (F) Long term states. The evolution rate is essentially constant. There are almost no three-sided bubbles and many-sided bubbles are rare. However, the fraction of bubbles with more than seven sides, $\rho(n)$, $n > 7$, increases slowly.

For large initial disorder ($\partial_0 = 0.85$), we observe a simpler pattern of evolution. We present detail photos of such a run in Fig. 9 (b).

(A') The lattice is relatively disordered but not in a long term scaling state. The rate of evolution increases monotonically (See Fig. 16 (f)).

(C') The lattice coarsens and the width of the distribution functions first decreases slightly as the system overshoots equilibrium, then increases to its final equilibrium value. The rate of evolution continues to increase monotonically to its final value without overshoot.

(F') Long term state. The state is indistinguishable from (E) and (F).

For an artificially broadened area distribution, including both well ordered and completely disordered patches, we again observe a monotonic equilibration (Fig. 10).

(A") Initial condition. Many small bubbles with a few very large bubbles with very many sides.

(C") The large bubbles gradually lose sides to the advantage of their neighbors. The relative area of many sided bubbles decreases.

(F") Long term states. Except for the presence of one eleven-sided bubble, the state is indistinguishable from (E), (F) and (F').

IV.c.ii von Neumann's Law: Experiment

Fu, Glazier, Gross and Stavans, and Glazier *et al.* have made experimental measurements of von Neumann's law.[85,93,94] Fu measured areas by cutting out the individual bubbles from his photographs and weighing them, an extremely tedious procedure that limited him to small samples. Glazier, Gross and Stavans and Glazier *et al.* made their measurements using a digitizing tablet (marginally less tedious), following around the edge of the bubble and selecting a few key points to digitize. For example a seven-sided bubble might have been digitized as fourteen- or twenty one-sided polygon depending on the degree of curvature of its sides. The digitization was repeated either three or six times for each bubble and the results averaged together to obtain an estimate for the bubble area.

This method had several disadvantages. The most serious problem was the difficulty of making repeated accurate measurements by hand. The typical variation in area estimates for a single bubble could be as high as 5%. Especially for images taken late in a run when the Plateau borders were broad, it was difficult to find the centers of the Plateau borders to obtain the correct perimeter. Enlarging the image increased the error from both

TABLE 3

VON NEUMANN'S LAW

da_n/dt	System				
n	Helium[94] 0.817 (hours)	Helium[94] 11.1 (hours)	Helium[94] 38.23 (hours)	Air[93]	Air[85]
3	–	–	–	-6.94	–
4	–	-1.21	-1.28	-5.28	-0.41
5	-0.59	-0.50	-0.70	-3.04	-0.41
6	0.00	0.00	0.00	0.06	0.005
7	0.71	0.67	0.47	1.39	0.38
8	0.89	1.28	1.04	4.13	0.74
9	–	–	1.82	5.25	1.13
10	–	–	–	8.42	1.29
11	–	–	–	24.47	1.88
12	–	–	–	18.97	–
14	–	–	–	31.18	–
15	–	–	–	19.93	–
17	–	–	–	28.78	–
21	–	–	–	25.13	–
22	–	–	–	47.59	–
24	–	–	–	37.52	–
25	–	–	–	35.00	–
36	–	–	–	23.01	–
66	–	–	–	46.54	–

Fig. 11 Von Neumann's Law. Growth rates for n-sided helium bubbles at (A) $t = 1.82$ hours, (B) $t = 12.10$ hours and (C) $t = 39.23$ hours, for the run given in Fig. 16 (d). Results are consistent with von Neumann's law with $\kappa = 4.57 \text{ x } 10^{-2} \pm 3.8 \text{ x } 10^{-3}$ $\frac{\text{mm}^2}{\text{min}}$ at all times. Error bars indicate the variation in κ among individual n-sided bubbles at 95% certainty (From Glazier, Gross and Stavans 1987).[94]

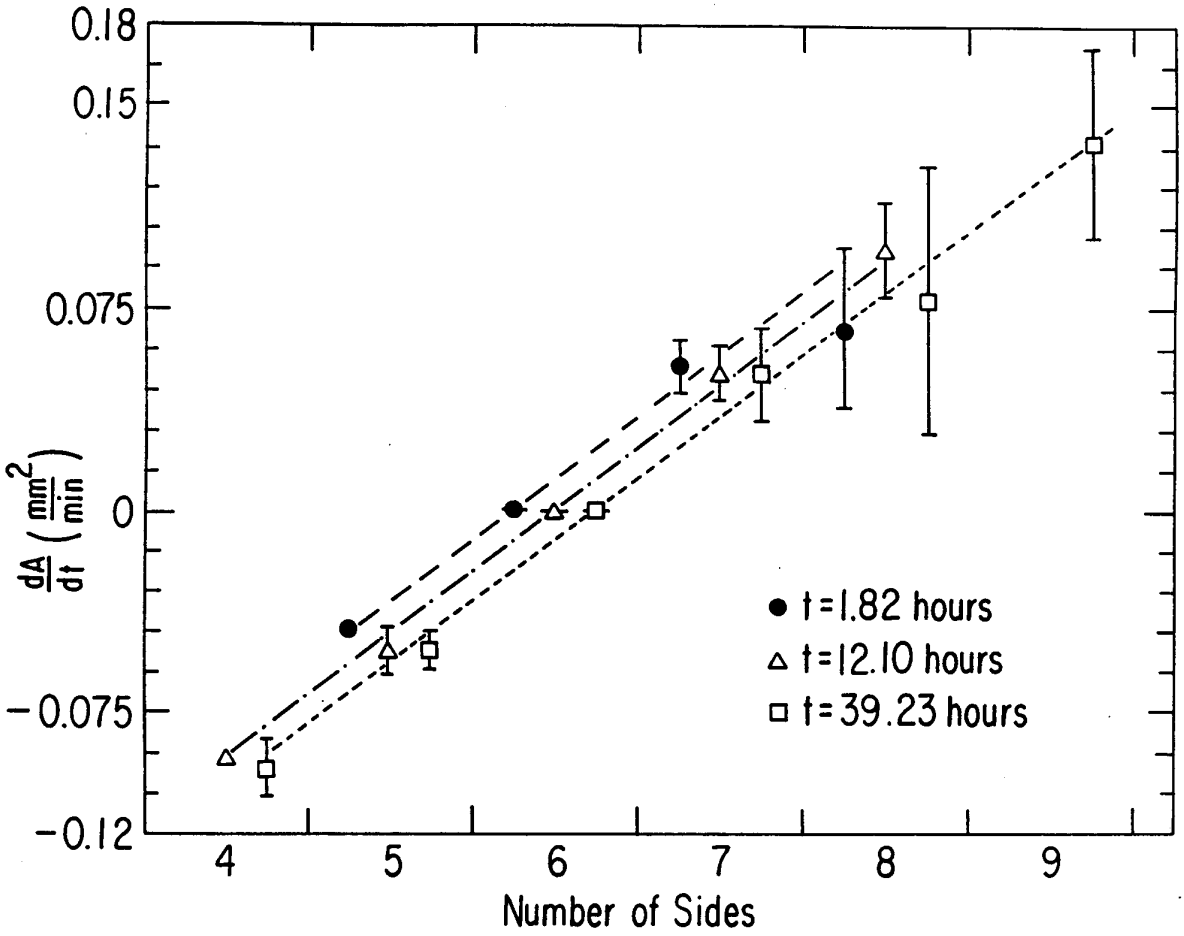
0.18
0.15
0.075
0
−0.075
−0.12
4
5
6
7
8
9
Number of Sides
$\frac{dA}{dt}\left(\frac{mm^2}{min}\right)$
● t=1.82 hours
△ t=12.10 hours
□ t=39.23 hours

Fig. 12 Von Neumann's Law. Growth rates for n-sided air bubbles. The result is consistent with von Neumann's law for n up to 24. Error bars show one standard deviation. Single points indicate that only one measurement was made for that number of sides (From Glazier *et al.* 1989).[93]

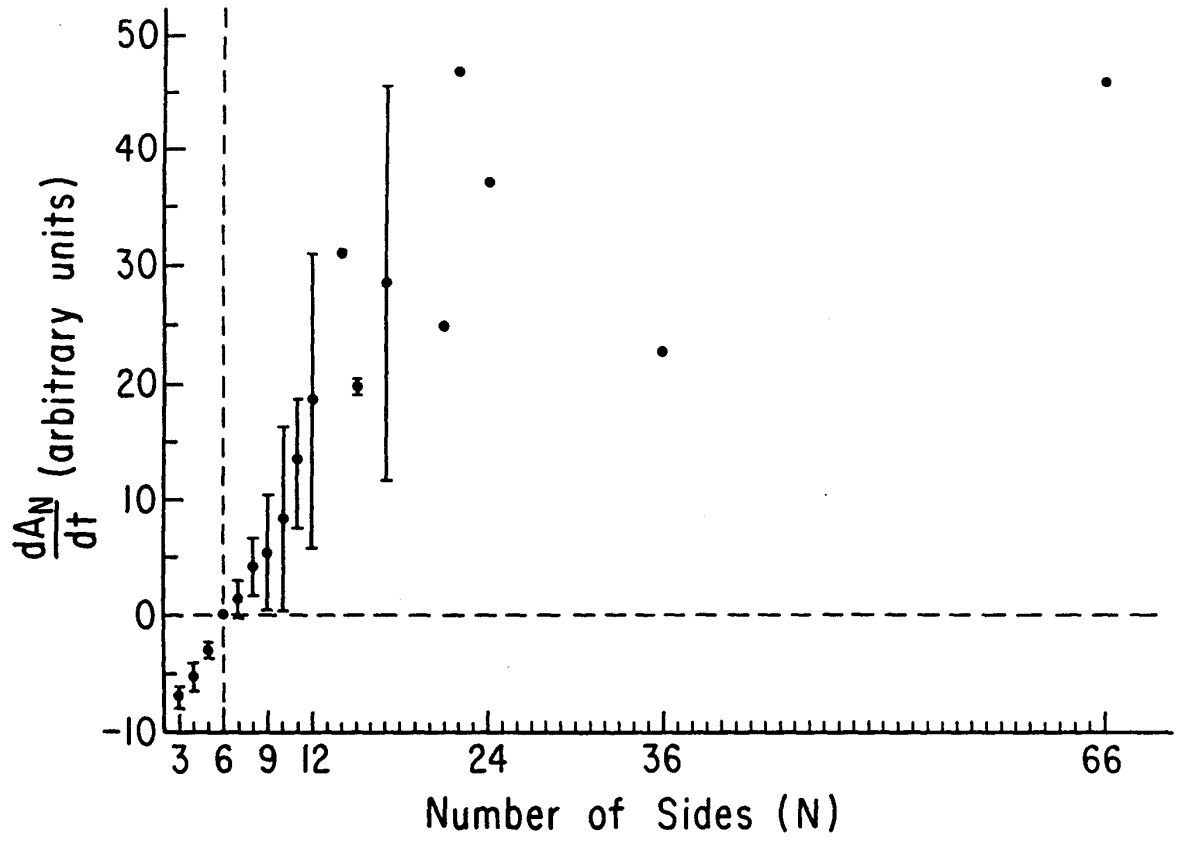
50
40
30
20
10
0
-10
$\frac{dA_N}{dt}$ (arbitrary units)
3 6 9 12 24 36 66
Number of Sides (N)

effects, and working with larger bubbles made the problem worse, since von Neumann's law predicts absolute not relative changes in area. Finally, the measured area depended on the number of points used in the approximating polygon and the exact position where they were set down, thus systematically underestimating the size of bubbles with fewer than six sides and overestimating the size of bubbles with more than six sides.

Measurements made over the longest possible time intervals, i.e. measuring the area of a bubble just after (and again just before) it changed its number of sides, minimize these errors. Large statistical samples reduce the random noise introduced by hand measurement. In the case of bubbles with three or more than ten sides, however, the rarity of the types limited Glazier *et al.*'s sample size to at most a few (sometimes only one) bubbles. Measurements of six-sided bubbles were easier because of the tendency of such bubbles to clump together at early times during a run. Treating a clump of six-sided bubbles as one many-sided bubble greatly reduced the measurement error. The essentially straight walls of six-sided bubbles further improved accuracy in this case.

In Table 3 and Figs. 11 and 12 we present experimental measurements of von Neumann's law by Fu, Glazier, Gross and Stavans, and Glazier *et al.*. Fig. 11 shows a series of measurements made by Glazier, Gross and Stavans in helium at different times during the same experimental run, and shows that the area diffusion constant κ (the slope of the line through each set of points) remained constant to within 5% during the period of the measure-

ments. 12 shows Glazier *et al.*'s results taken at a single time from an air system in which a large range of bubbles sizes and hence number of sides were purposely introduced, providing information on the growth rates of bubbles with up to twenty sides, although not in a scaling state nor with any great statistical accuracy. The indicated error bars in the measured values of $\frac{dA_n}{dt}$ at least partially represent real fluctuations in bubble growth rates. For example, some seven-sided bubbles do shrink. However, much of the scatter is probably due to measurement error rather than intrinsic fluctuations in growth rates. The calculated value of κ depends on the details like the cell thickness and the amount of fluid in the froth, so we neglect it. What is important is the linearity of the measured growth rates in n and the constancy of the diffusion constant in time for a given run.

All three groups obtained the expected linear relation between n and $\frac{dA_n}{dt}$ for bubbles with between five and roughly fifteen sides. Three- and four-sided bubbles shrink slightly more slowly than expected and bubbles with more than about fifteen sides perhaps grow slightly more slowly than expected. The deviation for few-sided bubbles may be due to the stabilizing effect of the Plateau borders on very small bubbles. It may also be due to the deviations observed in the internal angles of few-sided bubbles discussed below. The slow growth rate of many-sided bubbles may be due partially to angle deviations but since this cannot result in a saturation, merely a reduction in the slope of the n dependence, its origin is not completely explained.

Since it is not possible to produce an experimental cell large enough to

generate a twenty-sided bubble in a scaling state, Glazier *et al.* made the observations quoted above for many-sided bubbles using froths with artificially introduced many-sided bubbles.

Experimentally Stavans and Glazier observed (Fig. 10) that many-sided bubbles tend to lose sides continuously in time.[220] Mathematically, we may start from equation III.15:

$$\frac{dN}{dt} = -\sum_{n=3,4,5} \frac{\kappa\rho(n)N(n-6)}{\lambda_n < a >}, \tag{III.15}$$

the number of bubbles lost per unit time. If the total area of the experimental cell is A, then $< a >= A/N$ so

$$\frac{d < a >}{dt} = \sum_{n=3,4,5} \frac{\kappa\rho(n)(n-6)}{\lambda_n}, \tag{IV.1}$$

i.e.,

$$< a(t) >= t \cdot \left(\sum_{n=3,4,5} \frac{\kappa\rho(n)(n-6)}{\lambda_n} \right) + a_0, \tag{9}$$

where a_0 is the average area at the start of the experiment. Substituting approximate experimental values for $\rho(n)$ and λ_n, we find

$$< a >= a_0 + 0.8\kappa t. \tag{IV.3}$$

On the other hand, an n-sided bubble will have area

$$A_n = A_n(0) + (n-6)\kappa t \tag{IV.4}$$

The ratio is

$$\lim_{t\to\infty} \frac{A_n(0) + (n-6)\kappa t}{a_0 + 0.8\kappa t} = 1.25 \cdot (n-6). \tag{IV.5}$$

Fig. 13 Internal Angles in the Soap Froth. Average internal angles versus n for n-sided bubbles. Note that angles are smaller than 120° for few-sided bubbles and larger for many-sided bubbles so that bubbles are more polygonal than expected. Error bars show one standard deviation of the measurement. Ten bubbles were measured for small n, fewer for large n (From Stavans and Glazier 1989).[220]

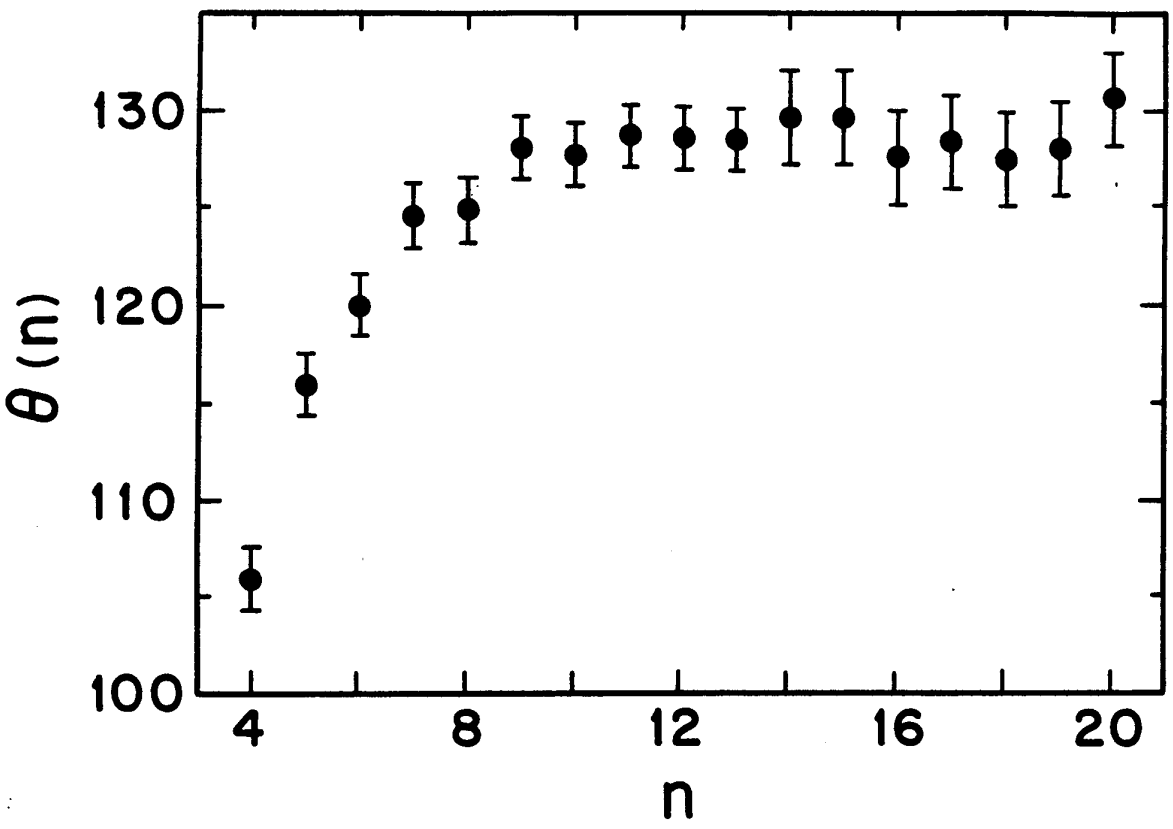
130
120
110
100
θ(n)
4
8
12
16
20
n

Fig. 14 Modified Von Neumann's Law. Growth rates for n-sided bubbles predicted by von Neumann's Law using the measured angle deviations in Fig. 13 (boxes) and ideal von Neumann's Law (solid line). The large error in the measured value of $\theta(3)$, means that we cannot tell if small bubbles shrink slower than a liner law would predict.

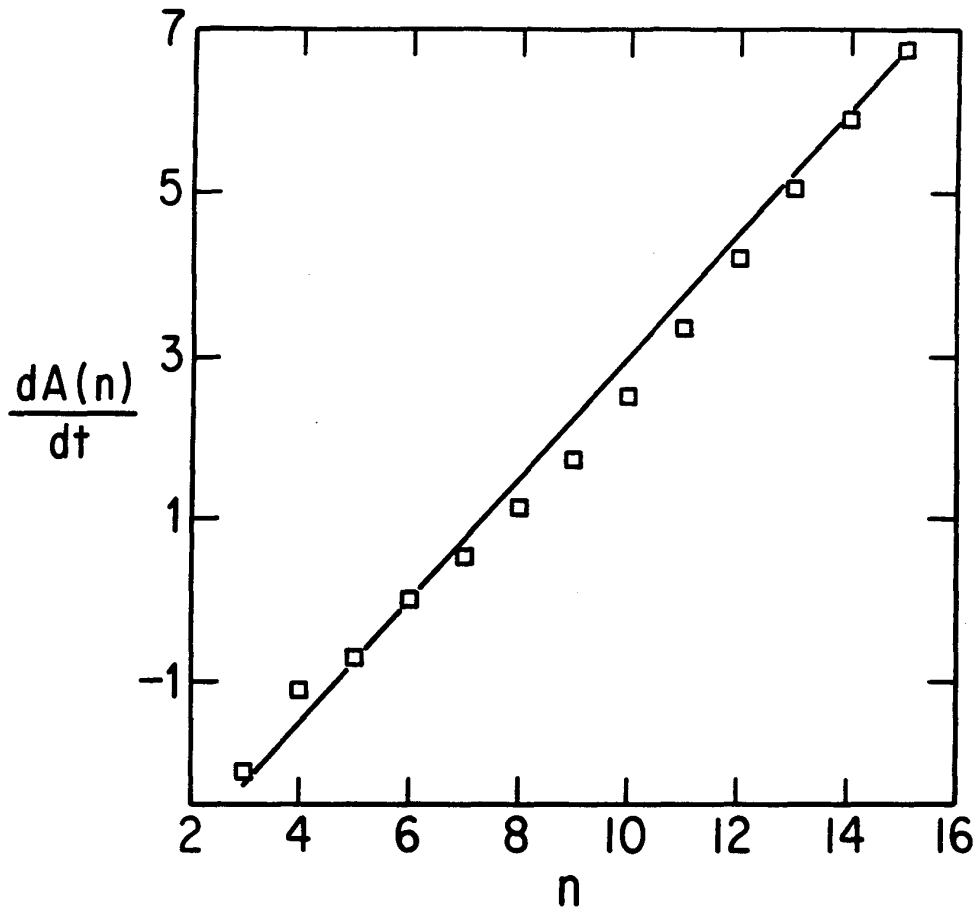
7
5
3
1
-1
dA(n)
dt
2
4
6
8
10
12
14
16
n

Fig. 15 Area Growth in Soap Froths. (A) Average area versus time in a low pressure two dimensional air froth (From Smith 1952).[206] (B) Number of bubbles (equivalent to normalized average area) versus time in a medium pressure two dimensional air froth. Circles are experimental data, x's Fullman's vertex model (From Fullman 1952).[86]

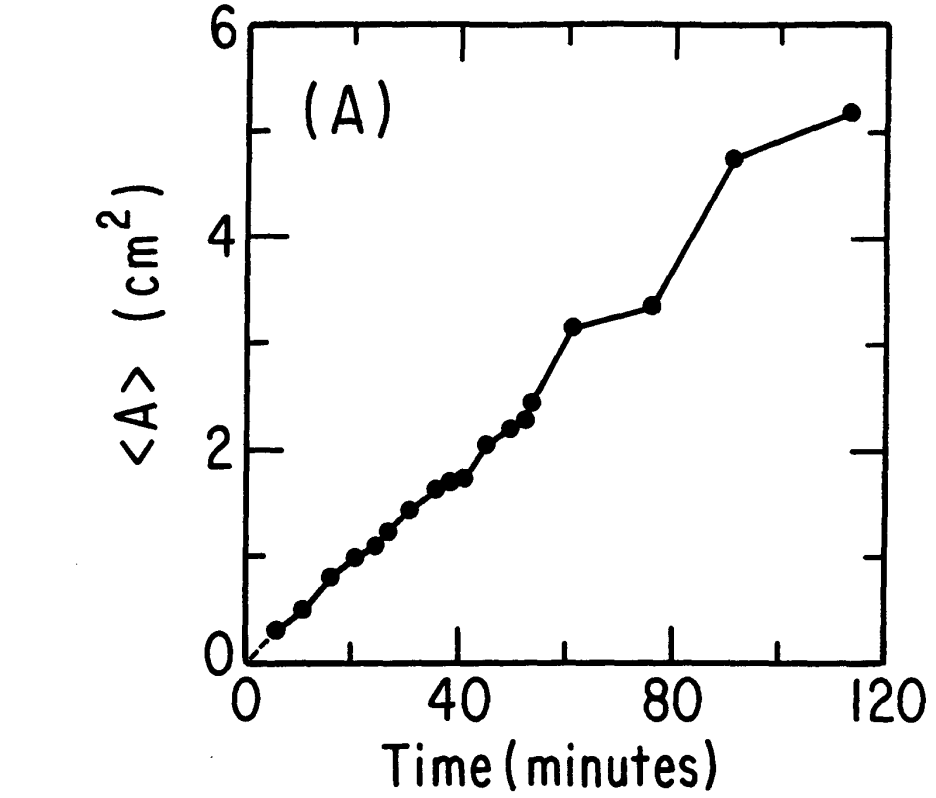
(A)
<A> (cm²)
6
4
2
0
0
40
80
120
Time (minutes)

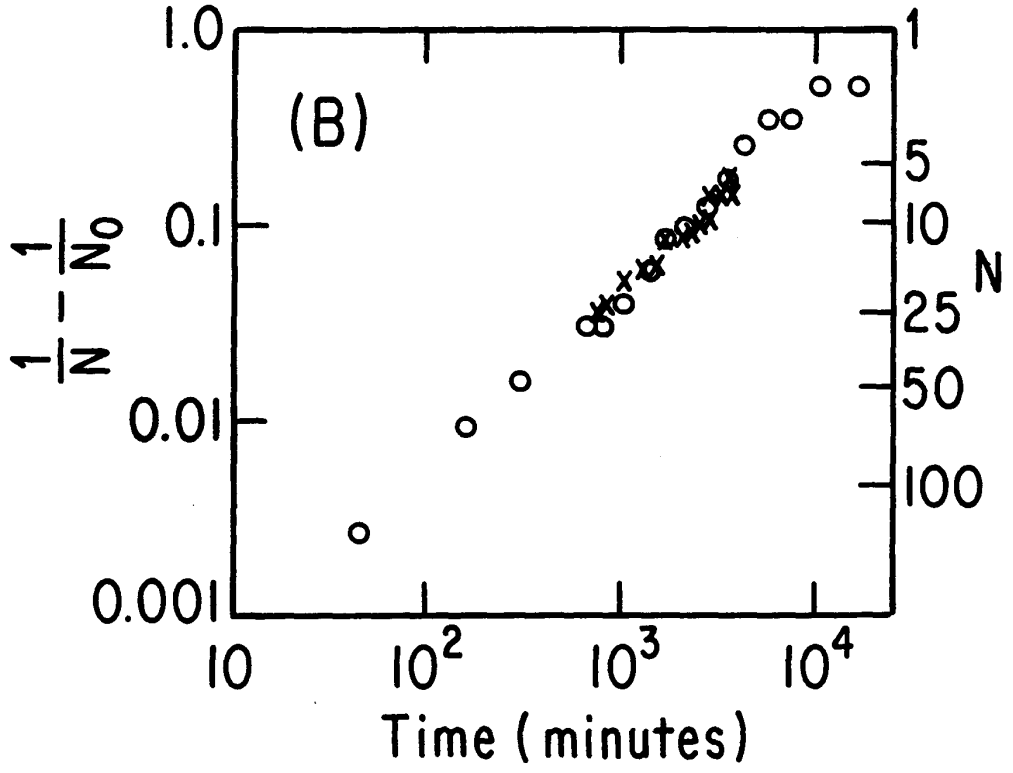
(B)
1 − 1/N
1 − 1/N₀
1.0
0.1
0.01
0.001
10
10²
10³
10⁴
Time (minutes)
1
5
10
25
50
100
N

Fig. 16 Area Growth in Soap Froths. Disorder parameter and number of bubbles in a fixed area cell (equivalent to average area) versus time for increasingly disordered initial conditions, (a) $\partial(0) = 0.04 \pm 0.02$, $\alpha = 0.63 \pm 0.03$ (Helium 1/16" cell thickness), (b) $\partial(0) = 0.08 \pm 0.01$, $\alpha = 0.50 \pm 0.01$ (Helium 1/8" cell thickness), (c) $\partial(0) = 0.11 \pm 0.02$, $\alpha = 0.50 \pm 0.04$ (Air 1/8" cell thickness), (d) $\partial(0) = 0.17 \pm 0.04$, $\alpha = 0.68 \pm 0.03$ (Helium 1/8" cell thickness), (e) $\partial(0) = 0.33 \pm 0.01$, $\alpha = 0.53 \pm 0.01$ (Helium 1/16" cell thickness), (f) $\partial(0) = 0.85 \pm 0.05$, $\alpha = 0.81 \pm 0.08$ (Air 1/8" cell thickness). Errors are at 90% certainty. Capital letters in (d) and (f) indicate times referred to in the text and in Fig. 9. Dots are experimental values. Solid lines and values of α are best fits computed from the phenomenological model of Glazier, Gross and Stavans.[94] Dashed lines are the disorder, ∂, as calculated from the model. Initial times are offset to 1 hour. For initially ordered conditions the rate of evolution overshoots its long term value, while for initially disordered conditions, the rate increases monotonically. In both cases the long term states obey a power law, $N \propto t^{-\alpha}$, where, $\alpha = 0.59 \pm 0.11$ (From Glazier, Gross and Stavans 1987).[94]

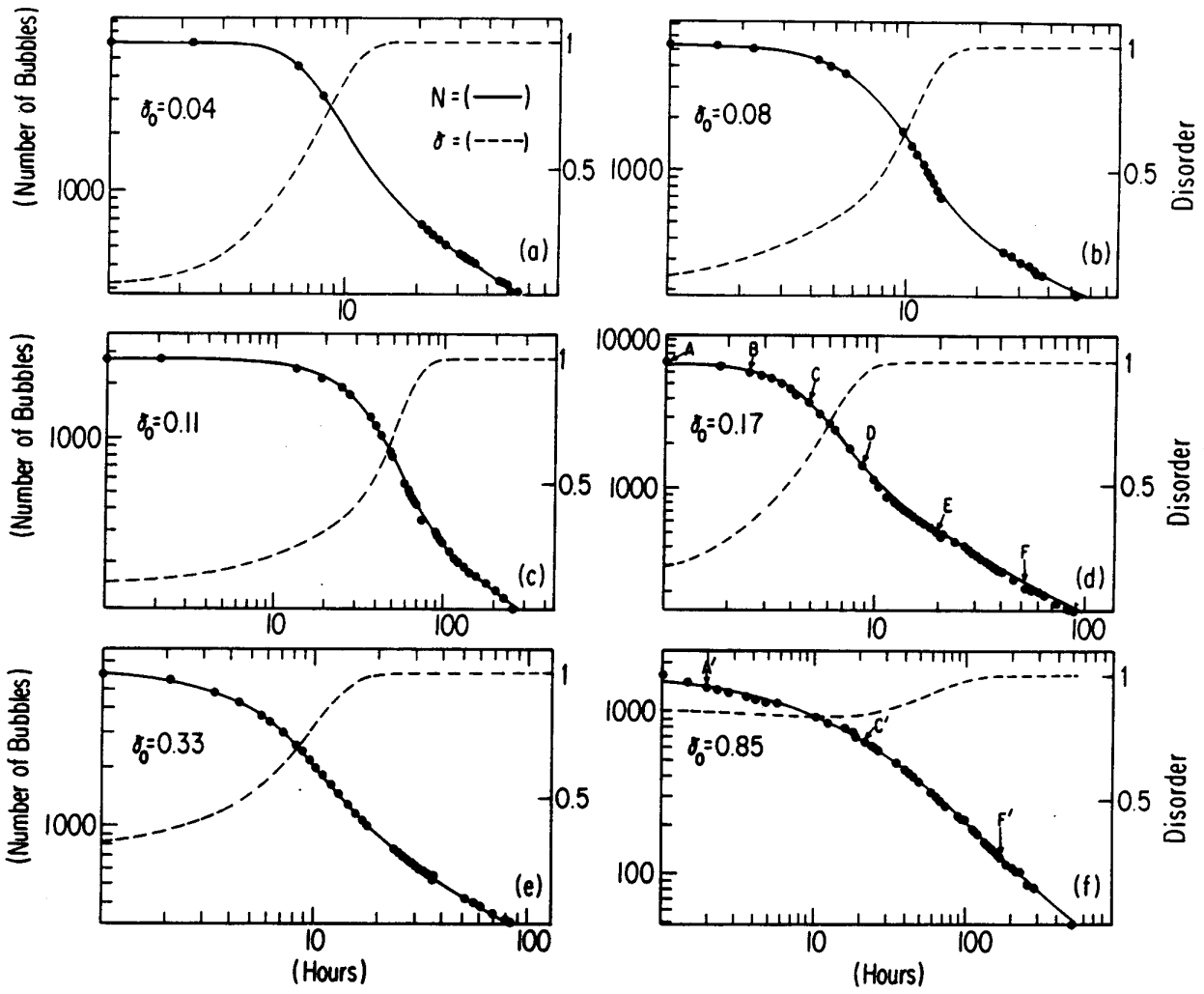
(Number of Bubbles)
Disorder
N = (——)
δ = (----)
δ0=0.04
δ0=0.08
δ0=0.11
δ0=0.17
δ0=0.33
δ0=0.85
(a)
(b)
(c)
(d)
(e)
(f)
A
B
C
D
E
F
A'
C'
F'
1000
10000
100
10
0.5
1
(Hours)

Fig. 17 Area Growth in Soap Froths. Average area (in pixels) versus time for a two dimensional air froth in a large cell. Dots are experimental data. Circles are values from a Potts model simulation starting from identical initial conditions (From Glazier *et al.* 1989).[93]

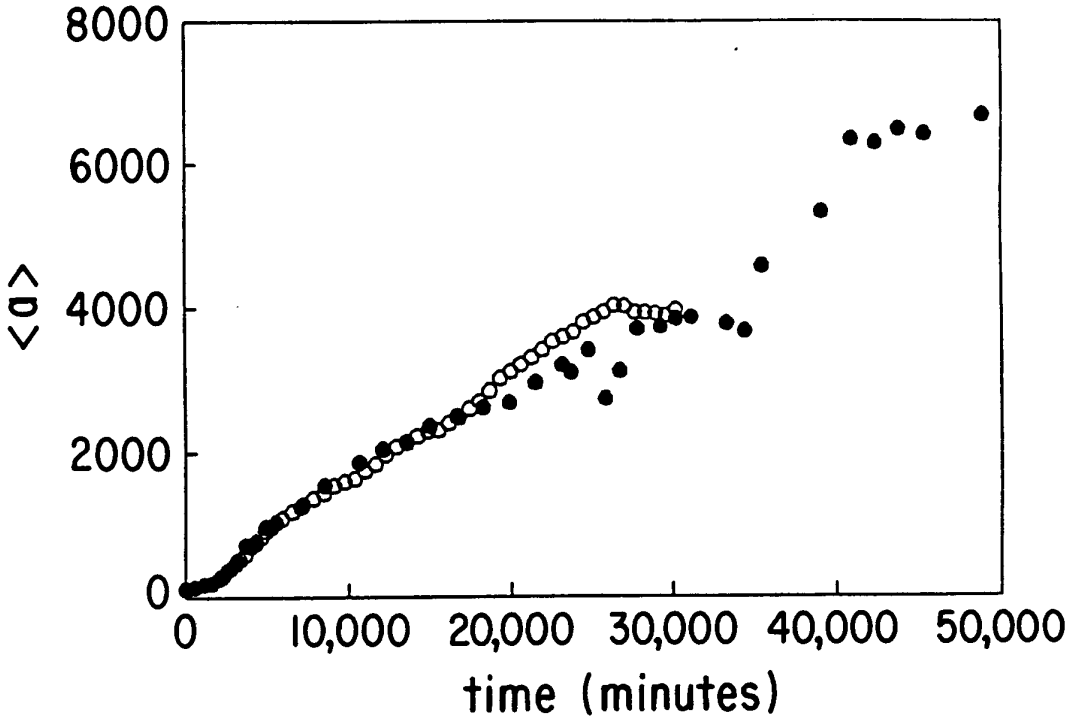
8000
6000
4000
2000
0
<D>
0
10,000
20,000
30,000
40,000
50,000
time (minutes)

Thus many-sided bubbles should equilibrate slowly, on a timescale of order $\frac{A_n(0)}{(n-6)\kappa}$. In the absence of side shedding this relation would predict that the average relative areas of n-sided bubbles would be proportional to $(n-6)$ which is non-sensical. The equilibration will happen much faster if the rate of side shedding is large. Unfortunately, no one has ever measured the mean rate of side shedding to check these hypotheses. Thompson and Frost have given an alternative argument for the equilibration of a froth.[229]

Stavans and Glazier also measured the average internal angle of an n-sided bubble, $\theta(n)$ by enlarging each vertex, bisecting the Plateau borders near the vertex, and measuring the internal angles with a protractor. Once again, their chief source of error was finding the true position of the centers of the Plateau borders.

In Fig. 13 we present their measurements of the average internal angles for the same run shown in the von Neumann's law calculation in Fig. 13. They found small but significant deviations from the expected 120° angles. In particular, the average wall curvature of all bubbles was smaller in magnitude, i.e. bubbles were more polygonal, than expected. In Fig. 14 we show the modified von Neumann's law obtained from these values of $\theta(n)$ and the linear predictions of the ordinary von Neumann's Law. Within the experimental error we cannot distinguish the two results, though the modified law predicts a smaller absolute rate of growth than the unmodified. The apparent rate of shrinkage of few-sided bubbles is smaller than predicted by a pure linear fit, as observed by Glazier *et al.*

IV.c.iii Quantitative Kinetics

We can begin to make our qualitative ideas about disordering and grain growth more precise by measuring the average area per bubble as a function of time, $< a >$ or $< \mathbf{A} >$. Such measurements have been made in two distinct ways. Fullman, and Glazier Gross and Stavans hand counted the number of bubbles in the experimental cell which were not in contact with the cell walls and used the total area of the interior of the froth to obtain the average bubble size.[86,94] Smith, Aboav, and Glazier *et al.* measured bubble areas directly, either by weighing cut outs from photographs or by digitizing the images.[8,93,206]

We present results for average bubble area versus time in Fig. 15 (A) (Smith's results), Fig. 15 (B) (Fullman's results), Fig. 16 (Glazier, Gross and Stavan's results, converted back into the number of bubbles needed to cover the experimental cell completely), and Fig. 17. (Glazier *et al.*'s results obtained by direct digitization of a 30% sample of an air run). The letters in Fig. 16 (d) and (f) key to the regimes of evolution presented in Fig. 9. In Fig. 17 the slight non-monotonicity results from the fact that large bubbles are more likely to touch the frame boundary and hence to be excluded from the ensemble.

These quantitative measurements confirm division of the evolution into distinct regimes. For an initially ordered froth we observe a period of slow growth, followed by a period of equilibration during which the average area per bubble increases roughly exponentially, and finally a scaling regime dur-

TABLE 4

GROWTH EXPONENTS

Experiment		Two Dim.	Three Dim.
Group	System	α	α
Soap Froths			
Smith[206]	Froth	1	–
Fischer[86]		1	–
Aboav[8]		2	–
Glasier and Stavans[94]		0.59 ±0.11	–
Glasier *et al.*[93]		1	–
Lipid Monolayers Metal Grains			
Moore *et al.*[169]	stearic acid	1.10 ± 0.10	–
	Lead		
Bolling and Winegard[32]	Pb 10^{-6} Pure	–	0.8 ± 0.05
	Pb + 0.005% Ag	–	0.96
	Pb + 0.01% Ag	–	0.96
	Pb + 0.02% Ag	–	1.04
	Pb + 0.04% Ag	–	1.14
	Pb + 0.005% Au	–	1.12
	Pb + 0.02% Au	–	1.20
Drolet and Galbois[59]	Ultra Pure	–	0.82
	Tin		
Holmes and Winegard[107]	10^{-5} Pure	–	1.00 ± 0.02
Drolet and Galbois[259]	Ultra Pure	–	0.86
	Aluminum		
Gordon[260]	Ultra Pure	–	0.5
Beck *et al.*[261]	High Purity		
	400° C	–	0.18
	600° C	–	0.64
	Al + 2% Mg		
	400° C	–	0.34
	600° C	–	0.90
	Al + .6% Mg		
	550° C	–	0.3
	650° C	–	0.68
Beck[24]	Pure		
	350° C	–	0.112
	600° C	–	0.644
	"Near Melting"	–	1
Fradkov *et al.*[262]	Al $+10^{-4}$ Mg Foil	1	–

TABLE 4, *continued*

Experiment		Two Dim.	Three Dim.
Group	System	α	α
Metal Grains			
	α-Brass		
Beck and Burke[259]	70:30	–	0.4
Beck[24]	Ultra Pure	–	1
	Commercial	–	0.4
Fullman[86]	450° C	–	0.42
	850° C	–	0.6
Beck[24]	High Purity		0.8
Burke[260]	500° C	–	0.7
	850° C	–	1
Fullman[86]	500° C	–	0.70
	850° C	–	1.2
	Iron		
Miller[261]	Carbon Steel		
	815° C	–	0.16
	1250° C	–	0.44
Hu[262]	Ultra Pure Fe	–	0.80
Ceramics			
Dutta and Sprigs[263]	ZnO	–	0.66
Kapadia and Liepold[264]	MgO	–	1
Gordon *et al.*[265]		–	0.66
Petrovic and Ristic[266]	CdO	–	0.66
Tien and Subbaro[267]	$Ca_{.16}Zr_{.84}O_{1.84}$	–	0.8
Kingery and François[268]	UO_2	–	0.66

TABLE 4, *continued*

Theory		Two Dim.	Three Dim.
Group	System	α	α
	Mean Field Theories		
Burke and Turnbull[42]	Radius Based	1	1
Hillert[106]		1	1
Feltham[259]		1	1
Mullins[172,173]		1	1
Rhines and Craig[260]		–	1
Louat[152]		1	–
Novikov[183]		0.91	–
Hunderi and Ryum[112]		1	–
Hunderi and Ryum[114]		0.77 ± 0.3	–
Mullins[173]	Topological	1	–
Marder[157]		1	–
	Boundary Models		
Frost *et al.*[52]		1	–
	Vertex Models		
Fullman[86]		1	–
Enamoto *et al.*[261]		1	–
Weaire and Kermode[242,243]		2	–
	Network Models		
Fradkov *et al.*[76]		1	–
Beenakker[27,26]		1	–
	Potts Models		
Anderson *et al.*[16]		0.83	–
Wejchert *et al.*[249]	Initial Voronoi	0.84 ± 0.06	–
	Initial Hard Sphere	0.98 ± 0.06	–
Anderson *et al.*[14]	Q=36	0.87	–
	Q=48	0.90	–
	Q=64	0.94	–
Anderson *et al.*[13,15]		0.98 ± 0.04	0.96 ± 0.12

ing which $< a >$ increases as a power law. For an initially disordered froth we find a monotonic increase in growth rate until it reaches the equilibrium power law. We have not measured growth rates for an artificially broadened initial distribution, but we expect that the growth rate will decrease monotonically to its equilibrium value, as observed in simulations of Frost and Thompson.[83] Smith and Fullman both begin with disordered states and obtain $< a > \sim t$ at all times.[86,206]

While finite size effects may well be important in the latter stages of pattern evolution, the range of rollover points from equilibrating to scaling behavior observed (ranging from 1000 bubbles for Fig. 16 (a) and (d) to 100 bubbles in Fig. 16 (c)) suggests that the transition between these two regimes is not an edge effect. To further control for edge effects Glazier, Gross and Stavans counted the number of bubbles touching the lateral walls of the cell (edge bubbles) as a function of time. If the average area of a bubble in contact with the edge were a constant times the average area of a bubble in the bulk, we would expect $N_{edge} \propto N_{bulk}^{0.5}$. This would be the case if the edge behaved as a non-interacting window on an infinite cell or as an infinite network of hexagonal bubbles. In either case the result would suggest that edge effects were insignificant. They found $N_{edge} \propto N_{bulk}^{0.56 \pm 0.14}$ which was consistent with either hypothesis.

In the scaling state the coarsening of the froth may be described by a scaling exponent, α, $< a(t) > \propto t^{\alpha}$. Smith and Fullman both measured $\alpha = 1$ but with relatively few bubbles. Aboav, reanalyzing Smith's data found $\alpha = 2$.[8]

Glazier, Gross and Stavans obtained a value of $\alpha = 0.59(^{+0.11}_{-0.09})$, where the scaling exponent was determined using an indirect method discussed below. Finally, Glazier *et al.*, working in a larger experimental cell, obtained results consistent with, though not conclusively demonstrating, $\alpha = 1$. Observations of coarsening in thin film and bulk metals, alloys and ceramics have yielded a similar variety of exponents, though non-von Neumann factors like impurity pinning and three dimensional effects complicate the interpretation. In general we find that higher impurity concentrations lead to lower growth exponents as impurities zone refine to grain boundaries and act as pinning centers which eventually reduce boundary mobilities to zero. Some impurities (e.g. Au in Pb), however, apparently enhance grain boundary mobility or grain coalescence, and thus increase the growth exponent. Higher temperatures nearly always result in higher growth exponents since they reduce grain freezing due to anisotropy and other pinning effects. In two dimensions, preferential etching or oxidation at grain boundaries can also reduce boundary mobilities and growth exponents. Measured exponents in bulk and thin films, metals, alloys and ceramics are all comparable. We summarize a few selected experimental measurements and theoretical predictions of the scaling exponent in Table 4. Where the original result was presented for the average radius rather than the average area, the quoted value of α is twice the radius exponent. This approximation is correct in the case of a scaling state. Three dimensional results are given for two dimensional sections of three dimensional volumes.

Summarizing: most experimental coarsening has $0.3 < \alpha < 1$ and the majority of models give $\alpha = 1$. We observe experimental results close to the theoretical values for α, only when the experiment is carefully controlled, a large experimental cell and many bubbles in the soap froth, high temperatures and pure materials in grain growth. At short times and for initially well ordered conditions the transient during which a soap froth equilibrates results in a larger apparent exponent measured by Glazier, Gross and Stavans, hence Aboav's measurement of a growth exponent of two (we will discuss later the reasons we believe that Aboav measured an equilibrating rather than a scaling state). At very long times in the froth, we suspect that the effective diffusion constant of the soap films decreases due to broadening of the Plateau borders, hence the smaller apparent exponent. In grain growth we have mentioned a variety of effects that can lead to smaller long term exponents and even the complete cessation of coarsening. The most important of these mechanisms are impurity segregation due to local zone refining resulting in pinning of grain boundaries (an effect which can be observed in a correctly designed soap froth experiment) and pinning of grain boundaries due to strong orientational anisotropies in surface energies (which can be duplicated in Potts model simulations).

The essential unanimity of the theoretical predictions of the growth exponent, and the experimental uncertainties in measuring it,

TABLE 5

PLATEAU BORDER BROADENING

Run 1		Run 2	
Time (hours)	Width(mm)	Time (hours)	Width(mm)
0.00	0.393 ± 0.028	0.00	0.309 ± 0.019
11.08	0.430 ± 0.027	2.50	0.313 ± 0.018
56.43	0.475 ± 0.019	18.47	0.312 ± 0.024
139.08	0.512 ± 0.028	42.75	0.313 ± 0.024
490.45	0.590 ± 0.034	74.20	0.394 ± 0.037
–	–	258.08	0.602 ± 0.031

Fig. 18 Plateau Border Broadening. Plateau border widths versus time for two air runs. Run 1 (circles). Run 2 (squares).

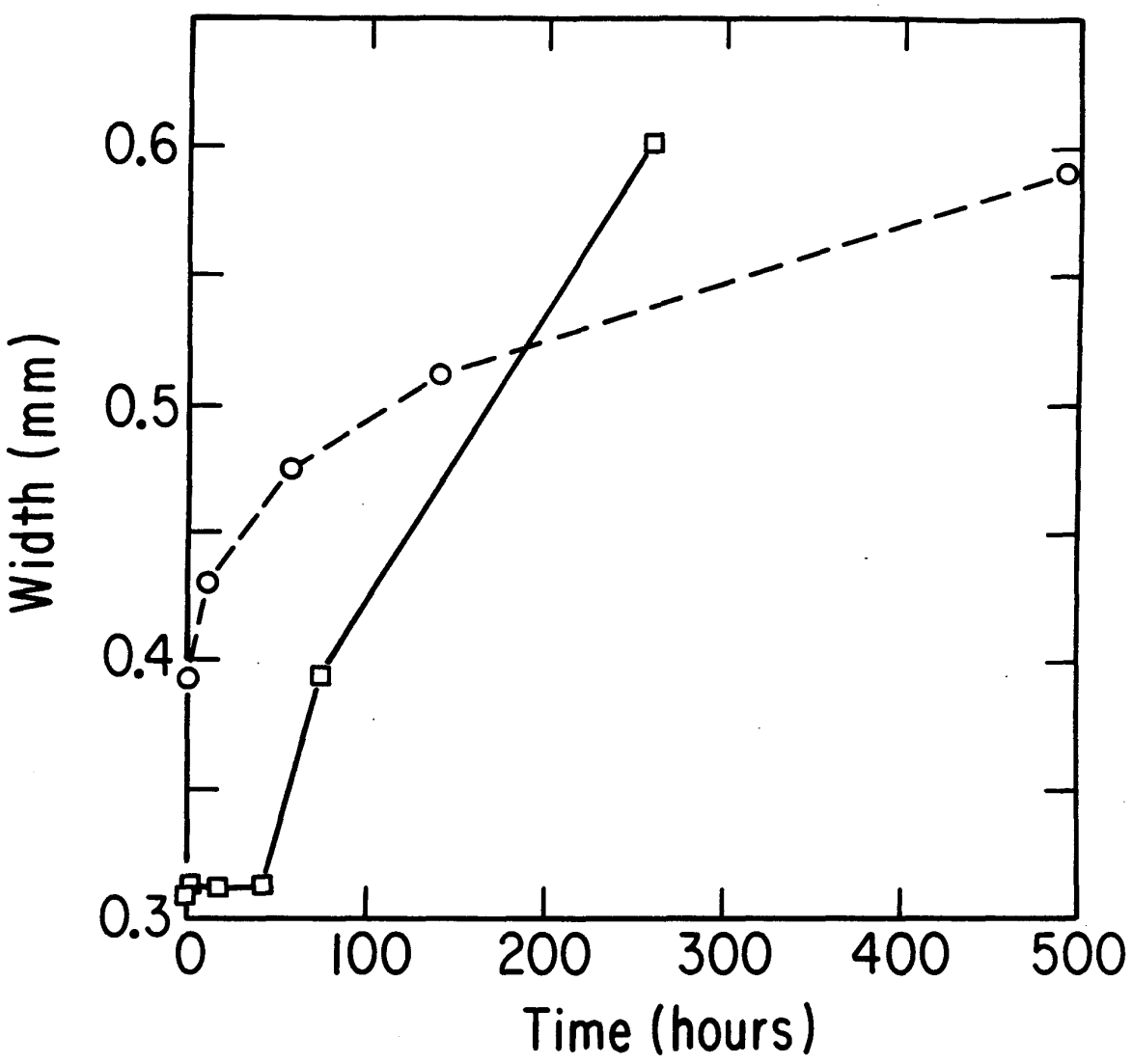
0.6
0.5
0.4
0.3
Width (mm)
0
100
200
300
400
500
Time (hours)

suggest that a better test of the agreement between theory and experiment is the theory's ability to duplicate the observed transient behaviors for initially ordered and initially disordered patterns.

IV.d Other Topics

IV.d.i Broadening of Plateau Borders

Glazier, Gross and Stavans originally proposed that the anomalous exponent they observed in the two dimensional soap froth resulted from the failure of the froth to reach a scaling state.[94] Later work has demonstrated that their froths did reach a well behaved scaling state.[93,220] Others have suggested that boundary effects play a role when many bubbles are in contact with the walls of the experimental cell.[157,200] However, the experiments of Smith, and Fullman showed no such anomalous exponent though they worked with even fewer bubbles.[86,206] The Potts model simulations of Glazier *et al.* did show a boundary effect glitch in the long time tail of the simulation (See Fig. 17), just where the experiment showed a sudden decrease in growth rate, but this similarity may be fortuitous.[93] One possible source of the difference is that Glazier, Gross and Stavans used a rectangular cell, while Smith and Fullman used a round cell. A later experiment by Glazier *et al.* in a larger cell where edge effects should have been less important was consistent with an exponent of $\alpha = 1$.

The observation of anomalously low growth exponents is common in metals, where initially well dispersed impurities gradually segregate to the grain

boundaries and reduce boundary mobility and hence slow (or even stop) grain growth. Inversely, the presence of impurities which increase boundary mobility can result in growth exponents larger than 1.[24] In a froth the equivalent to a decreased boundary mobility is a decreased diffusion constant of the soap films. While changes in the chemical structure of the films as they age are possible, it seems more likely that any decrease in diffusion constant is due to the increase of the amount of fluid per unit length of soap film in the sealed cell, as bubbles disappear and the total length of the soap film decreases. Film thickening *per se* is probably not too important since the thickness of the soap films depends on the competition between van der Waals attractive forces and electrical double layer forces between the lipid monolayers on the surface of the film,[176] and since the Plateau borders take up most of the excess fluid.[220] However, even a small amount of film thickening would result in a large decrease in diffusion constant.

An additional experimental problem is that we have no techniques to measure the film thickness directly during a coarsening run. The Plateau border width can be measured directly. Since we might expect that the film thickness would increase with the widths of the Plateau borders which indicate the amount of excess fluid present in the froth, a measurement of Plateau border broadening cannot hope to separate the two effects definitively. Of course, if we could measure the von Neumann κ accurately as a function of time we could check the constancy of the diffusion constant directly, and correct our models without recourse to physical explanations.

Against the diffusion constant explanation lies Glazier, Gross and Stavans' measurement of the constancy of the von Neumann κ discussed in the previous section. The helium run in question, however, gave a growth exponent of $\alpha = 0.68$ and would have given a still larger exponent (nearly 1) if the data had been cut at the time of the last diffusion constant measurement. There is thus no real evidence for the constancy of κ in the tail of the time evolution where the anomalous growth rates occurred.

Determining the fraction of the soap film obstructed by the Plateau borders was not straightforward. Glazier could measure only the widths of the borders, not their vertical extent, and even measuring the widths from the experimental photocopies proved unreliable, because the changes in width during the experiment were comparable to the uncertainties in the widths in the copies. In particular, the photocopier proved to be anisotropic in its treatment of lines. Some orientations produced smooth well defined lines, and some irregular lines with great variations in line width. Examination of an actual froth with a magnifying glass showed that this was indeed an artifact of the photocopies and not an exotic wetting effect of the plexiglass. He therefore measured only lines oriented within 30° of the axis giving the smoothest line profiles. We present the results for two air runs in an $\frac{1}{8}$" cell in Table 5 and Fig. 18. In the first run the width of the Plateau borders doubled during the run, in the second the increase was approximately 50%.

If we assume that the vertical extent of a Plateau border is roughly one half its horizontal extent we obtain the following results (A larger wetting

angle would result in a relatively larger obstructed area and hence in an effect of greater magnitude). In the first run the fraction of the film obstructed by the Plateau Borders ranged from approximately 12.4% at the beginning of the run to 18.7% at the end. The growth exponent for this run was $\alpha = 0.81$. In the second run the obstructed fraction grew from 9.9% at the beginning of the run to 19.0% at the end. The growth exponent for this run was $\alpha = 0.50$. The Plateau border width in the second run did not increase significantly until the number of bubbles decreased to fewer than two hundred. The fact that a lower exponent corresponds to a larger percentage increase in obstructed area is suggestive but hardly conclusive. Even more suggestive was the exponent of nearly one obtained by Glazier *et al.* in a much larger cell which showed little Plateau border broadening. Also favoring Plateau border broadening is the difference in average exponent between cells with a height of 1/8" ($\alpha = 0.71$) and 1/16" ($\alpha = 0.58$). We would expect that Plateau border broadening, but not film thickening, would have a larger effect in a thinner cell.

To obtain a definitive measure of the growth exponent in the soap froth, we need to repeat the grain growth measurement in a drained cell where the width of the Plateau borders, and hence the film thickness, is held constant.

IV.d.ii Disappearance of Four- and Five-Sided Bubbles

Many of the models we will discuss require the enumeration of the different fundamental processes by which a bubble can change its number of sides. In particular, they depend on the rate of side swapping ($T1$ processes) and

the rate at which three-, four- and five-sided bubbles disappear. Smith, in his original article, claimed that only three-sided bubbles could disappear directly, and that four- and five-sided bubbles always shed sides as they shrank to become three-sided when they were very small.[206] Glazier, Gross and Stavans, on the other hand, claimed that 50% of four-sided bubbles and 10% of five-sided bubbles disappeared directly.[94] Later Stavans and Glazier revised their estimate for the rate of direct disappearance by five-sided bubbles to 24%.[220] Fu also observed direct disappearance, though he did not publish estimates for the relevant rates.[85] A theoretical study by Weaire supports the contention that arbitrarily small four- and five-sided bubbles may be stable against side shedding.[237] However, the distinction may be more a matter of definition than a true physical difference. Very small bubbles are sensitive to the thickness of the cell and are hence no longer two dimensional in their properties. In particular, when a cylindrical bubble disappears, it first pinches off on the bottom plate (where the Plateau borders are broader due to gravity) to form a conical bubble, and then shrinks rapidly before disappearing on the top plate. Since Smith took his photographs from the top, he recorded the disappearance of the conical bubble, while Glazier *et al.* photocopying from below, recorded the initial separation. Since the conical bubbles behave in a manner qualitatively different from the ensemble of cylindrical bubbles, the latter definition seems more sensible.

CHAPTER V

THEORY OF COARSENING

The range of model types that have been used to simulate grain growth is extremely large. Broad categories include pure phenomenological models, pure statistical models, mean field theories, "exact" vertex and boundary evolution models, and Potts model simulations. All have been successful to varying degrees. An important division exists between models that attempt to predict equilibrium distribution functions based on purely statistical or geometrical considerations and dynamical models which focus primarily on grain growth rates, though they may supply information on distribution functions as well. We will first examine static models and then move on to the many categories of dynamic simulation.

V.a Static Models

The construction of pure geometric models based on random partitions of the plane, and attempts to determine their properties analytically, have amused geometers for at least two hundred years.[34,52,90,164,245] The elegance of some of the solutions and the complicated analytic geometry of others is impressive in its own right, but these models also have some claim to be considered as models for grain growth (in the case of nucleation they can work very well). In addition, the exact solutions of the properties of these models provide an extremely useful baseline for comparison to experiment and less rigorous simulations. Especially for the Voronoi type models there are

many analytic results for area and side distributions and correlations which are difficult or impossible to obtain for more complicated constructions.[164] Perhaps, the simplest approach to modeling the soap froth is to examine the statistical properties of its long term state considered as a fixed polygonal lattice. Taking this idea to an extreme we might study the regular hexagonal honeycomb as a model of the froth. Such a model is not very useful for studies of coarsening, but as we noted above, it gives useful results in studies of foam rheology.

V.a.i Voronoi Type Models

Slightly more realistic models must take into account the fundamental disorder of the froth and attempt to duplicate it geometrically. Most simply we may throw down a set of points at random locations with some average density, and assign to each point that subset of the plane which is closer to it than to any other point, a process known as the **Voronoi Construction** (see Fig. 27 (A)).[34,52,88,89,90,151,245,254] This construction subdivides the plane into a unique network of polygons with straight sides and vertices with coördination number three, but with a range of vertex angles and a very broad area distribution. In nucleation, this model corresponds to throwing down a set of nucleation centers at a fixed time and growing a circular domain from each at a fixed rate. The area distributions can be regularized by establishing an excluded volume during seeding, so that the initial particles are separated by a minimum distance (see Fig. 24 (A)). This narrows both the area and number-of-sides distributions, and results in angles more nearly

Fig. 19 Glass Models. (A) Triangle raft. (B) Triangle-Line raft (From Shackelford 1982).[204]

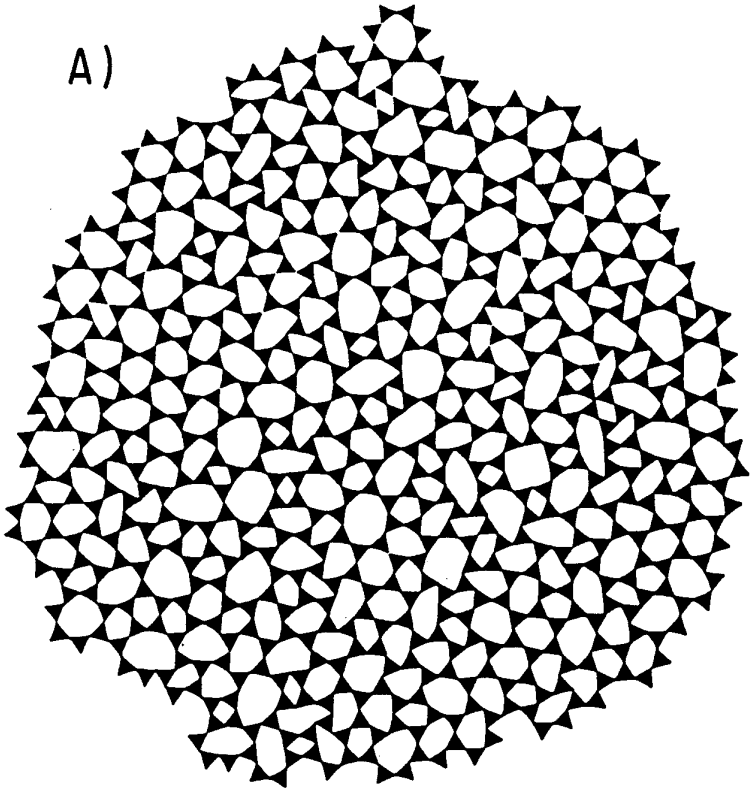
A)

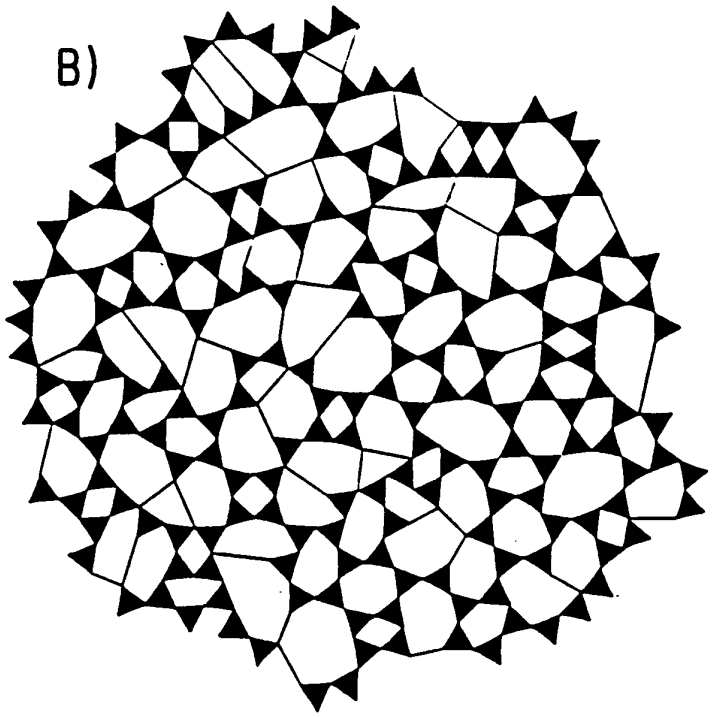
B)

Fig. 20 Dual Lattice. Sample of a two dimensional soap froth (solid lines) with the triangular dual lattice (dashed lines) indicated. Points replace bubbles, and dashed lines between points replace edges between neighbors (From Kikuchi 1956).[121]

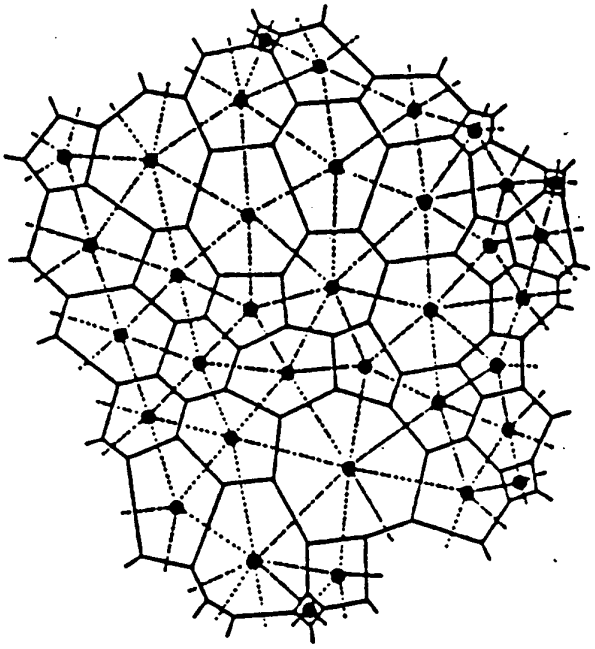

120°. The resulting pattern looks more like a real froth but still has non-120° angles and too narrow a side distribution.[80]

The fundamental problem with models of this sort is that they freeze in large scale inhomogeneities present in the seed pattern which would be rapidly relaxed in a real froth. We can approximate this relaxation geometrically by iteratively performing the Voronoi construction and moving each nucleation center to a new position at the center of its polygon until we reach an invariant pattern. This is known as a relaxed Voronoi construction.[105]

A third approach is to seed continuously but randomly in time in the "uncrystallized area" while growing uniformly (the **Johnson-Mehl model**), again producing a more irregular pattern than that observed in experiments, but which can be regularized using an excluded volume or relaxation.[164] Frost and Thompson have studied extensively,[80] the effects of changing the rates and types of nucleation and relaxation on the final distributions. In no case do they find the observed experimental dominance of five-sided bubbles, but the range of distributions they obtain is impressive.

One place where Voronoi networks are useful is to generate initial conditions for simulations. In this case, any initial stresses equilibrate quickly, and the patterns are sufficiently random to converge rapidly to a scaling state. Both Frost and Thompson and Anderson *et al.* have discussed the consequences of the choice of initial conditions.[80,15]

An additional application of the Voronoi construction in two dimensions is to determine adjacencies when the widths of the boundaries between

bubbles are comparable to the bubble size as happens in magnetic and lipid monolayer froths. In this case the Voronoi construction applied starting with the centers of each bubble, gives a unique assignment of areas and neighbors.

We also mention briefly a class of glass models originally proposed by Zachariasen.[204,256,258] We place equilateral triangles successively with vertices touching and without overlap, in a clockwise spiral around a seed triangle. At each step we randomly choose a number between four and eight and attempt to build a closed ring with that number of links. Since not all target rings sizes are possible at any given time we obtain a nontrivial side distribution function for the number of triangles per ring (See Tables 7 and 8 and Fig. 19 (A)). Shackelford also proposed an extended model which gave a narrower side distribution by allowing the use of lines as well as triangles, a line being inserted if it would a) close a loop with six or more triangles which had its target number of sides or more, and b) have a length between one and two times the length of a triangle edge (See Tables 7 and 8 and Fig. 19 (B)).

V.a.ii Maximum Entropy Models

We may extend our geometrical models a little more (as we did by introducing relaxation), by considering the final distribution to be the limit of a repetitively applied geometrical process. Kikuchi looked for the most probable network configuration based on independent weighting of configurations in the dual lattice (the pure triangular lattice obtained by replacing each bubble by a point at its center, and each edge by a line connecting

the centers of the neighbors (See Fig. 20).[121] In his first model (Kikuchi I) he assumed that the bubble centers lay on a regular triangular lattice and calculated the relative frequency of nearest neighbor and next nearest neighbor links which gave the largest number of possible configurations, i.e. the highest entropy. Then he calculated the distribution functions for this most probable state. In his second model (Kikuchi II) he allowed vacancies in his triangular lattice and third nearest neighbor links, again calculating the most probable state and its distribution functions (See Tables 7 and 8). Weaire has used a similar argument employing the probabilities of various topological transforms on a lattice to obtain the nearest neighbor number of sides correlation for an equilibrated froth (See Table 11).[134,135]

We can be slightly more sophisticated and try to guess the constraints on a topological lattice. If the constraints are correctly chosen, then in statistical equilibrium, the actual distribution functions should be such as to maximize the distribution function's entropy subject to those constraints, for example the first three or four moments of the distribution functions.[50,115,116,139] The difficulty in this "Maximum Entropy" method is to choose the constraints correctly.

Rivier has championed maximum entropy models and done extensive analyses to predict the soap froth's distribution functions.[199] He solves the joint distribution function $\rho(n, A)$ to maximize the entropy,

$$S \equiv -\sum_{n,A} \rho(n, A) \log(\rho(n, A)) \qquad \text{(V.1)}$$

subject to the constraints that $< n >= 6$, that $< a >$ is known, and that that either Lewis' law for areas, $< A_n > \propto n$, or the radius law, $< r_n > \propto n$ (where $< r_n >$ is the average radius of an n-sided bubble) applies. The two predictions of interest are that the area distribution function will decay exponentially,

$$\rho(A) \propto \exp^{-\lambda_1 A}, \tag{V.2}$$

where λ_1 is a fitting parameter, or, defining $a' \equiv \log(\frac{A}{<a>})$,

$$\rho(a') = \log(a') \exp^{-a'}. \tag{V.3}$$

The number of sides distribution takes the form

$$\rho(n) = \epsilon(n - c_1) \exp^{-\gamma n}, \tag{V.4}$$

where γ and ϵ are fitting parameters, and c_1 is a constant taken from Lewis' Law (described in section VII.a).

Almeida and Iglesias have done the same thing adding a bulk energy, proportional to bubble area.[10] This has the peculiar effect of making $< a_n >$ roll over rapidly in n so that many-sided bubbles all have the same area, and $\rho(n)$ is monotonically decreasing in n. A later paper by the same authors instead assumes that the average side length of bubbles is uniform and, taking the second moment of the side distribution as a parameter, obtains acceptable results for $\rho(n)$ and $< a_n >$ (See Tables 7, 8 and 11).[11]

V.b A Phenomenological Model

Another approach is to discard microscopic considerations entirely and to try to model the disordering process directly, considering only its salient physical features. Such an approach cannot hope to predict the growth exponent in the scaling regime, but it can provide a check on how well we understand the froth's approach to equilibrium. Based on the observations that disordered regions eat away at islands of hexagons from the edges, and that the long term rate of area growth is a power law in time, Glazier, Gross and Stavans wrote the following phenomenological model.[94]

They divided the population of bubbles into two classes, the bubbles in ordered regions and the bubbles in disordered regions, denoting the number of bubbles in each class by $O(t)$ and $D(t)$ respectively, with the total number of bubbles, $N(t) \equiv O(t) + D(t)$. They next assumed that ordered bubbles did not evolve but were converted into disordered bubbles at a rate proportional to the total contact area between order and disorder (making use of the experimental observation that ordered patches were stable except where they were eaten away by disorder from their edges). To lowest order, assuming random distributions, contact area is proportional to $\frac{O(t) \cdot D(t)}{O(t)+D(t)}$ which implies:

$$\frac{dO(t)}{dt} = -\kappa_1 \frac{O(t) \cdot D(t)}{O(t) + D(t)} \tag{V.5}$$

where κ_1 is a constant to be determined and represents the rate at which disorder diffuses into ordered patches.

They also assumed that the rate of disappearance of bubbles in disordered regions was independent of $O(t)$ and was uniform in t, since experimentally

they obtained nearly power law behavior for the area atlong times, when the system appeared completely disordered, i.e., $N(t) \propto t^{-\alpha}$. These assumptions yield an equation for $D(t)$ including terms for the conversion of order to disorder and for power law dissipation:

$$\frac{dD(t)}{dt} = \kappa_1 \frac{O(t) \cdot D(t)}{O(t) + D(t)} - \kappa_2 D(t)^{\beta}, \tag{V.6}$$

where $\alpha = \frac{1}{\beta - 1}$. While both $O(t)$ and $D(t)$ are abstract quantities, since $O(t)$ in particular is not simple to measure (there are six-sided bubbles in disordered regions as well as ordered regions), combining them produces a quantitative measure of the system disorder which we can then compare to other possible measures, the **Disorder**

$$\partial \equiv \frac{D(t)}{O(t) + D(t)}. \tag{V.7}$$

The parameter ∂ runs from zero for a perfect hexagonal lattice, to one for an equilibrated froth in a power law scaling state. Thus its time evolution provides information about the transition from order to disorder. It has significant advantages over most other measures of disorder since it can be computed from $N(t)$ directly without calculating the distribution functions. It is also an intrinsically averaged quantity, much less sensitive to small fluctuations than high order moments and therefore is usable in smaller scale systems. Glazier, Gross and Stavans calculated ∂ by fitting $N(0)$, β, κ_1, κ_2 and $\partial(0)$ to give a minimal least squares error against the experimental $N(t)$, but β, κ_2 and $N(0)$ can all be measured independently.

We present Glazier, Gross and Stavans' values for ∂ in Fig. 16 (dashed lines). For initially ordered runs, Fig. 16 (a)-(e), ∂ behaved as expected,

increasing smoothly to 1, and reaching its final value where the experimental value of $N(t)$ rolled over into a power law. For the initially disordered run shown in Fig. 16 (f), the rate of conversion from order to disorder was slower than the rate of loss of disorder, and ∂ decreased slightly before increasing to one at the rollover. While Glazier, Gross and Stavans originally dismissed this decrease as an artifact of the model, Stavans and Glazier have since shown that it accurately reflects the disordering of the pattern.[220] We will return to this point in our discussion of the moments of the distribution functions. As expected, ∂ was small for apparently well ordered conditions, e.g. $\frac{\rho(5)}{\rho(6)} < 0.1$ and large for disordered conditions, e.g. $\frac{\rho(5)}{\rho(6)} > 1.0$.

In Fig. 16 we also show Glazier, Gross and Stavans' fits for $N(t)$ (solid lines). The fits yielded a value of $\beta = 2.7 \pm 0.3$ corresponding to $\alpha = 0.59(^{+0.11}_{-0.09})$. We believe that their error estimate was rather optimistic because of the systematic boundary effects we have discussed, but it did accurately reflect the numerical range in the estimate of the exponent. The typical error of their fits for $N(t)$ was better than 3%, and the maximum observed error was 5%. In the two runs with the most complete time series, Fig. 16 (d) and Fig. 16 (f), the apparent power law behavior held over a full decade, so the deviation in exponent from $\alpha = 1$ was not due simply to noisy measurements. The excellent quantitative agreement between the behavior of the model and the experiment, with a perfect matching of the transient over a wide range of initial disorders strongly suggests that the model contains most of the essential physics of the transition.

V.c Radius Based Mean Field Theories

The term mean field theory is a broad one and we will discuss three separate categories, roughly in their historical order of development: dynamic theories based solely on the distribution of grain radii, theories based on both area and side distributions, and semi-exact models which keep track of the structure of the topological network defined by the dual lattice. In our discussion we will examine the predicted growth exponents and ability to duplicate transients as indicators of the reasonableness of the theory.

Many of the models we present in this section emphasize simplicity at the expense of much of the basic physics of grain growth. Historically, part of the difficulty developing an adequate theory of coarsening was the focus on grain growth in metals, in which it was impossible to measure the key parameter, namely how the growth rate of a grain depended on its size and geometry. It was therefore a common practice to start with an experimental result (like a distribution function) and to work backwards to determine the basic dynamical laws. In the absence of experimental checks on the dynamics this procedure allowed essentially any result to be obtained. Another result of the focus on metals was a general neglect of geometrical factors which were hard to measure. Models tended to assume the proverbial spherical cow, neglecting transients and equilibration processes, and frequently, for good measure, invoking log-normal area distributions. Since von Neumann showed that it is the number of sides a grain has and not its size that determines the grain's growth rate, it is somewhat surprising that radius

based models work at all. What saves them is the strong correlation between number of sides and grain (or bubble) area. One decided advantage of radius based models is that they are independent of dimension, giving useful results for bulk grain growth, when the absence of an equivalent to von Neumann's law in three dimensions makes it difficult to develop more sophisticated models. Additionally the success of radius based theories in explaining Ostwald ripening (the growth of widely separated grains interacting with a gas) suggests that these theories may be more relevant to the case of liquid-gas phase transitions than they are to coarsening of froths.[117,231]

In our discussion we will consider only the mathematical formalism of these theories, not the elaborate attempts to evaluate the various physical parameters such as activation and surface energies and temperature dependencies, which were of specific interest in metallurgical applications.

V.c.i Burke and Turnbull: a Zeroth Order Model

In a long review, primarily concerned with microscopic properties of metal grains, Burke and Turnbull,[42] discussed the coarsening dynamics of metal grains, drawing a specific analogy to the evolution of a soap froth. Their analysis neglected all interactions between grains which they considered as circular or spherical, so it certainly qualifies as a mean field theory. They assumed, based on both microscopic energy considerations and surface tension arguments, that for any grain, the rate of boundary migration was,

$$v = \mu\sigma\frac{V}{\rho}, \tag{V.8}$$

where μ is a temperature dependent mobility, σ a surface energy, ρ the integrated radius of curvature, and V the atomic volume. This is just a scalar form of equation (III.8). Assuming that all these constants were indeed constant, that the radius of curvature was proportional to the grain radius, r, and that the change in average grain diameter was proportional to the rate of boundary migration, they obtained

$$\frac{dr}{dt} = \frac{\kappa}{r}, \tag{V.9}$$

where κ is a diffusion constant. Integrating this differential equation (which is essentially equivalent to the second term in the phenomenological model presented previously), produced

$$< a(t) >= \sqrt{\kappa t + a_0}. \tag{V.10}$$

So for long times $\alpha = 1$. The analysis is completely independent of whether the grain growth occurs in two or three dimensions. Burke and Turnbull noted agreement with scaling measurements in a two dimensional soap froth by Fullman,[86] and rather optimistically concluded "The fact that $< r > \propto t^{1/2}$ indicates that the geometrical analysis is essentially correct." They then suggested several mechanisms to explain the observed deviations from this scaling law in real metal systems. Unfortunately, as shown in the section on von Neumann's law, any mean field theory must yield a long term scaling exponent of one, so the agreement with experiment was fortuitous.[173,174]

Rhines and Craig took a view similar to that presented in the phenomenological model above,[194] looking at coarsening as the progressive elimination

of individual grains with average area $< a >$. They derived the dynamics of their equation by assuming a bubble like diffusive motion of grain boundaries,

$$v = \mu \Delta P = \mu(\frac{1}{\rho_1} + \frac{1}{\rho_2}), \tag{V.11}$$

which meant that the change in volume per unit time of a grain was

$$\frac{dV}{dt} = \mu M S, \tag{V.12}$$

where, M is the grain's integrated curvature and S the grain's surface area. They next cited as an experimental fact that the product, $MS = \Sigma$, was proportional to the length scale in any given experiment, and defined a **sweep constant**, Θ, the number of grains lost per unit distance of boundary motion. There has been some debate as to whether this choice of sweep constant was correct, but for our purpose we need only note that in a scaling state it must scale inversely with length scale.[58,111,195] Swallowing Θ, μ and Σ into a single rate constant κ they concluded that the number of grains in a given volume goes as

$$\frac{d}{dt}\frac{1}{N} = \frac{1}{N_0}(1 + \kappa), \tag{V.13}$$

putting in the initial condition $N(0) = N_0$. Again we obtain $\alpha = 1$ at long times in three dimensions.

V.c.ii Diffusional Radial Mean Field Theories

The most obvious defect with the Burke and Turnbull and Rhines and Craig models is their inability to predict radius or area distribution functions. Several authors have proposed models which address directly the mean field

evolution of the area distribution. The basic formalism of these models is the same. Consider the distribution function of radii, $\rho(r)$. The evolution of this function may be described in terms of a probability current,

$$j(r) = -D\frac{\partial \rho(r)}{\partial r} + \rho(r)v(r), \tag{V.14}$$

where the first term describes diffusional processes tending to broaden the distribution function and the second deterministic evolution, D being a diffusion constant and $v(r)$ the growth rate as a function of radius. As we shall see later, when applied to a distribution function including number of sides as well as areas, this probability current formalism is completely appropriate to a correct mean field theory of froth coarsening. The difficulty in this case is that there is no simple way to reduce diffusion in the number of sides distribution to diffusion in area distribution. Assuming the appropriateness of this current, the continuity equation gives the time evolution of the distribution as:

$$\frac{\partial \rho(r)}{\partial t} = -\frac{\partial j(r)}{\partial r} = \frac{\partial}{\partial r}(D\frac{\partial \rho(r)}{\partial r}) - \frac{\partial}{\partial r}(\rho(r)v(r)). \tag{V.15}$$

We are now free to speculate on various values for D and $v(r)$. We note that this is the basic structure of the famous Lifschitz-Slyozov model for Ostwald ripening.[148,149]

V.c.iii Deterministic Models

We first consider models that neglect the diffusive term in the evolution equation (i.e. set $D = 0$). In essence these models neglect the possibility that a grain can gain or lose sides in time. One can either hypothesize a form for

$v(r)$ and solve for the area distribution or vice versa. Feltham hypothesized a log normal limiting distribution of areas

$$\rho(r) = \frac{1}{r}\exp\{-|\frac{1}{k_2}\ln\frac{r}{<r>}|^2\} \tag{V.16}$$

and applied an areal approximation to von Neumann's law to obtain the result that for a given grain:

$$\frac{dr^2}{dt} = \kappa\ln(\frac{r}{<r>}). \tag{V.17}$$

Assuming self similar distributions, he then obtained the unsurprising result that $< a > \propto t$.[64] Hunderi and Ryum solved $v(r)$ for several different proposed area distributions.[112,113,114]

Hillert began with our equation (III.8), assuming the basic relation that interface velocity is proportional to the curvature driven pressure difference:[106]

$$v = \mu\Delta P = \mu\sigma(\frac{1}{\rho_1} + \frac{1}{\rho_2}), \tag{V.18}$$

where the ρ_i are the principle radii of curvature. He then assumed that small grains shrink and large grains grow. Since many sided grains tend to be large this was not too unreasonable an assumption. In this case he proposed a specific relation between grain curvature and grain size, of

$$v(r) \propto (\frac{1}{r_{crit}} - \frac{1}{r}), \tag{V.19}$$

where r_{crit} is the average radius of a grain in two dimensions (derived by working backwards from von Neumann's Law!) and an experimentally determined parameter in three dimensions. Substituting he obtained

$$\frac{dr}{dt} = \kappa(\frac{1}{r_{crit}} - \frac{1}{r}), \tag{V.20}$$

which, assuming equilibrated distribution functions yielded the expected $< a > \propto t$. He also made a detailed prediction for the area distributions using the Lifschitz-Slyozov method. Letting $r' \equiv \frac{r}{r_{crit}}$ he found

$$\rho(r') = (2e)^{\delta} \cdot \frac{\delta r'}{(2-r')^{2+\delta}} \cdot \exp \frac{-2\delta}{2-r'}, \tag{V.21}$$

where δ is the dimension.

Kirchner has applied a similar argument to obtain the size distribution function for lens shaped (two-sided) grains growing in grain boundaries.[122] Thompson has also extended the model to include anisotropy and pinning effects to study the growth of free grains in a medium.[227]

Hunderi and Ryum set up a radius based model of this sort in three dimensions, which explicitly considered grain-grain interactions.[112,114] where

$$\frac{dr_i}{dt} = -\frac{\kappa}{{r_i}^2} \sum_{\substack{neighbors \\ j}} A_{ij}(\frac{1}{r_i} - \frac{1}{r_j}), \tag{V.22}$$

where $A_{ij} \equiv \pi \min({r_i}^2, {r_j}^2)$ is the contact area between grains. They assigned grain contacts by position in the index list rather than by looking at a network topology, so this is a pure mean field theory rather than a network model. In their first paper they obtained a scaling exponent of $\alpha = 1$ but later revised their figure to $\alpha = 0.76 \pm 0.04$.

Novikov produced a closely related interaction model.[183] He discretized the radius distributions (bin width Δ, $r_i = \Delta \cdot i$, $N_i \equiv$number of grains in bin i), and assumed completely random attachments and constant grain

boundary mobility. As before

$$\Delta P_{ij} = 2\sigma(\frac{1}{\rho_j} - \frac{1}{\rho_i}). \tag{V.23}$$

However, he used a different, nonsymmetric contact area:

$$A_{ij} = \frac{{r_j}^2}{4(r_i + r_j)^2}. \tag{V.24}$$

So the change in radius from any one contact between class i and class j was:

$$\frac{dr_i}{dt} = 2\sigma \frac{{r_j}^2}{4(r_i + r_j)^2}(\frac{1}{\rho_j} - \frac{1}{\rho_i}). \tag{V.25}$$

As in the phenomenological model, the number of contacts between class i and class j is

$$N_i{}^j = k_i \frac{N_i N_j}{N}, \tag{V.26}$$

where k_i is a normalization to make the total areas come out consistent. This yields

$$\frac{dN_i{}^j}{dt} = \frac{k_v}{8} N_i{}^j \frac{dr_j}{dt}, \tag{V.27}$$

where k_v is the averaged renormalization constant. Finally, summing over classes, yields a master equation:

$$\frac{dN_i}{dt} = -\sum_{j=1}^{i-1} \frac{dN_i{}^j}{dt} + \sum_{j=1}^{i-2} \frac{dN_{i-1}{}^j}{dt} \tag{V.28}$$

$$-[outscatter\ down] + [inscatter\ up]$$

$$-\sum_{j=i+1}^{i_{max}} \frac{dN_i{}^j}{dt} + \sum_{j=i+2}^{i_{max}} \frac{dN_{i+1}{}^j}{dt}$$

$$-[outscatter\ up] + [inscatter\ down].$$

Novikov solved the master equation using a montecarlo method and deleting downscattered grains in class 1. Depending on the absolute length scale of his initial conditions he obtained either $\alpha = 0.792 \pm 0.016$ or $\alpha = 0.720 \pm 0.01$, suggesting some problems in reaching complete convergence. Using the same model with two values of grain boundary mobility he has measured the distribution functions and exponents for anomalous grain growth, and he has also studied boundary pinning using a damped equation for boundary motion:

$$\frac{dr_i}{dt} = 2\sigma(\frac{1}{\rho_j} - \frac{1}{\rho_i} - F), \tag{V.29}$$

where F is a pinning force.[184]

Abbruzzese and Lücke have examined the effects of defect pinning[2,5] and anisotropy[4] on models of this type. For normal grain growth they have compared the theoretical predictions for experimental values obtained in thin sheets of iron alloy, with reasonable success.

Beenakker has also written a radius based mean field theory, which began with von Neumann's law,[25] but then made an *ad hoc* assumption that the free energies of individual grains were minimized, resulting in a nonlinearly increasing dependence of $< a_n >$ on n. The model has the peculiar property that the area distribution broadens to a width of 3.2 and then narrows again to a width of 0.25. The long term growth exponent is $\alpha = 1$.

V.c.iv Diffusive Models

An alternative approach is due to Louat, whose two dimensional analysis

began by noticing that von Neumann's law held only on average experimentally.[152] He proposed that the rate of side swapping could be regarded as so large that the von Neumann's law component of the distribution function evolution could be completely neglected. He therefore wrote the basic evolution equation as:

$$\frac{\partial \rho(r)}{\partial t} = D\frac{\partial^2 \rho(r)}{\partial r^2}. \tag{V.30}$$

Assuming that there are no zero sized or infinite sized grains, the resulting evolution is:

$$\rho(r,t) = cr \exp\left(\frac{-r^2/4Dt}{Dt^{3/2}}\right), \tag{V.31}$$

where c fixed the mean area at the starting time. As expected, $\alpha = 1$. A time or scale dependent diffusion constant (like that hypothesised for the soap froth, and observed in impure metals) leads to a variety of other growth laws.

V.d Topological Mean Field Theories

The simplest approach to a model which includes topological transformations as well as von Neumann's law, is to neglect spatial structure entirely and treat the system as homogeneous and completely described by its distribution functions. Hillert proposed a model basically of this type looking at the spread of topological charge as a series of defect climbs, but he did not develop the model to any great extent nor did he derive equilibrium distribution functions.[43,106]

Fig. 21 Elementary Topological Processes. (a) Side Swapping or $T1$ process. (b) Disappearance of a three-sided bubble or $T2(3)$ process. (c) Disappearance of a four-sided bubble or $T2(4)$ process. (d) Disappearance of a five-sided bubble or $T2(5)$ process. (e) Wall breakage next to an n-sided bubble, $Break(n)$. Numbers are keyed to Table 6.

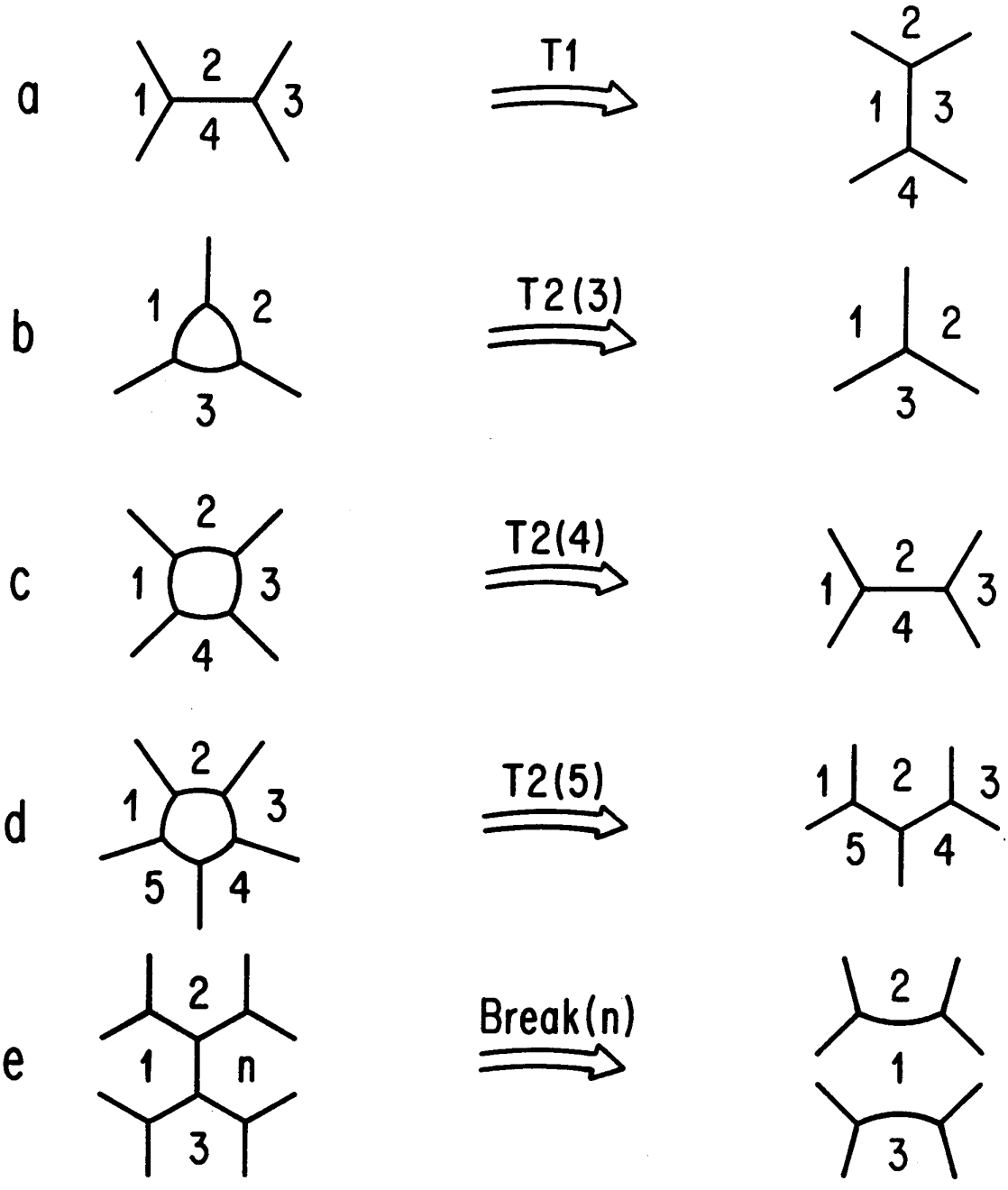
a
1
2
3
4
T1
2
1
3
4
b
1
2
3
T2(3)
1
2
3
c
2
1
3
4
T2(4)
1
2
3
4
d
2
1
3
5
4
T2(5)
1
2
3
5
4
e
2
1
n
3
Break(n)
2
1
3

TABLE 6

SCATTERING PROCESSES

Change	Bubble Number				
Process	1	2	3	4	5
T1	+1	−1	+1	−1	-
T2(3)	−1	−1	−1	-	-
T2(4)	−1	0	−1	0	-
T2(5)	−1	+1	−1	0	0
Break(n)	$+n-4$	−1	−1	-	-

Blanc, Carnal and Mocellin appear to have been the first to apply a topological mean field theory (they used only the number of side distribution) to grain growth.[30,46] We originally attempted such a mean field theory approach using separate distribution functions for the number of sides and areas with some qualitative but little quantitative success. This model was later refined by Marder who employed a joint probability distribution $\rho(n, A)$,[157] and by Beenakker.[26,27,28]

Any topological mean field theory for the soap froth starts with two basic components, the dynamics given by von Neumann's law, and a list of fundamental processes, scattering processes if you like, which describe the allowed changes in the distribution function. In general there can be an arbitrary number of different scattering processes, but all the possible behaviors of the soap froth can be described by five fundamental processes, of which only four enter into the models we will discuss.

When shear stresses are present in the froth, a pair of adjacent bubbles can be squeezed apart by another pair, as shown in Fig. 21 (a). This is known as a $T1$ process or **side swapping**. In this case the two bubbles that were neighbors each lose a side and the new adjacent bubbles each gain a side. Topological charge, $\mathcal{T} \equiv (n-6)$ is conserved since the total number of sides of the four bubbles before and after the swap is the same.

The disappearance of a bubble, a $T2$ process, also results in changes to its neighbors' number of sides. Topological charge is conserved in all disappearances so once again the results depend only on the number of sides

of the disappearing bubble. When a three-sided bubble disappears (Fig. 21 (b)) each of its neighbors loses a side. The equation for topological charge is $\mathcal{T} = -3 = 3 \times -1$. When a four-sided bubble disappears (Fig. 21 (c)) two of its neighbors stay the same and two lose a side. The equation for topological charge is $\mathcal{T} = -2 = 2 \times -1 + 2 \times 0$. Finally, when a five-sided bubble disappears (Fig. 21 (d)), one of its neighbors gains a side, two stay the same and two lose sides. The equation for topological charge is $\mathcal{T} = -1 = 1 \times 1 + 2 \times 0 + 2 \times -1$.

Wall breakage (Fig. 21 (e)) is only a slightly different problem. When a wall between an n-sided bubble and an m-sided bubble breaks, the resulting bubble has $n + m - 4$ sides and the two common neighbors each lose a side. Thus there is a total loss of 6 sides and 1 bubble, preserving topological charge. Note that wall breakage is the only mechanism that favors the creation of many-sided bubbles. The $T1$ process by itself is in equilibrium with a slowly decreasing $\rho(n)$ (See Table 7 under Fradkov ∞) and bubble disappearance results in exponential cutoff for large n. We may represent all these relationships conveniently in a table (Table 6) which encodes all the basic topological information about scattering in a connection number three lattice.

While the rates for disappearances of bubbles are fixed by the distribution functions and von Neumann's law, side swapping and wall breakage depend on different mechanisms and thus have rates independent of the basic froth evolution. Experimentally we observe little side swapping at long times since

the soap froth is soft and tends to eliminate stresses quickly and over short range. Some side swapping does occur, however, in the immediate vicinity of disappearing bubbles. Therefore some of the models discussed include side swapping as an external parameter. None of the models considers wall breakage, but that rate too could easily be included. One peculiarity of three dimensional models that examine two dimensional sections is that they must include the creation of three-sided grains caused by the growth of a previously unseen grain into the plane being examined.

V.d.i Pure Topological Theories

Blanc, Carnal and Mocellin have solved the equilibrium distribution function $\rho(n)$ subject to three scattering processes, side swapping, three-sided bubble disappearance and three-sided bubble creation.[30,46] The presence of three-sided bubble creation makes this model appropriate to three dimensions where three-sided bubbles can "nucleate" in a planar section as growing bubbles come to intersect the section. They require two parameters to specify their model, the proportion of three-sided bubbles $\rho(3)$, and the rate of side swapping. In their first paper they fixed the rate of three-sided bubble creation and adjusted the rate of side swapping to achieve a target $\rho(3)$. In their second paper they kept the rate of side swapping as a free parameter and adjusted the rate of three-sided bubble creation to achieve the target $\rho(3)$. The probability that a given $T1$ process affects an n-sided grain (n

restricted to be > 3) is just

$$\phi_n \equiv \frac{n\rho(n)}{6}. \tag{V.32}$$

The probability that a three-sided grain appears or disappears next to an n-sided grain is not *a priori* defined. They choose to use the value

$$\psi_n \equiv \frac{n^\gamma \rho(n)}{\sum_n n^\gamma \rho(n)}, \tag{V.33}$$

where γ is rather arbitrarily defined to be the solution to

$$\sum_{n=3}^{\infty} n^{\gamma+1}\rho(n) = \sum_{n=3}^{\infty} n^\gamma \rho(n) \left[7 + \frac{1}{3}\sum_{n=3}^{\infty}(n-6)^2\rho(n)\right]. \tag{V.34}$$

They then solved for the equilibrium of the system using montecarlo techniques. We present their results for no swapping and for a fixed rate of side swapping in Tables 7 and 8. The parameter β is approximately the reciprocal of the rate of $T1$'s.

Kurtz and Carpay, in a paper chiefly devoted to three dimensional grain growth considered a two dimensional topological mean field theory subject to von Neumann's Law.[132] They took the distribution of grain areas in each topological class to be a fixed log normal distribution,

$$\rho(r_n) = \frac{1}{(2\pi\sigma^2)^{1/2}}\frac{1}{r_n}\exp\left(-\frac{(\ln r_n - < r_n >)^2}{2\sigma^2}\right), \tag{V.35}$$

where $< r_n > \equiv c\ln(\frac{n}{<n>})$. This distribution is approximately correct for a two dimensional section of a three dimensional froth, but is not a very good description of a true two dimensional froth. They assumed everything else was random and solved by montecarlo as above. We present their results in Tables 7 and 8. They have also performed the entire calculation in three dimensions.

Fig. 22 Average Area versus Time. (A) For Marder's mean field theory (From Marder 1987).[157] (B) From Fradkov, Shvindlerman and Udler's network model (From Fradkov, Shvindlerman and Udler 1985).[261] (C) Average radius versus time for Beenakker's network model for ordered (O) and disordered (D) initial conditions (From Beenakker 1988).[262]

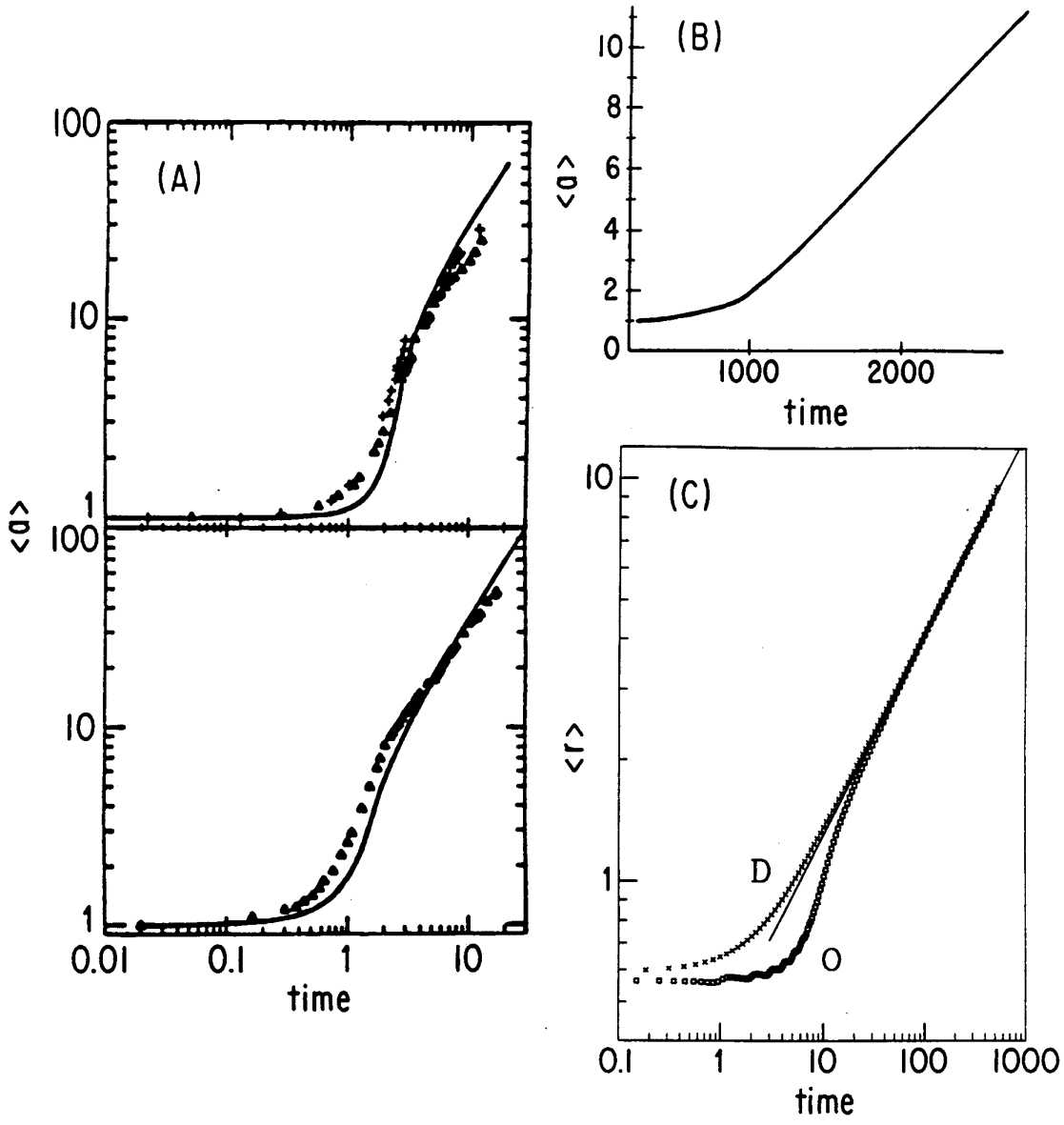
(A)
100
10
1
<D>
100
10
1
0.01
0.1
1
10
time
(B)
10
8
6
4
2
0
<D>
1000
2000
time
(C)
10
1
<r>
D
O
0.1
1
10
100
1000
time

V.d.ii A Complete Mean Field Theory

Marder attempted a true mean field theory depending only on the evolution of the distribution functions. He built his model as follows: Let $\rho(n, A, t)$ be the joint distribution function, and $g(n, A, t) \equiv N(t) * \rho(n, A, t)$. At any given time each n-sided bubbles obeys von Neumann's law, so it shifts the distribution per unit time as

$$\frac{dg(n, A)}{dt} = \frac{\partial A}{\partial t}\kappa(6 - n)g(n, A, t), \tag{V.36}$$

where the diffusion constant κ is now dimensionless. The change in number of bubbles with area A and n sides is now just the result of von Neumann's law plus the probability that a bubble with area A and $n+1$ sides loses a side or a bubble with area A and $n-1$ sides gains a side minus the probability that a bubble with area A and n sides either loses or gains a side, i.e.,

$$\begin{aligned} \frac{\partial}{\partial t}g(n, A) &= \frac{\partial}{\partial A}\kappa(6 - n)g(n, A, t) \\ &+u(A)\frac{n-1}{S}g(n-1, A) + d(A)\frac{n+1}{S}g(n+1, A) \\ &-[u(A) + d(A)]\frac{n}{S}g(n, A), \end{aligned} \tag{V.37}$$

where S is the total number of sides (a bubble with more sides is more likely to be chosen at random), $u(A)$ is the probability that a bubble of area A gains a side, and $d(A)$ is the probability that a bubble of area A loses a side.

Marder next assumed that the smallest bubbles neighboring a disappearing bubble tend to lose a side and the largest to gain a side. In this case

$$d(A) = d_5(A) + d_4(A) + d_3(A), \tag{V.38}$$

where:

$$d_5(A) \equiv \kappa g(5,0)5!(\frac{p^4(A)}{4!} + (1-p(A))\frac{p^3(A)}{3!}) \qquad \text{(V.39)}$$

is the probability to be next to a disappearing five-sided bubble and smallest or next smallest among the bubble's neighbors.

$$d_4(A) \equiv \kappa g(4,0)4!(\frac{p^3(A)}{3!} + (1-p(A))\frac{p^2(A)}{2!}) \qquad \text{(V.40)}$$

is the probability to be next to a disappearing four-sided bubble and smallest or next smallest among the bubble's neighbors.

$$d_3(A) \equiv \kappa g(3,0)3! \qquad \text{(V.41)}$$

is the probability to be next to a disappearing three-sided bubble. Similarly,

$$u(A) = \kappa g(5,0)5!\frac{[1-p(A)]^4}{4!} \qquad \text{(V.42)},$$

is the probability that a bubble is next to a disappearing five-sided bubble and is the largest. We present results from Marder's direct solution of the model in Table 7. Impressively for a model with no free parameters, Marder obtained quite good quantitative agreement with actual experimental time series for $< a(t) >$ (see Fig. 22 (A)), including the correct transient behavior for two different initially well ordered experimental runs.

If we assume that there is no correlation in side shedding we instead obtain

$$u(A) = \kappa g(5,0)5!\frac{2}{5} + g(4,0)4!\frac{2}{4} + g(3,0)3!\frac{3}{3} \qquad \text{(V.43)}$$

and

$$u(A) = \kappa g(5,0)5!\frac{1}{5}. \qquad \text{(V.44)}$$

This last is essentially a discretized version of the equations used in early work by Beenakker.[26] Fradkov has also taken this approach and solved for the equilibrium distributions retaining the rate of $T1$'s as a free parameter.[74]

V.e Evolution on a Network

Conceptually, the most satisfying approach to a mean field theory is that of the topological network. This was originally described by Fradkov, Shvindlerman and Udler, and apparently rediscovered independently by Beenakker[27,76] They model the froth as a connected network of bubbles where each bubble is completely described by its area, number of sides and list of neighbors. The mean field theory assumption is that side redistribution occurs randomly upon the disappearance of a bubble. The simulation is then straightforward. Von Neumann's law is applied to each bubble in the network, and the first time at which any bubble disappears, calculated. Next, the areas of all bubbles in the network are recalculated. The disappearing bubble is then deleted, its neighbors have their numbers of sides updated according to Table 6 and the list of neighbor connections is corrected according to Fig. 21. Almost any function of interest, $< a(t) >$, side and area distributions and correlations, etc., can be directly calculated from the state of the network as it evolves in time. The only aspect of the froth abandoned by the model is the deterministic redistribution of sides upon bubble disappearance. We may also include wall breakage processes without any detailed modifications.

Fradkov, Shvindlerman and Udler assumed direct disappearance of

three-, four- and five-sided bubbles with no redistribution correlations and included the rate of $T1$ processes as an adjustable parameter to obtain a family of side distributions.[76,77] For non-zero rates of side swapping they allowed the creation of two-sided bubbles. The greater the rate of T1's the lower the value of n at which the distribution peaked and the larger the value of $\rho(3)$ (See Table 7). They also observed the expected monotonic increase in growth rate to equilibrium for initially disordered states (See Fig. 22 (B)).

Beenakker employed the same model setting the rate of T1's to zero and assuming no redistribution correlations. He obtained excellent results for λ_n and the area distributions (See Table 7). Particularly striking was his observation of the characteristic features of both initially ordered growth (slow, fast, equilibrium) and initially disordered growth (monotonic increase to equilibrium rate), as well as the broadening and subsequent narrowing of the side distribution for initially well ordered distributions (See Fig. 22 (C)).

V.f "Exact Models"

As we shall see in the next chapter, mean field theories can predict well experimentally observed distribution functions. What they cannot do is generate an actual image of an evolving froth. To produce such a real space picture we must simulate the behavior of the froth directly as a combination of soap films and diffusing gas (or in the next section, as an array of hopping atoms). For want of a better term we call these "exact" models, though they are by no means always exact. "Exact" models come in two types. They either move the films and then adjust the vertex positions (boundary

dynamic models), or adjust the position of the vertices and then recalculate the positions of the soap films (vertex models). We begin by examining boundary dynamic models.

V.e.i Boundary Dynamic Models

Ceppi and Nasello[47,48] assumed a radius based dynamics, $v = \frac{\mu}{\rho}$, where v is the velocity of a given boundary, and ρ its averaged curvature. They then discretized to a lattice and defined the function

$$F_i(\vec{x}) \equiv \int_{C(\vec{x},a)} f_i(\vec{x}\prime) d\vec{x}\prime, \tag{V.45}$$

where $f_i(\vec{x})$ is one inside the ith bubble and zero outside, and $C(\vec{x},a)$ is a circle of radius a (in their paper, six lattice constants) centered at $\vec{x}$. The boundary between bubble i and bubble j was then given by solving implicitly for the position that yielded $F_i(\vec{x}) = F_j(\vec{x})$. They claimed that this evolution law was equivalent to the velocity relation with a time step of $\Delta t = a^2/6\mu$. Disappearing grains were eliminated from the list, and boundary reconnection was taken care of automatically by the definition. We show a typical example of the evolution they obtained in Fig. 23. Taking iterations of the algorithm as equivalent to time, they obtained $\alpha = 1$.

Frost, Thompson and their collaborators, in a long series of articles,[79,81,82,83,84,109,229] tried to duplicate the physical situation more realistically. They took equation (III.8):

$$\vec{v}(\vec{x}) = \mu(\vec{x}) \frac{\hat{n}(\vec{x})}{\rho(\vec{x})}, \tag{V.46}$$

as their basic dynamics, and discretized by segmenting the boundary into short, nearly flat sections represented by a point. The boundary segments were then moved perpendicular to the boundary a distance $v\Delta t$, to obey the dynamical law. Vertices were separately adjusted to give 120° angles, and radii of curvature calculated by local fitting of circular arcs. Boundary points were added or removed as needed to minimize errors in the curvature calculations. Side readjustments were made locally when vertices moved too close together. In spite of the numerous opportunities for error in the various discretizations, the model satisfied von Neumann's law to within 3%, convincing evidence that it captured the basic dynamics correctly.[80] It was straightforward to measure distribution functions and growth rates. We present a typical pattern evolution from their model in Fig. 24. Since the model stored only information describing the positions of boundaries they could run extremely large simulations, to obtain $\alpha = 1$ over three full decades for a variety of initial conditions. Unfortunately all of their initial conditions were fully disordered so they were not able to observe the disordering transient. One particularly attractive feature of this model is that it is simple to include a whole variety of evolution equations once the basic structure of the model has been established. Frost and Thompson have considered anomalous grain growth (by locally increasing the boundary mobility, μ), continuous nucleation of new grains, and non-linear curvature dependence among many other effects.

Fig. 23 Boundary Dynamic Grain Growth. (A) Initial Condition. (B) After 5 iterations of the algorithm. (C) After 20 iterations. (D) After 40 iterations (From Ceppi and Nasello 1984).[47]

A)

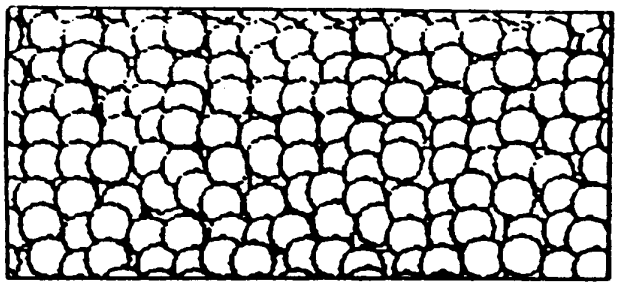

B)

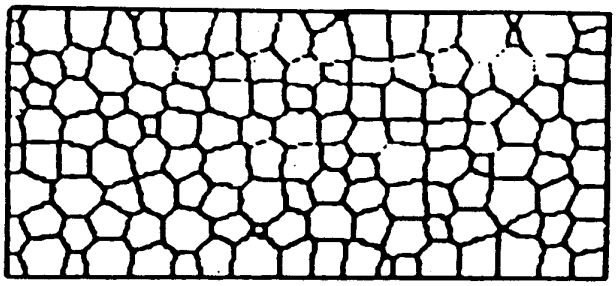

C)

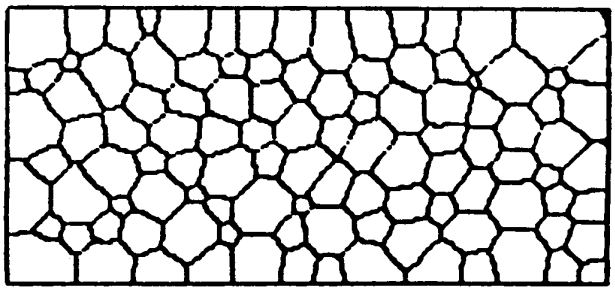

D)

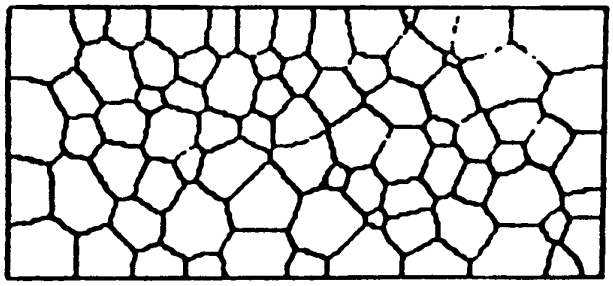

Fig. 24 Boundary Dynamic Grain Growth. Grain growth in the boundary dynamic model of Frost *et al.*. (A) Initial excluded volume Voronoi construction. (B) $t = 0.5$ diffusion times. (C) $t = 1.0$ diffusion times. (D) $t = 3.0$ diffusion times. (E) $t = 10.0$ diffusion times. (F) $t = 30.0$ diffusion times (From Frost and Thompson 1988).[260]

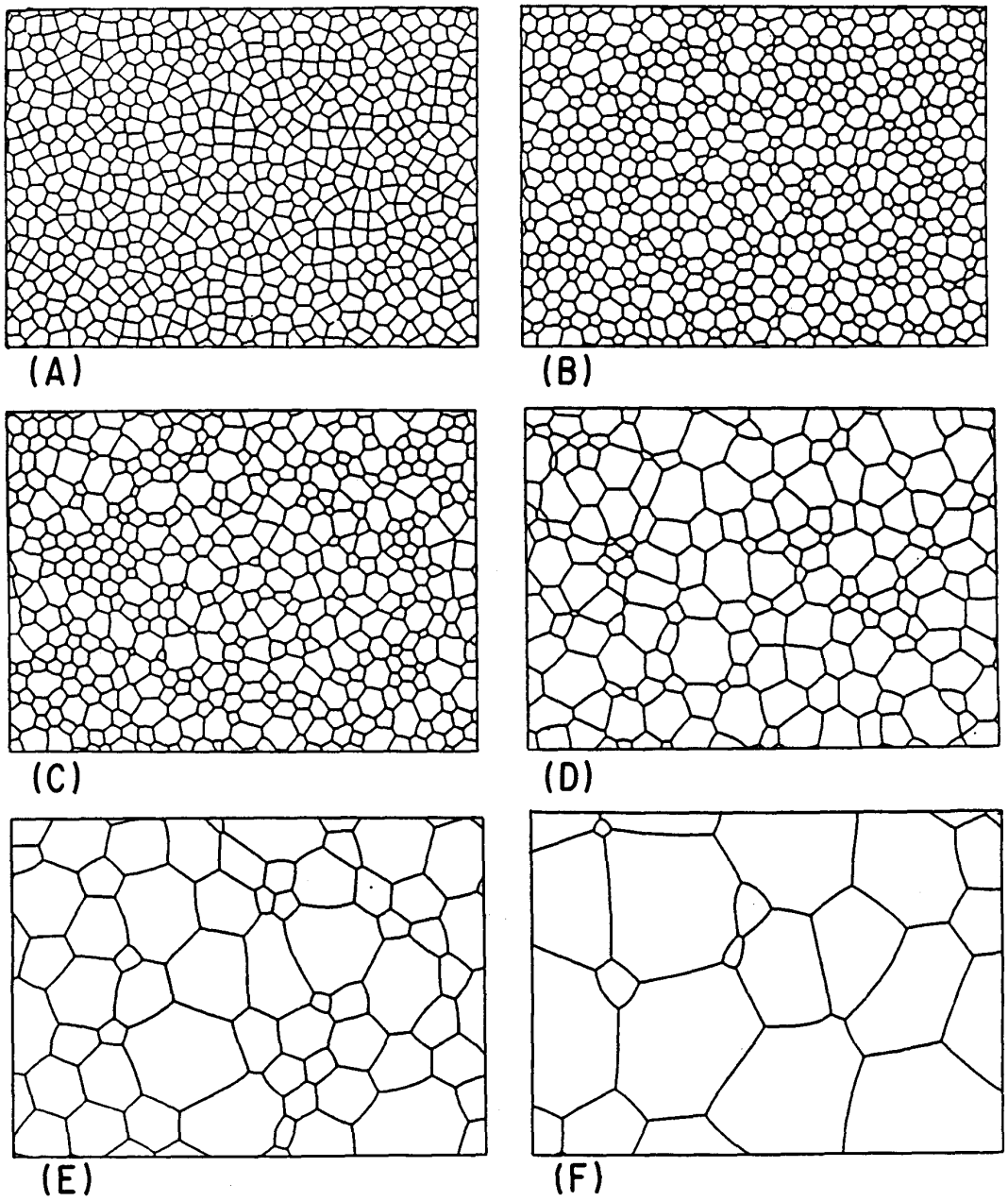
(A)
(B)
(C)
(D)
(E)
(F)

Fig. 25 Vertex Dynamic Grain Growth. Left hand side of each column shows the evolution of an experimental two dimensional soap froth, right hand side shows the evolution of a vertex model starting from identical initial conditions. (A) (left) $t = 990$ minutes. (A) (right) $t = 820$ minutes. (B) (left) $t = 1319$ minutes. (B) (right) $t = 1236$ minutes. (C) (left) $t = 1620$ minutes. (C) (right) $t = 1652$ minutes. (D) (left) $t = 2040$ minutes. (D) (right) $t = 2068$ minutes. (E) (left) $t = 2690$ minutes. (E) (right) $t = 2692$ minutes. (F) (left) $t = 3525$ minutes. (F) (right) $t = 3525$ minutes. Theoretical times were assigned by fitting $N(t = 0)$ and $N(t_{final})$ (From Fullman 1952).[86]

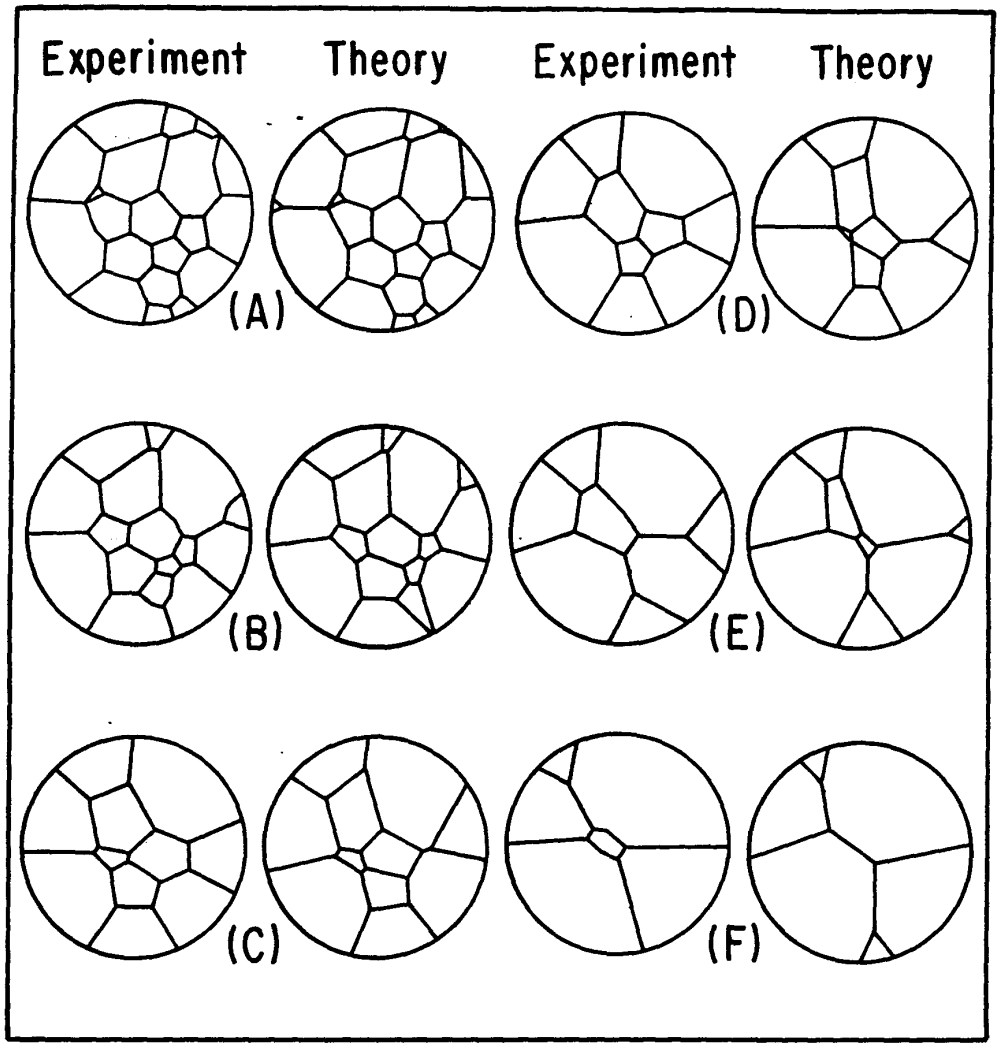
Experiment
Theory
Experiment
Theory
(A)
(D)
(B)
(E)
(C)
(F)

Fig. 26 Vertex Dynamic Grain Growth. (A) Voronoi network initial condition. (B) $t = 50$ time steps. (C) $t = 156$ time steps. (D) $t = 300$ time steps. (E) $t = 500$ time steps (From Soares, Ferro and Fortes, 1985).[210]

(A)

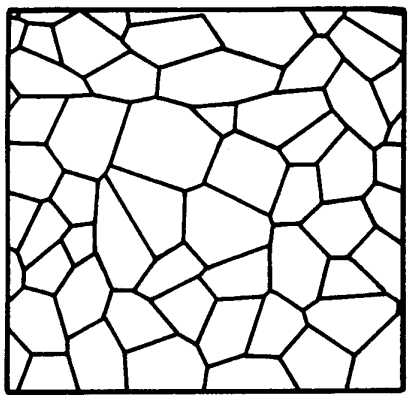

(B)

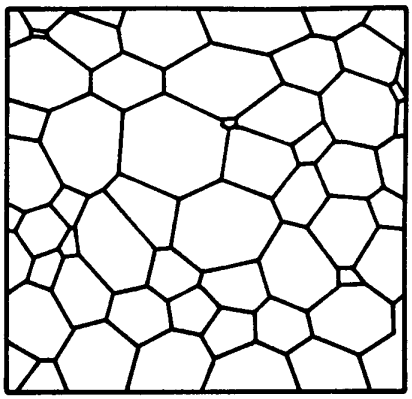

(C)

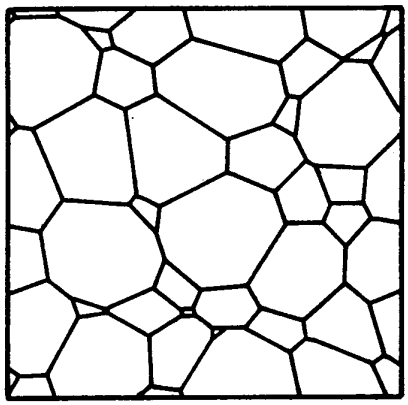

(D)

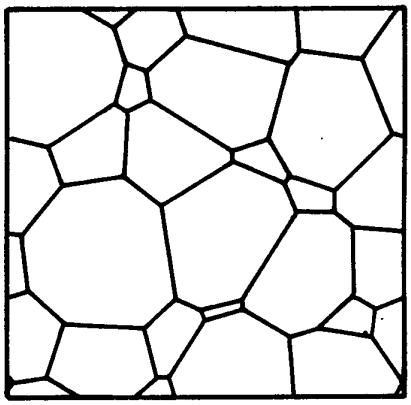

(E)

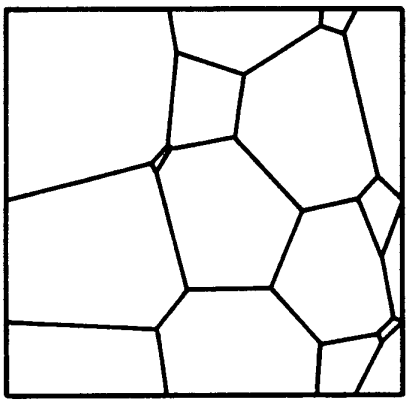

Fig. 27 Vertex Dynamic Grain Growth. Small samples of grain growth in the vertex model of Kawasaki, Nagai and Nakashima. They begin with a Voronoi lattice, $N = 48,000$. (A) $t = 5.0$ montecarlo steps (MCS). (B) $t = 20$ MCS. (C) $t = 50$ MCS (From Kawasaki, Nagai and Nakashima 1988).[259]

(A)

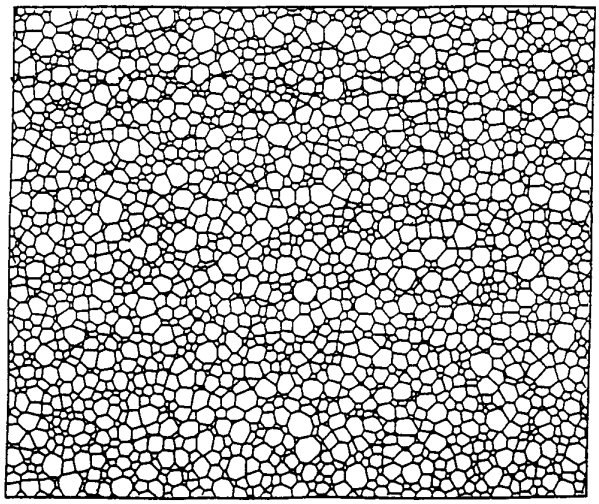

(B)

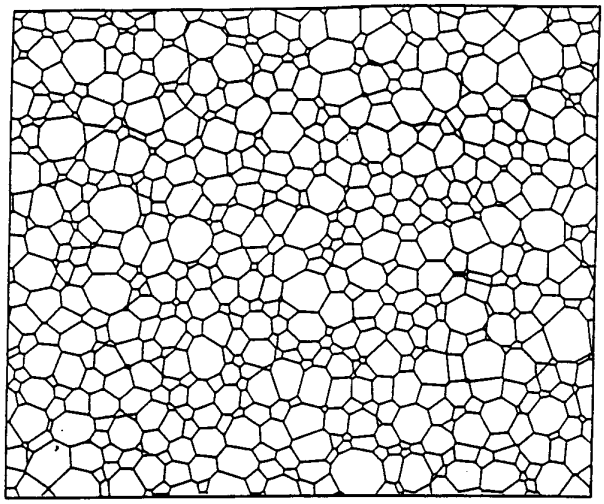

(C)

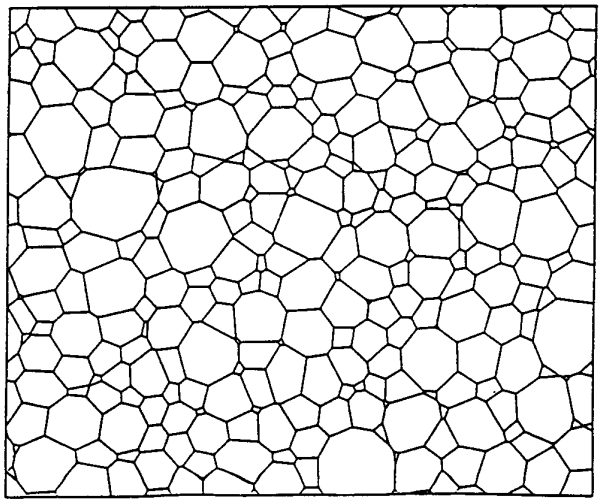

V.e.ii Vertex Dynamics

One appealing way to simplify the computation of bubble evolution is to treat the vertices as particles pulled by the grain boundaries. Such models have the advantage of extreme simplicity, but are not in any obvious way dependent on the real physics. We might expect them to work best in a different limit, when the diffusion rate across the grain boundaries was large compared to the rate of boundary motion. However, by choosing correctly the dependence of the vertex motion on applied force, we can obtain reasonable agreement with experiment.

The earliest example of a vertex model is that of Fullman (largely forgotten by later researchers).[86] He treated interfaces as flat and defined the force on a vertex j by

$$\vec{F}_i = \sum_{\substack{j=1,3 \\ neighbors}} \frac{\vec{x}_i - \vec{x}_j}{|\vec{x}_i - \vec{x}_j|}, \tag{V.47}$$

and the resulting velocity of the vertex by

$$\vec{v}_i = \vec{F}_i \frac{|\vec{F}_i|}{\sum_{\substack{j=1,3 \\ neighbors}} (\vec{x}_i - \vec{x}_j) \cdot \vec{F}_i} \tag{V.48}.$$

This effective mobility is a pretty good method to absorb an integrated wall curvature into an angle deviation at the vertex. Fullman did not discuss his treatment of bubble disappearance or side swapping (he did all his calculations by hand! which limited the number of bubbles he could work with), but it appears that he removed zero area bubbles directly, and swapped sides whenever vertex pairs overlapped. With this model, starting with an actual

soap bubble configuration, he was able to obtain good agreement both for the rate of area growth (Fig. 15 (B)) and for the detailed geometrical evolution of the froth (Fig. 25).

Soares, Ferro and Fortes also assumed that the froth behaves like a damped network of springs, and that pressure and diffusion could be neglected entirely.[210] That is, they assumed that wall mobilities were much greater than vertex mobilities. There is no reason *a priori* to expect that this should be true in the soap froth. They further assumed that boundary walls were flat, and the velocity of the ith vertex in the network given by

$$\vec{v}_i = \mu \vec{F}_i, \tag{V.49}$$

where μ is the mobility of the vertex, and F_i is the force on the vertex from equation (V.47). They performed side swaps whenever a given line connecting vertices shrank below a cutoff length l_0. Triangular cells with sides smaller than l_0 were deleted and replaced with a single vertex at the mid point of the triangle's shortest edge. As with all "exact" models, calculating distribution functions, etc. was straightforward. We show their sample evolution in Fig. 26, beginning with a Voronoi network and employing periodic boundary conditions. They obtained a value of $\alpha = 1.04$ for the area exponent.

Kawasaki, Nagai and Nakashima have developed a series of vertex based models that include a realistic description of the energetics of the soap films.[62,118,119,179] Instead of merely assuming a constant force dependent velocity, they included an explicit velocity dependent damping term. Let

$\vec{r}_i$ be the position of the ith vertex and σ be the surface tension. The free energy of the whole network then is :

$$\mathcal{F} \equiv \sigma \sum_{i,j} |\vec{r}_i - \vec{r}_j|. \tag{V.50}$$

If v_i is the velocity of the ith vertex and $\hat{n}_{ij} \equiv \frac{\vec{r}_i - \vec{r}_j}{|\vec{r}_i - \vec{r}_j|}$ is the normal between vertex i and vertex j, the dissipation is:

$$\mathcal{R} = \frac{\sigma}{6L} \left(\sum_i \sum_{\substack{j \\ neighbors(i)}} (\vec{v}_i \cdot \hat{n}_{ij})^2 + \sum_{\substack{i,\ j \\ (connected\ pairs)}} (\vec{v}_i \cdot \hat{n}_{ij})(\vec{v}_i \cdot \hat{n}_{ij}) \right), \tag{V.51}$$

where L sets the length scale of the pattern relative to the typical velocity. In terms of $\mathcal{F}$ and $\mathcal{R}$ the equation of motion for the ith vertex is given by:

$$\frac{\partial \mathcal{F}}{\partial \vec{r}_i} + \frac{\partial \mathcal{R}}{\partial \vec{v}_i} = 0. \tag{V.52}$$

These equations are not soluble for large numbers of bubbles. They may, however, be reduced to a soluble form by neglecting any anisotropy in the dissipation to obtain a simplified equation for the motion of a vertex

$$\frac{1}{6L} \sum_{\substack{j \\ neighbors(i)}} |\vec{r}_i - \vec{r}_j| \vec{v}_i = - \sum_{\substack{j \\ neighbors(i)}} \frac{\vec{r}_i - \vec{r}_j}{|\vec{r}_i - \vec{r}_j|}. \qquad \text{Model I (V.53)}$$

Averaging over the nearest neighbor lengths on the left hand side reduces the equation to an even simpler form:

$$\frac{1}{2L} \vec{v}_i = - \sum_{j,\ neighbors(i)} \frac{\vec{r}_i - \vec{r}_j}{|\vec{r}_i - \vec{r}_j|}, \qquad \text{Model II (V.54)}$$

equivalent to the model of Soares, Fero and Fortes. Kawasaki, Nagai and Nakashima treated swapping by setting any two vertices within a critical

distance to be equivalent, and replacing small triangles with a single vertex at the midpoint of the shortest side. They solved the equations by direct integration. We show the typical evolution of their Model II in Fig. 27 in a configuration beginning with a 48,000 bubble Voronoi lattice. The distributions were clearly much broader than in a real froth. Neither model obeyed von Neumann's law, with six-sided bubbles shrinking and few sided bubbles shrinking much slower than expected. In later papers they drew on the work of Fullman,[119] substituting the velocity dependence:

$$\vec{v}_i = \frac{\vec{F}_i \cdot \vec{v}_i / |\vec{v}_i|}{\sum_{\substack{j=1,3 \\ neighbors}} \frac{r_{ij}}{3L} \sin^2 \theta_{ij}}, \tag{V.55}$$

where θ_{ij} is the angle to the jth vertex. They also tried a local vertex mobility[62]

$$\mu_i \equiv \left(\frac{\sum_{\substack{j \\ neighbors(i)}} |\vec{r}_i - \vec{r}_j|}{6L} \right)^{-1}, \tag{V.56}$$

which gave more attractive distribution functions, with $\alpha = 1$, and obeyed both the Aboav-Weaire Law, and the radius law that $< r_n > \propto n$.

V.f.iii Other

Weaire and Kermode wrote a hybrid between a vertex and a boundary dynamic model.[243,244] They used von Neumann's law to adjust cell areas and then relaxed the positions of the vertices to produce 120° angles connected by minimal length circular arcs. They performed $T1$'s whenever vertex relaxation would have caused crossings in the boundaries and deleted very small three-, four-, and five-sided bubbles. They started their model with a

randomized lattice using periodic boundary conditions. Unfortunately limitations on the availability of computer time limited them to two hundred initial bubbles. Probably because of the small size of the simulation, they never seem to have reached a scaling state (their side distribution widened continuously), and they observed a growth exponent of $\alpha = 2$, typical of high growth rate equilibration. It is difficult to believe that they would not have obtained $\alpha = 1$ for a larger system. They did obtain good fits to experimental correlation functions and were able to perform a variety of rheological simulations.

V.g Potts Model

The vertex and boundary dynamic models we have been discussing arise naturally from a consideration of the basic physics of a soap froth, in which gas diffuses across well defined soap films. In a metal the grain boundaries are just regions of high concentrations of defects and move by the hopping of atoms between regions of different crystalline orientation. The Potts model simulation takes a quasi-microscopic view of froth evolution. It was developed by metallurgists who found it natural to think of the interior of a grain as being composed of a lattice of "atoms," and the grain boundaries, as the interface between different types (or orientations) of those "atoms." Philosophically this is as far as one can get from a mean field theory, but the starting point is not too different. The mean field theories begin with von Neumann's law, the Potts models with surface tension. The chief exponents of the Potts model approach have been the Exxon group of Anderson, Grest,

Sahni and Srolovitz who have published a monumental series of papers investigating every aspect of the model.[12,15,16,93,99,100,202,215,216,217,218,219]

We have mentioned in our discussion of von Neumann's Law that the basic driving force in a coarsening system is surface tension (or more generally surface energy) which creates pressure differences which result in gas diffusion. The Potts model puts surface tension on a lattice by defining an energy which is proportional to the total length of grain boundary in the system.

Mathematically we may do this by defining on each site of our lattice, a spin $\sigma_{(i,j)}$, where all the lattice points lying within a given grain in our initial configuration are assigned the same value of spin, with a different spin for each grain. In practice to increase computational efficiency, we may reuse spins, using a finite number Q of spins, but taking enough that the probability of two grains with like spins coming in contact and coalescing is small. will discuss below. The energy of interaction between like spins is defined to be zero, and between unlike spins to be one. We may thus write the total Hamiltonian for our spin system as:

$$\mathcal{H} = \sum_{i,j} \sum_{\substack{neighbors \\ i,j}} \delta_{\sigma(i,j),\sigma(i',j')} - 1, \qquad \text{(V.57)}$$

where the range of the second sum will affect the nature of the interaction. The spins are flipped using a montecarlo selection, where a spin is chosen at random and flipped only if the flip would lower system energy. This corresponds to the zero temperature limit, which is appropriate if we

Fig. 28 Potts Model Grain Boundary Migration. (A) Flat boundary, second nearest neighbor interaction. All boundary spins have energy 3, flips would increase energy to 5. (B) Curved boundary. Circled spins lose energy by flipping (6 → 3). The 2 grain will grow at the expense of the 1 grain.

A

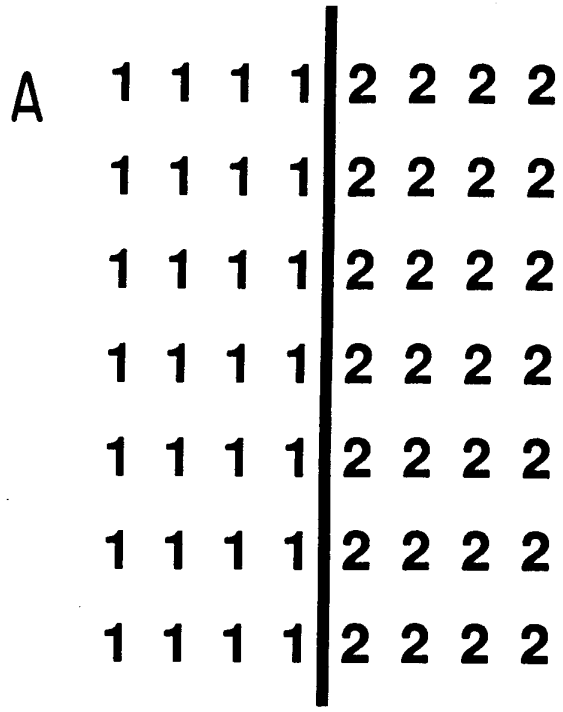
1 1 1 1 2 2 2 2
1 1 1 1 2 2 2 2
1 1 1 1 2 2 2 2
1 1 1 1 2 2 2 2
1 1 1 1 2 2 2 2
1 1 1 1 2 2 2 2
1 1 1 1 2 2 2 2

B

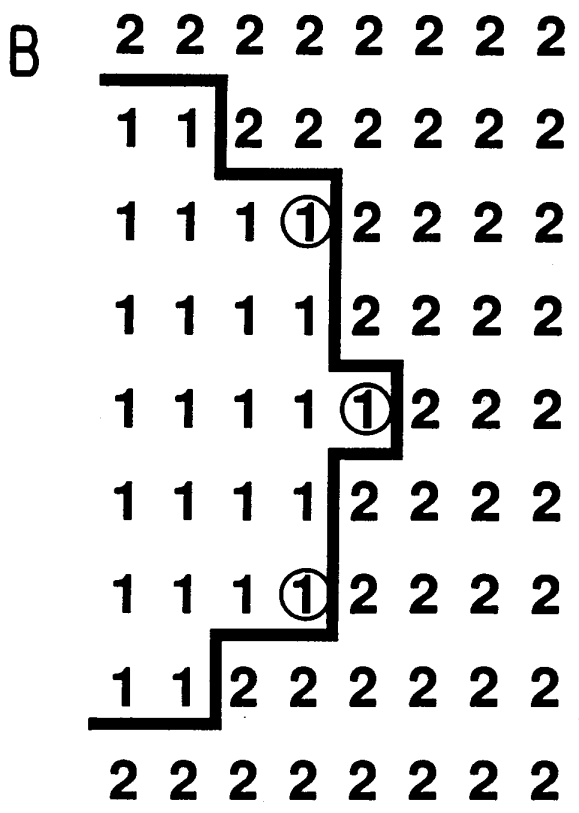
2 2 2 2 2 2 2 2
1 1 2 2 2 2 2 2
1 1 1 1 2 2 2 2
1 1 1 1 2 2 2 2
1 1 1 1 1 2 2 2
1 1 1 1 2 2 2 2
1 1 1 1 2 2 2 2
1 1 2 2 2 2 2 2
2 2 2 2 2 2 2 2

Fig. 29 Potts Model Anisotropies. Energy per unit surface length as a function of surface angle. (a) For nearest neighbor hexagonal lattice (From Srolovitz *et al.* 1983).[216] (b) For nearest neighbor square lattice. (c) For next nearest neighbor square lattice. Labelled arrows show energy extrema and values.

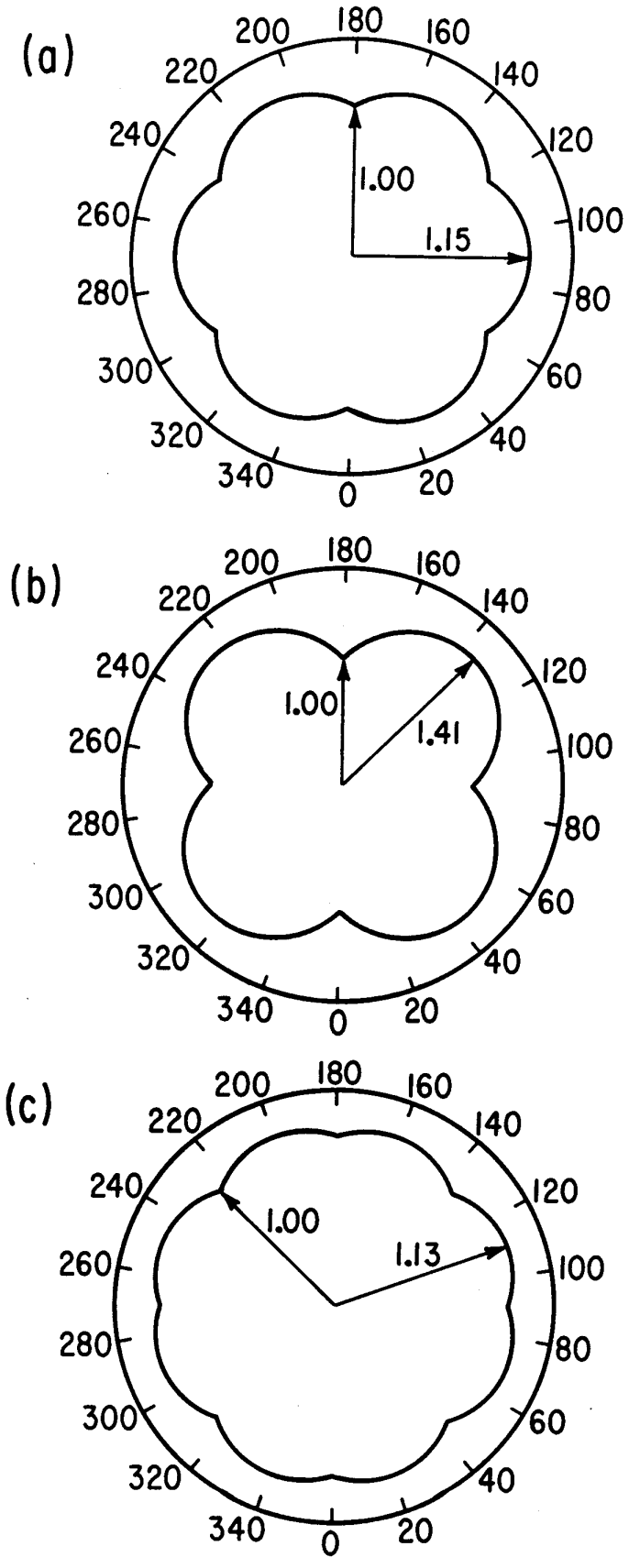
(a)
180
200
160
220
140
240
120
1.00
260
100
1.15
280
80
300
60
320
40
340
0
20
(b)
180
200
160
220
140
240
120
1.00
260
100
1.41
280
80
300
60
320
40
340
0
20
(c)
180
200
160
220
140
240
120
1.00
260
100
1.13
280
80
300
60
320
40
340
0
20

Fig. 30 Potts Model Anisotropy. Shrinking of an initially circular grain in an hexagonal nearest neighbor Potts model simulation. Times from outermost contour moving inwards are, $t = 0$, $t = 1200$, $t = 2100$, and $t = 3000$ montecarlo steps. Some hexagonal anisotropy is evident at later times (From Srolovitz *et al.* 1983).[216]

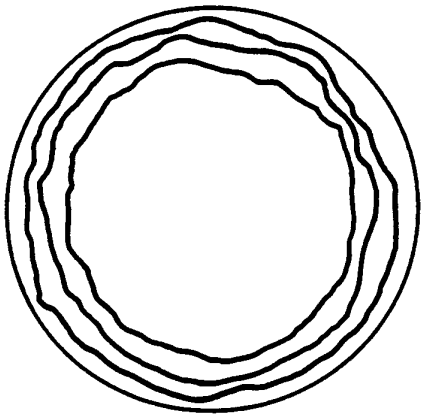

Fig. 31 Potts Model Grain Growth. Grain Growth in the next nearest neighbor $Q = 48$ Potts model starting with random initial conditions on a periodic lattice. (A) $t = 4,000$ montecarlo steps. (B) $t = 8,000$ montecarlo steps (C) $t = 12,000$ montecarlo steps. (D) $t = 20,000$ montecarlo steps (Figure supplied by G. S. Grest 1989).

(A)

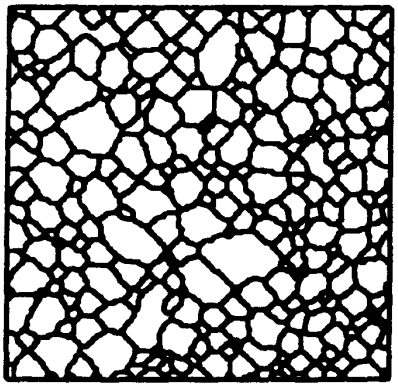

(B)

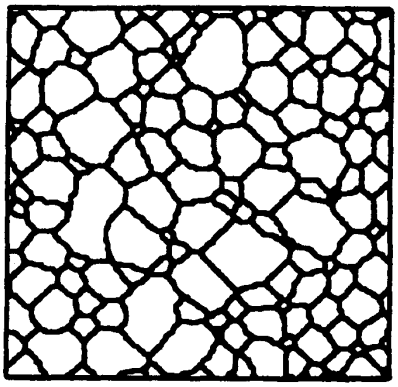

(C)

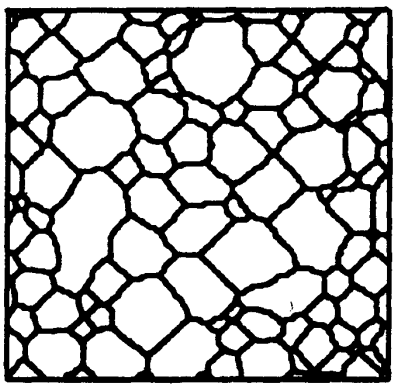

(D)

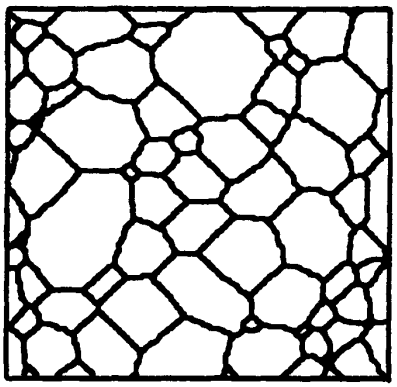

Fig. 32 Potts Model Grain Growth. Comparison of two dimensional soap froth (left) and next nearest neighbor square lattice Potts model simulation starting from identical initial conditions (right). Areas shown are 30% details of the soap froth and the entire 600 x 500 Potts model simulation. Note the missing walls along the lower boundary in the $t = 1640$ minute image and the spurious two-sided bubbles in the $t = 559$ minute and $t = 1119$ minute images (From Glazier *et al.* 1989).[93]

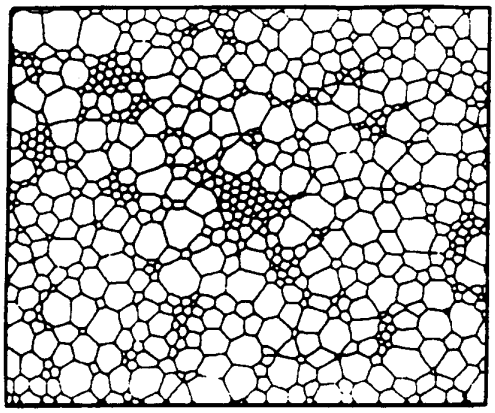

559 Minutes

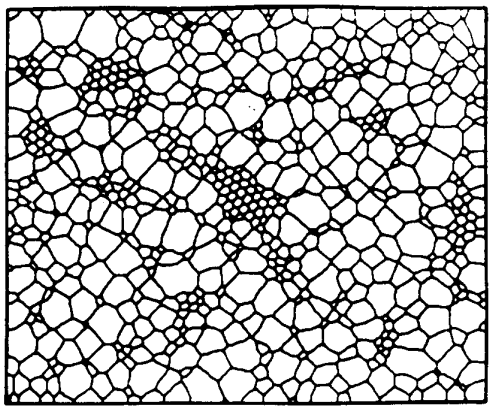

2000 MCS

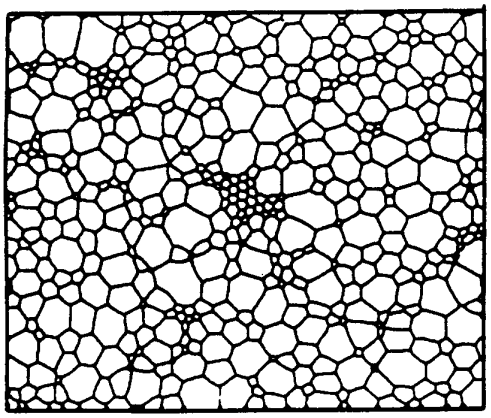

1119 Minutes

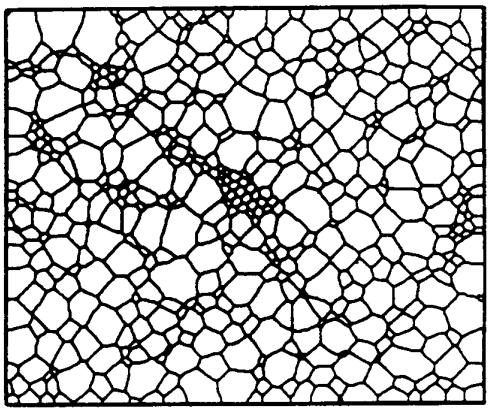

4000 MCS

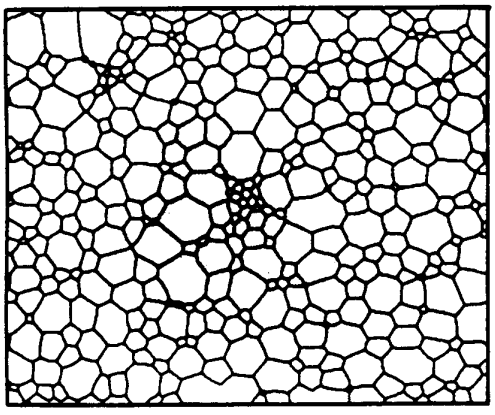

1640 Minutes

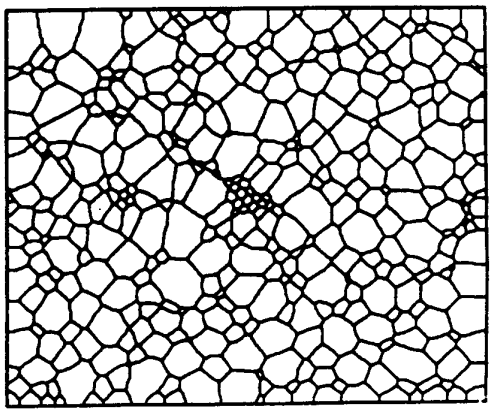

6000 MCS

want to study relaxation processes rather than phase transitions (The temperature remains a useful control parameter, however, for the analysis of conditions where fluctuations are significant).

We may understand why this surface energy results in a von Neumann like diffusion if we look closely at a region of grain boundary (Fig. 28). If the boundary is straight (Fig. 28 (A)) there is no tendency for spins to flip, since all spins border more of their own kind than of others. If a boundary is curved (Fig. 28 (B)), however, spins on the convex side will tend to see more of the opposing type and thus to flip. The result is that the boundary recedes at a rate proportional to its curvature. The original version of this argument was given by Plateau in his study of soap bubbles.[189,190] Since the system attempts to minimize surface length the same factors that favor 120° angles at vertices are at work, so the rest of the von Neumann's law derivation follows. One difficulty with this argument is that a simple nearest neighbor interaction on a square lattice results in a strongly anisotropic surface energy (the ratio of lowest to highest surface energies as a function of orientation is 1.41) which allows stable vertices deviating from the 120° rule (See Fig. 29 (b)). As a result grain growth in a nearest neighbor square lattice Potts model tends to gradually slow and finally stop altogether (as observed in many real metals with a high anisotropy), rather than coarsening continuously. One way to treat this problem is to work at a higher temperature where fluctuations overcome anisotropy pinning (experimentally in metals, higher temperatures result in larger growth exponents so this choice

is reasonable in simulations of grain growth). However, the soap froth is essentially fluctuation free, and therefore should be simulated in the zero temperature limit. A better solution is to use a nearest neighbor hexagonal lattice (Fig. 29 (a), energy ratio 1.15) or a next nearest neighbor square lattice (Fig. 29 (c), energy ratio 1.13), to reduce pinning. There is still some preferred boundary alignment in both cases, but no evidence of freezing. Anderson *et al.* have checked the anisotropy effect in the hexagonal lattice by tracking the evolution of an initially round grain (Fig. 30). It becomes slightly hexagonal, but continues to shrink essentially uniformly.

A second difficulty with the Potts model grain growth simulation is the range of length scales it requires. To successfully measure the scaling exponent for the growth of average grain area, for example, the following relation must hold:

$$L_{Lattice\ Spacing} << L_{Grain\ Initial} << L_{Grain\ Final} << L_{Lattice\ Size}, \tag{V.58}$$

i.e. each grain must contain many spins, the grains must grow a substantial amount, and the final configuration must have many grains. This means that for truly reliable results the lattice needs to be at least 1000 spins per side. An insufficient appreciation of this problem lead to some confusion over the actual scaling exponent of the model.[16,83] In their most recent paper the Exxon group obtained good agreement with von Neumann's Law. While they originally obtained a growth exponent of $\alpha = 0.76$ possibly due to non-equilibrium and anisotropy effects,[202] they have since revised their estimate

up to $\alpha = 0.98 \pm 0.04$.[15] In the same paper they obtained a growth exponent in three dimensions of $\alpha = 0.96 \pm 0.11$.

It is, perhaps, not too surprising that the Potts model shows excellent qualitative agreement with the coarsening of a soap froth. We show a simulated evolution of an initially random distribution of 48 different spin types ($Q = 48$) in Fig. 31.

In the case of the Potts model, we had the advantage of doing the simulations ourselves and could therefore match the conditions of the experiment and simulation more closely. We ran the simulation using a 600 x 500 square lattice with open boundary conditions (in which spins on the boundary were assumed to interact with frozen impurities) employing the digitized image at $t = 2044$ minutes as the initial state. As seen in Fig. 32, this time was late enough that there were few islands of six-sided bubbles remaining from the initial fill. We used a value of $Q = 48$ to minimize wall breakage without unreasonably increasing the time required for the computation. To prevent freezing of the domain boundaries at long times, we set the nearest and next nearest neighbor coupling constants equal. The resulting anisotropy appears as a preferential alignment of grain boundaries along 45° and 90° angles, which does not appear in the triangle lattice. However, grain areas and topological distribution functions appear to be independent of the lattice type, for simulations in which the boundaries do not freeze.

In Fig. 32 we show the soap froth (30% detail) and the Potts model at various stages of evolution, beginning with identical initial patterns. The

qualitative features of the disordering are similar, though the differing boundary conditions (the sample of the froth is taken from the bulk whereas the simulation has open boundary conditions) result in a rapid divergence between the actual patterns. A clear example of the difference in boundary conditions is the contact angle between the domain walls and the edges of the cell. In the experiment, the boundary of the viewing window does not affect the froth and the films can cross the boundary at an arbitrary angle. In the simulation (and adjacent to the cell walls in the experiment) the angle of contact is always close to 90°. The digitization can also result in the appearance of spurious small bubbles near the image boundaries and occasional wall breakage that they attempt to correct for in calculations. The disappearance of residual order occurs in both systems at comparable length scales (after approximately an one order of magnitude increase), and the qualitative patterns remain comparable. At long times in the Potts model grain boundaries appear to lie preferentially along 45° angles. This effect is not seen in simulations on the triangular lattice and presumably reflects the anisotropy remaining in the second nearest neighbor Hamiltonian.

In Fig. 17 we compare the average bubble size versus time for the froth and the model. Since the initial condition of the model was taken from the same digitized image used to measure the areas of the bubbles in the froth, there was no freedom in assigning areas to bubbles. The multiplicative constant relating real time to montecarlo steps is a free parameter, however. If we believe the result that the soap froth does show a growth in average area

slower than t at long times, we obtain from a least squares fit, t (minutes) $= t_m * .32 + 2044$, where t_m is the number of montecarlo steps. In this case we have essentially exact agreement between the froth and the model up to 20,000 minutes where the statistics are best, after which the rate of evolution of the soap froth slows noticeably. If we neglect the long term effect, we obtain a best fit with t (minutes) $= t_m * .38$, which gives agreement over the whole time period within approximately 20%. In both cases the typical dynamics for an initially ordered froth appear, slow initial evolution, followed by rapid growth during which any residual order disappears, and a long term tail with slower, approximately power law growth. We even obtain a purely fortuitous agreement in the long time tails of the two areas, where the soap froth and simulation both show non-monotonic changes in average area (at the same time) due to the contact with the cell boundary (and hence loss from the ensemble) of a large bubble.

Wejchert, Weaire and Kermode modeled the froth using a slightly different Potts model technique. They included von Neumann's law explicitly to control the dynamics in their calculations and used the hexagonal lattice Potts model only to relax the grain boundaries. They therefore used a different Hamiltonian,

$$\mathcal{H} = \frac{1}{2N} \sum_{i,j} \sum_{\substack{neighbors \\ i,j}} \delta_{\sigma_{(i,j)},\sigma_{(i',j')}} - 1 + \frac{\lambda}{N} \sum_{cells\ k} (a_k - \hat{a}_k)^2, \qquad \text{(V.59)}$$

where k indexes the bubbles, $\hat{a}_k$ is the von Neumann's law determined target area for the kth bubble, and λ specifies the strength of the area constraint. This Hamiltonian relaxes to the surface tension case with the constraint that

each bubble has a fixed target area $\hat{a}_k$. The target areas were updated according to von Neumann's law, $\frac{d\hat{a}_k}{dt} = \kappa(n_k - 6)$, at each time step. This had the advantage over the Exxon model that even bubbles small relative to the lattice constant properly obey von Neumann's law, since they are not dependent on statistical averaging along their walls, but the basic requirement of a large lattice remains.

The Potts model has several significant points in its favor. First is simplicity. Its one assumption is that wall energy is the only mechanism driving coarsening. Redistribution of sides occurs automatically without making further assumptions. $T1$ processes are also automatically included with the correct rate. Second, it can be easily extended to include grain coalescence and wall breakage. If, instead of assigning a different spin to each grain, a fixed number, Q, of spins are used, then the probability of a broken wall between two grains meeting as a result of a reorganization of the lattice is just $\frac{1}{Q}$. Thus one can study in detail the effects of wall breakage on froth evolution.[16,217] Other straightforward extensions include three dimensional lattices (limited by the availability of computer time to do 1000^3 monte-carlo calculations),[15] the consideration of pinning centers,[218] orientational anisotropies,[100] and anomalous grain growth in which volume dependent terms are added to the surface energy in the Hamiltonian.[219]

V.h Summary

We have examined seven basic types of models for coarsening in two dimensions: static models, phenomenological models, radius based mean

field theories, topological mean field and network models, boundary dynamic models, vertex dynamic models, and the Potts model. We draw the following conclusions about the physics of two dimensional coarsening. The phenomenological model's success shows that we understand the basic mechanism of disordering, that regions of homogeneous, unstable disorder eat away at regions of stable order along the boundaries between the regions. The ability of network models to reproduce the dependence of disordering on initial disorder confirms our basic statistical assumption, that the dynamics is independent of any correlations in side shedding. The ability of boundary dynamic models to predict both pattern evolution and dynamics goes a step further, demonstrating that local wall length minimization and the geometrical constraints of a coördination number three network can provide a complete description of two dimensional coarsening. Finally, the Potts model extends our understanding to the microscopic level, proving that purely local energy considerations at the "atomic" level can give rise to the correct diffusive and geometrical laws.

In this limited respect our understanding of the universal dynamics of two dimensional coarsening is complete. We have only hinted at the many types of non-universal behavior, which would be of paramount importance in any real application, because they are still poorly understood. We have also neglected three dimensional coarsening, another problem of great practical importance.

CHAPTER VI

DISTRIBUTION FUNCTIONS

In the next two chapters we examine in more detail the agreement between experiment and the predictions of the models discussed previously. We focus on those properties which should distinguish among different classes of systems. We examine, in particular, the distributions of number of sides and area, and the correlation between area and number of sides and between the number of sides of neighboring bubbles. Because of the large uncertainties in the experimental measurements our conclusions will be indicative rather than definitive.

Besides the mean bubble area, the two basic measures of the state of a froth are the distribution of the number of sides, $\rho(n)$, the probability a randomly selected bubble has n sides, and the normalized area distribution, $\rho(A/ < a >)$, the probability that a bubble has an area which is a given fraction of the mean bubble area. Such measurements have been made even in systems for which the dynamics are not well studied. A typical example is three dimensional grain growth in a metal, where measurement of the size distribution usually involves sectioning and hence precludes measurements in time.

A basic problem with any distribution function measured in a finite area is that large bubbles are more likely to touch the area's boundary (and hence to be excluded from the statistics) than are small bubbles. We therefore have a systematic bias against large (and many-sided) bubbles in our distribution

functions and their moments. To the accuracies that we are able to measure, this error is not significant, but we have given two examples of corrected distributions in Table 7 and 8. For the second moment, the effective correction is of the order of 5%. It is relatively smaller for higher moments. The mathematics of distribution function correction is discussed in detail in Miles, Lantuejoul and Blanc and Mocellin.[30,137,166]

VI.a Side Distributions

We define the mth moment of the side distribution as:

$$\mu_m \equiv \sum_{n=2}^{\infty} \rho(n)(n - < n >)^m, \qquad \text{VI.1}$$

and the width of the distribution,

$$W \equiv \sum_{n=2}^{\infty} \rho(n)|n - < n > |. \qquad \text{VI.2}$$

For experimental distributions, $< n >$ may differ from six so our calculated values for the moments may differ slightly from those given elsewhere. The larger the difference between $< n >$ and six, the less reliable the distribution and the larger the error in the moment estimate. Moments higher than μ_2 are sensitive to the large n tail of the distribution, which is hard to measure, and thus are frequently only useful as qualitative indicators. W is useful because it is much less sensitive to small counting error fluctuations for large n than are the higher moments. We will also refer to the ratio $\mathcal{R} \equiv \frac{\rho(5)}{\rho(6)}$, another simple reduction of the distribution.

While there are no general rules for correcting for statistical errors, we find that small sample sizes tend to reduce average moments. For example, if

there is a nominal 1% probability for twelve-sided bubbles, the contribution to μ_2 should be 0.36, which we shall see is a large effect. With a typical sample of thirty bubbles, however, we will usually not see any twelve-sided bubbles, and our estimate of μ_2 will be correspondingly low. The problem is worse for higher moments. Occasionally we will attempt to correct for this bias by averaging several distributions, but most of the time we do not have multiple samples to average.

Let us begin our discussion by examining the typical evolution of the side distribution for two dimensional soap bubble coarsening. In Fig. 33 we plot Glazier *et al.*'s data for the directly digitized air froth shown in Fig. 17, which began a well ordered pattern with a side distribution sharply peaked at six. As a function of time, they observed a monotonic decrease in the fraction of six-sided bubbles $\rho(6)$ and a monotonic increase in the fraction of five-sided bubbles, $\rho(5)$. The large n tail of the distribution first broadened, then narrowed to an equilibrium width. At long times, just after the rate of evolution rolled over to a power law ($t > 10,000$ minutes) they observed an essentially time independent distribution function, with $\mathcal{R} = 1.03$, implying the existence of a scaling state. We may see this scaling state more clearly in Fig. 34 (from Stavans and Glazier, taken from the helium froth shown in Figs. 16 (d) and 9 (left)). In this figure, Glazier and Stavans have superimposed the side distributions for three different times

Fig. 33 $\rho(n)$ versus Time. Side distribution versus time for an initially ordered air froth. In order of decreasing $\rho(6)$, measurement times were: $t = 0$ minutes, $t = 545$ minutes, $t = 1124$ minutes, $t = 1565$ minutes, $t = 2044$ minutes, and $t = 3163$ minutes. Note that the distribution first broadens and then narrows to its equilibrium shape (From Glazier *et al.* 1989).[93]

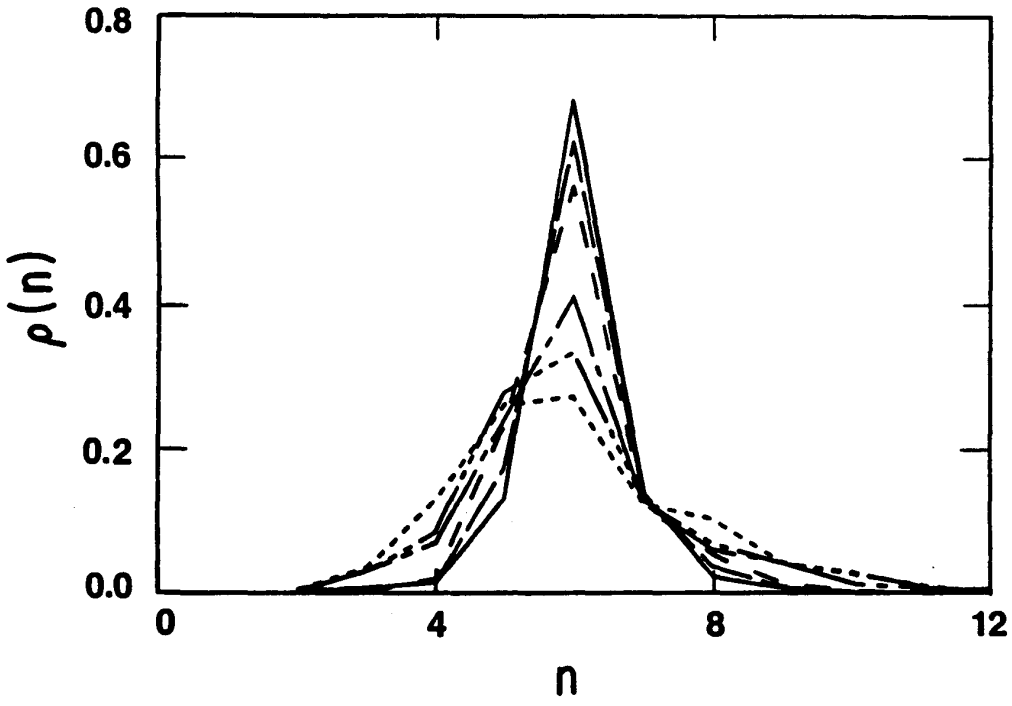
0.8
0.6
0.4
0.2
0.0
ρ(n)
0
4
8
12
n

Fig. 34 $\rho(n)$ versus Time. Side distribution versus time for an initially ordered two dimensional helium froth. Taken at three different times in the scaling regime: $t = 15.25$ hours (open circles), $t = 29.48$ hours (solid circles), and $t = 32.9$ hours (crosses). Number of bubbles ranges from a few hundred to about sixty (From Stavans and Glazier 1989).[220]

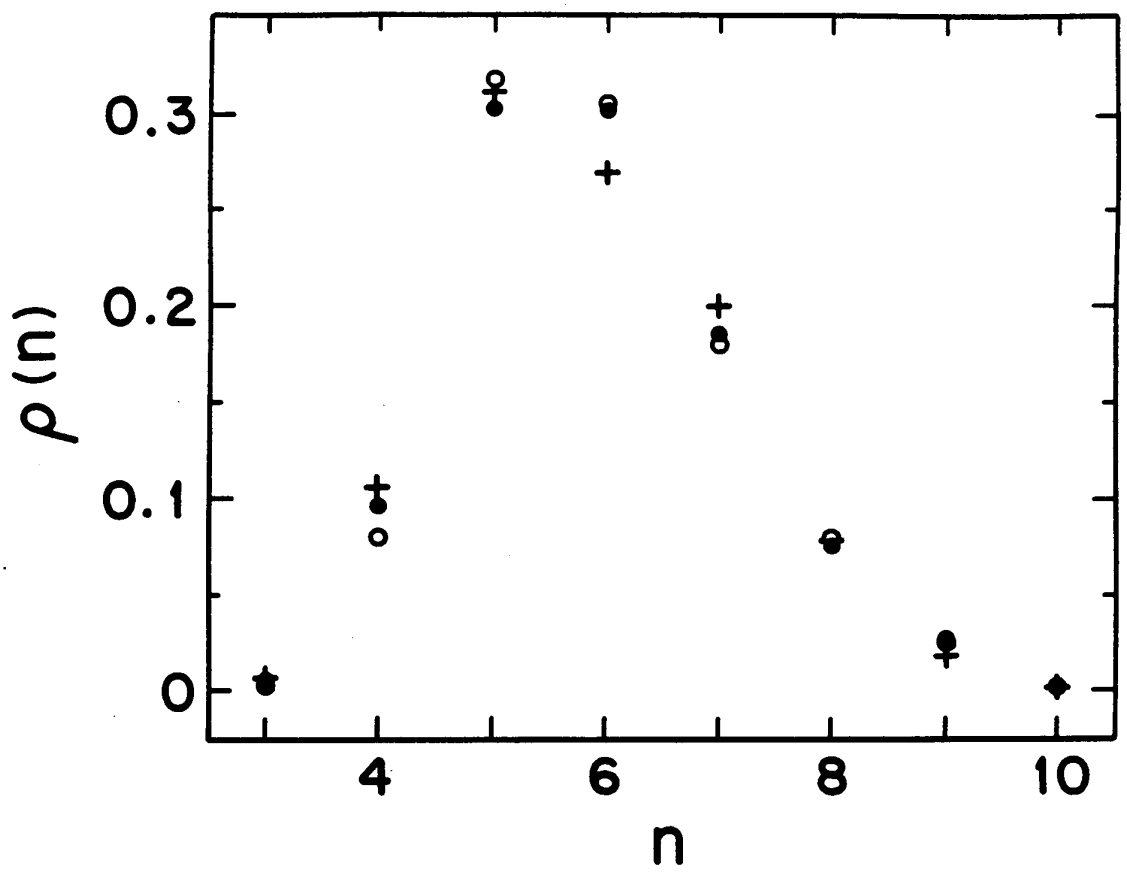
0.3
0.2
0.1
0
ρ(n)
4
6
8
10
n

Fig. 35 Side Distributions. Side distribution for the scaling state of an initially disordered two dimensional air froth (solid) and for the $Q = 48$ hexagonal lattice, nearest neighbor Potts model (dashed) (From Glazier *et al.* 1989).[93]

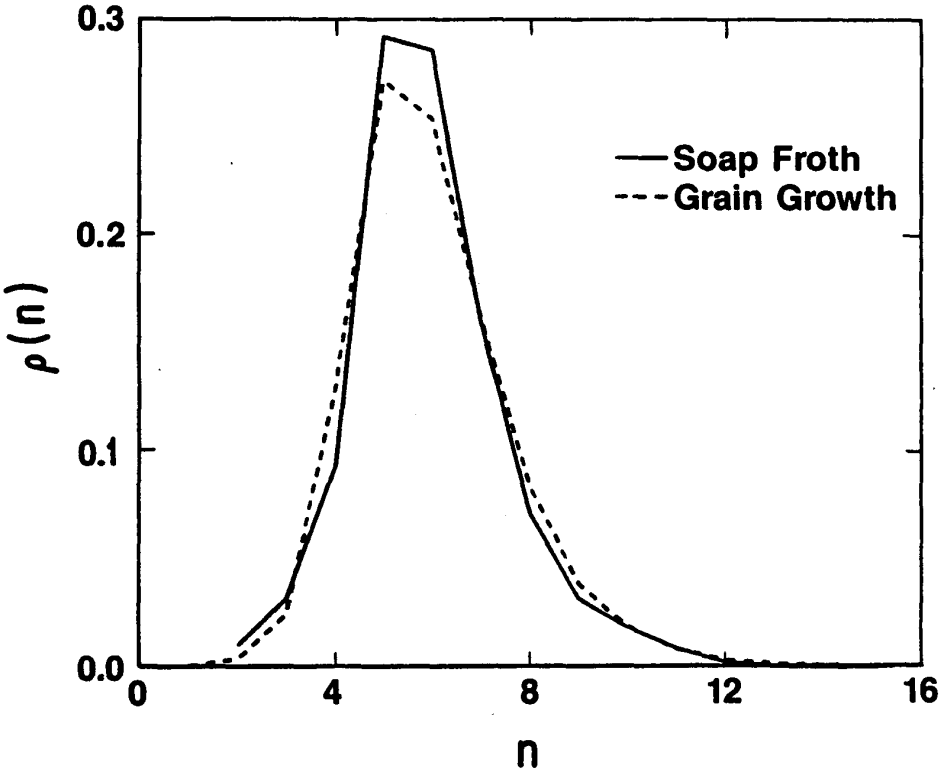
0.3
0.2
0.1
0.0
ρ(n)
0
4
8
12
16
n
Soap Froth
Grain Growth

Fig. 36 μ_2 versus Time. Second moment of the side distribution versus time for an initially ordered helium froth (dots), and an initially disordered air froth (circles). The time scale of the initially ordered run has been multiplied by three (From Stavans and Glazier 1989).[220]

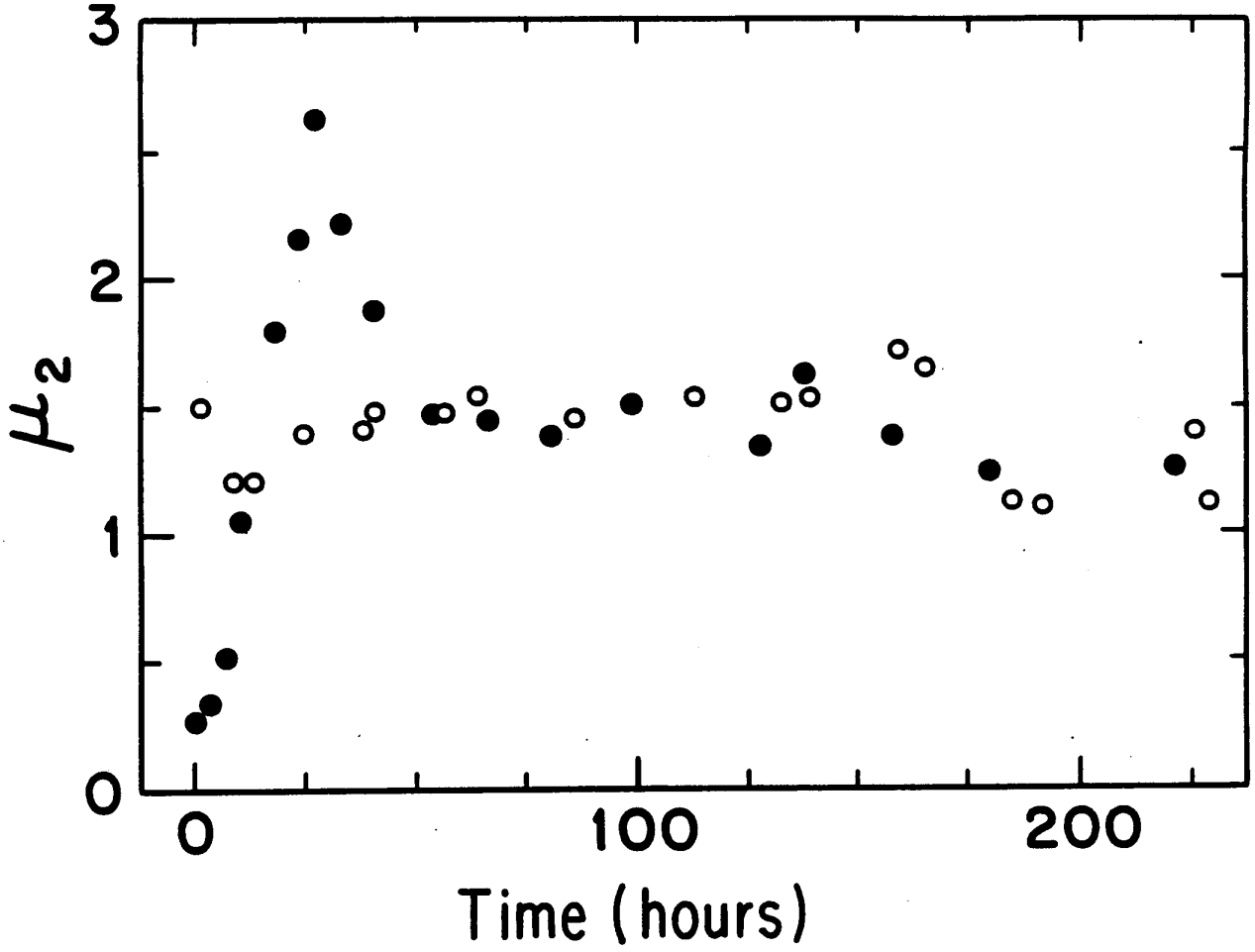
3
2
1
0
μ_2
0
100
200
Time (hours)

Fig. 37 μ_2 versus Time. Second moment of the side distribution versus time for two dimensional initially ordered air froth (From Glazier *et al.* 1989).[93]

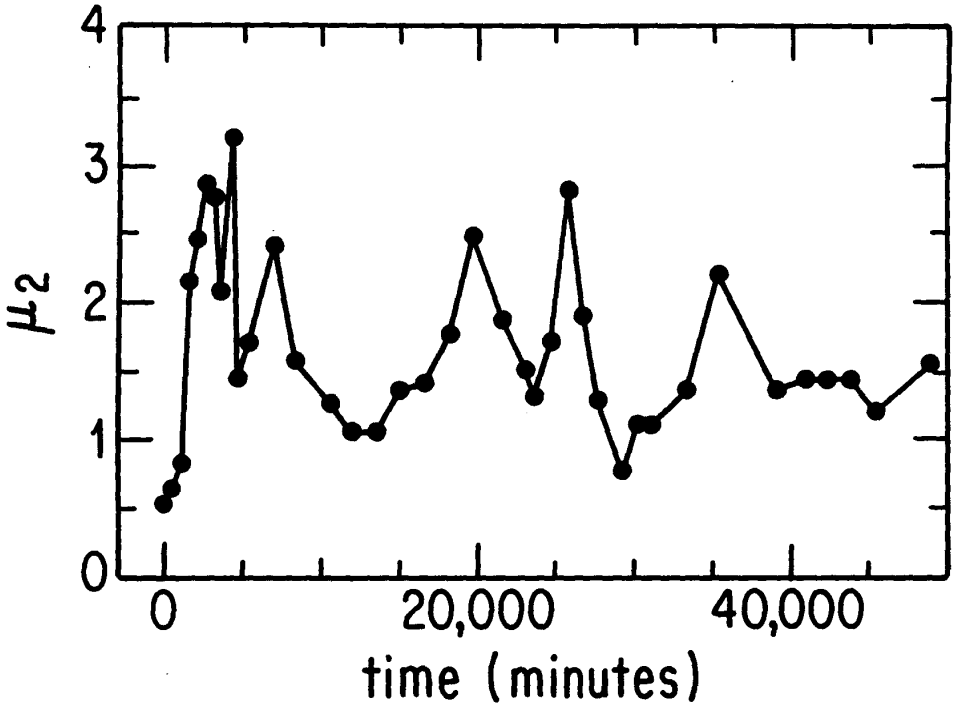
4
3
2
1
0
μ_2
0
20,000
40,000
time (minutes)

Fig. 38 μ_3 versus Time. Third moment of the side distribution versus time for two dimensional initially ordered air froth (From Glazier *et al.* 1989).[93]

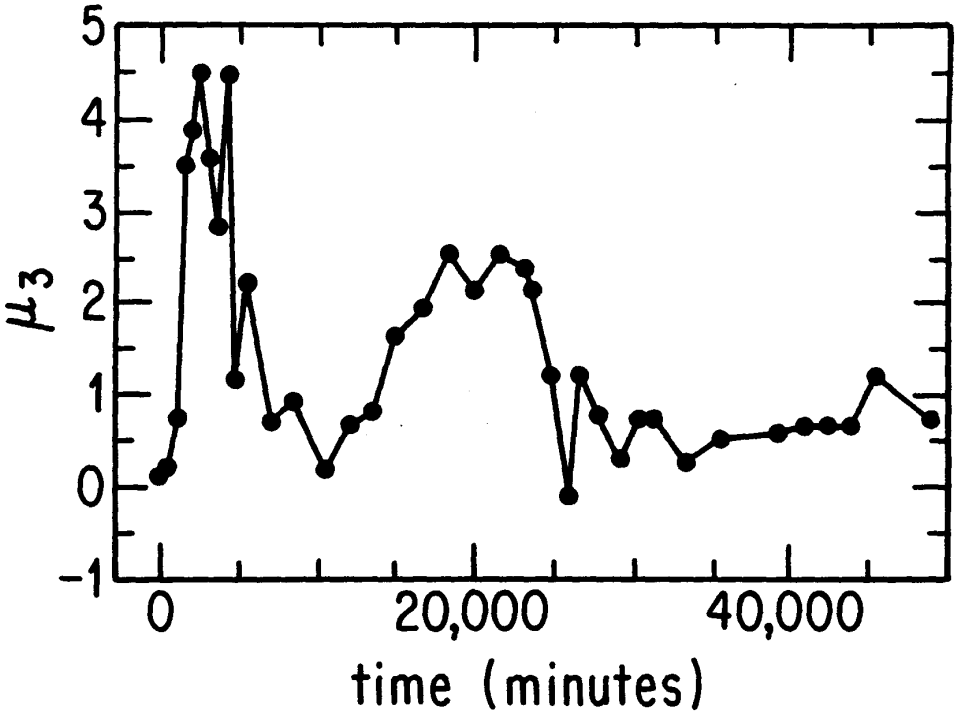
5
4
3
2
1
0
-1
μ_3
0
20,000
40,000
time (minutes)

Fig. 39 μ_4 versus Time. Fourth moment of the side distribution versus time for two dimensional initially ordered air froth (From Glazier *et al.* 1989).[93]

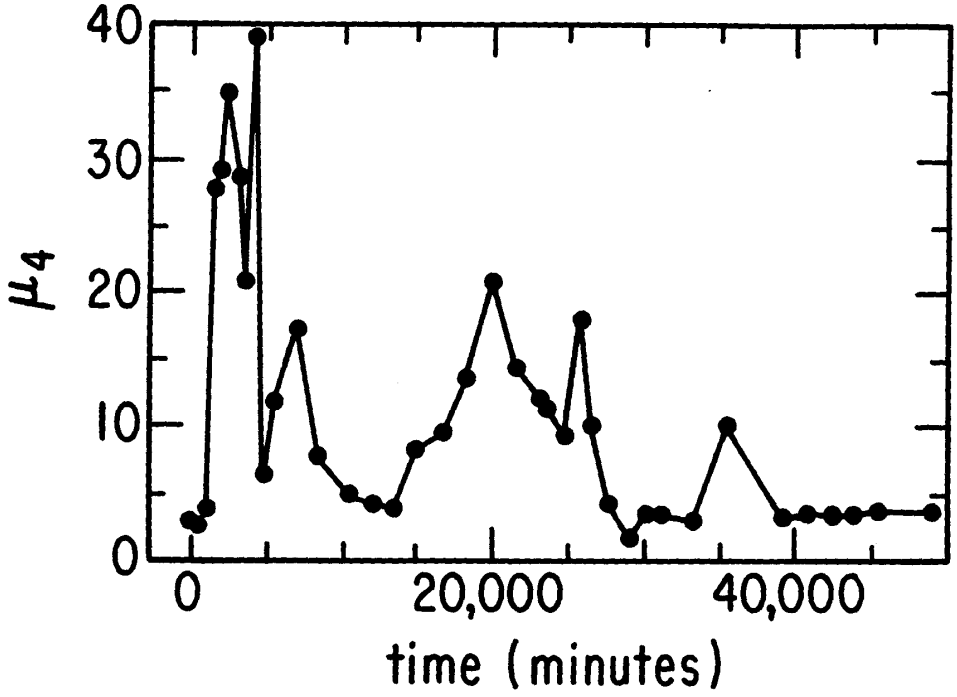
40
30
20
10
0
μ_4
0
20,000
40,000
time (minutes)

Fig. 40 W versus Time. Width of the side distribution versus time for two dimensional initially ordered air froth (From Glazier *et al.* 1989).[93]

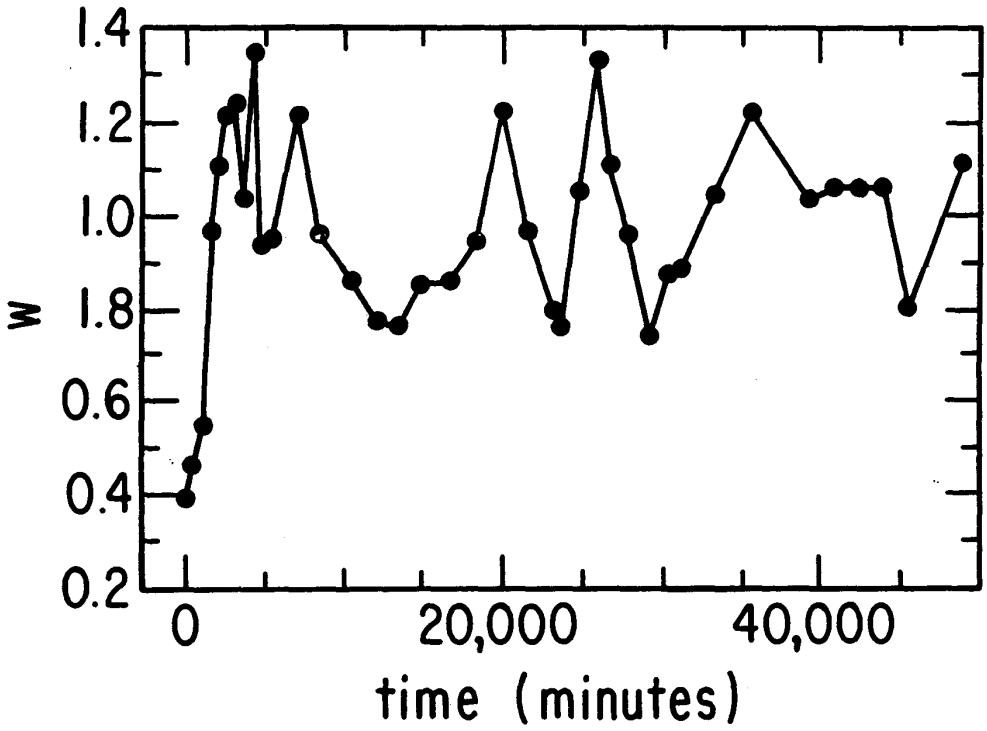
1.4
1.2
1.0
1.8
0.6
0.4
0.2
W
0
20,000
40,000
time (minutes)

TABLE 7

SIDE DISTRIBUTION FUNCTIONS

System	$\rho(3)$ ($\rho(10)$)	$\rho(4)$ ($\rho(11)$)	$\rho(5)$ ($\rho(12)$)	$\rho(6)$ ($\rho(13)$)	$\rho(7)$ ($\rho(14)$)	$\rho(8)$ ($\rho(15)$)	$\rho(9)$ ($\rho(16)$)
Experiment							
Two D Soap Froth							
Smith[206]							
Air[206]	0.01	0.08	0.27	0.35	0.18	0.11	
Air[121]	0.018 (0.009)	0.096 (0.0006)	0.282	0.318	0.161	0.083	0.031
±	0.009 (0.009)	0.043 (0.0006)	0.032	0.036	0.025	0.025	0.021
Aboav[8]							
$t = 0$h $N = 4612$	-	-	0.126	0.731	0.112	0.001	
$t = 0$h $N = 5687$	0.002	0.022	0.212	0.537	0.204	0.022	0.001
$t = 15$h $N = 3550$	0.012 (0.0003)	0.050 (0.0003)	0.217	0.461	0.206	0.050	0.004
$t = 30$h $N = 3623$	0.011 (0.001)	0.059 (0.0006)	0.265 (-)	0.373 (0.0003)	0.198	0.074	0.018
$t = 75$h $N = 1372$	0.026 (0.011)	0.080 (0.004)	0.284 (0.0007)	0.308 (0.0007)	0.174	0.077	0.035
$t = 105$h $N = 584$	0.034 (0.017)	0.111 (0.010)	0.291 (0.010)	0.262 (0.003)	0.149	0.077	0.033 $[\rho(18)]$ [0.002]

TABLE 7, *continued*

System	$\rho(3)$ ($\rho(10)$)	$\rho(4)$ ($\rho(11)$)	$\rho(5)$ ($\rho(12)$)	$\rho(6)$ ($\rho(13)$)	$\rho(7)$ ($\rho(14)$)	$\rho(8)$ ($\rho(15)$)	$\rho(9)$ ($\rho(16)$)
Experiment							
Two D Soap Froth							
Glasier *et al.*							
Air[93]	0.032	0.093	0.292	0.285	0.159	0.072	0.032
	(0.018)	(0.018)	(0.002)				
Air[94]	0.003	0.102	0.277	0.329	0.201	0.073	0.009
$N = 343$	(0.009)	(0.003)					
$N = 111$	0.000	0.090	0.333	0.315	0.144	0.072	0.045
Helium[94]	0.004	0.101	0.321	0.314	0.137	0.058	0.041
$N = 1696$	(0.017)	(0.008)	(0.003)	(0.002)			
$N = 423$	0.000	0.071	0.333	0.298	0.187	0.073	0.038
	0.003	0.090	0.325	0.289	0.193	0.064	0.032
$N = 311$	(0.003)						
Average of	0.010	0.091	0.314	0.305	0.170	0.069	0.033
Above	(0.008)	(0.005)	(0.0008)	(0.0003)			
$\pm$	0.013	0.011	0.023	0.017	0.027	0.006	0.013
	(0.008)	(0.007)	(0.001)	(0.0007)			
Metal Grains							
Al $+10^{-4}$ Mg .22mm Foil[75]							
$T = 0$	0.031	0.153	0.252	0.252	0.156	0.078	0.044
	(0.016)	(0.012)	(0.002)	(0.003)	(–)	(0.003)	
$T = 1.5$h	0.034	0.153	0.274	0.254	0.161	0.090	0.033
							[$\rho(2)$]
	(0.015)	(0.006)					[0.003]
$T = 3.25$h	0.031	0.134	0.275	0.241	0.161	0.078	0.037
	(0.022)	(0.008)					
$T = 4.25$h	0.045	0.120	0.236	0.236	0.152	0.084	0.032
	(0.026)	(0.009)	(0.006)	(0.007)	(0.005)	(0.003)	[0.003]
Averaged	0.035	0.140	0.259	0.246	0.157	0.082	0.036
	(0.020)	(0.009)	(0.002)	(0.0025)	(0.0012)	(0.0013)	[0.0016]
$\pm$	0.002	0.007	0.016	0.019	0.009	0.005	0.006
	(0.005)	(0.003)	(0.003)	(0.003)	(0.002)	(0.002)	[0.002]

TABLE 7, *continued*

System	$\rho(3)$ ($\rho(10)$)	$\rho(4)$ ($\rho(11)$)	$\rho(5)$ ($\rho(12)$)	$\rho(6)$ ($\rho(13)$)	$\rho(7)$ ($\rho(14)$)	$\rho(8)$ ($\rho(15)$)	$\rho(9)$ ($\rho(16)$)
			Experiment				
Biological							
Cucumber[142]	–	0.023	0.265	0.445	0.231	0.035	0.003
Dividing[147]	–	–	0.016	0.255	0.478	0.224	0.026
	(0.001)						
Eupatorium[147]	–	0.026	0.265	0.436	0.238	0.034	0.001
Human Amnion[142]	0.004	0.054	0.248	0.397	0.241	0.049	0.007
Mouthbreeder Fish[105]	–	–	0.214	0.643	0.143		
Rock Fracture							
Pieri[191]							
Basalts							
Giant's Causeway	–	0.040	0.347	0.507	0.081	0.024	
Devil's Postpile	0.025	0.091	0.368	0.440	0.076		
Mt. Rodeix	–	0.148	0.499	0.328	0.024		
Devil's Tower	–	0.169	0.422	0.354	0.055		
Europa Type 1,2	0.038	0.171	0.4623	0.2517	0.078		
Coörd # 4							
Circle Cliffs	0.329	0.624	0.048				
Zendan, Iran	0.406	0.524	0.061	0.008			
Colorado	0.324	0.656	0.020				
Europa Type 3	0.404	0.463	0.124	0.008			
Europa Mixed	0.182	0.491	0.243	0.074	0.002	0.007	
Other 2 D							
Photo Emulsion[142]	0.031	0.222	0.253	0.171	0.129	0.070 [$\rho(17)$]	0.053 [$\rho(19)$]
$N = 1000$	(0.034)	(0.019)	(0.009)	(0.004)	(0.001)	[0.001]	[0.001]
Lipid Monolayers							
Stearic Acid[169]	0.071	0.125	0.269	0.269	0.125	0.089	–
	(0.035)	(–)	(–)	(0.018)			
Pentadecanoic							
Ordered[92]	–	0.054	0.258	0.462	0.140	0.077	0.009
Disordered[92]	–	0.097	0.340	0.262	0.233	0.039	0.010
	(0.010)						
Wax Convect.[147]	–	0.023	0.357	0.377	0.220	0.023	

TABLE 7, *continued*

System	$\rho(3)$ ($\rho(10)$)	$\rho(4)$ ($\rho(11)$)	$\rho(5)$ ($\rho(12)$)	$\rho(6)$ ($\rho(13)$)	$\rho(7)$ ($\rho(14)$)	$\rho(8)$ ($\rho(15)$)	$\rho(9)$ ($\rho(16)$)
				Experiment			
Two D Sections of 3 D Materials							
Froths							
Polyurethane Foam[250]	0.049 (0.002)	0.145	0.229	0.318	0.175	0.067	0.016
Metal Grains							
Tin							
Champur[64]	0.100 (0.008)	0.227 (0.005)	0.290 (0.003)	0.206 (0.001)	0.097	0.043	0.019
Aluminum							
High Purity	0.038 (0.019)	0.161 (0.009)	0.256 (0.005)	0.250	0.148	0.076	0.039
Pure 500° C[24]							
1m	0.014 (0.020)	0.152 (0.009)	0.261 (0.001)	0.267	0.156	0.074	0.047
25m	0.023 (0.012)	0.167 (0.005)	0.257 (0.005)	0.253	0.149	0.096	0.035
125m	0.073 (0.008)	0.198 (0.005)	0.286 (0.005)	0.230	0.114	0.048	0.034
625m	0.029 (0.031)	0.146 (0.012)	0.251 (0.009)	0.225	0.174	0.071	0.053
Average	0.035 (0.018)	0.166 (0.008)	0.264 (0.005)	0.244	0.148	0.072	0.042
±	0.026 (0.010)	0.023 (0.003)	0.015 (0.003)	0.019	0.025	0.019	0.009
α Iron[206]	0.063	0.083	0.104	0.396	0.271	0.063	0.021
β-Brass[206]	0.025	0.202	0.436	0.287	0.046	0.007	
Ceramics							
Blanc *et al.*[30]							
Al_2O_3 Uncorrected	0.04 (0.02)	0.17 (0.01)	0.29	0.21	0.12	0.10	0.04
Corrected	0.036 (0.024)	0.158 (0.013)	0.276	0.213	0.127	0.108	0.045

TABLE 7, *continued*

System	$\rho(3)$ ($\rho(10)$)	$\rho(4)$ ($\rho(11)$)	$\rho(5)$ ($\rho(12)$)	$\rho(6)$ ($\rho(13)$)	$\rho(7)$ ($\rho(14)$)	$\rho(8)$ ($\rho(15)$)	$\rho(9)$ ($\rho(16)$)
Experiment							
Two D Sectns of 3 D Mats							
Ceramics							
Sintered Alumina[137]	0.021 (0.009)	0.153 (0.007)	0.258 (0.001)	0.281	0.131	0.131	0.100
Corrected	0.018 (0.010)	0.141 (0.008)	0.246 (0.001)	0.281	0.140	0.111	0.044
MgO + LiF[9] $N = 9906$	0.024 (0.013)	0.160 (0.005)	0.279 (0.0013)	0.248	0.155	0.081	0.034
Biological Materials							
Vegetable Cells[206]	0.051	0.273	0.397	0.254	0.063	0.008	0.001
Theory							
Geometrical Models							
Pure Geometrical							
Voronoi[34] $N = 1377$	0.012 (0.008)	0.105 (0.0007)	0.264 (0.0007)	0.295	0.197	0.088	0.031
$N = 57,000$[52]	0.0110 (0.0075)	0.1078 (0.0014)	0.2594 (.00018)	0.2952 (.00005)	0.1984	0.0896	0.0296
Clumped	0.013	0.108	0.266	0.289	0.192	0.079	0.041
Relaxed[105] $N = 1366$	– (0.011)	0.022 (0.0007)	0.258 (0.0007)	0.467	0.211	0.037	0.006
Glass Models[204]							
Triangle Raft	–	0.062	0.256	0.392	0.196	0.095	
Triangle-Line Raft	0.009 (0.004)	0.078	0.245	0.363	0.183	0.107	0.010
2 D Sectns of 3 D Arrays[250]							
Pentagonal Dodecahedra	0.089 (0.008)	0.128	0.212	0.293	0.204	0.061	0.007
Tetrakaidecahedra	0.073 (0.011)	0.134	0.118	0.3144	0.185	0.130	0.037
Coordination # 4							
Poisson[191]	0.354	0.377	0.191	0.059	0.009		

TABLE 7, *continued*

System	$\rho(3)$ ($\rho(10)$)	$\rho(4)$ ($\rho(11)$)	$\rho(5)$ ($\rho(12)$)	$\rho(6)$ ($\rho(13)$)	$\rho(7)$ ($\rho(14)$)	$\rho(8)$ ($\rho(15)$)	$\rho(9)$ ($\rho(16)$)
				Theory			
Maximum Entropy							
Kikuchi I[121]	0.035 (0.015)	0.141 (0.001)	0.233	0.238	0.185	0.107	0.045
Kikuchi II	0.025 (0.009)	0.107 (0.001)	0.243	0.274	0.189	0.109	0.042
Almeida *et al.*[10]	0.210 0.035	0.195 0.025	0.159 0.018	0.118 0.013	0.086 0.009	0.063 0.007	0.047
Vertex Models							
Weaire *et al.*							
"Exact"[244]	– (0.008)	0.145	0.251	0.261	0.194	0.103	0.038
"Exact"[243]	0.003 (0.003)	0.078	0.259	0.358	0.200	0.091	0.008
Soares *et al.*[210] Straight Sides	0.027 (0.009)	0.149	0.229	0.223	0.198	0.125	0.040
Kawasaki *et al.*[259]							
Model I	0.054 (0.027)	0.153 (0.010)	0.236 (0.005)	0.216 (0.002)	0.151	0.091	0.055
Model II	0.031 (0.019)	0.141 (0.006)	0.253 (0.002)	0.237	0.173	0.094	0.045
Enomoto *et al.*[62]	0.068 (0.023)	0.134 (0.014)	0.255 (0.005)	0.213 –	0.147 (0.005)	0.082	0.053
Mean Field Theories							
Marder[157]	0.011 (0.015)	0.076 (0.008)	0.263 (0.006)	0.414	0.123	0.056	0.029

TABLE 7, *continued*

System	$\rho(3)$ ($\rho(10)$)	$\rho(4)$ ($\rho(11)$)	$\rho(5)$ ($\rho(12)$)	$\rho(6)$ ($\rho(13)$)	$\rho(7)$ ($\rho(14)$)	$\rho(8)$ ($\rho(15)$)	$\rho(9)$ ($\rho(16)$)
				Theory			
Network Models							
Fradkov *et al.*[76]							
T1's per T2	0.002	0.046	0.288	0.390	0.193	0.064	0.016
0	(0.002)						
1	0.018	0.115	0.262	0.273	0.184	0.089	0.033
	(0.010)	(0.003)					
2	0.048	0.145	0.224	0.222	0.158	0.099	0.046
				[$\rho(2)$]			
	(0.022)	(0.009)		[0.010]			
10	0.127	0.145	0.145	0.135	0.110	0.080	0.046
	0.033	0.022		[0.073]			
∞	0.127	0.107	0.093	0.077	0.065	0.053	0.049
	(0.038)	(0.032)		[0.152]			
Potts Model							
Potts Model[93]	0.025	0.128	0.271	0.253	0.161	0.084	0.039
Triangle Lattice	(0.019)	(0.008)	(0.003)				

TABLE 7, *continued*

System	$\rho(3)$ ($\rho(10)$)	$\rho(4)$ ($\rho(11)$)	$\rho(5)$ ($\rho(12)$)	$\rho(6)$ ($\rho(13)$)	$\rho(7)$ ($\rho(14)$)	$\rho(8)$ ($\rho(15)$)	$\rho(9)$ ($\rho(16)$)
			Theory				
Two D Sect of 3 D Mat							
Carnal & Mocellin[46]							
$\beta = 0$	0.297 (0.029)	0.190 (0.022)	0.129 (0.018)	0.092 (0.014)	0.067 (0.011)	0.050	0.038
$\beta = 2$	0.065 (0.028)	0.174 (0.015)	0.222 (0.008)	0.205 (0.004)	0.138 (0.002)	0.086	0.050
$\beta = 4$	0.011 (0.013)	0.118 (0.005)	0.264 (0.002)	0.297 (0.001)	0.171	0.083	0.035
$\beta = 6$ (T1 rate)	0.002 (0.006)	0.070 (0.001)	0.273	0.373	0.184	0.069	0.021
Blanc & Mocellin[30]							
	0.036 (0.025)	0.173 (0.009)	0.231 (0.003)	0.215 (0.0008)	0.154	0.099	0.054
Depends on $\rho(3)$ as	0.100 (0.033)	0.146 (0.013)	0.194 (0.004)	0.194 (0.001)	0.151	0.101	0.064
a parameter no T1's	0.050 (0.026)	0.169 (0.009)	0.227 (0.003)	0.212 (0.0006)	0.155	0.104	0.056
	– (0.021)	0.190 (0.006)	0.259 (0.0009)	0.230	0.160	0.094	0.050
Kurtz & Carpay[132]							
Potts Model[15]							
	0.076 (0.027)	0.185 (0.010)	0.230 (0.005)	0.212 (0.004)	0.121 (0.002)	0.082 (0.001)	0.046

TABLE 8

SIDE DISTRIBUTION MOMENTS

System	$< n >$	μ_2	μ_3	μ_4	W
Experiment					
2-D Soap Froth					
Smith[121]	5.928	1.759	1.148	10.21	1.005
Smith[259]	5.94	1.296	0.114	4.30	0.877
Aboav[8]					
$t = 0$ hours $N = 4612$	5.988	0.242	0.003	0.26	0.249
$t = 0$ hours $N = 5687$	5.990	0.620	-0.011	1.38	0.519
$t = 15$ hours $N = 3550$	5.968	0.976	-0.068	3.56	0.687
$t = 30$ hours $N = 3623$	5.993	1.30	0.486	6.00	0.827
$t = 75$ hours $N = 1372$	5.982	1.98	1.763	15.62	1.028
$t = 105$ hours $N = 584$	6.010	2.86	8.153	76.10	1.247
Glazier *et al.*					
Air[93]	5.999	2.490	2.490	26.66	1.144
Air $N = 343$[94]	5.935	1.492	1.090	8.623	.925
Air $N = 111$	5.910	1.523	1.295	7.113	.951
Helium $N = 1696$	5.983	2.151	3.933	24.29	1.045
Helium $N = 423$	5.972	1.437	1.017	6.01	0.927
Helium $N = 311$	5.915	1.491	1.017	6.87	0.958
Average of Above	5.952	1.764	1.980	13.26	0.992
$\pm$	0.037	0.445	1.366	9.53	0.0087
Metal Grains					
Al + 10^{-4} Mg .22mm Foil[75]					
$t = 0$ hours	5.975	2.993	5.824	49.58	1.277
$t = 1.5$ hours	5.835	2.353	1.921	18.24	1.210
$t = 3.25$ hours	5.916	2.465	2.644	20.97	1.214
$t = 4.25$ hours	6.091	3.791	9.257	84.07	1.414
Average of Above	5.952	2.900	5.013	43.90	1.269
Biological Systems					
Cucumber[142]	5.998	0.748	0.137	1.62	0.619
Dividing Cucumber[147]	6.992	0.656	0.092	1.23	0.570
Eupatorium[147]	5.992	0.752	0.082	1.55	0.629
Human Amnion[142]	5.987	1.00	0.068	3.02	0.734
Mouthbreeder Fish[105]	5.929	0.352	0.004	0.35	0.398

TABLE 8, *continued*

System	$< n >$	μ_2	μ_3	μ_4	W
Experiment					
Rock Fracture[191]					
Giant's Causeway	5.702	0.596	0.165	1.33	0.624
Devil's Postpile	5.448	0.733	-0.325	1.80	0.719
Mt. Rodeix	5.228	0.522	0.005	0.69	0.592
Devil's Tower	5.296	0.657	0.019	1.03	0.687
Europa Type 1,2	5.161	0.858	-0.018	2.14	0.708
Coördination # 4 Rock Fracture[191]					
Circle Cliffs	3.720	0.297	-0.008	0.22	0.473
Zendan, Iran	3.671	0.392	0.144	0.52	0.545
Colorado	3.696	0.252	-0.046	0.14	0.451
Europa Type 3	3.739	0.495	0.198	0.67	0.596
Europa Mixed	4.243	0.791	0.553	2.69	0.692
Other 2-D Systems					
Photo Emulsion $N = 1000$[142]	6.00	4.344	12.402	111.66	1.580
Lipid Monolayers					
Stearic Acid[169]	5.836	3.309	7.705	66.37	1.313
Ordered[92]	5.955	1.001	0.444	3.29	0.704
Disordered[92]	5.874	1.432	1.125	7.28	0.958
Wax Convection[147]	5.863	0.742	0.171	1.32	0.702
Two D Sections of 3 D Materials					
Froths					
Polyurethane Foam[250]	5.697	1.771	0.172	8.70	1.076
Metal Grains					
Champur Tin[64]	5.278	5.278	4.074	30.62	1.200
High Purity Aluminum[64]	5.877	2.746	3.739	29.40	1.271
Pure Aluminum at 500° C[24]					
1 minute	5.967	2.445	3.047	21.68	1.188
25 minutes	5.883	2.440	2.849	22.48	1.216
125 minutes	5.500	2.534	3.779	28.64	1.243
625 minutes	6.081	3.118	4.534	35.33	1.362
α Iron[206]	6.000	1.708	-1.125	9.46	0.917
β-Brass[207]	5.148	0.812	0.781	2.03	0.698

TABLE 8, *continued*

System	$< n >$	μ_2	μ_3	μ_4	W
Experiment					
Ceramics					
Blanc and Mocellin Al_2O_3[30]					
Uncorrected	5.82	2.748	3.290	24.41	1.32
Corrected	5.939	2.901	3.386	26.25	1.343
Sintered Alumina uncorrected[137]	5.895	2.278	2.269	18.02	1.164
Sintered Alumina corrected[137]	5.998	2.348	2.226	18.31	1.162
MgO + LiF flux $N = 9906$[9]	5.835	2.279	2.415	18.51	1.188
Biological Materials					
Vegetable Cells[206]	5.032	1.022	0.244	3.07	0.760
Theory					
Geometrical Models					
Pure Geometrical					
Voronoi $N = 1377$[34]	6.00	1.79	1.089	10.41	1.014
Voronoi $N = 57,000$[52]	5.997	1.777	1.026	10.68	1.013
Negative Binomial Voronoi[34]	6.00	1.91	1.367	11.97	1.047
Relaxed Voronoi[105]	6.000	0.754	0.222	1.858	0.603
Coörd. # 4 Poisson[191]	3.981	0.869	0.604	2.28	0.702
Glass Models[204]					
Triangle Raft	6.007	1.079	0.185	2.95	0.768
Triangle-Line Raft	6.015	1.409	0.400	6.01	0.879
2-D Sections of 3-D Arrays					
Pentagonal Dodecahedra[250]	5.646	2.032	-0.032	11.61	1.162
Tetrakaidekahedra	5.993	2.506	-0.212	16.03	1.202
Topological Transforms					
Kikuchi I[121]	5.982	2.399	1.208	15.51	1.223
Kikuchi II	6.041	2.072	0.876	12.22	1.120
Maximum Entropy Models					
Almeida *et al.*[10]	5.98	∞	∞	∞	2.130(?)
Vertex Models					
"Exact"[244]	6.005	1.907	1.116	9.516	1.089
"Exact"[243]	5.996	1.286	0.403	4.86	0.844
Soares *et al.*[210]	5.997	2.273	0.740	12.63	1.213

TABLE 8, *continued*

System	$< n >$	μ_2	μ_3	μ_4	W
Theory					
Vertex Models					
Kawasaki *et al.*[259]					
Model I	5.993	3.277	4.085	36.41	1.401
Model II	5.979	2.544	2.288	20.75	1.239
Enomoto *et al.*[62]	5.980	3.609	6.390	57.50	1.437
Mean Field Theories					
Marder[157]	6.005	1.909	3.287	21.57	0.905
Network Models					
Fradkov *et al.*[76] T1's per T2					
0	5.991	1.111	0.560	4.14	0.765
1	5.554	2.758	0.983	20.36	1.358
2	5.929	2.984	2.089	26.56	1.357
10	5.502	5.170	5.129	66.72	1.886
∞	5.159	7.136	11.168	114.65	2.254
Beenakker[25]	6.00	max=3.2 final=0.25			
Potts Model					
Potts Model[93]	5.978	2.490	2.971	23.22	1.196
Two D Sections of 3 D Mater.					
Blanc and Mocellin[30]					
$\rho(3) = 0.036$	5.264	3.969	5.172	44.41	1.654
$\rho(3) = 0.100$	5.984	3.839	3.660	41.45	1.558
$\rho(3) = 0.050$	5.989	3.174	3.300	30.78	1.403
$\rho(3) = 0.000$	5.976	2.489	2.881	19.18	1.244
Carnal and Mocellin[46]					
$\beta = 0$	5.37	7.156	24.918	206.69	2.120
$\beta = 2$	5.97	3.881	6.921	59.42	1.510
$\beta = 4$	6.005	2.107	2.475	18.77	1.073
$\beta = 6$	5.995	1.342	0.946	6.73	0.835
Kurtz and Carpay[260]	5.748	2.308	0.992	12.91	1.253
3 D Potts Model[15]	5.830	3.736	7.189	61.80	1.492

and found them identical within experimental error, thus showing that the distribution was indeed time invariant. We give Glazier *et al.*'s measurement for the scaling distribution in Fig. 35.

Smith's data for the two dimensional froth had $\mathcal{R} < 1$ (See Table 7), suggesting that he never saw a fully equilibrated froth. His actual distributions were not too different from those of Stavans and Glazier, however, considering the large counting error in his small sample. His measured growth exponent of $\alpha = 1$, on the other hand, suggests that he did observe a scaling state. If his side distribution came from early in the run (he never indicates when he made the measurement), it would resolve the apparent contradiction. Aboav observed the same sequence of events, with $\mathcal{R}$ increasing monotonically, and the large n tail of the distribution broadening (See Table 7), but, as we noted in discussing his value for the growth exponent, stopped his measurement just before the froth reached its scaling state (only his last data point had $\mathcal{R} > 1$) so he did not observe the subsequent narrowing and equilibration of the distribution.

In Fig. 36 we show evidence from Stavans and Glazier, that the scaling state is universal for the soap froth. They measured the second moment versus time for an initially ordered helium froth (that shown in Fig. 16 (d) and 9 (a)) and an initially disordered air froth (that shown in Fig. 16 (f) and 9 (b)). The initially ordered froth started with a very small μ_2 which increased rapidly to a maximum value of $\mu_2 = 2.65$, (at about 9 hours, corresponding to Fig. 16 (d) point D and Fig. 9 (D)) at the time when the rate of area

increase was maximal. μ_2 then dropped rapidly, reaching a constant value of $\mu_2 = 1.4 \pm 0.1$, at around 15 hours when the rate of growth rolled over into a power law (Fig. 16 (d) point E and Fig. 9 (E)). In the initially disordered froth the value of μ_2 first dropped for about five hours (thus confirming the initial drop in ∂ shown in Fig. 16 (f)). At these early times there were many bubbles and the moment estimates were sufficiently accurate that the drop cannot be a counting error fluctuation. μ_2 then recovered, reaching a constant value of $\mu_2 = 1.4 \pm 0.1$, at around 50 hours when the rate of growth rolled over into a power law (Fig. 16 (f) point C' and Fig. 9 (C')). Thus the final value of μ_2 was independent of the diffusing gas and of the initial configuration of the froth. In both cases the scatter increased as the number of bubbles decreased at long times. There was no evidence of any significant trend at long times, the slight decrease in the last few values of μ_2 apparently occurring when the expected number of nine-sided bubbles dropped below one. If we reject these points, our estimate of the equilibrium value of μ_2 would increase slightly to $\mu_2 = 1.45 \pm 0.1$ for both the initially ordered and initially disordered froths. In contrast, Aboav observed a monotonic increase in μ_2 from 0.242 to 2.86, as we would expect for observations made during the froth's equilibration (See Tables 7 and 8).

We show the same quantities calculated by Glazier *et al.* (for the air froth shown in Fig. 17) in Fig. 37. The scatter is larger than in Fig. 36 because they analyzed only a 30% sample of the total experimental image. The last few points represent only about six bubbles each. Digitization errors also

resulted in the creation of some spurious many- and few-sided bubbles. The distributions were rechecked by hand, but some errors doubtless remained to contribute to the scatter. We observe the same basic pattern as in Fig. 36. The initially narrow distribution (small value of μ_2) widened to a maximum width of $\mu_2 \approx 3.25$, then narrowed to a stable value of $\mu_2 = 1.6 \pm 0.2$, in agreement with the value of Stavans and Glazier, at the same time as the rate of area growth rolled over into a power law ($\approx 10,000$ minutes, see Fig. 17).

The higher moments behaved similarly. We have calculated the evolution of μ_3 (Fig. 38), μ_4 (Fig. 39) and W (Fig. 40) from the data of Glazier *et al.*. The third moment, which measures the asymmetry of the distribution, in this case mostly the strength of the large n tail, began near zero, increased rapidly to a maximum during equilibration when the frequency of many-sided bubbles was maximal ($\mu_4 \approx 4.5$), then dropped to a stable value of $\mu_3 = 1 \pm 0.5$. The graph suggests that μ_3, may have undergone a second oscillation, undershooting the stable value around 10,000 minutes and reaching a second slightly lower maximum of $\mu_3 \approx 2.5$ around 20,000 minutes. If so, it is a surprising confirmation of the prediction by Beenakker that equilibration should require multiple oscillations.[25] Nothing changes if we look at the fourth moment which represents the flatness of the distribution, essentially the relative strength of $\rho(4)$, $\rho(7)$, and $\rho(8)$ versus $\rho(5)$ and $\rho(6)$. The initial value was $\mu_4 \approx 5$. It then grew to $\mu_4 \approx 40$ and decreased, with a possible oscillation and second peak at 20,000 minutes, to a stable value of $\mu_4 =$

6 ± 3.5. We call the initial maximum in all the distribution functions, the **equilibrating maximum.**

We might speculate that the second maximum we observe in the third and fourth moments represents the decay of next nearest neighbor correlations while the first peak represents the decay of nearest neighbor correlations. In that case the time between the peaks would represent the time for an average bubble to disappear, and hence for disorder to propagate a distance of one bubble radius. The oscillation might also result from a phase lag caused by different time constants for area and side equilibration. However, without experimental values for μ_3 and μ_4 from other experimental runs (in particular those of Stavans and Glazier), we must presume that the apparent oscillation is a statistical artifact, which could result if, for example, a single very many-sided bubble appeared at roughly 15,000 minutes and gradually began to shed sides after 20,000 minutes. We mention this scenario as an example only, since we see no single many-sided bubble in the data to throw off our calculations.

The width (Fig. 40) increased from an initial minimum of $W \approx 0.4$ to a stable value ($W = 1.1 \pm 0.3$) at around 10,000 minutes, with a possible weak maximum of $W \approx 1.3$ at 5000 minutes. Any oscillation at 20,000 minutes was lost in noise.

Returning to our comparison of Glazier *et al.*'s results to those of Smith and Aboav: Smith's original distribution came within one standard deviation of the Glazier *et al.* values for all moments, suggesting that he was reasonably

close to equilibrium.[206] The distribution given by Kikuchi, however, gives unexpectedly low values for all moments, suggesting that it was taken early in a run before the initial equilibrating maximum. If we look at Aboav's final state at $t = 105$ hours, we find elevated values of all moments as expected near the equilibration maximum.

In Table 7 we summarize side distributions for the soap froth, several biological systems, metallic grain growth, rock fracture, and several other systems, as well as many of the models we have discussed. We give corresponding moments in Table 8. We note that in this table we give the moments exactly as calculated from the published distributions, even when it is clear that the exact distribution would give infinite values for the higher moments.

In spite of the large scatter in our measurements, the scaling state side distribution of the soap froth is surprisingly difficult to match theoretically. As typical froth distributions we take the averaged long time distributions of Glazier *et al.* (the first line in the appropriate section of Table 7) and an average of unpublished data of Glazier and data of Stavans and Glazier (the last line of the appropriate section in Table 7) . None of the geometrical models is within range, nor are the maximum entropy models of Rivier, Kikuchi, or Almeida and Iglesias. Among the topological mean field theories, Marder's model is generally within range, but gives an excessively high value of μ_3 because of its correlated side redistribution which tends to make many-sided bubbles gain sides and thus stretches the large n tail. Blanc and

Mocellin's model for two dimensional growth (no nucleation of three-sided bubbles) is equally tail heavy. Fradkov, Shvindlerman and Udler's network model has difficulty matching both μ_2 and μ_3 for a given rate of side swapping, but does a reasonable qualitative job. Kawasaki's vertex Model II does reasonably well with the moments but has far too many four-sided bubbles. Weaire and Kermode's vertex model never reached equilibrium and Frost and Thompson never published side distributions for their boundary dynamics model so we have no data for comparisons from the two most physically appealing "exact" models. The boundary dynamics model of Soares, Ferro and Fortes is very tail heavy.

We plot the side distribution for the hexagonal lattice Potts model in Fig. 35. Referring to Table 7 we find that the predicted values for the $\rho(n)$ are within the measured experimental scatter for all n, though the averaged froth distribution has fewer four- and many-sided bubbles. Looking at the moments, we find that the Potts model again gave consistently larger values than the averaged froth, though within the experimental scatter in all cases. If we compare to the distribution from Glazier *et al.*, the agreement is much better: exact for μ_2 and within 10% for all other moments, with μ_3 a little high, as we expect from the stretched tail.

If we try to match the froth to other experimental coarsening patterns the only experiment that provides a reasonable match is Fradkov, Shvindlerman and Udler's measurement of two dimensional grain growth in Al $+10^{-4}$ Mg foil. The side distributions are similar in shape with $\mathcal{R} = 1.05$ for the

grain growth and $\mathcal{R} = 1.03$ for the froth. The chief difference is the prominence of the tail in the metallic grain growth. Nevertheless, because of the large scatter in both measurements, the measured range of distributions and moments overlap in all categories. Unsurprisingly, Fradkov, Shvindlerman and Udler's network model with the rate of $T1$'s set to be about 5 times the rate of $T2$'s agrees well with their experimental data for the foil. The Potts model also is within range of the results for the foil for all values, though consistently on the low side for the moments.

The apparent failure of topological mean field theories and network models to predict the moments in the soap froth correctly is surprising– but given the large uncertainties in the experimental distributions hardly conclusive. There may be an anti many-sided bubble bias built into the soap froth. Perhaps, we need to include an anticorrelation in side shedding: that many-sided bubbles preferentially lose sides and few-sided bubbles preferentially gain sides, a possible source for this anticorrelation being the deviation of internal angles from the predicted 120°. Another factor may be statistical. Theoretical distributions are usually calculated for large samples, and thus avoid the anti many-sided bias that we have noted in the experimental data.

In the case of the Potts model and metallic grain growth the discrepancy may arise from stiffness caused by anisotropy. The excess curvature which opposes increases in number of sides for many-sided bubbles is masked in the presence of anisotropy. In this case we would expect that the third moment would increase with increasing anisotropy. Unfortunately we have no

data on the dependence of the distribution functions on the relative orientational anisotropies of the Potts model and metal films, though it would be straightforward to design an experiment to test the hypothesis. In particular, for lower anisotropies and higher temperatures, the frequency of many-sided bubbles should decrease. An additional factor may come from the relative rates of diffusion along and across grain boundaries. We expect that the Potts model and metal grains will be further from equilibrium than a soap froth, and hence may eliminate many sided bubbles more slowly, since a bubble may not "know" how many sides it really has. Again, careful measurements using different materials and temperatures could test the hypothesis. Any theory must explain why the metal film gives a larger tail than the Potts model.

We tentatively assert the existence of a universal distribution function for two dimensional coarsening including the soap froth, two dimensional grain growth in metals and the Potts model. It seems that the soap froth has a lower frequency of many-sided bubbles than the Potts model, and the Potts model than real grain growth. However, with our current data we cannot really distinguish the three cases. In particular we have no way to determine whether a larger or smaller frequency of many-sided bubbles is "ideal." We cannot tell whether disequilibria or anisotropies in the Potts model cause a deviation from the ideal coarsening of the soap froth, or whether an anti many-sided bubble bias causes the soap froth to deviate from the ideal coarsening of the Potts model. The mean field and network models may also

belong to this class if proper side shedding anticorrelations are included. All our speculation may be premature, however, since our current poor experimental accuracy cannot distinguish any given soap froth distribution from a Potts model distribution or a metal film distribution. We certainly need better experimental data, especially scaling states for the soap froth with many (i.e. thousands) of bubbles.

Proceeding down our list of experimental categories we come to two dimensional biological systems. Bénard-Marangoni convection patterns in wax also belong in this group. These have narrow side distributions, tightly and symmetrically centered around $n = 6$, with $\mathcal{R} = 0.45 \pm 0.2$, μ_2 between 0.35 and 1, $\mu_3 < 2$, $\mu_4 < 3$ and W between 0.4 and 0.7. The sharp cutoffs in the distributions at $n = 4$ and $n = 7$ are distinctive. The dividing cucumber cells are a special case since they represent a selection rather than an entire pattern, as the large value for $< n >$ shows. We have no difficulty distinguishing these distributions from two dimensional coarsening. The models that work for these systems are the pure geometrical constructions, particularly the relaxed Voronoi, which gives excellent agreement. The network model of Fradkov, Shvindlerman and Udler with no $T1$'s to redistribute sides is also not too far off. In both the models and the experiments the basic physics seems clear. The mobility of cells and territories is small and their area range limited (if they grow too large they split, if too small they die and disappear). The pattern can readjust locally to eliminate stress, but diffusive equilibration does not occur.

Fracture patterns in rock belong to the same non-equilibrating class, with distributions composed almost entirely of five-, six- and seven-sided bubbles. $\mathcal{R}$ ranges from 0.7 for the Giant's Causeway to 1.8 for cracks on Europa, but the moments stay small, with $\mu_2 = 0.6 \pm 0.2$, $\mu_3 = 0 \pm 0.2$, $\mu_4 \approx 1.4 \pm 0.6$ and $W \approx 0.6 \pm 0.1$. Once again we have no trouble distinguishing such patterns from two dimensional coarsening. The models described for biological systems work for geological as well. A slight complication are the various coördination number four patterns whose distribution functions are radically different from the others but which give similar moments to coördination number three fracture, suggesting that the non-relaxational physics is similar in the two cases. It also serves as a warning not to accept similarity of moments as definitive without looking at the actual distribution functions.

We next come to two polymer systems. The photo emulsion has frozen in a broad area distribution generated by a spray from a nozzle. The lipid monolayer began with a similarly broad area distribution but had time to at least partially equilibrate diffusively. The emulsion distribution is exceptionally broad, with $\mathcal{R} = 1.5$, and $\rho(4) > \rho(6)$, with a tail extending to $n = 19$. The monolayer is less extreme, with $\mathcal{R} = 1$, $\rho(4) = 0.125$, and a cutoff at $n = 13$. The moments are correspondingly large and are well separated from those of two dimensional coarsening. We are clearly in a regime where side exchange is a dominant process, and our best agreement with models comes from Fradkov, Shvindlerman and Udler's high $T1$ rate network model (∞ or 10 $T1$'s per $T2$), or the mean field theory of Blanc and Mocellin in the same

limit ($\beta = 0$ or $\beta = 2$). Again, the physical motivation seems clear. The well separated drops can move freely, and easily slide past one another to reduce stress. However their large separation results in slow diffusion rates, hence the failure to reach equilibrium. We will discuss the equilibration of lipid monolayers in a later chapter.

Finally we consider two dimensional sections of three dimensional systems. If we neglect Smiths's measurements for α-iron, a reasonably consistent picture emerges for grain coarsening. The constancy of Beck's measurements of the distributions in aluminum as a function of time suggests that we are safe to assume that the all metallic distribution functions are in scaling states. Taking a rough average over the various metals and ceramics we obtain a "typical" three dimensional coarsening distribution with $\mathcal{R} \approx 1$, $\rho(3) \approx 0.04$, with a relatively long tail, $\rho(9) \approx 0.05$ and $\rho(10) \approx 0.02$. The moments are quite consistent, with $\mu_2 \approx 2.6 \pm 0.2$, $\mu_3 \approx 3.5 \pm 1.5$, $\mu_4 \approx 25 \pm 5$, and $W \approx 1.3 \pm 0.2$. The moments for the polyurethane foam are slightly smaller, probably because its initial condition consisted of nearly uniform volumes and it cured before reaching equilibrium. The vegetable cells, where, as we have discussed, both areas and mobility are constrained, also show lower moments. The poor value of $< n >= 5$ warns us to be cautious in interpreting the vegetable cell data, but both the froth and the cells are in reasonable agreement with the sectioning of a *regular* array of tetrakaidekahedra or dodecahedra, which is reasonable if they are relaxed close packings of nearly equal volume bubbles. The agreement between random and regular

structures also reminds us just how much information is lost taking a two dimensional section of a three dimensional structure.

Two dimensional coarsening distributions and three dimensional coarsening distributions are clearly distinct. The best results for the three dimensional distributions come from the mean field theories of Blanc and Mocellin and Carnal and Mocellin which were designed precisely for this purpose.[30,46] Interpolating for $\rho(3) \approx 0.04$ and $\beta \approx 3$ respectively fits the distribution and all the moments to well within the experimental error. The actual distribution function of the Carnal and Mocellin model is particularly impressive. The three dimensional Potts model gives values of moments much too large and a tail much more extended than our hypothetical "typical coarsening." Whether this disagreement results from finite size or anisotropy effects, or the particular choice of comparisons (we note that the comparisons given in the paper of Anderson, Grest and Srolovitz fit only marginally better),[15] is unclear.

There does seem to be a typical side distribution for two dimensional sections of three dimensional grain growth (and hence, presumably for three dimensional grain growth itself). It is striking that the simplest of topological mean field theories, which assumes no side shedding correlations and independent creation and destruction of three-sided bubbles, and which requires only one rate constant, seems perfectly adequate to describe all of the measured patterns in three dimensions. In two dimensions, on the other hand, none of our theories is entirely satisfactory, and the one that works the

best is also the most complicated and microscopically detailed. As in two dimensions, structures with limited area distribuitions have distinctly different side distributions. The range of scatter in the distributions is narrower in three dimensions than in two, as if the details of what was coarsening mattered less (this is partly an effect of the loss of information from taking a section, but we are still perfectly able to distinguish coarsening from non-equilibrating cellular aggregates and foams). The extra dimension seems to reduce the effects of topological constraints, anisotropy, etc., and paradoxically to simplify the physics, while making exact modeling more difficult.

VI.b Area Distributions

Because we have much less reliable data on the equilibrium area distribution of the soap froth, we will treat the topic of area distributions more briefly than the side distributions, focusing on comparisons to the Potts model simulation. In particular we lack the distributions of bubble radii which are the probabilities calculated by most models. We will not quote the many distribution functions available for metals. We refer the interested reader to the papers of Beck or Anderson *et al.*.[15,24]

If we examine the time evolution of Glazier *et al.*'s area histograms (Fig. 41) for the two dimensional soap froth, $\rho(A/ < a >)$, we find roughly the same scenario that we found for side distributions. At short times the distribution peaks sharply around the average area (corresponding to a pattern composed primarily of uniform sized six-sided bubbles). In time, the most probable size gradually decreases to zero while the large area tail of the dis-

Fig. 41 Area Distribution versus Time. Evolution of the area distribution for an initially ordered two dimensional air froth. Times are: (a) $t = 0$ minutes. (b) $t = 545$ minutes. (c) $t = 1124$ minutes. (d) $t = 1565$ minutes. (e) $t = 2044$ minutes. (f) $t = 3163$ minutes (From Glazier *et al.*1989).[93]

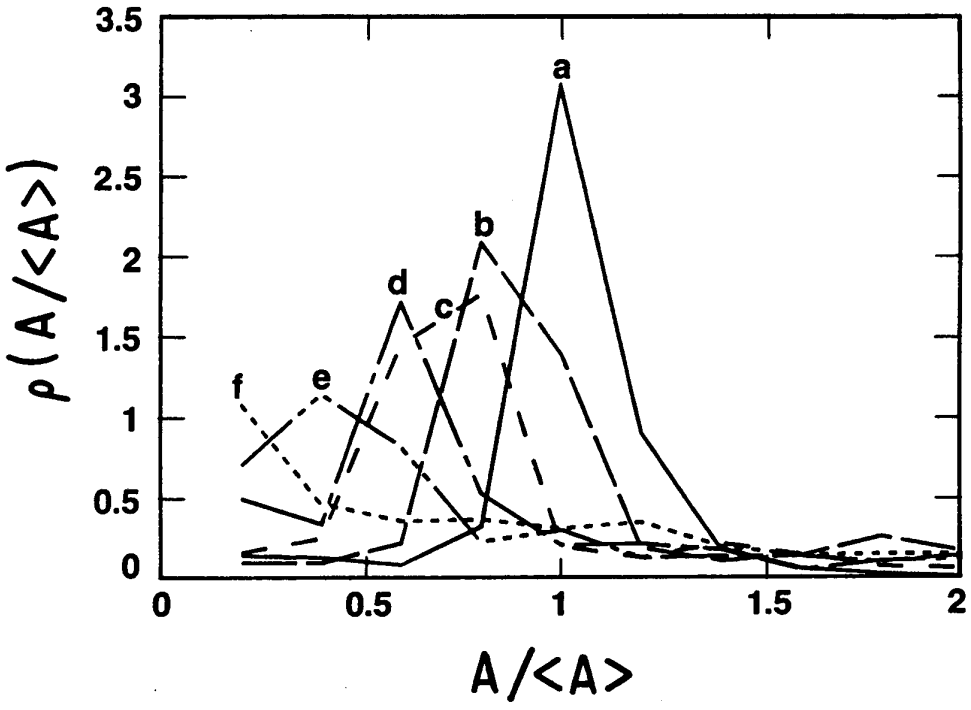
3.5
3
2.5
2
1.5
1
0.5
0
0
0.5
1
1.5
2
ρ(A/<A>)
A/<A>
a
b
c
d
e
f

Fig. 42 Correlated Area Distributions. Area distributions for five-, six-, seven- and eight-sided bubbles in the scaling state. Measurements in air froth (solid line) and Potts model with identical starting conditions (heavy dashed line). Total area distributions are shown for reference for the soap froth (dotted line) and Potts model (light dashed line) (From Glazier *et al.* 1989).[93]

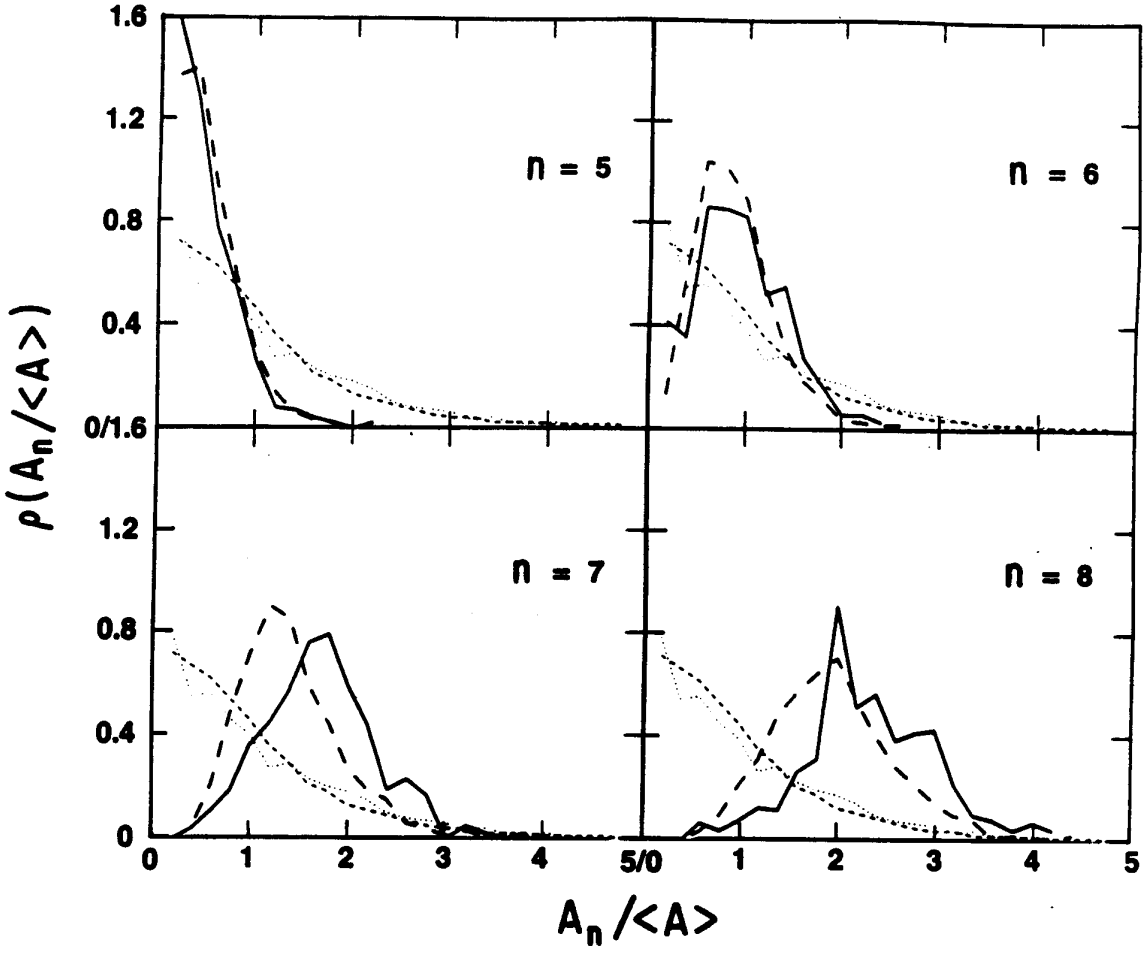
1.6
1.2
0.8
0.4
0/1.6
1.2
0.8
0.4
0
0
1
2
3
4
5/0
1
2
3
4
5
n = 5
n = 6
n = 7
n = 8
ρ(A_n/<A>)
A_n /<A>

tribution gradually lengthens. This broadening comes about because the fraction of shrinking small bubbles with near zero absolute area remains essentially constant, while their relative size decreases as the total length scale increases. Eventually the distribution reaches a time invariant scaling state.

We next examine the scaling state distributions more closely. In Fig. 42 we plot Glazier *et al.*'s area distributions for five-, six-, seven-, and eight-sided bubbles and compare them to the total distribution functions and the equivalent results from the Potts model simulation. As we might expect for bubbles which shrink, the most probable area for a five-sided bubble is zero, agreeing with the Potts model result. Six-sided bubbles have a relatively narrow width around the average area, with good agreement between the experiment and the Potts model. Both seven- and eight-sided bubbles are larger, with broader distributions than the six-sided bubbles. The Potts model seems to give a higher third moment than the actual froth for these types (again we may suppose that this is an anisotropy effect), but the difference is statistically significant only for seven-sided bubbles.

Comparing to other models we find comparable distributions from the various mean field theories, network models and boundary dynamic models. Unfortunately, the error in our measurement of the area distribution and the difficulty of determining exactly how the histograms were constructed, makes the area distribution useless as a diagnostic.

CHAPTER VII

CORRELATIONS

In this chapter we continue our examination of the experimental results looking at correlations between area (or radius) and number of sides, "Lewis' Law," and correlation's between the number of sides of neighboring bubbles, the Aboav-Weaire relation.

VII.a "Lewis' Law"

Of the aggregate quantities derivable from the area distribution functions, the average area of an n-sided bubble as a function of n is the most robust diagnostic. The relationship had been evaluated by Fradkov, Shvindlerman, and Udler, Beenakker, Marder, and others.[27,28,76,77,157] The most commonly assumed relation is that of Lewis, originally proposed for the epithelial cells of the cucumber, that the area of a polygonal cell should be a linear function of its number of sides,[141] i.e.,

$$< a_n >= c_1 + c_2 \cdot n \qquad \text{(VII.1)}$$

at any fixed time, where c_1 and c_2 are fitting parameters.

Glazier, Gross and Stavans have measured this relation by hand for various stages in the evolution of a two dimensional helium froth and Glazier *et al.* from directly digitized images. The hand measured results cover several different times during the helium run indicated in Figs. 16 (d) and 9 (a). The direct digitization results are available for the entire run shown in Fig.

17 and allow us to calculate an ensemble average of different times to improve our statistics. In their hand measurements Glazier, Gross and Stavans estimated areas by connecting the vertices and centers of sides of bubbles by straight lines and measuring the area of the resulting polygon using a digitizing tablet. Since the walls of few-sided bubbles are convex and the walls of many-sided bubbles concave, this method caused them to systematically underestimate the area of few-sided bubbles and overestimate the area of many-sided bubbles by up to a few percent. Glazier *et al.* measured areas directly by counting pixels and should thus have achieved better accuracy.

We present experimental measurements of normalized bubble areas (i.e. $\lambda_n \equiv \frac{<a_n>}{<a>}$) as a function of n in Fig. 43 for the hand measured data and in Fig. 44 for Glazier *et al.*'s directly digitized data along with their results of the Potts model simulation starting with identical initial conditions on the next nearest neighbor square lattice. Beginning with random initial conditions on the nearest neighbor hexagonal lattice gave identical results. We observe that the area for few-sided ($n = 3, 4$) bubbles is larger than that predicted by Lewis' hypothesis, in agreement with the models of Fradkov, Shvindlerman and Udler, Beenakker, Marder, and Weaire and Kermode, but disagreeing with the predictions of Rivier.[198] Lewis' Law is seen to work poorly for few-sided bubbles. Indeed, for many runs, a linear fit actually predicts negative areas for three- and four-sided bubbles. Many-sided ($n > 8$) bubbles are smaller than predicted as well, though this discrepancy may be due to memory of the initial length scale. The correlation seems to be

independent of the degree of equilibration of the froth and the distributions of normalized area are constant to within experimental error (typically 5%) at all times, suggesting that they depend on local rather than long range equilibration. For example, a very large few-sided bubble can rapidly shed sides by $T1$ processes without having to wait for bubbles to disappear.

In Table 9 we present side-area correlations for a few models and experimental systems. We normalize A_6 to one, which is not ideal (we would prefer to look at λ_n) but is at least consistent and does not require us to know $< a >$ for all categories. We can easily distinguish the biological patterns which obey Lewis' law from the coarsening patterns which do not. The correlations for the soap froth and two dimensional grain growth in aluminum are comparable for large n. For small n, the grains are much larger than the bubbles, suggesting a mechanism stabilizing small few-sided grains in the metal. Of the models, the Potts model gives almost identical results to the froth. The vertex model of Nakashima *et al.* also does well. The mean field theories all tend to have both few- and many-sided bubbles too large, again suggesting a failure to consider an anticorrelation in side redistribution. Large few-sided bubbles are less likely to lose sides than small few-sided and large many-sided bubbles, and thus there are fewer large few-sided bubbles produced than predicted by the uncorrelated mean field theories. As we might expect neither the Voronoi construction nor the first model of Almeida and Iglesias are within range. The second model of Almeida and Iglesias does better but is still too weakly correlated.

Fig. 43 Lewis' Law. Normalized average area of an n-sided bubble versus n for a two dimensional helium froth at four different times during a run. (a) $t = 2.52$ hours. (b) $t = 8.63$ hours. (c) $t = 12.45$ hours. (d) $t = 64.32$ hours. To within experimental error the four correlations are identical (From Glazier, Gross and Stavans 1987).[94]

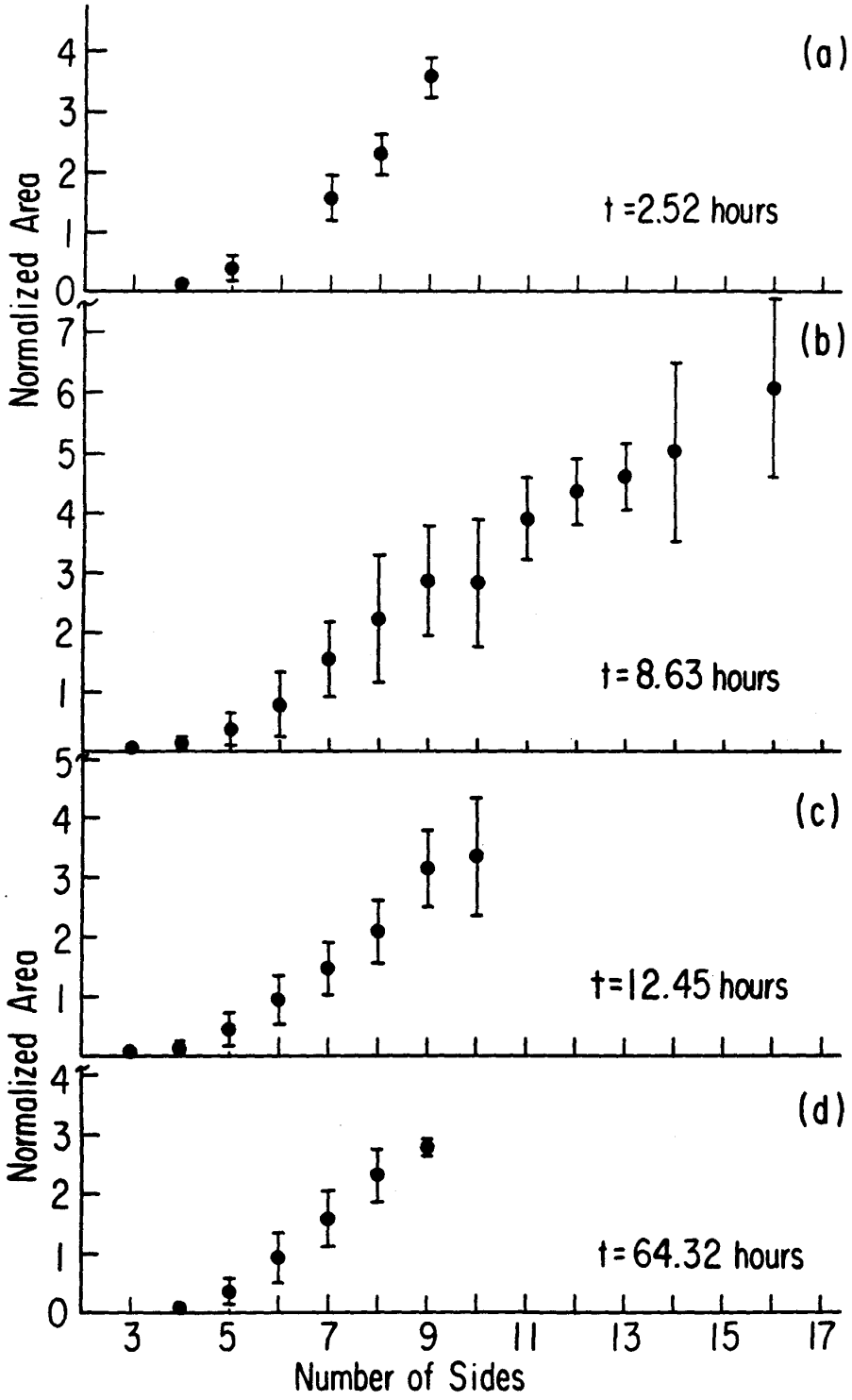
(a)
t =2.52 hours
(b)
t=8.63 hours
(c)
t=12.45 hours
(d)
t=64.32 hours
Normalized Area
Normalized Area
Number of Sides
0
1
2
3
4
5
6
7
3
5
7
9
11
13
15
17

Fig. 44 Lewis' Law. Normalized average area of an n-sided bubble versus n for a two dimensional air froth (circles), $Q = 48$ hexagonal lattice Potts model (triangles), and $Q = 48$ next nearest neighbor square lattice Potts model (diamonds). To within experimental error the correlations are identical (From Glazier *et al.* 1989).[93]

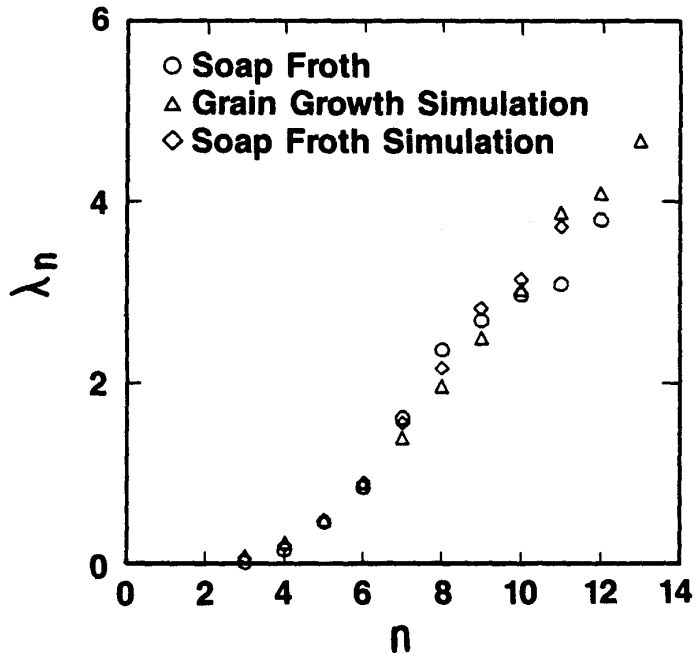
Soap Froth
Grain Growth Simulation
Soap Froth Simulation
λn
n
0
2
4
6
8
10
12
14

Fig. 45 Radius Law. Normalized average radius of an n-sided bubble versus n for a two dimensional air froth (circles), $Q = 48$ hexagonal lattice Potts model (triangles), and $Q = 48$ next nearest neighbor square lattice Potts model (diamonds). To within experimental error the correlations are identical (From Glazier *et al.* 1989).[93]

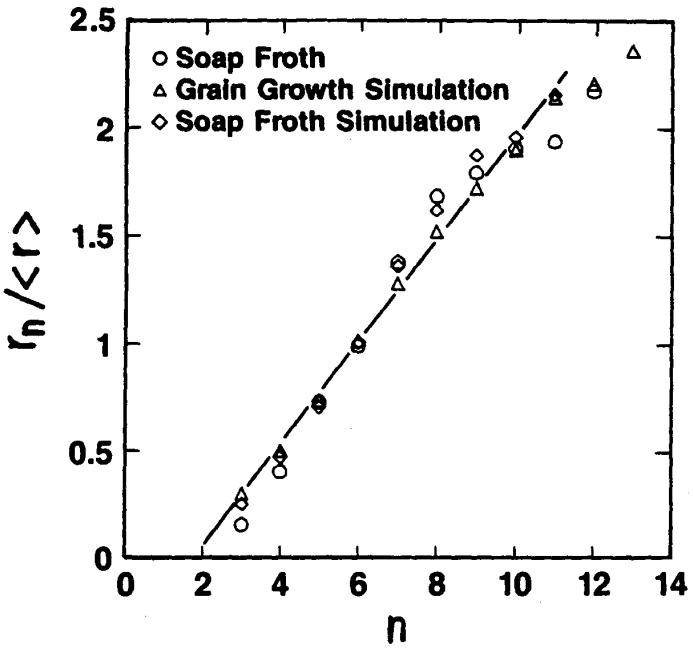
Soap Froth
Grain Growth Simulation
Soap Froth Simulation
$r_n/\langle r\rangle$
n
0
0.5
1
1.5
2
2.5
0
2
4
6
8
10
12
14

TABLE 9

LEWIS' LAW

System	A_3 [A_2]	A_4	A_5	A_6 (A_{11})	A_7 (A_{12})	A_8 (A_{13})	A_9 (A_{14})	A_{10} (A_{15})
Experiment								
Soap Froths								
Averaged Air[95]	0.04	0.18	0.56	1.00 (4.61)	1.96	2.84	3.19	3.75
Averaged Helium	0.05	0.17	0.44	1.00 (4.61)	1.73	2.38	2.96	
Metal Grains								
Al Foil[75]	0.12 [0.16]	0.37	0.56	1.00 (4.35)	1.41 (5.15)	2.12	3.25	3.55
Biological[142]								
Cucumber 100mm	–	0.51	0.76	1.00	1.29	1.49	1.60	
Cucumber 200mm	–	0.52	0.78	1.00	1.21	1.44	1.64	
Amnion	0.42	0.59	0.82	1.00	1.20	1.35	1.59	
Other Materials								
Agfa Film[142]	0.08	0.20	0.46	1.00	1.68	2.43	3.49	4.49
Theory								
Weaire[244]	–	0.12	0.38	1.00	1.39	1.87	2.87	3.17
Almeida & Iglesias (I)[10]	0.66	0.85	0.94	1.00	1.02	1.05	1.06	1.07
Almeida & Iglesias (II)[11]	0.17	0.36	0.63	1.00 (3.60)	1.40 (4.29)	1.89	2.40	2.99
Marder[157]	0.24	0.35	0.56	1.00 (3.18)	1.53 (3.60)	2.04	2.49	2.93
Fradkov *et al.*[76]	0.53	0.53	0.71	1.00 (6.47)	1.96 (7.71)	2.80	3.95	4.91
Beenakker[26]	0.38	0.46	0.62	1.00 (5.35)	1.75	2.63	3.49	4.39
Voronoi[82]	0.51	0.66	0.82	1.00	1.17	1.35	1.55	1.67
Potts Model[98]	0.03	0.23	0.53	1.00 (4.37)	1.83 (4.70)	2.35 (–)	3.07 (5.37)	3.53
Nakashima *et al.*[179]	0.002	0.17	0.45	1.00 (4.36)	1.72 (5.13)	2.39	3.06	3.64

TABLE 10

RADIUS LAW

System	r_3	r_4	r_5	r_6 (r_{11})	r_7 (r_{12})	r_8 (r_{13})	r_9 (r_{14})	r_{10} (r_{17})
Experiment								
Two Dimensional Growth								
Air Froth[93]	0.15	0.40	0.73	1.00 (1.96)	1.40 (2.21)	1.71	1.82	1.93
Al Foil[75]	–	0.48	0.72	1.00 (2.23)	1.13 (2.52)	1.58 (–)	1.93 (2.76)	2.10
Two Dimensional Sections of Three Dimensional Grain Growth								
Tin[64]	0.26	0.49	0.69	1.00 (2.83)	1.23 (2.91)	1.63 (3.31)	1.83 (3.23)	2.37 (3.49)
MgO + LiF[9]	0.25	0.47	0.72	1.00 (2.23)	1.27 (2.45)	1.53	1.73	1.96
Theory								
Topological[76]	0.57	0.61	0.76	1.00 (2.21)	1.38	1.67	1.96	2.13
Vertex Model[179]	0.15	0.36	0.64	1.00 (2.40)	1.56	1.76	1.93	2.15
Vertex[62]	0.16	0.27	0.64	1.00	1.34	1.59	1.66	
Topological[28]	0.62	0.66	0.77	1.00	1.37	1.70	1.99	2.23
Potts Model[250]	0.27	0.49	0.73	1.00 (2.17)	1.34 (2.22)	1.60 (2.39)	1.82	1.95

If we plot instead $r_n \equiv \frac{<a_n>^{.5}}{<a>^{.5}}$ the graph is significantly more linear, with just a hint of S-curve rollover for large n. We show Glazier *et al.*'s result for an air froth in Fig. 45. In this case because of the scarcity of many-sided bubbles we may well be observing a subtle selection effect: large many-sided bubbles are more likely to intersect the frame boundary than small bubbles and are hence more likely to be excluded from consideration, resulting in a lower apparent size for large n. Once again we find that the soap froth, the hexagonal lattice Potts model and the next nearest neighbor square lattice Potts model give essentially identical results.

We have fewer examples where radius correlations are quoted than we have area correlations. We summarize the available data in Table 10. Once again we have used the normalization, $r_6 = 1$. The agreement between the soap froth and the aluminum foil is reasonable, though the foil has slightly larger many-sided grains. Surprisingly, the two dimensional sections of three dimensional grains give results essentially indistinguishable from true two dimensional coarsening. As we would expect, the Potts model and the vertex model of Nakashima *et al.* give the best agreement with experiment. The uncorrelated mean field theories predict excessively large few-sided bubbles. In all cases the overall linearity of the correlation is good, and the radius law

$$< r_n >= c_1 + c_2 \cdot n \qquad \text{(VII.2)}$$

seems verified for both two and three dimensional grain growth, at least for n small enough that we are able to obtain reasonable statistics.

Our conclusion is twofold. First: the radius law seems to work for grain

growth while Lewis' law fails (though the latter works for biological aggregates with constrained area distributions). Second: all of the models that seem physically reasonable give good agreement with experiment, the models that we think of as coming closest to the actual physics, like the Potts model giving the best results. The agreement also provides added evidence for the existence of an anticorrelation in side redistribution, which is apparent in the mean field theory's predictions of larger size few-sided bubbles.

VII.b Aboav-Weaire Law

The simplest side correlation function to measure (and the only one that can be reliably calculated given the available statistics) is the average number of sides of the neighbors of an n-sided bubble, $m(n)$. Assuming statistical equilibrium and short range interactions, Rivier and Weaire have both provided arguments for the form of this function.[134,135,199,236]

Rivier's argument is particularly elegant. In this case $nm(n)$ is the average total number of sides of the neighbors of an n-sided bubble. Consider a bubble with n sides next to a three-sided bubble, and the two common neighbors, a and b. Then

$$nm(n) = n_a + n_b + 3 + n_{other}, \tag{VII.3}$$

where n_{other} is the number of sides of the remaining grains adjacent to the bubble. If the three-sided bubble disappears, the original bubble and its neighbors each lose a side, and the total number of sides of the remaining

neighbors decreases by 2, so

$$(n-1)m(n-1) = n_a + n_b - 2 + n_{other}. \tag{VII.4}$$

Assuming that $m(n)$ is unchanged by the disappearance as it must be in a scaling state yields a recursion relation

$$(n-1)m(n-1) + 5 = nm(n), \tag{VII.5}$$

which is solved by

$$m(n) = 5 + \frac{c}{n}, \tag{VII.6}$$

where c is an arbitrary constant.

We may argue even more simply as follows. Assume that there are no long range correlations or stresses in the lattice. Then topological charge (which represents residual stress) should be locally screened. Consider an n-sided bubble. Its topological charge is $\mathcal{T} = n-6$. Therefore nearest neighbor charge screening requires that the bubble's nearest neighbors must have a total topological charge of $\mathcal{T} = 6-n$. Thus the average topological charge of each neighbor is $\mathcal{T} = \frac{6-n}{n}$, so

$$m(n) = 6 - \frac{6-n}{6} = 5 + \frac{6}{n}. \tag{VII.7}$$

A longer range interaction with weak local correlation will change the constants, but we expect a general form:

$$m(n) = \kappa_1 + \frac{c}{n}. \tag{VII.8}$$

Weaire has argued on physical grounds that the correct form of the relation is

$$m(n) = 6 - a + \frac{6a + \mu_2}{n}, \qquad \text{(VII.9)}$$

where μ_2 is the second moment of the side distribution and a is a constant of order one.[134,135] This relation is known as the **Aboav-Weaire Law.**

In Fig. 46 we present experimental results for $nm(n)$, measured by Stavans and Glazier for a scaling state of a two dimensional helium froth. They found excellent agreement with the Aboav-Weaire law with the second moment of the distribution $\mu_2 = 1.4$ and $a = 1$. Aboav also obtained good agreement for soap froth patterns with μ_2 ranging from 0.24 to 2.86 during the initial transient, using $a = 1.2$. It is reasonable to expect that longer range correlations (i.e. larger values of a) would obtain during a transient which retains some residual order. Similar results also obtain in metal films, and two dimensional sections of three dimensional polycrystals. Since the Aboav-Weaire law depends on the ability of the froth to equilibrate stress locally, it is not surprising that it does not apply to either the Voronoi or Johnson-Mehl models. It does apply to almost all the other models we have discussed. We present a summary of Aboav's Law results in Table 11.

Since the Aboav-Weaire law has two fitting parameters, a and μ_2, the best we can hope for is a general agreement in form among the data presented. In Fig. 47 we show Glazier *et al.*'s comparison between $m(n)$ for the

TABLE 11

ABOAV's LAW

System	$m(3)$ ($m(11)$)	$m(4)$ ($m(12)$)	$m(5)$ ($m(13)$)	$m(6)$	$m(7)$	$m(8)$	$m(9)$	$m(10)$
Experiment								
Soap Froth								
Aboav[8]								
V/1	-	-	6.29	6.03	5.84			
IV/1	-	6.68	6.33	6.09	5.91	5.76		
IV/2	7.49	6.82	6.44	6.11	5.93	5.80		
IV/3	7.86	6.96	6.49	6.19	5.99	5.87	5.76	
IV/6	7.97	7.09	6.59	6.28	6.10	5.95	5.78	
IV/8	8.4	7.4	6.7	6.4	6.2	6.1	6.0	
Glasier *et al.*[93]	8.13 (5.90)	7.31	6.65	6.34	6.19	6.07	6.04	5.87
±	2.43 (1.85)	2.09 (-)	1.58 (-)	1.55	1.55	1.72	2.11	2.01
Grain Growth								
Al_2O_3[30]	8.08 (5.76)	7.06	6.55	6.37	6.23	5.97	5.99	6.04
±	0.34 (0.17)	0.17	0.08	0.08	0.08	0.08	0.11	0.28
Al Foil[77]	6.99 6.06	6.78 (-)	6.60 (6.03)	6.45	6.30	6.22	6.17	6.12
±	0.13 (0.10)	- (-)	- (0.10)	-	-	-	-	0.10
Biological								
Cucumber[142]	-	6.67	6.50	6.18	5.82	5.73	5.79	
Theory								
Network[77]	7.71 (5.75)	7.21 (5.80)	6.69 (5.75)	6.39	6.24	6.14	5.97	5.78
Vertex Model[179]	8.51 (5.82)	7.34	6.64	6.42	6.22 6.04	6.12	5.96	5.88
Potts Model[93]	8.28 (5.82)	7.23 (5.68)	6.65 (5.70)	6.34 (5.63)	6.19	6.07	6.04	5.87
±	2.09 (1.84)	1.77 (1.75)	1.58 (1.75)	1.55 (1.75)	1.55	1.55	1.75	1.65
Static[34]								
Voronoi	6.96	6.68	6.44	6.26	6.10	6.05	5.81	5.74
Johnson-Mehl	7.14	6.60	6.36	6.21	6.13	6.09	5.95	6.02

Fig. 46 Aboav-Weaire Law. Correlation between the number of sides of neighboring bubbles. $m(n)$ is the average number of sides of a bubble next to an n-sided bubble. The dots are taken from an equilibrated two dimensional helium froth. The dashed line shows the prediction of the Aboav-Weaire law using $a = 1$ and the measured value of $\mu_2 = 1.4$ (From Stavans and Glazier, 1989).[220]

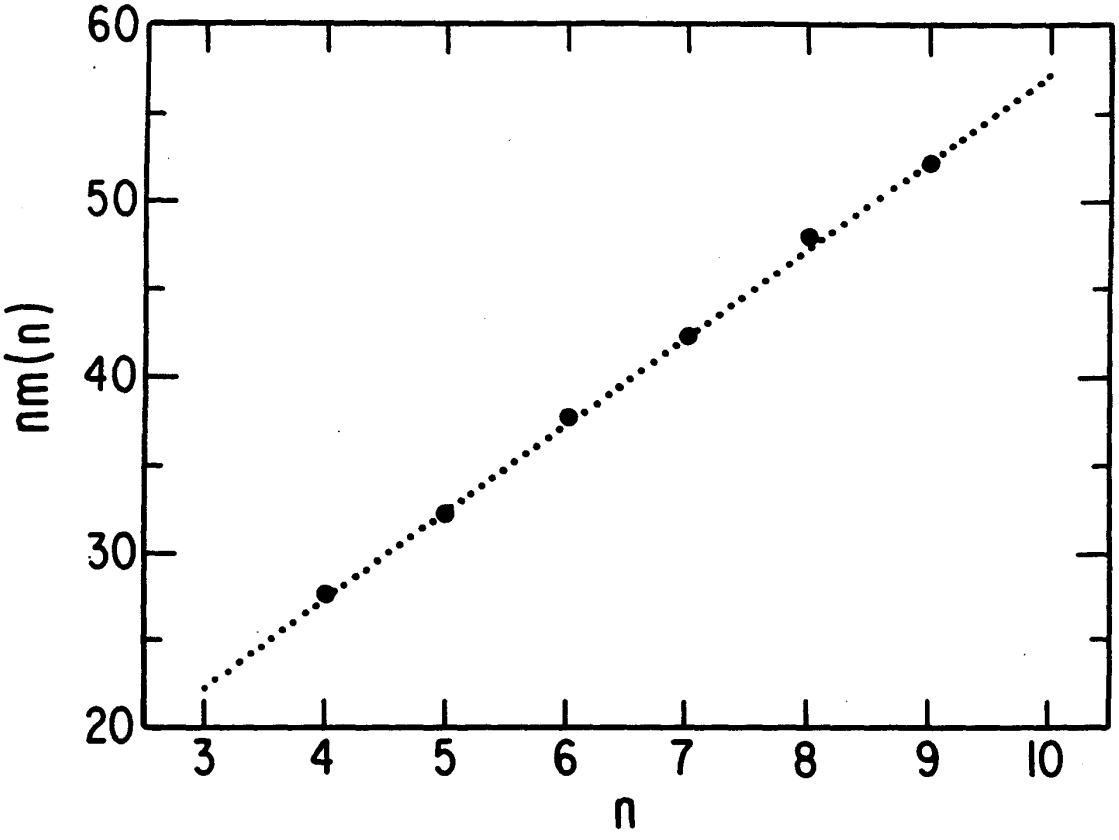
60
50
40
30
20
nm(n)
3
4
5
6
7
8
9
10
n

Fig. 47 Nearest Neighbor Side Correlations. Correlation between the number of sides of neighboring bubbles. $m(n)$ is the average number of sides of a bubble next to an n-sided bubble. The upper points show the value of $m(n)$, the lower points the standard deviation, for a two dimensional air froth (circles), the $Q = 48$ hexagonal lattice Potts model (triangles), and the $Q = 48$ next nearest neighbor square lattice Potts model (diamonds). To within experimental error the correlations are identical (From Glazier *et al.* 1989).[93]

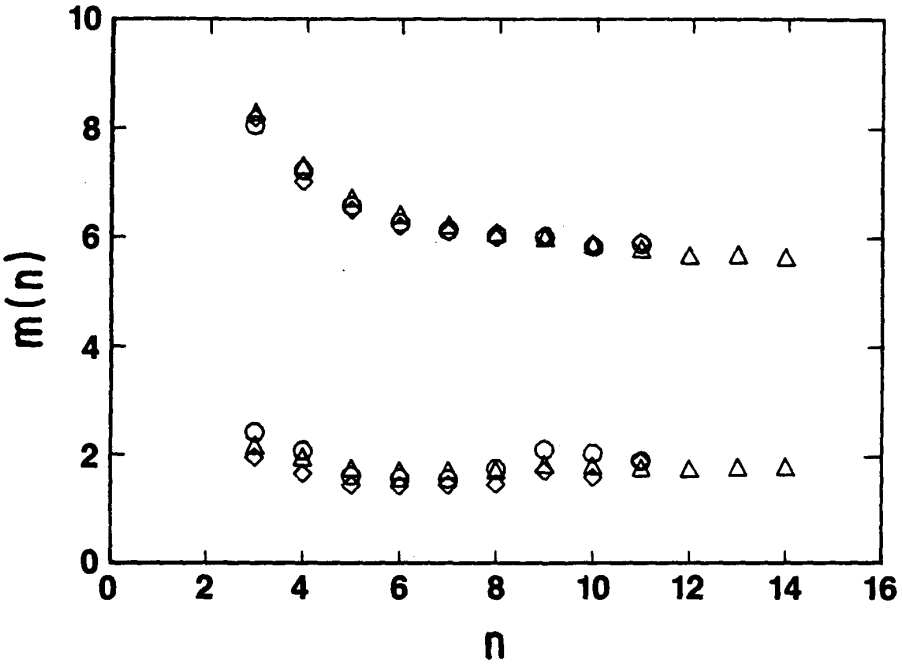
10
8
6
4
2
0
m(n)
0
2
4
6
8
10
12
14
16
n

Fig. 48 Correlated Side Distributions. Side distributions of bubbles next to m-sided bubbles in the scaling state. Solid lines show distributions for a two dimensional air froth, heavy dashed lines for Potts model. The total distribution function, $\rho(n)$, is given for reference, dotted lines for the air froth and light dashed lines for the Potts model (From Glazier *et al.* 1989).[93]

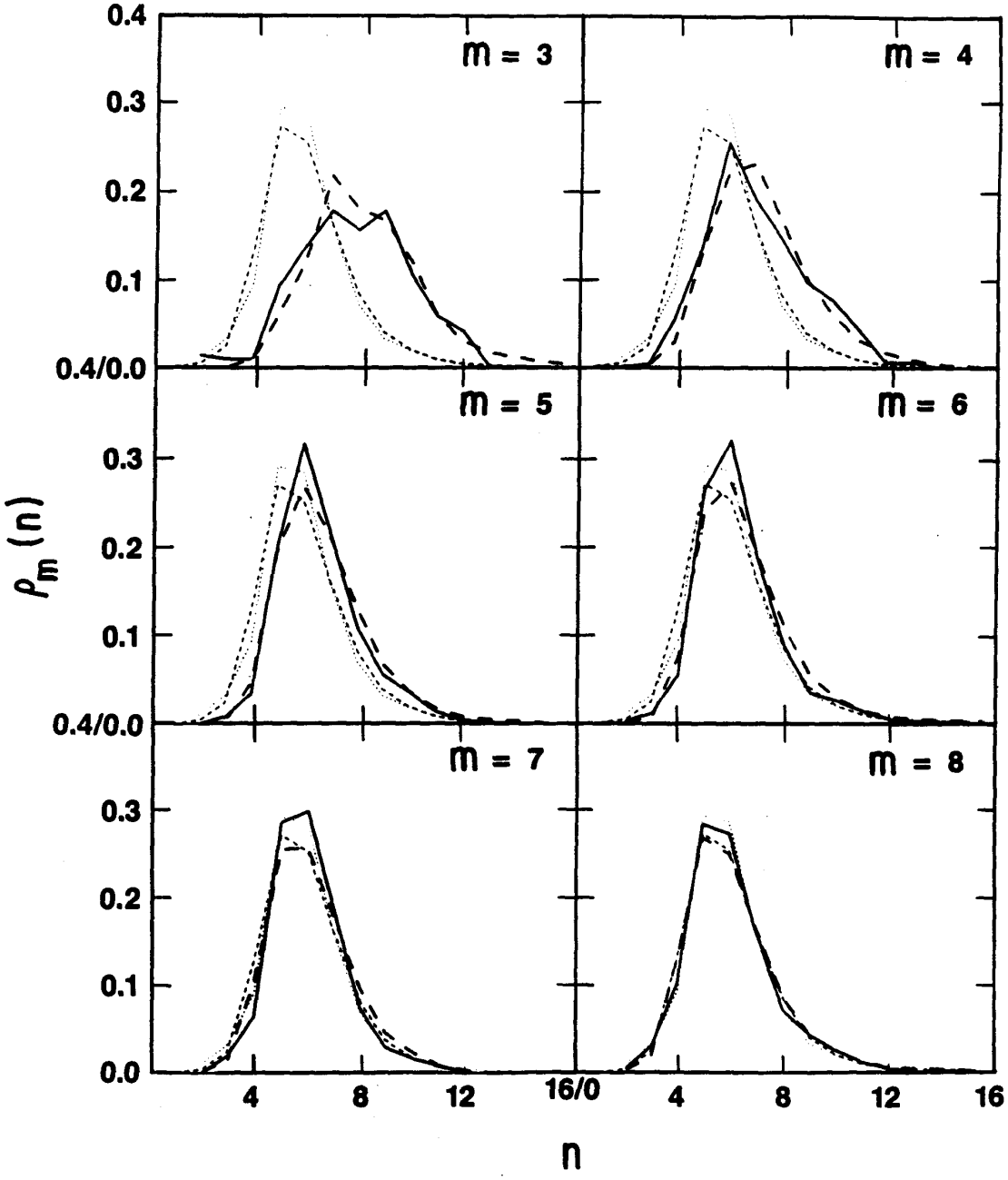
m = 3
m = 4
m = 5
m = 6
m = 7
m = 8
0.4
0.3
0.2
0.1
0.4/0.0
0.0
$\rho_m(n)$
4
8
12
16/0
16
n

soap froth and the Potts model. The results are essentially identical with no free parameters. We can extend the comparison by plotting $\rho_m(n)$ the probability that a bubble next to an m-sided bubble has n sides. We present Glazier *et al.*'s results in Fig. 48 for the soap froth and the Potts model starting with identical initial conditions. As expected we find that few-sided bubble tend to be near many-sided bubbles. The converse does not hold, however. Six-sided bubbles like to cluster together, and seven-sided bubbles attract six-sided bubbles. Even more surprising, the distribution of neighbors of eight-sided bubbles is essentially the total distribution. Discounting the bias towards many- and few-sided bubbles that we have noted in the Potts model, the behavior of the distributions as a function of m is identical for the model and the froth. Of the remaining models for which data are available, only the vertex model of Nakashima *et al.* comes close to reproducing the soap bubble correlation.

CHAPTER VIII

OTHER MEASURES OF DISORDER

We have previously discussed several ways to quantify the equilibration and disordering of a cellular pattern, including dynamical and distribution function measures. One natural way to look at disorder is to calculate an entropy. However, calculating the entropy of a pattern directly is sensitive to low amplitude noise and to lattice discretization. We therefore follow a suggestion made by Gollub for the analysis of the pattern of convective rolls in a large aspect ratio Rayleigh-Bénard cell and measure the entropy of the azimuthally averaged two dimensional Fourier transform of the pattern:[97]

$$\tilde{f}_0(\bar{\mathbf{k}}) \equiv \int f(\bar{\mathbf{x}}) e^{i\bar{\mathbf{x}}\cdot\bar{\mathbf{k}}} d\bar{\mathbf{x}}$$

$$\tilde{f}(\bar{\mathbf{k}}) \equiv \frac{\tilde{f}_0(\bar{\mathbf{k}})}{\int \tilde{f}_0(\bar{\mathbf{k}}) d\bar{\mathbf{k}}} \qquad \text{(VIII.1)}$$

$$S(f(\bar{\mathbf{x}})) \equiv \int \tilde{f}(\bar{\mathbf{k}}) \log(\tilde{f}(\bar{\mathbf{k}})) d\bar{\mathbf{k}}$$

This function depends in a simple way on the length scale, L, of the pattern $\tilde{f}(\bar{\mathbf{x}})$ as

$$S(f(L\bar{\mathbf{x}})) = S(f(\bar{\mathbf{x}})) + \delta \log(L), \qquad \text{(VIII.2)}$$

where δ is the dimension of the Fourier transform. For two patterns with the same basic length scale, a larger value of S indicates a more disordered pattern. In Fig. 49 (a) we plot $S(f(\bar{\mathbf{x}}))$ versus $\log(\langle a^{.5} \rangle)$ for Glazier *et al.*'s two dimensional air froth. For moderate length scales (late times) we observe (with some scatter due to poor statistics) the expected linear relationship.

Fig. 49 Spectral Entropy. (a) Spectral entropy versus time for a two dimensional air froth. (b) Spectral entropy versus the logarithm of the mean bubble radius for the same froth (From Glazier *et al.* 1989).[93]

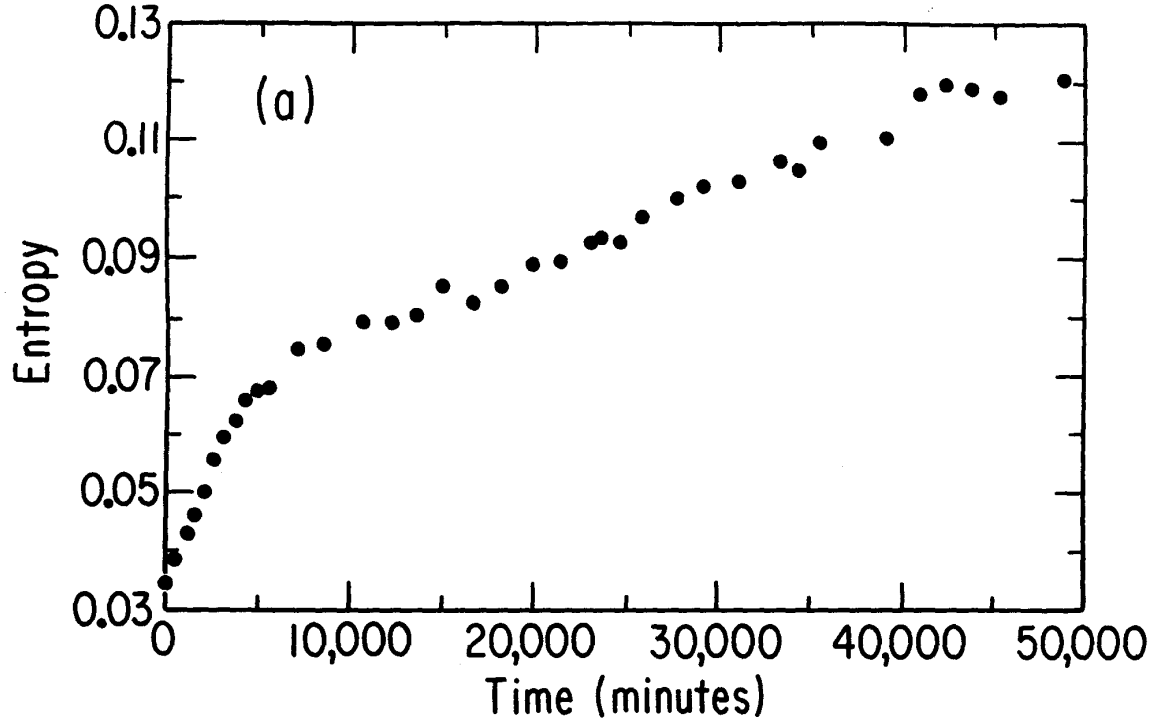
(a)
Entropy
0.13
0.11
0.09
0.07
0.05
0.03
0
10,000
20,000
30,000
40,000
50,000
Time (minutes)

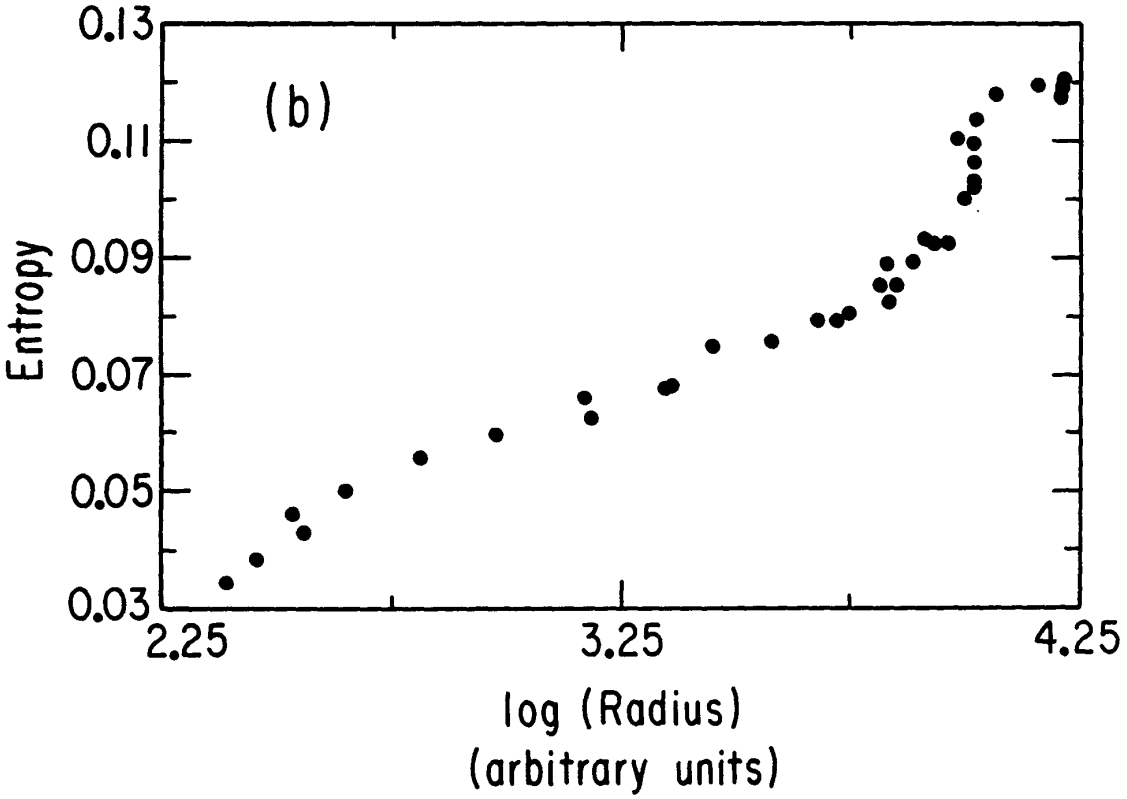
(b)
Entropy
0.13
0.11
0.09
0.07
0.05
0.03
2.25
3.25
4.25
log (Radius)
(arbitrary units)

Fig. 50 Radius versus Time. Mean bubble radius versus time for the two dimensional air froth shown in Fig. 49. Note the nonmonotonic scatter at long times due to edge effects (From Glazier *et al.* 1989).[93]

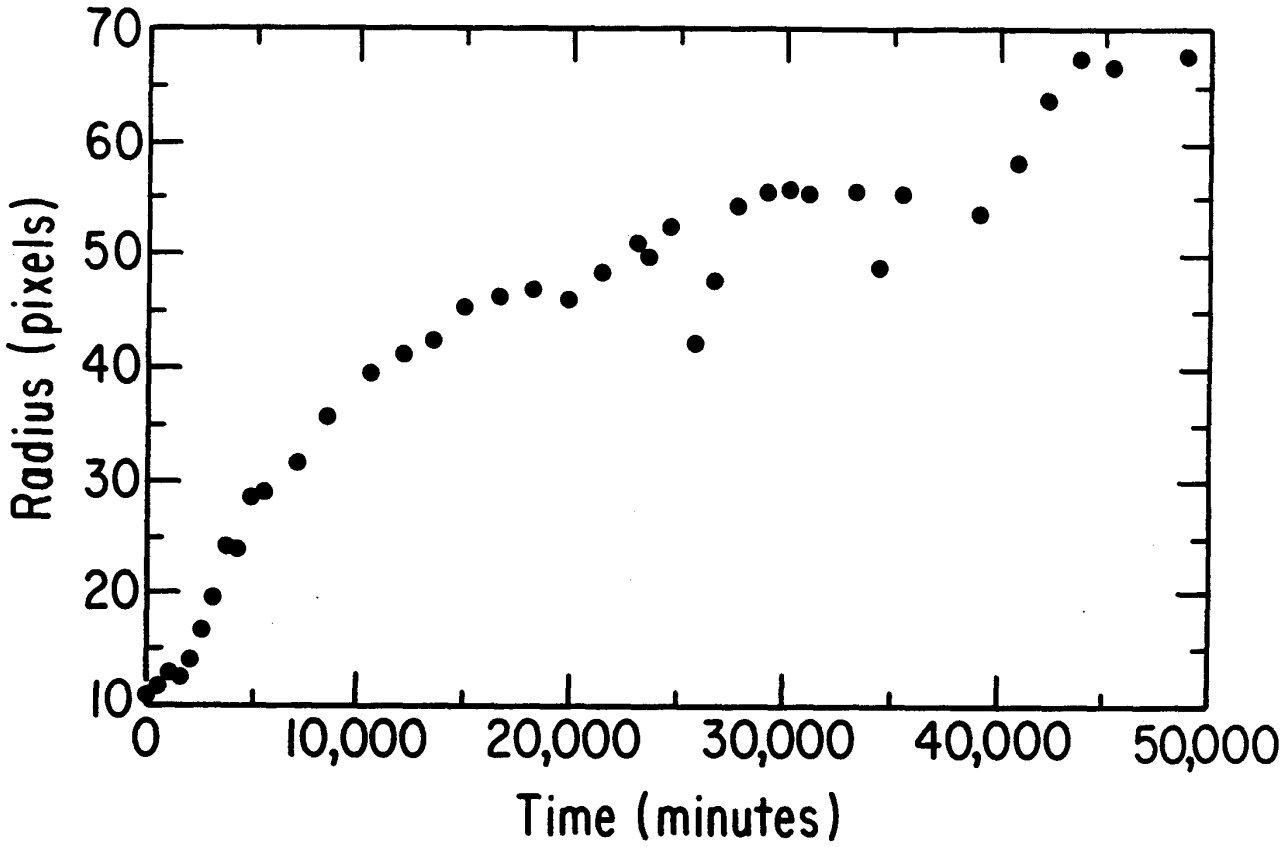
70
60
50
40
30
20
10
Radius (pixels)
0
10,000
20,000
30,000
40,000
50,000
Time (minutes)

Fig. 51 Perimeter/Area Ratio. Ratio of perimeter to area as a function of time for the two dimensional air froth shown in Fig. 49. The ratio reaches a constant value around 8000 minutes, when the froth reaches its scaling state (From Glazier *et al.* 1989).[93]

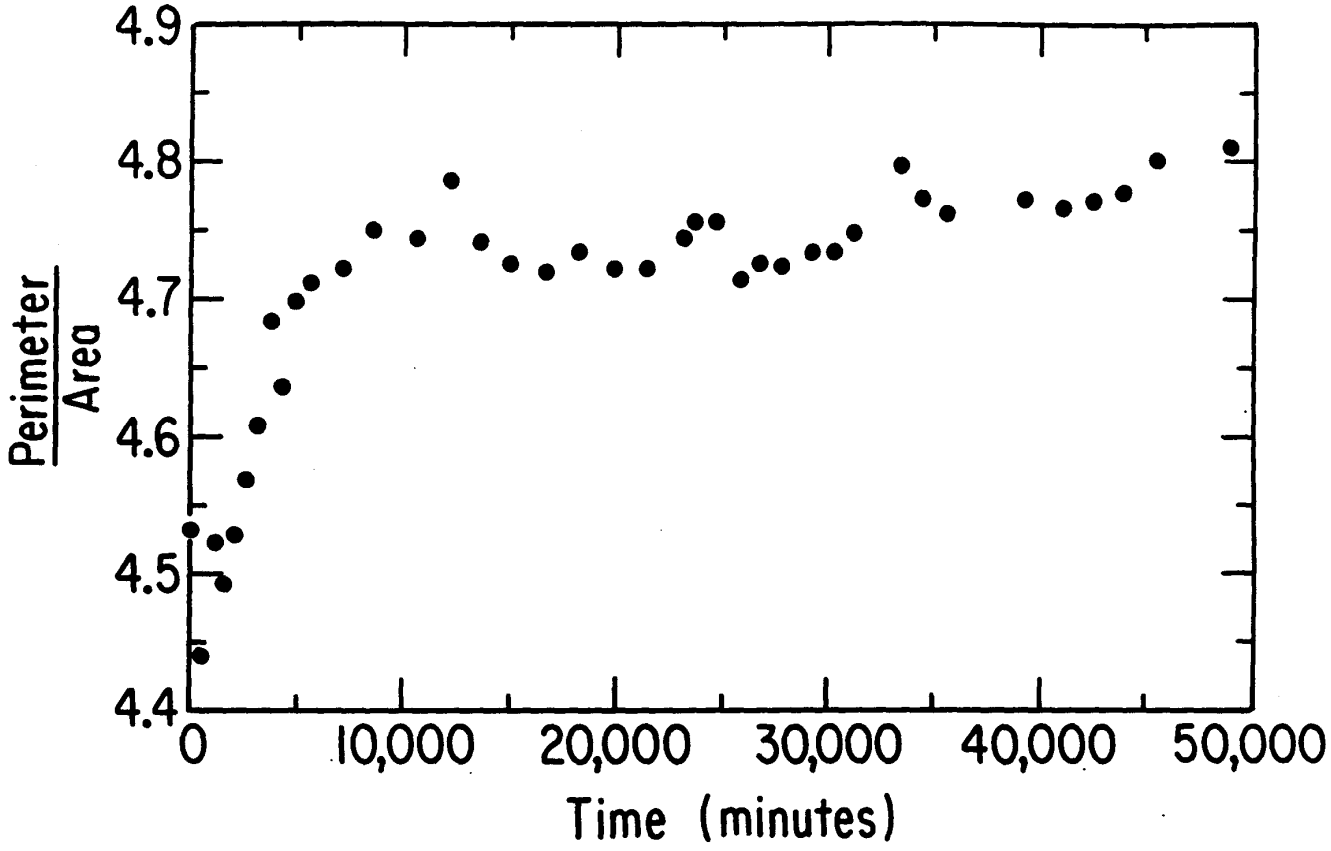
4.9
4.8
4.7
4.6
4.5
4.4
Perimeter / Area
0
10,000
20,000
30,000
40,000
50,000
Time (minutes)

At short length scales (early times), $S(f(\bar{x}))$ lay below the extrapolated line, indicating that the disorder of the pattern was increasing. As expected, the entropy reached equilibrium at approximately the same time as other measures of the disorder. At very long times the entropy rose abruptly above the extrapolated line. Most of this rise was due to non-monotonic fluctuations in the measured average bubble radius (See Fig. 50) at long times and does not represent a real change in the rate of entropy growth. If we plot instead, $S(f(\bar{x}))$ versus time (Fig. 49 (b)) we see a smooth increase in entropy, with a large slope during equilibration when the pattern was increasing in disorder and a smaller constant slope at long times when the pattern was merely increasing in length scale.

A disadvantage of the entropy method is its sensitivity to noise due to our difficulty in accurately measuring the average length scale of the pattern. However, its general applicability makes it a technique worth developing further.

Another technique to examine the stationarity of the pattern is to measure the ratio of the mean bubble circumference to the mean bubble radius as a function of time. We plot Glazier *et al.*'s values for the ratio versus time in Fig. 51. The ratio reached its equilibrium value of $4.73 \pm .4$ after approximately 8000 seconds, agreeing with the other measures of system equilibration.

CHAPTER IX

THREE DIMENSIONAL FROTHS

IX.a Some Thoughts On Three Dimensional Froths

While we have briefly discussed two dimensional sections of three dimensional materials, our previous discussion has focussed on true two dimensional coarsening, like that found in a flat soap bubble cell or a thin metal film. For most applications, however, coarsening occurs in an open geometry in three dimensions and it is the real three dimensional properties, not the properties of sections which are important. In spite of the importance of the problem few detailed studies of the development of true three dimensional structures exist. In the 1940's Marvin and Matzke did some beautiful work on the shapes resulting when spherical lead shot is subject to high pressure and reduced to a dense polygonal mass,[158,160] Matzke *et al.* studied the shape distribution of carefully stacked regular soap bubbles,[161,162] and Lewis studied the shape distributions of three dimensional biological cells.[140,144,147] In the first two cases the systems were not allowed to coarsen in time, either by the nature of the material (lead shot) or the design of the experiment. In the last, biological constraints on the growth of vegetable cells (mitosis of large cells) introduced additional processes which are not typical of normal coarsening. The one complete study of an evolved froth is that of White and Van Vlack,[250] who studied the area and side distributions of a slowly cured polymer foam. Unfortunately, as we mentioned earlier, it appears that the foam had not reached a true scaling state. In addition, Williams' and

Smith measured the shape distribution in Al-1.2%Sn,[252] using stereographic pairs taken with X-rays and viewed under a microscope. Earlier work on grain shapes was done by Desch in β-brass,[54] and Scheil and Wurst in ingot iron.[24] None of these studies examined the dynamics of the pattern evolution.

Theoretical studies of regular and pseudo-regular polyhedral packings are more common, beginning with Lord Kelvin's famous paper demonstrating that a modified tetrakaidekahedron is the minimal regular packing.[120] The distributions produced by plane sections of regular three dimensional packings have also been extensively studied. Fortes and Ferro have enumerated the allowed three dimensional polyhedra, in order to define the elementary three dimensional processes.[72,73] Besides the studies of Blanc and Mocellin and Carnal and Mocellin on two dimensional sections, direct simulations of three dimensional coarsening are few. Kurtz and Carpay go to great length to develop the formalism for a true topological mean field theory, but then make a variety of *ad hoc* assumptions that greatly reduce the usefulness of their model.[132] The generality of the various radius based mean field theories means that their predictions are usually independent of dimension, and so they may be considered three dimensional models, but the only true three dimensional models of grain coarsening are the Potts model simulations of Anderson *et al.*.[12,15] Without more detailed experimental data, it is difficult to evaluate the accuracy of their results.

Except for the Potts model studies, none of this work is of the sort to appeal to a physicist. Besides the now discredited idea that a froth was

an imperfect realization of an optimal regular packing, the work on three dimensional froths has concentrated on details and special cases with little effort to elucidate general principles.

IX.b Why is the Three Dimensional Case Difficult?

Why is the three dimensional case so relatively neglected? The basic problem is experimental. It is much harder to measure a three dimensional than a two dimensional structure. Just recording the state of the system in an unambiguous way becomes difficult. Measuring the volume of foam grains with a syringe or the volume of metal grains by serial sectioning is extraordinarily tedious and slow, while the much broader range of shapes possible in three dimensions means that many more bubbles need to be analyzed to obtain reasonable statistics. Small wonder that most researchers have contented themselves with examining the two dimensional sections of three dimensional materials. This method has two unfortunate consequences. First, since sectioning is destructive, it is impossible to follow the evolution of a pattern. Second, the distribution functions of the two dimensional section are only second order dependent on the real three dimensional distributions. For example, a section of a perfectly regular tetrakaidekahedral packing can result in broad area and number of sides distributions in the section.[53] It is not surprising therefore, that all the mean field theory models which give (or assume) log-normal area distributions agree reasonably well with the

experimental results. They essentially describe the process of taking two dimensional sections rather than the properties of the materials being modeled.

Besides the virtual absence of good experimental data, any theory of the three dimensional froth faces an even more serious obstacle. The basic equations which allow one to write mean field theories for two dimensional froths, von Neumann's law, and the rule that $< n >= 6$, both fail in three dimensions. In fact, the average number of faces, $< f >$ of bubbles in a three dimensional froth can vary considerably, though most experiments yield a value near 14. Instead the relation is

$$< n >= 6 - \frac{12}{< f >}, \tag{IX.1}$$

which adds an inconvenient level of self consistency to any models. Similarly, in three dimensions the average surface curvature of a bubble with tetrahedral angles (109.5°), is not determined solely by its number of sides. Rivier has proposed patching things up with the relation

$$\frac{dA_f}{dt} = \kappa(< f > -f), \tag{IX.2}$$

but his argument is not entirely convincing,[198] and at best applies only to ensembles of bubbles. An additional problem is that the basic scattering processes and elementary shapes are much more complicated. There are many different types of fourteen-sided bubbles, for example. Trying to simulate two dimensional sections in the manner of Carnal and Mocellin's and Blanc and Mocellin's phenomenological mean field theories, though extremely successful at giving distributions does not help us understand the real physics of

the three dimensional froth. Non 120° angles and spontaneous nucleation of bubbles at vertices, remove the characteristic geometrical constraints which are typical of two dimensional froths, without suggesting any way to recover their three dimensional equivalents, and leave us without either von Neumann's law or rates for the elementary processes.

Computer time is the chief problem for the Potts model simulation (which is the one true three dimensional model which has been successfully implemented), especially because the fraction of volume affected by edge effects is much larger in three than in two dimensions. Equilibration times are similarly stretched out making very large systems imperative. Unfortunately, running long time montecarlo simulations on 1000 x 1000 x 1000 lattices is costly to say the least.

IX.c Existing Results

For detailed distributions broken down by topological categories of bubbles, we refer the reader to the papers of Matzke and Fortes and Ferro.[72,73,161] Rhines and Craig have measured the steady state face distribution in Aluminum.[194] Anderson, Grest and Srolovitz have summarized the existing data on metallic grain growth and the Potts model.[15] Besides the Potts model work, the only interesting theory for three dimensional grains is the topological mean field theory of Kurtz and Carpay.[132] Their comparisons to experiment are elaborate but not well chosen from a physicist's point of view, since they never really show that the model reproduces the most important characteristics of a real metal (for example the side distribution).[133]

IX.d Where do we go from here?

Fortunately many of the two dimensional models we have described can be extended in a straightforward manner to three dimensions. We describe briefly a few possible methods for extending simulations to three dimensions.

Three dimensional topological network models are no more difficult than network models in two dimensions, provided that we accept Rivier's three dimensional von Neumann's law. The scattering table is longer, but no more complicated in principle than in two dimensions, the chief inconvenience being that there are ten or more types of disappearing bubbles rather than three.

Three dimensional vertex models are extremely attractive because their dynamics is identical to that in two dimensions. If we select, for example, the model of Fullman, [86] we may immediately write the three dimensional equations of motion:

$$\vec{v}_i = \vec{f}_i \frac{|\vec{f}_i|}{\sum_{\substack{j=1,4 \\ neighbors}} (\vec{x}_i - \vec{x}_j) \cdot \vec{f}}, \tag{IX.3}$$

where we define the force on a vertex j by

$$\vec{f}_i = \sum_{\substack{j=1,4 \\ neighbors}} \frac{\vec{x}_i - \vec{x}_j}{|\vec{x}_i - \vec{x}_j|}. \tag{IX.4}$$

We note again that we have no *a priori* physical argument to derive these equations. However, their excellent agreement with two dimensional experiment suggests that if we accept them as phenomenologically correct we will not be too far wrong, especially since the work of Blanc and Mocellin and

Carnal and Mocellin indicates that three dimensional models are less dependent on details than two dimensional models. One minor difficulty in three dimensions is that it becomes much harder to define the inside and outside of a bubble. Perimeter tracing no longer works. Thus we need to set the dynamics on top of a topological network that we can use for bookkeeping purposes. Computationally, the effort goes up linearly in the number of vertices, allowing us to contemplate extremely large simulations, which should be able to reach the scaling regime in an unambiguous fashion. We are currently designing a model along these lines.

Boundary dynamic models also extend well from two to three dimensions with the added bonus that the underlying physics is correctly expressed. Indeed, we might hope to measure the three dimensional analogue to von Neumann's law from such a simulation. Laplace's law relating pressure differences to wall curvature is certainly true in three as well as two dimensions so there should be no surprises in the physics. Fortes and Ferro have described such a model but apparently never solved it numerically.[73] Once again the main problems are in bookkeeping. We need to maintain a topological network, and keep track of patches of two dimensional bubble walls, resulting in a computational load proportional to the total surface area of bubble in the system. Nonetheless, the method should still prove much more practical than Potts model simulations and should allow an empirical determination of an extended von Neumann's law.

Experimentally the picture is less promising. In principle it should be

possible to determine the three dimensional structure of a froth using either CAT, NMR or optical tomography. Whether the needed accuracy of resolution is achievable, and if achievable compatible with the timescales of the coarsening process (true three dimensional imaging still uses the ancient method of serial sectioning–though in these cases non-destructive–and therefore remains painfully slow), are unsolved questions, because no one has ever tried the experiments. Clearly, any three dimensional tomographic experiment will generate vast quantities of image data. Nevertheless, the potential payoff would be large both in applications and in providing hard data to the theorists, and the experiment is worth trying. The biological possibilities are even more exciting. One might imagine, in the spirit of Lewis, that cancer cells with their fast division, would produce aggregates with different side distributions from normal cells, and hence provide a diagnostic tool. But such speculations lead us too far from our topic.

CHAPTER X

OTHER COARSENING SYSTEMS

In this chapter we briefly consider two two dimensional systems that coarsen in a manner that appears qualitatively similar to coarsening in the soap froth and in metals: bubble patterns in the liquid-gas phase transition in lipid monolayers and in the magnetic domains of doped iron garnets. Both are distinguished by the presence of long range interactions which lead to a greater variety of phenomena than observable in normal coarsening. Both are also only beginning to be studied experimentally, with few hard theoretical results. Indeed, in the case of the magnetic bubbles it is still not clear what sort of theory is appropriate.

X.a Lipid Monolayers

If we distribute a small quantity of a lipid surfactant on a water surface, the polar lipid molecules align with their heads at the surface of the fluid and their long polymer tails in the air. Depending on the areal density of the lipid and the temperature, "solid", liquid or gaseous two-dimensional phases may form. We can visualize the phase transition if we add a small amount of a second lipid with a tail marked by a fluorescent dye, the fluorescent group being active only in the liquid phase regions. Illuminating the liquid surface with light of the dye excitation frequency then makes it straightforward (with correct filtering) to observe the patterns of the different phase domains, a technique pioneered by Lösche and Möhwald, and McConnell, Tamm and

gas condenses and the interface grows. If we assume that the total surface energy is small compared to bulk energy, then the temperature and pressure of the lipid remain essentially constant (provided the water temperature is carefully controlled). Since we remain at the same point in the coëxistence curve, the total area of liquid and gas remains constant. Since the thermal diffusion time is long compared to the molecular diffusion time, the patterns are well equilibrated, with minimal surface (circular) shapes. Thus the basic mechanisms driving the pattern evolution are similar to those in coarsening.

A fundamental difference from the soap froth is that , since pressure is carried by the connected matrix phase as well as by the fragmented bubble phase, interactions between bubbles can be long range. When the separation between bubbles is small compared to their size we would expect this effect to be small. When the bubbles are well separated it should dominate, and the behavior should be closer to that of Ostwald ripening.

Depending on the point in the coëxistence region chosen, we can obtain either bubbles of gas in a liquid matrix, bubbles of liquid in a gas matrix, or mixtures of both (e.g. patterns with regions of both types, or hierarchical patterns with gas bubbles inside liquid bubbles, inside gas bubbles, etc.). This range of initial patterns is a fascinating topic in its own right which we will not discuss here. Moore *et al.* studied stearic acid monolayers, looking at gas bubbles in a liquid matrix.[169] They were particularly interested in the possible analogy with the two dimensional soap froth. Qualitatively the phenomena they observed seemed very much like those seen in a soap

froth. The pattern itself looked similar to soap bubbles, with small bubbles shrinking and large bubbles growing. They observed both $T1$ (side swapping) and $T2$ processes (bubble disappearance). The overall length scale of the pattern increased monotonically in time. An obvious difference from the soap froth was the variable width of the walls. At short times bubbles were more round than polygonal, becoming progressively more polygonal with time (a behavior more typical of nucleation than coarsening). Quantitatively, they measured the side distribution for their patterns and the mean bubble area versus time. They obtained a growth exponent of $\alpha = 1.1 \pm 0.1$ (See Table 4), in agreement with the expected value for ideal grain growth. Their measured distribution function is rather tail heavy including a thirteen-sided bubble (See Tables 7 and 8), and depends on measurements of only about forty bubbles. They note that the second moment of the distribution was still increasing at the end of their run, a sure indication that they had not yet reached a scaling state. A problem with lipid monolayer patterns is that, because they form by a nucleation process, they tend to start with many very small bubbles and very broad area distributions and therefore take a long time (and a large relative increase in length scale) to equilibrate. The experiment is much faster than in the soap froth since the typical timescales are a few hours and the absolute length scales typically 10 μm to 100 μm. Even so, maintaining temperature and concentration stability over that time is difficult.

Berge *et al.* have recently extended Moore *et al.*'s work, studying gas

bubbles in a liquid matrix using pentadecanoic acid, with a hexadecylamine label.[29] Unfortunately experimental difficulties with image stability and analysis have so far prevented them from making quantitative measurements, but they did observe coarsening with well defined $T1$ and $T2$ processes for a wide range of ratios of matrix area to bubble area. For patterns dominated by bubbles, the evolution looked very similar to that of the soap froth, with walls of uniform width and polygonal bubbles (See Fig. 52). For patterns with more matrix the bubbles were rounder (See Fig. 53) and some ambiguity crept in in determining the number of sides (See Fig. 54), though it is always possible to formally determine nearest neighbors using the Voronoi construction. In the former case the rates of growth appeared to be close to von Neumann's law, in the latter, the rate of shrinkage of small bubbles appeared to depend on the bubbles' size as well as their number of sides. In patterns with extremely narrow walls, wall breakage and grain coalescence occured, but were rare otherwise. Glazier has measured side distributions from ordered ($N = 221$) and disordered ($N = 103$) patterns supplied by Berge (See Tables 7 and 8 and Fig. 55).[92] The "disordered" pattern probably still contained some residual order but its side distribution lay within the experimental range for the scaling state soap froth. On the basis of these observations we may tentatively conclude that the narrow matrix lipid monolayer behaves like an ideal two dimensional coarsening system. The crucial piece of missing information is the dynamics, a measurement of the dependence of the growth rate for bubbles on their number of sides and size.

Fig. 52 Lipid Monolayer Bubbles. Pattern of lipid monolayer bubbles showing well separated round bubbles (Figure supplied by B. Berge 1989).

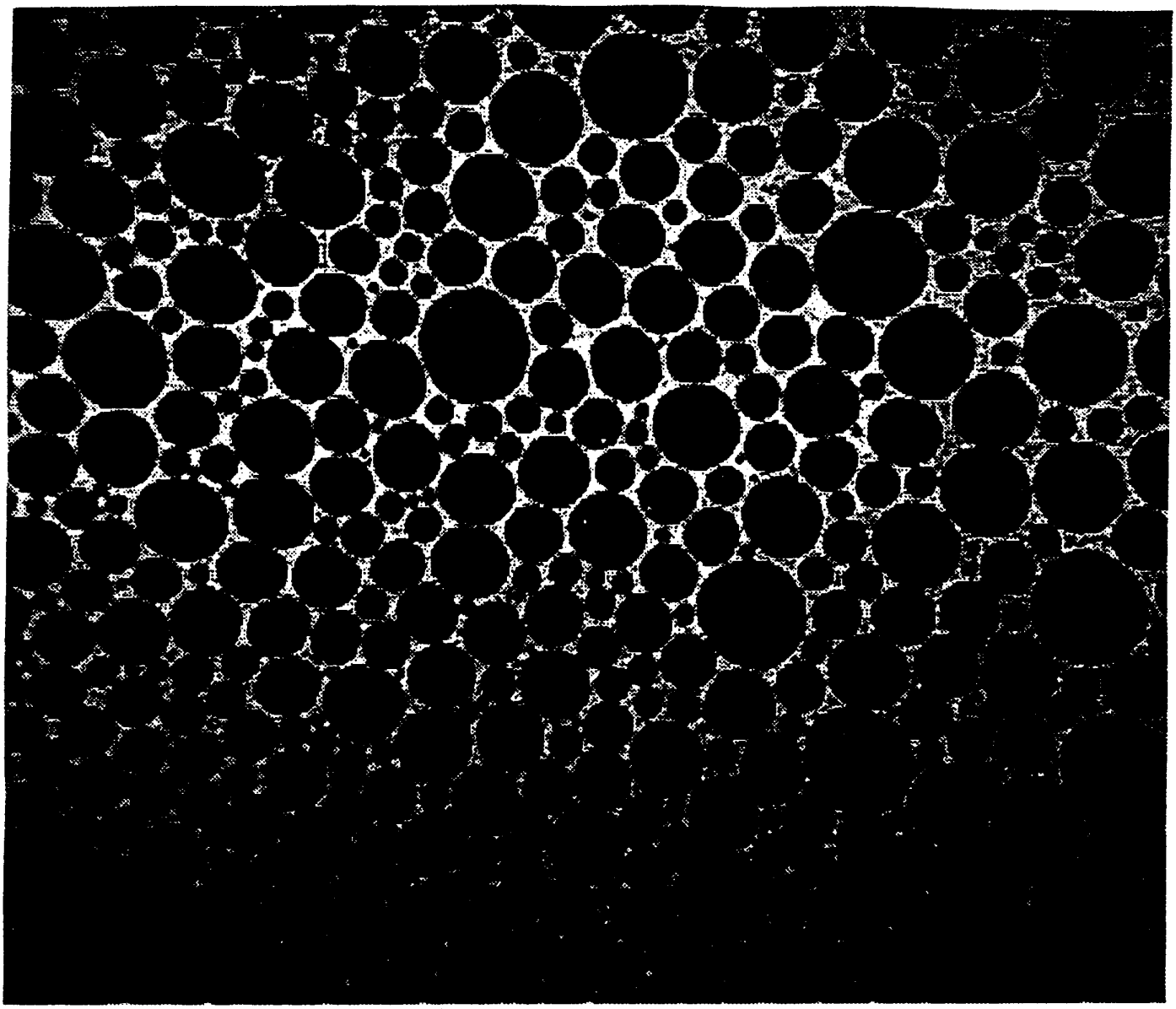

Fig. 53 Lipid Monolayer Bubbles. Pattern of lipid monolayer bubbles showing close packed polygonal bubbles (Figure supplied by B. Berge 1989).

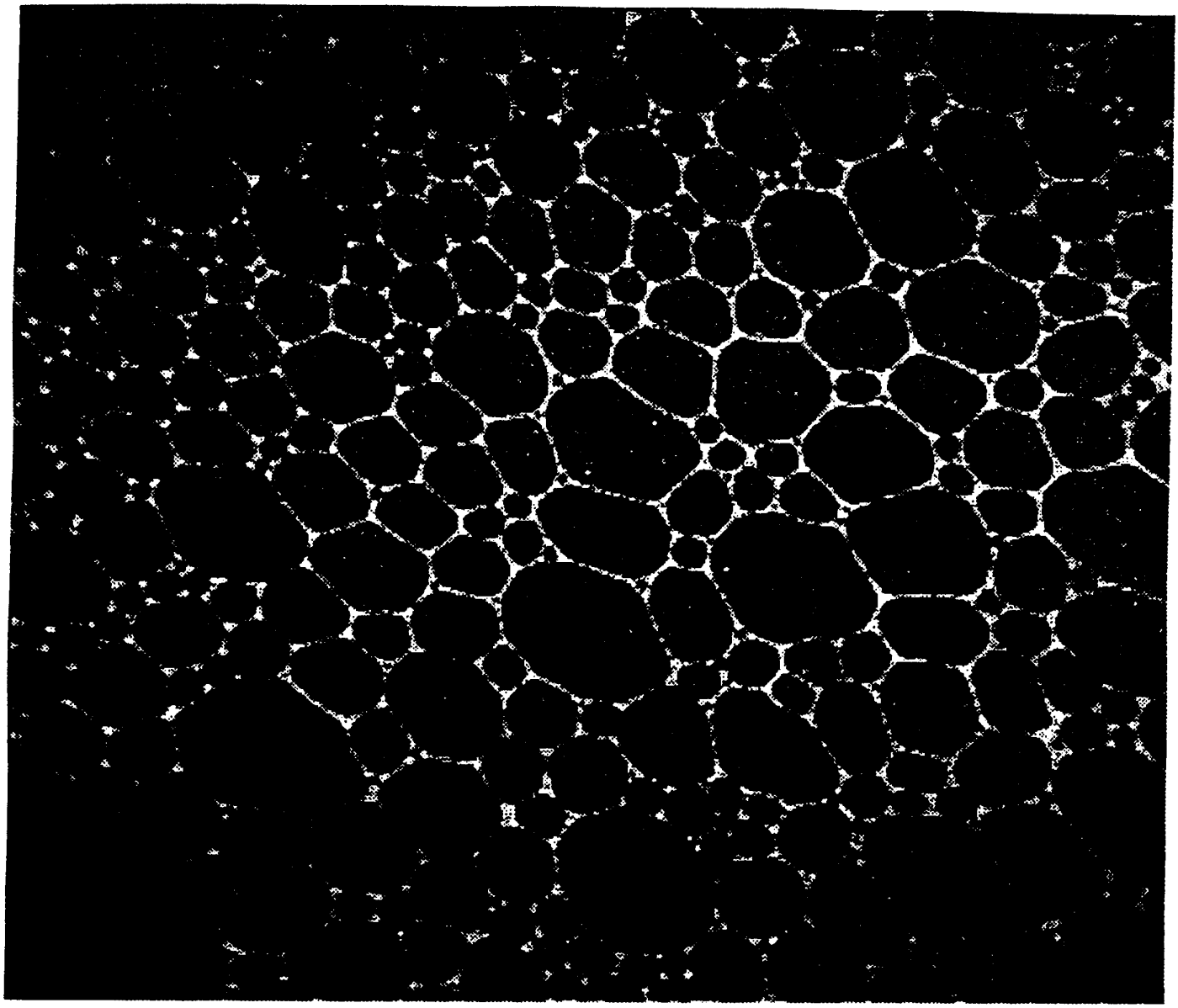

Fig. 54 Ambiguity in Separated Bubbles. (a) A four-sided bubble. (b) A three-sided bubble. In some situations only the Voronoi construction can to distinguish the two cases.

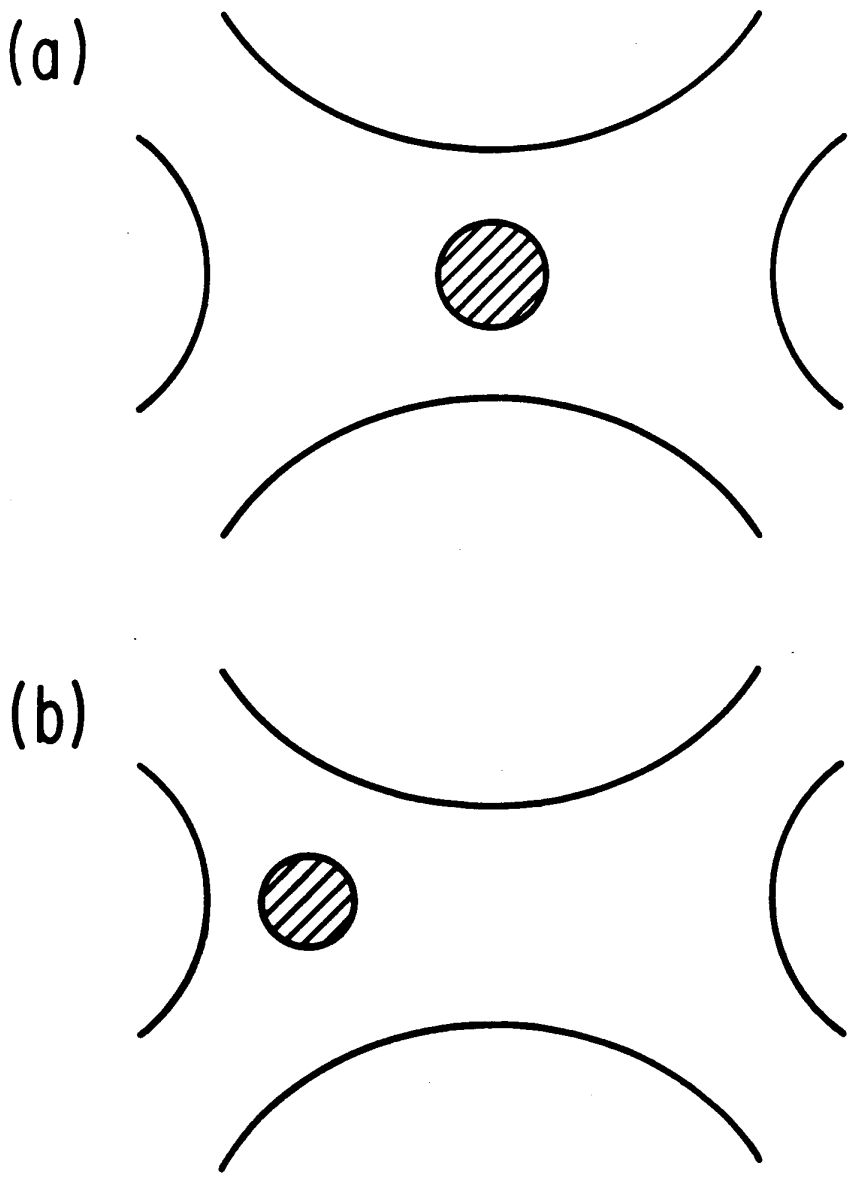
(a)
(b)

Fig. 55 Side Distribution. Side distribution for an ordered and a disordered lipid monolayer pattern. A typical soap froth distribution is given as a comparison.

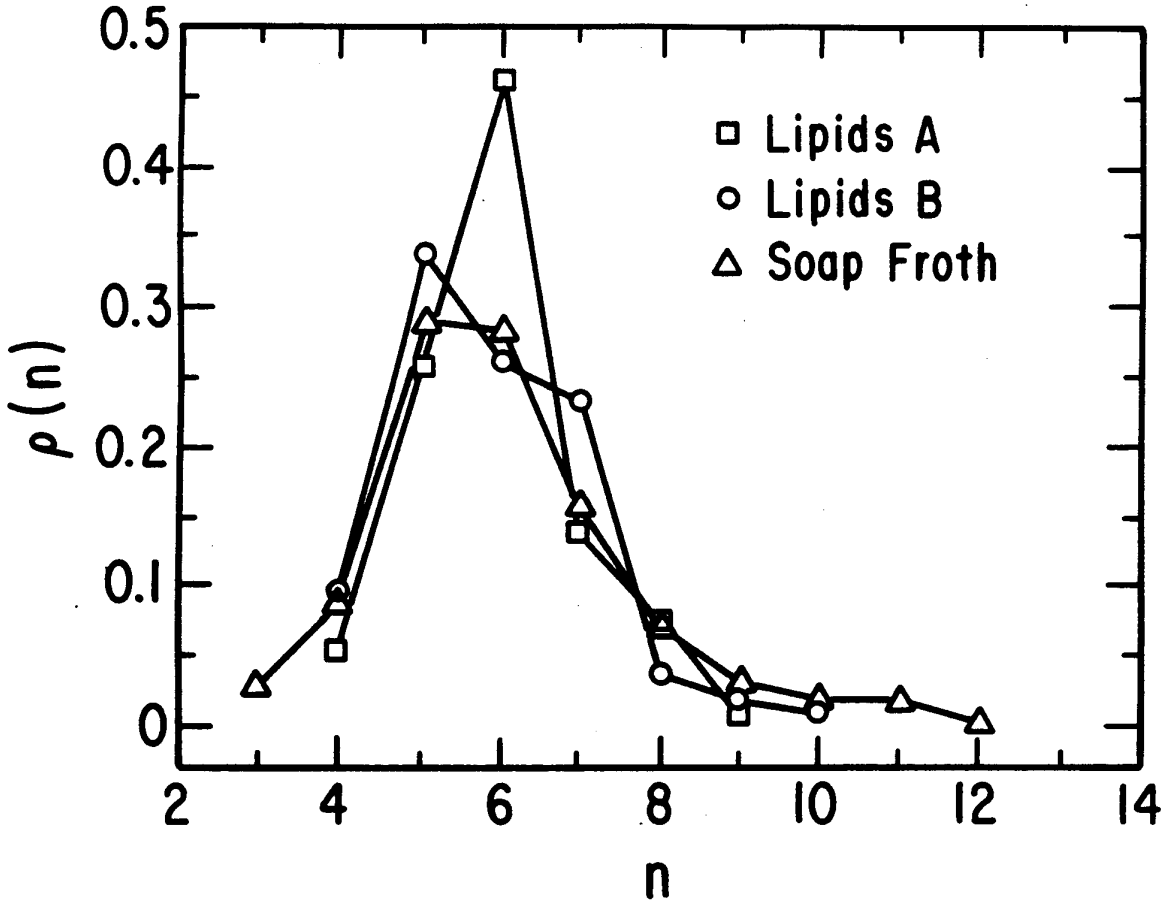
0.5
0.4
0.3
0.2
0.1
0
ρ(n)
2
4
6
8
10
12
14
n
Lipids A
Lipids B
Soap Froth

Based on our concept of the lipid monolayer as intermediate between the soap froth and Ostwald ripening, we suggest that a reasonable form for the growth rate should be:

$$\frac{dA(n,r)}{dt} = (1-\epsilon)\kappa(n-6) + \epsilon\frac{\kappa}{2\pi}(1 - \frac{r}{< r >}), \qquad \text{(X.1)}$$

where ϵ is a fitting parameter that describes the degree of polygonality of the bubbles, being zero for purely polygonal bubbles, and one for infinitely separated bubbles. The form of the second term comes from the requirement that area be conserved. We can easily rewrite any of our mean field and network models using this sort of a fundamental dynamics. We could also write a next order theory to include the dependence of a bubble on the properties of its neighbors, in which we explicitly consider area exchange between all pairs of bubbles:

$$\frac{dA_i}{dt} = (1-\epsilon)\kappa(n_i-6) + \epsilon\frac{\kappa}{2\pi}\sum_j f(|\vec{x}_i - \vec{x}_j|)(\frac{1}{r_j} - \frac{1}{r_i}), \qquad \text{(X.2)}$$

where i indexes the bubbles, $\vec{x}_i$ is the position of the center of the ith bubble and f describes the drop off with distance of the interaction between bubbles. We might also wish to make ϵ a local function of bubble size and separation. Without further experimental data we cannot begin to discuss correlations in side redistribution, local fluctuations, or other second order effects.

X.b Magnetic Bubbles

Throughout our previous discussion we have examined coarsening in time, the basic mechanism in all cases being diffusion driven by energy gra-

dients. Magnetic bubble patterns, in contrast, are usually time independent, with the control parameter being the strength of an applied magnetic field. Generally when the applied magnetic field changes, the pattern evolves rapidly and then reaches a time independent state (sometimes with a few noise driven adjustments at later times). This difference of control parameter allows a variety of experiments impossible in normal coarsening, since it allows us to move "backwards in time" towards smaller length scales. Further complications come in two types. The long range interactions in magnetic systems are longer range and less intrinsically self averaging and support larger gradients than in lipid monolayers. They are also fundamentally nonlinear, which makes them harder to model.

The magnetic bubble patterns that we will discuss are regions of particular spin orientation in thin samples of doped ferri-magnetic iron garnets. The anisotropy of the material is such that the spins tend to align either up or down perpendicular to the material. When viewed in a microscope under crossed polarizers, the Faraday effect makes one spin orientation look light and the other dark. Since the basic exchange interaction is ferromagnetic, like spins clump into macroscopically large patches of a given orientation, and the patterns are easy to visualize.

Because they were once thought to have industrial applications, iron garnet magnetic bubble materials have been studied extensively by engineers and applied physicists.[31,45,63,186,224] There have been analytic calculations of the behavior of isolated bubbles and regular bubble lattices as well as

pattern instabilities.[156,187,212,225,226,235,253] There are a number of interesting questions concerning residual twists in domain walls (Bloch lines), and various kinds of anisotropy which need not concern us directly here.

While a full Hamiltonian for a magnetic bubble pattern would be difficult to write down (and even a moderately complete one is complicated) we need concern ourselves with only a few terms.[63] An applied magnetic field will tend to align spins with it. The domain walls between regions of reversed spin have an energy associated both with the mismatch between neighboring spins and with the local spin misalignment relative to the crystal as the spins rotate (spatially) from one orientation to the other. Finally, regions of uniform spin orientation have a dipole energy created by the self-interaction with the total generated field. In schematic form we may express this as an Hamiltonian:[63]

$$\mathcal{H} = \sum_i \left(-\vec{\sigma}_i \cdot \vec{\mathrm{H}} - \sum_{neighbors\ i} 2J\vec{\sigma}_i \cdot \vec{\sigma}_j \right) + J' \int_{Area} \sin^2(\psi(\vec{x}))d\vec{x} + 2\pi \int_{Area} \mathrm{M}^2(\vec{x})d\vec{x}, \tag{X.3}$$

where i indexes the spins, $\vec{\sigma}_i$ is a spin, J is a positive exchange strength, J' an anisotropy strength, ψ the angular mismatch between local spin orientation and the preferred crystalline orientation, $\vec{\mathrm{H}}$ the applied magnetic field, and M the local magnetization per unit area. The four terms correspond respectively to the external field energy, the exchange energy, the anisotropy energy, and the dipole energy.

The basic mechanism controlling the formation of magnetic bubble patterns is the competition between the wall energy which favors the creation

of large domains, and the dipole energy which favors the creation of small domains. Thus the basic dynamics differ from the soap froth in the presence of long range forces. Also if the size of the domains is very small, the wall energy per unit area is very large. If the domains are very large, the dipole energy per unit area is very large. Thus for any given value of the external magnetic field (and control parameters like temperature) the pattern has a preferred wavelength which minimizes the sum of the wall and dipole energies. The wall energy has the additional function of a surface tension, tending to straighten (or reduce to smooth arcs) the domain walls. Because of the presence of long range forces we cannot expect rigorous minimal surfaces however. Recurved walls reminiscent of metal grains are also common. The applied magnetic field controls the balance between the two spin orientations and also increases the preferred wavelength.

If the sample is raised above the temperature at which it undergoes its ferrimagnetic phase transition (the Néel temperature, T_N, is approximately 130° C in Molho *et al.*'s samples) and is then cooled, it forms at zero field (depending on the individual sample and the applied field when the Néel temperature is crossed on cooling) one of two basic types of pattern, a more or less regular array of bubbles (See Fig. 57 (A)), or a continuous folded labyrinth (See Fig. 56 (a)).

If we apply a magnetic field to the labyrinth favoring one spin orientation (by convention we will assume that we favor the white spins in our pictures), the black regions first narrow and then begin to unwind, keeping close to

Fig. 56 Coarsening of a Labyrinth. Stages in the coarsening of a magnetic bubble labyrinth subject to an external magnetic field. (a) H= 0 Oe. (b) H= 1470 Oe. (c) H= 2250 Oe. (d) H= 2700 Oe. (e) H= 3080 Oe. (f) H= 3300 Oe (From Kooy and Enz 1960).[124]

(a)

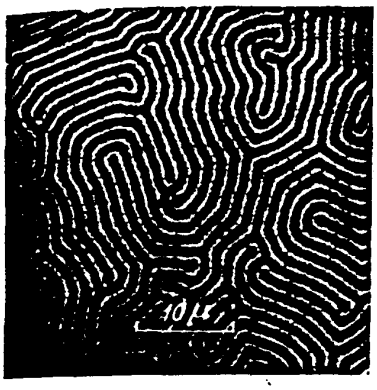

(b)

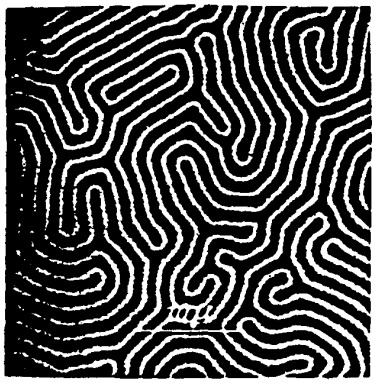

(c)

(d)

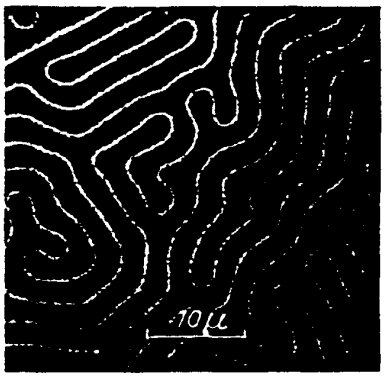

(e)

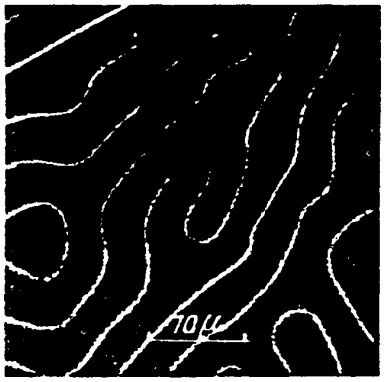

(f)

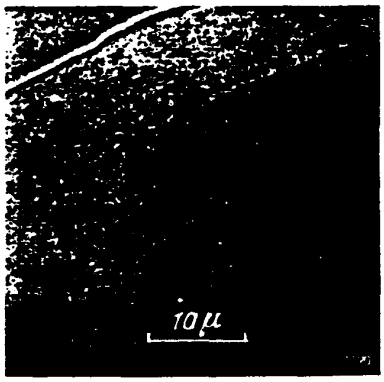

Fig. 57 Coarsening of Magnetic Bubbles. Normal coarsening at $T = 20°$ C of a magnetic bubble pattern with applied magnetic field. (A) H= 0 Oe. (B) H= 54.1 Oe. (C) H= 73.8 Oe. (D) H= 85.2 Oe (Figure supplied by P. Molho 1989).

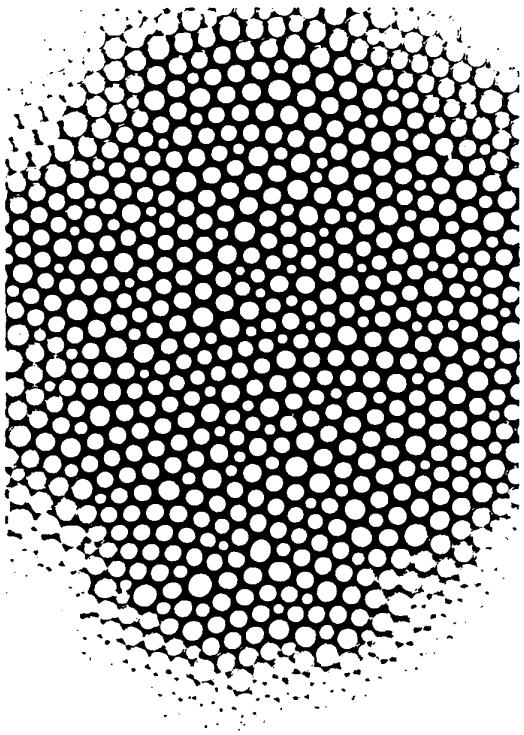

(A)

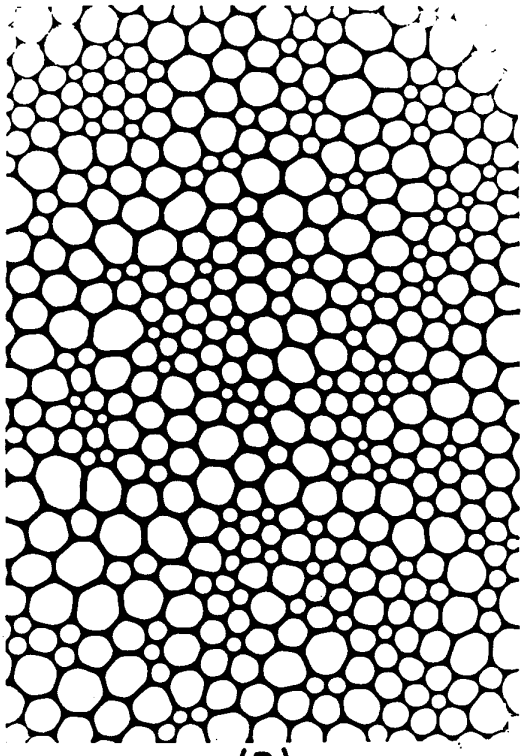

(B)

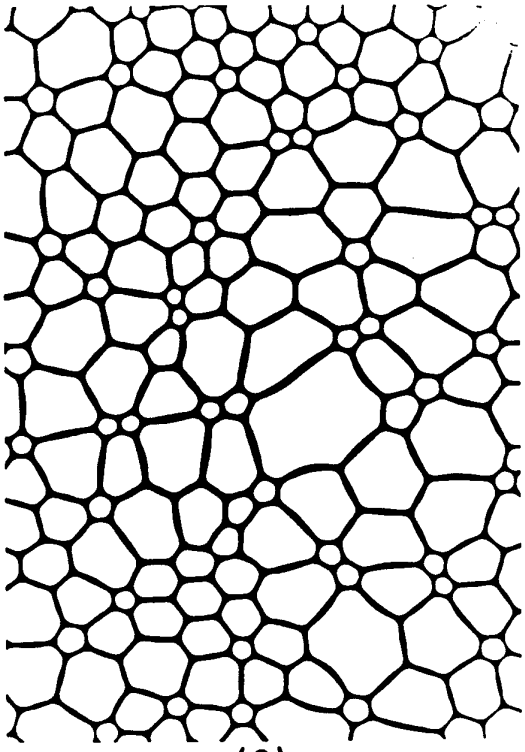

(C)

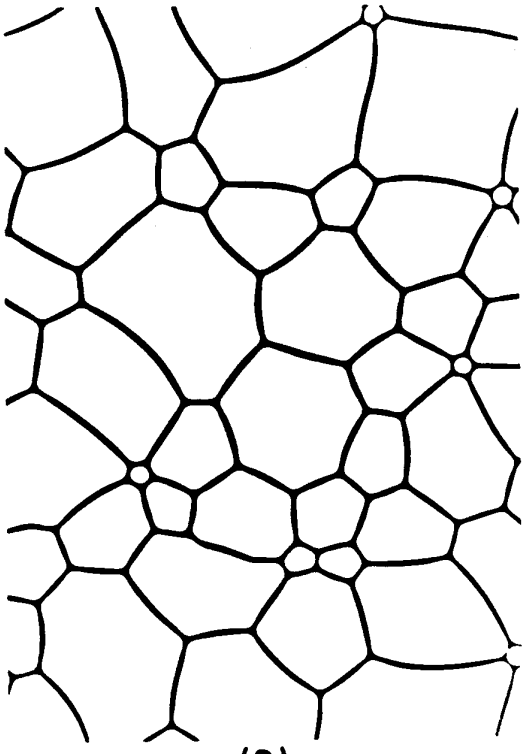

(D)

both the favored ratio between white and black and the selected wavelength, until at some critical field, the last black line collapses and the sample has uniform magnetization. We show an early example of this process by Kooy and Enz in Fig. 56.

In the case of a bubble pattern at a temperature much below T_N, the process is different (See Fig. 57). Because it takes energy to change the topology of a three-connected vertex (to break a wall), bubble patterns cannot change scale smoothly in the way a labyrinth can. If we apply an external field to favor the bubble orientation, the walls initially narrow, but soon reach a size below which they are unstable. The next stage consists of the shrinking of few-sided (small bubbles) but the wall energy prevents small bubbles from shrinking indefinitely. Bubbles that are too small increase in energy when they shrink (hence the absence of three- and four-sided bubbles). These stable uniform area five-sided bubbles freeze the pattern evolution (note the presence of many uniform five-sided bubbles in Fig 57 (A)-(C)). They can also maintain a size much smaller than the optimal wavelength. For the ratio of white to black to increase further the small bubbles must collapse entirely and this is the fundamental mechanism of coarsening in magnetic bubbles. Because of the long range dipole interaction and the pinning of five-sided bubblesi which results in large areas having mismatched wavelength, the reorganization of the pattern tends to happen abruptly, with large patches reorganizing together rather than continuously with bubble by bubble reorganization as in normal coarsening. In particular, five-sided bubbles near

Fig. 58 Coarsening of Magnetic Bubbles. Number of bubbles in a fixed area pattern versus applied magnetic field (Figure supplied by P. Molho 1989).

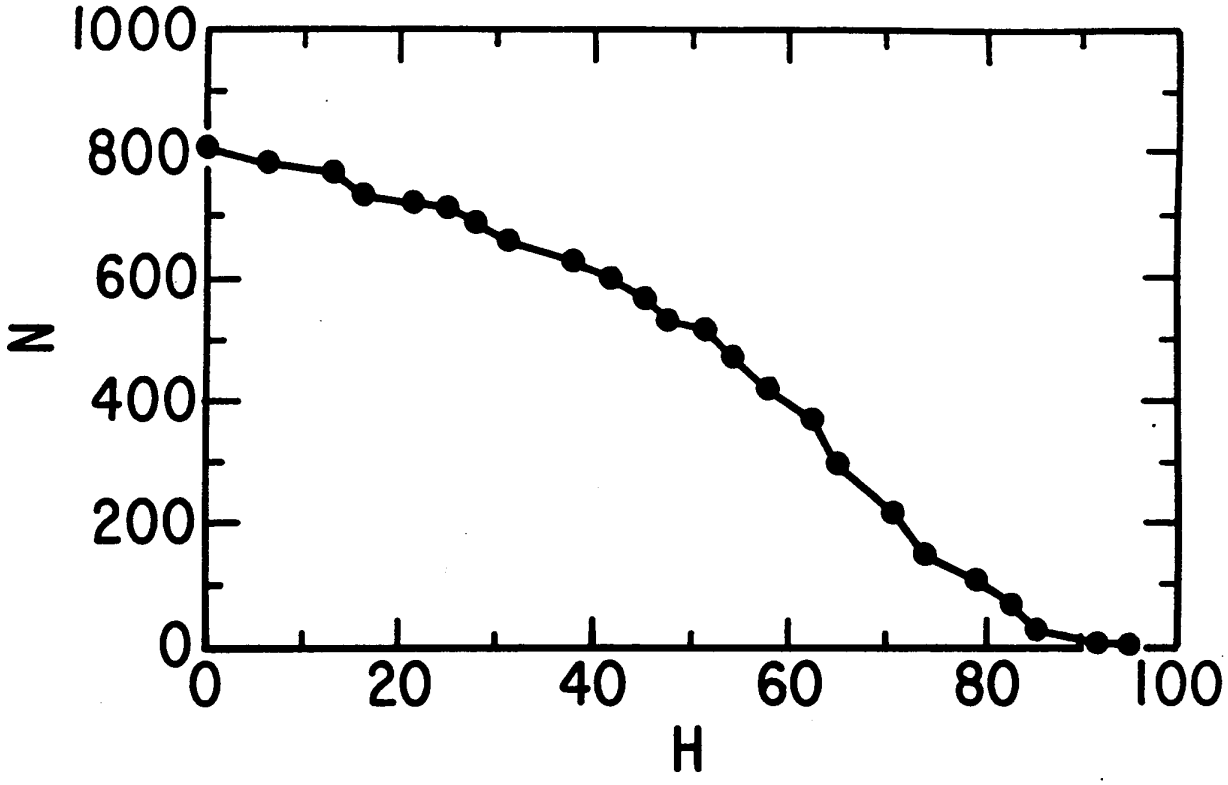
1000
800
600
400
200
0
N
0
20
40
60
80
100
H

Fig. 59 Coarsening of Magnetic Bubbles. Average area per bubble in a bubble pattern versus applied magnetic field (Figure supplied by P. Molho 1989).

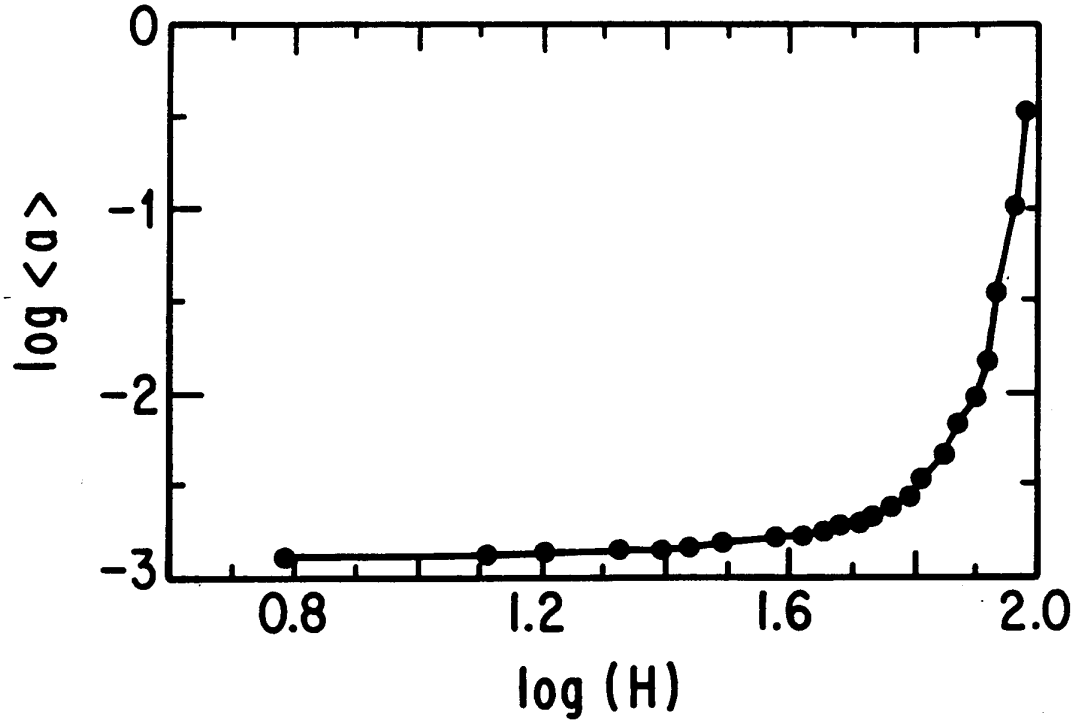
0
-1
-2
-3
log <a>
0.8
1.2
1.6
2.0
log (H)

Fig. 60 Coarsening of Magnetic Bubbles. Moments of the side distribution in a bubble pattern versus applied magnetic field (A) Second moment. (B) Third moment. (C) Fourth moment. (D) Width (Calculated from data supplied by P. Molho 1989)

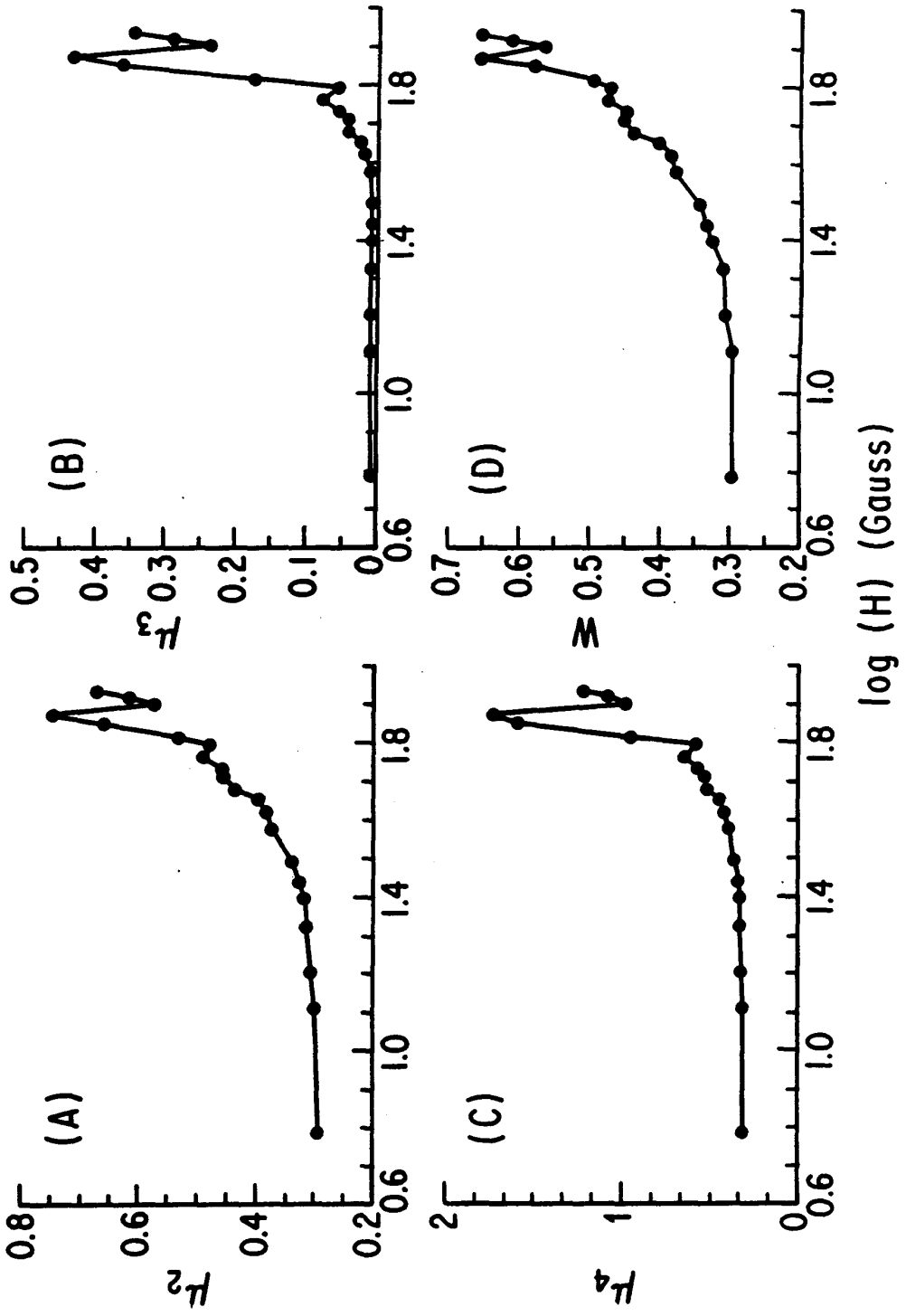
(A)
(B)
(C)
(D)
μ_2
μ_3
μ_4
W
log (H) (Gauss)

Fig. 61 Coarsening of Magnetic Bubbles. Area Distributions. (A) Total area distribution. (B) Area distribution for five-sided bubbles. (C) Area distribution for six-sided bubbles. (D) Area distribution for seven-sided bubbles (Figure supplied by M. Magnasco 1989).

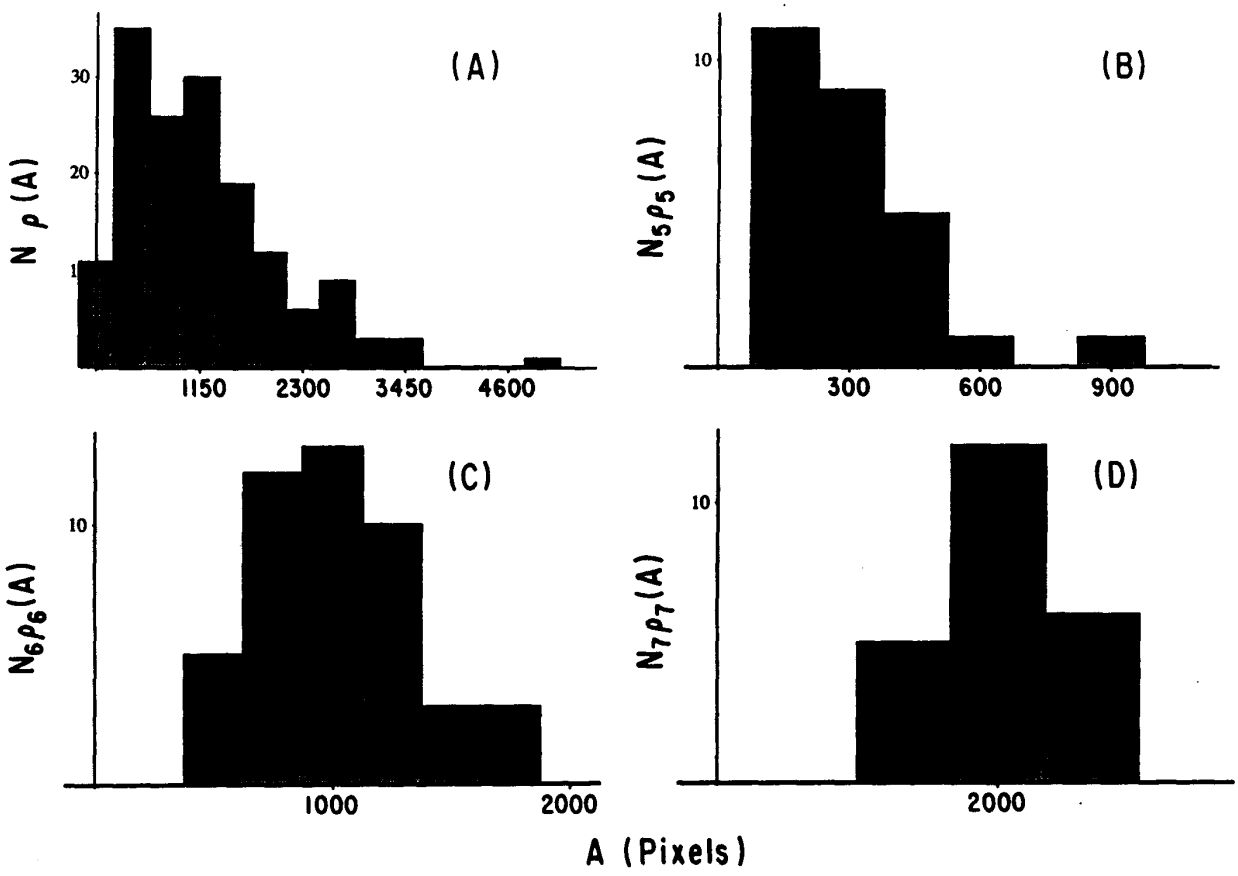
(A)
(B)
(C)
(D)
N ρ (A)
N5ρ5(A)
N6ρ6(A)
N7ρ7(A)
30
20
1
10
10
1150
2300
3450
4600
300
600
900
1000
2000
2000
A (Pixels)

each other tend to be destabilizing so there is a critical field above which groups of three five-sided bubbles lose stablity, then a field above which pairs become unstable, and finally a field above which single five-sided bubbles become unstable. At this field there are no more topological structures to stabilize the pattern and the length scale grows explosively (see Fig. 59). For high applied fields the size of the reorganizing patches is large and wall breakage and domain coalescence are common. One way to make the evolution more like a soap froth is to apply a small alternating bias field on top of the main field.[22]

If we calculate our usual quantities using Molho *et al.*'s measurements for coarsening magnetic bubbles ($< a(H) >$, moments, etc.) we see a very different general pattern from that of the soap froth. The number of bubbles decreased slightly faster than linearly in H (Fig. 58). On a log-log plot, there was a clear but smooth rollover around 50 Gauss, where the rate of area growth suddenly increased (Fig. 59). The monotonic increase of average area with applied magnetic field at least suggests that we are not too far wrong to associate field strength with time. As the field increased, $\rho(6)$ decreased monotonically and $\rho(5)$ and $\rho(7)$ increased monotonically, but the distributions themselves remained very narrow.

The moments all showed the same behavior, with μ_2 gradually increasing from 0.29 to 0.39 before taking off (Fig. 60 (a)), μ_3 staying constant at 0.008 before increasing (Fig. 60 (b)), μ_4 staying nearly constant around 0.33 (Fig. 60 (c)), and W increasing in step with the area from about 0.30 to 0.38

over the same range (Fig. 60 (d)). If we wanted to identify any of these patterns as a scaling state we would have to choose those at low magnetic field, but this seems unsatisfactory. Instead it seems more reasonable to accept that magnetic patterns never find an equilibrium. At all applied magnetic fields six-sided bubbles dominated (except perhaps at very high fields where our statistics are abysmal), there were no three- or four-sided bubbles. Bubbles with more than eight sides were extremely rare and the moments were much smaller than observed in normal coarsening systems, resembling much more the distribution functions we associate with biological materials or basalt fracture. The basic reason is the same in both cases. Wavelength or area selection results in strong limitations on the possible width of the side distributions. The total area distribution (Fig. 61 (A)) resembled that of the soap froth with a few significant differences. As in the soap froth, $\rho(A)$ decreased with increasing area for large areas, but more rapidly as befits a wavelength selected distribution. Unlike the soap froth, the number of very small bubbles was small. Five-sided bubbles (Fig. 61 (B)) formed a well defined class with a well defined non-zero most probable area. Six- and seven-sided bubbles, which do not feel the constraint on minimum bubble size, showed distributions close to those found in the soap froth (Fig. 61 (C) and (D)). To the extent that such a measurement is meaningful for a distribution in which only five- though nine-sided bubbles occur, the patterns appeared to follow the Aboav-Weaire law.

In spite of these differences between magnetic bubbles and our other

coarsening patterns, we can still approximate our coarsening as a competition between surface tension energy minimization and topological constrains. We have already noted the stabilizing effect of five-sided bubbles. In fact, any three-connected vertex is stabilizing in the same way because (at least at temperatures well below the Néel temperature) breaking a wall costs energy.[168] We see this most clearly when we perform the experiment impossible in normal coarsening of increasing and then decreasing the magnetic field. We show Molho *et al.*'s example in Fig. 62. He began with an initial bubble pattern at moderate field and temperature (Fig. 62 (A)) and reduced the magnetic field. Since the pattern could not nucleate new bubbles it adjusted to its smaller optimal wavelength by having its walls buckle and stretch (Fig. 62 (B)). Where the presence of pinned five-sided bubbles resulted in a local wavelength smaller than the optimal, the five-sided bubbles grew but the walls remained smooth (e.g. in the lower middle left of Fig. 62 (B)). Decreasing the applied field to near zero resulted in a labyrinth with almost uniform areas of black and white (Fig. 62 (C)). Looking carefully at Figs. 62 (B) and (C) shows that the three-connected vertices moved slightly but did not disappear. Increasing the field back to its original value restored a pattern topologically close to the original (Fig. 62 (D)). While the sizes of the bubbles changed slightly, most of the vertices remained unchanged. In a few places, bubbles which were much smaller than the optimal wavelength

disappeared. Presumably the changes in pattern detail affected the stability of nearly unstable bubbles as the field was increased, resulting in the disappearance of a few additional bubbles.

For the sake of the pictures and to stimulate further thought on the significance of anisotropy and long range interactions we include a few examples of exotic coarsening behavior for which we do not yet have quantitative analyses.

Near the Néel temperature the presence of a defect in the sample crystal can allow the nucleation of labyrinth at no energy cost. Molho *et al.* began with a pattern at $T = T_N - 5°$ C (Fig. 63 (A)), indistinguishable from that shown in Fig. 56 (a). As they increased the applied field a region of labyrinth nucleated from a defect (Fig. 63 (B)). At higher fields weaker defect centers also began to nucleate labyrinth (Fig. 63 (C)). Finally the labyrinth pushed aside the bubbles to dominate the pattern (Fig. 63 (D)). The wavelength of the labyrinth was substantially larger than the wavelength of the bubbles. It is also interesting to note that this entire evolution took place at fields too small to cause the collapse of bubbles. One could scarcely ask for a clearer demonstration that the labyrinth pattern has a lower energy than the bubble pattern, and that the energy advantage increases with field. The only thing that kept the labyrinth from swallowing the bubbles completely was the boundary of stretched bubbles (looking rather like the epithelium of a tree) which apparently add an extra "domain energy" to the labyrinthine

Fig. 62 Pattern Conservation in Magnetic Bubbles. (A) A bubble pattern at a fixed field, $T = 20°$ C. (B) The field is decreased and the walls buckle. (C) At small fields a nearly symmetric labyrinth forms. (D) Returning the field to its initial value restores the topology of the original pattern with minor changes (Figure supplied by P. Molho 1989).

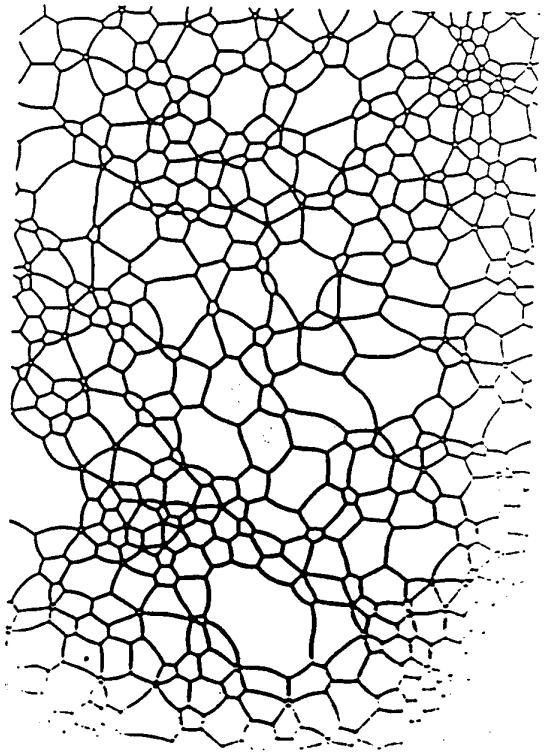

(A)

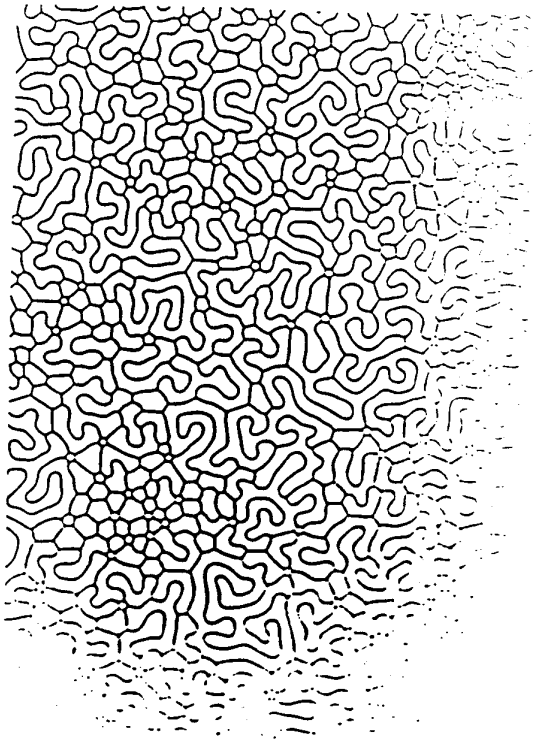

(B)

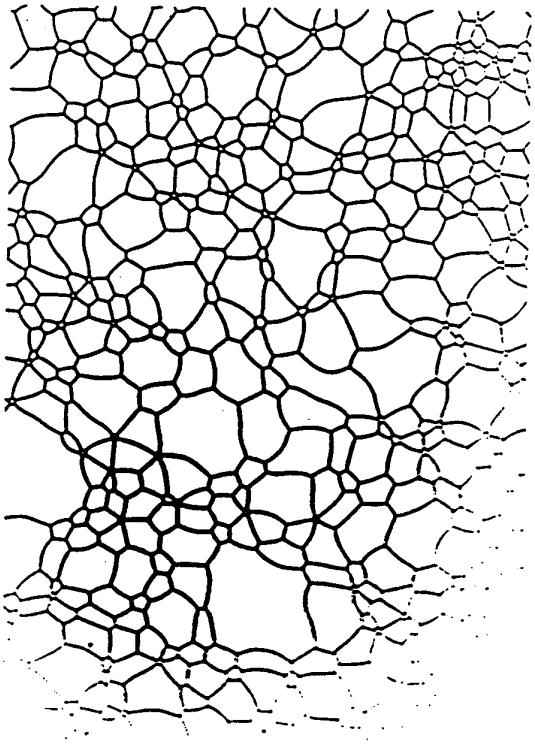

(D)

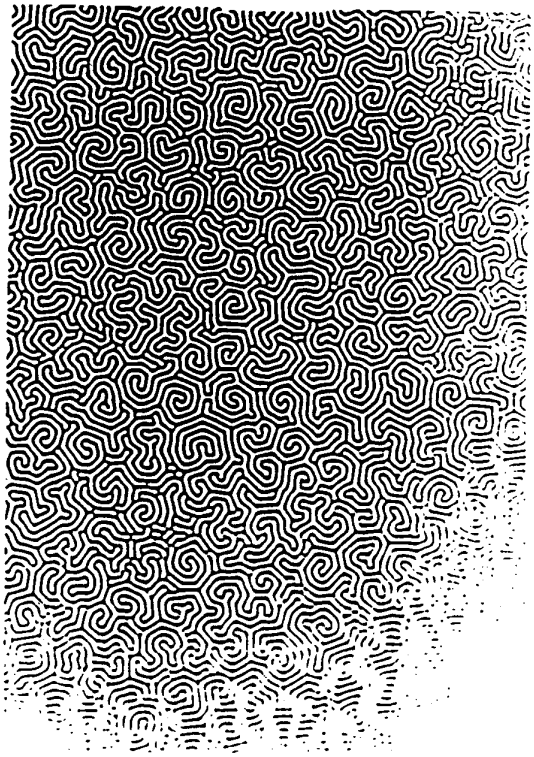

(C)

Fig. 63 Nucleation of Labyrinth. Nucleation of labyrinth from a defect with applied magnetic field, $T = T_N - 5°$ C. (A) H= 0 Oe. (B) H= 17 Oe, beginning of nucleation. (C) H= 19.1 Oe, labyrinth begins to nucleate at additional locations. (D) H= 19.4 Oe, Labyrinth grows rapidly at the expense of bubbles (Figure supplied by P. Molho 1989).

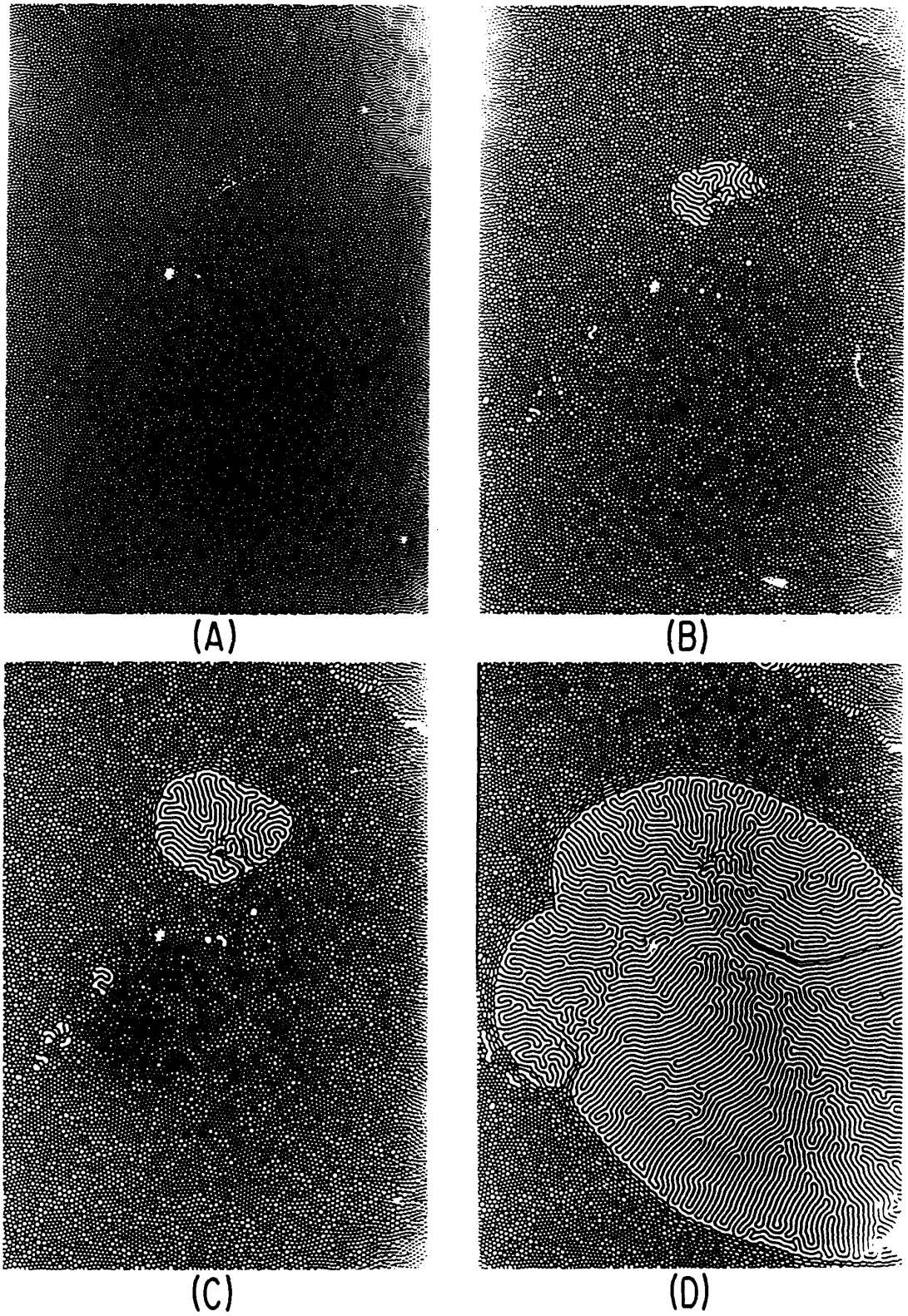
(A)
(B)
(C)
(D)

Fig. 64 Anisotropic Coarsening of Bubbles. Effect of anisotropy on bubble growth near T_N. $T = T_N - 1°$ C. (A) H=16.5 Oe. (B) H=17.5 Oe, bubbles begin to stretch. (C) H=19.0 Oe, growth of elongated bubbles. (D) H=21.5 Oe, bubbles grow by the motion of three-connected vertices to lower left (Figure supplied by P. Molho 1989).

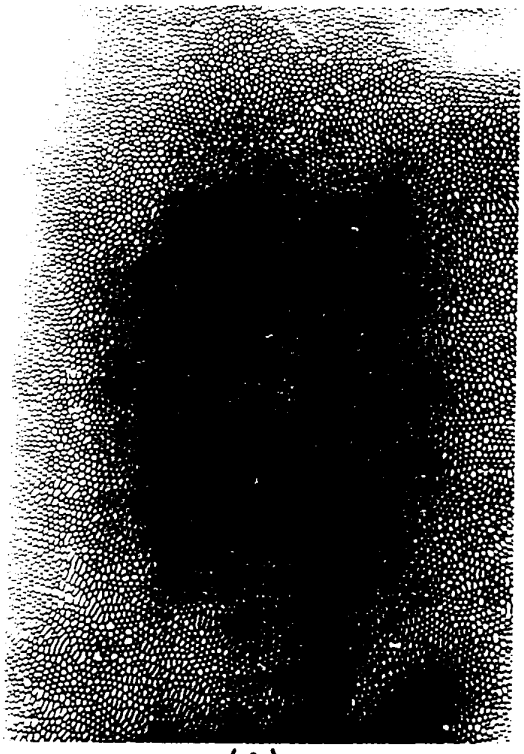

(A)

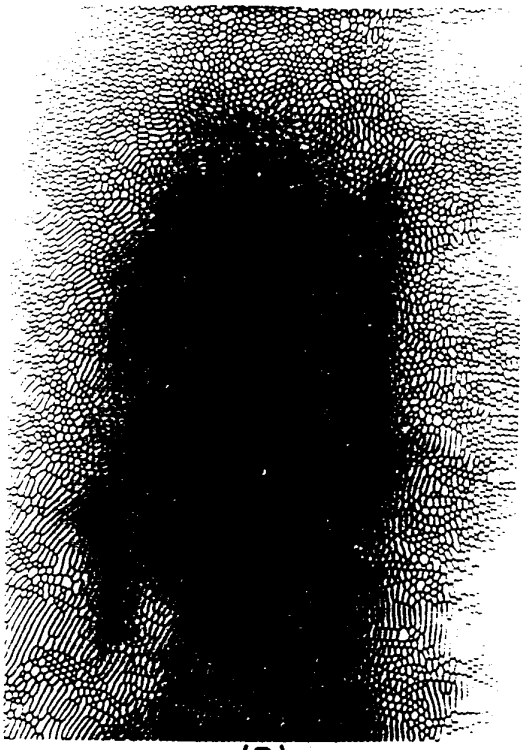

(B)

(C)

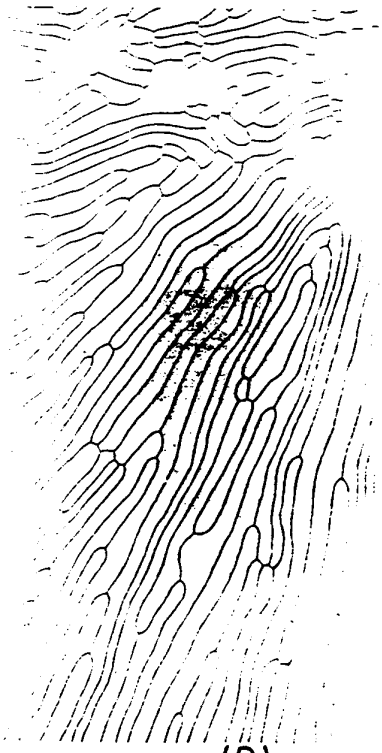

(D)

Fig. 65 Anomalous Bubble Growth in Magnetic Bubbles. Anomalous bubble growth in a magnetic bubble pattern near T_N, $T = T_N - 4°$ C. (A) H= 0 Oe. (B) H= 28 Oe, a few bubbles grow bigger as the field increases. (C) H= 30 Oe. (D) H= 31 Oe, THe larger bubbles grow rapidly. (E) H= 32.1 Oe, the large bubbles dominate the pattern. (F) H= 36 Oe, the initial length scale has disappeared and the pattern resembles that produced by normal bubble growth (Figure supplied by P. Molho 1989).

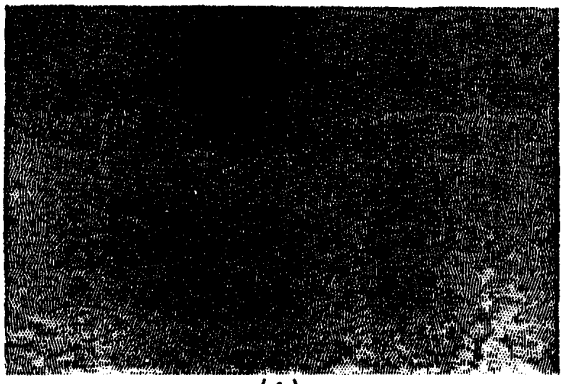

(A)

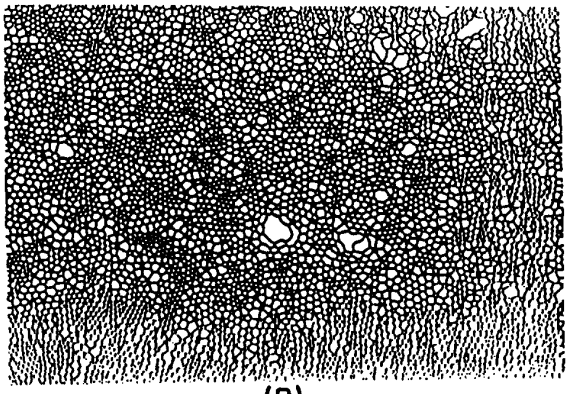

(B)

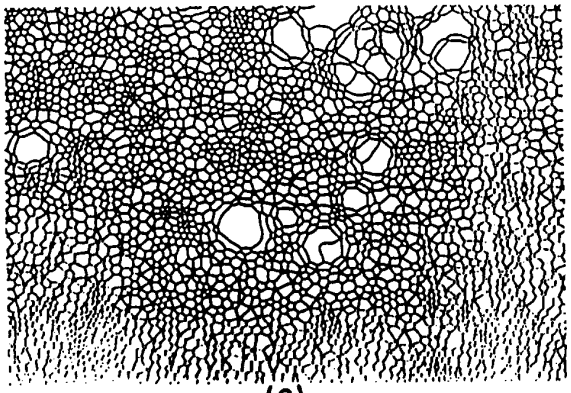

(C)

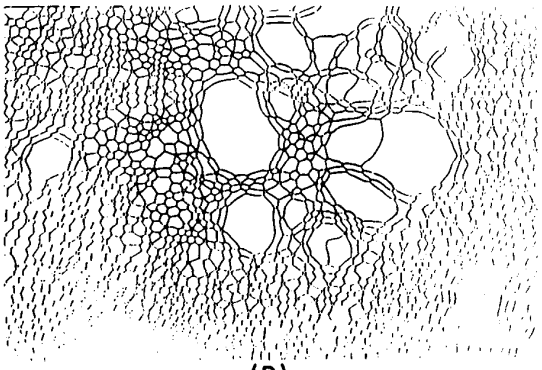

(D)

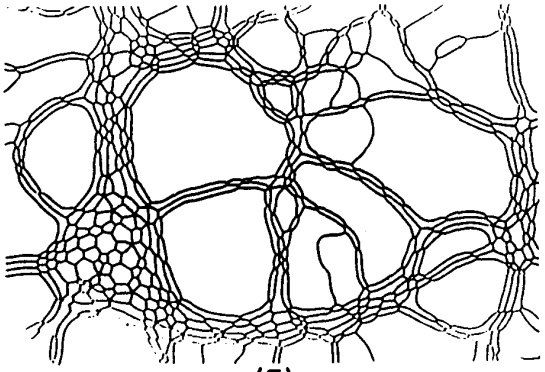

(E)

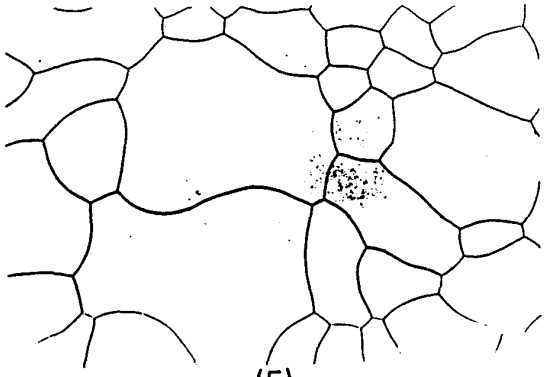

(F)

Fig. 66 Coarsening of Magnetic Bubbles. Bubble growth for the ensemble of n-sided bubbles as a function of applied magnetic field. Note that this is not the same as von Neumann's law (Figure supplied by M. Magnasco 1989).

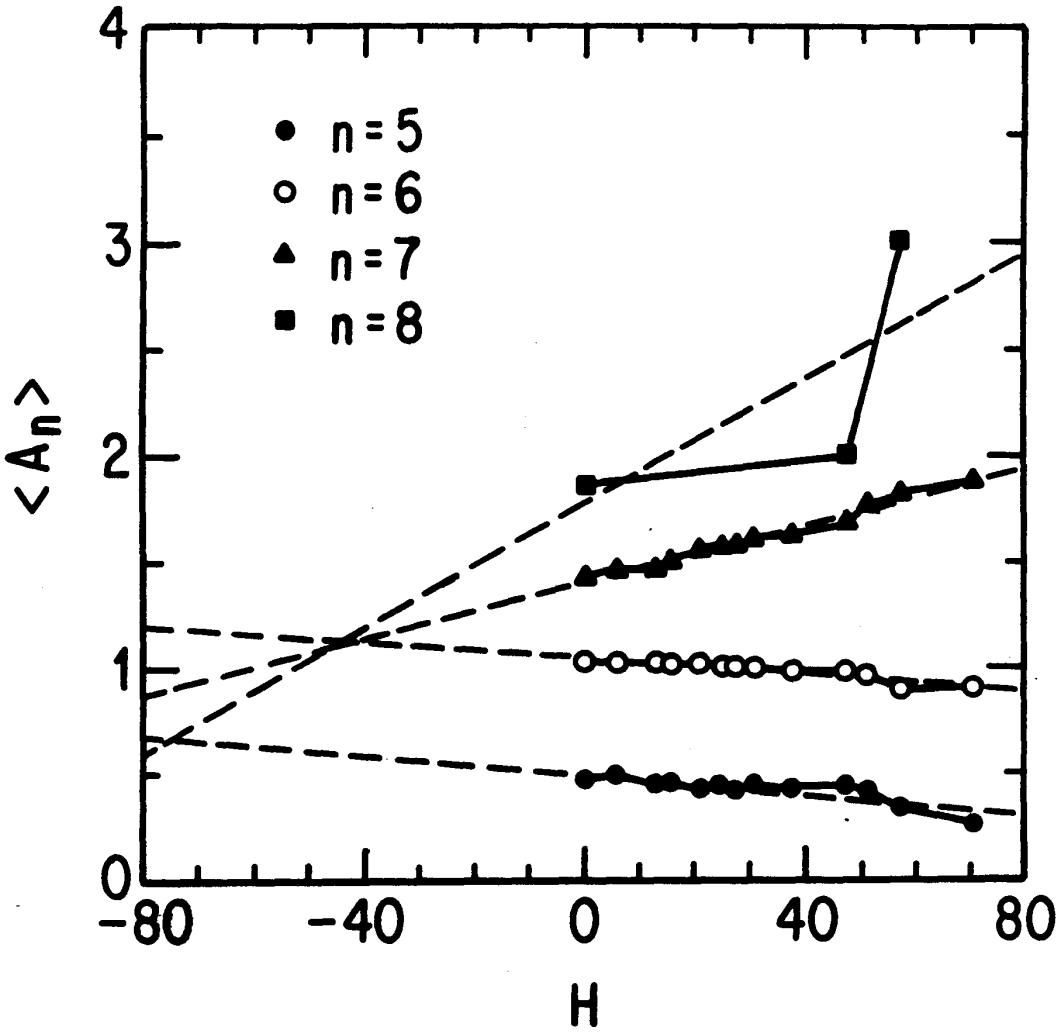
4
3
2
1
0
-80
-40
0
40
80
H
<A_n>
n=5
n=6
n=7
n=8

patch. However, besides retarding the growth of the labyrinth, these bubbles also facilitate the collapse of the original bubble pattern. In their absence the nucleated pattern cannot grow.[167] The temperature determines whether the labyrinth is energetically favorable enough to cause wall breakage.

Anisotropy can also have a decisive effect on coarsening. In Fig. 64 we show Molho *et al.*'s observation of coarsening in a material at $T = T_N - 1°$ C, which allowed walls with a particular orientation to break more easily (ranging from east-west at the right of the picture to northwest -southeast at the upper left). Because this type of anisotropy is small the effect occurs only near T_N where the wall breakage energy is very small. Once again the zero field pattern (Fig. 64 (A) was indistinguishable from Fig. 56 (a). As the field was increased however, bubbles with borders aligned along easy breaking directions began to coalesce (Fig. 64 (B)), producing a pattern of elongated bubbles reminiscent of cloth stretched near the point of failure. For larger fields the coalescence perpendicular to the preferred direction continued (Fig. 64 (C)), eventually producing a strongly grained pattern which grew by the sliding of three-fold vertices (Fig. 64 (D)). The final pattern was nearly as well behaved as one composed of well ordered parallel stripes.

Finally we show Molho *et al.*'s example of orientationally isotropic but spatially varying rates of bubble growth, analogous to the case of anomalous grain growth in metals. Again, working near T_N is crucial since the small anisotropy can only have an effect when it is comparable to the wall breakage energy. A sample that exhibits anomalous bubble growth near T_N will show

normal bubble growth at lower temperatures. They began with the usual zero field bubbles at $T = T_N - 4°$ C (Fig. 61 (A)). For small fields they observed normal grain growth with a few bubbles slightly larger than their neighbors (Fig. 61 (B)). As the field increased further these larger bubbles grew explosively at the expense of their neighbors (Fig. 61 (C)-(E)) producing the characteristic bark-like pattern of elongated bubbles lying along the surface of the growing bubbles which we noted in Fig. 11 (D). Finally the anomalously growing bubbles swallowed all the small length scale pattern and returned to a situation indistinguishable from that produced by normal bubble growth (Fig. 61 (F) compare Fig. 56 (d)). This return to a normal looking scaling pattern is also observed in metals. Of course if we were to look at the distribution functions for this pattern as a function of field they would be bimodal, and vastly broader than the corresponding stages in normal growth. The energy to drive this anomalous grain growth presumably comes from the mismatch between the wavelength of the bubble pattern and the optimal wavelength, but the mechanism which selects the anomalously growing grains is unclear.

Existing theories of magnetic bubbles treat either regular arrays or isolated bubbles. There have also been a few attempts to deduce large scale statistical properties of random lattices. The difficulties are several. Since bubbles evolve in patches and wall breakage is a dominant mechanism in some types of coarsening, we do not expect a simple description like our network models to suffice. In extreme cases the growth or shrinkage of an

individual bubble becomes an ill defined concept. Surprisingly if we take the naive zeroth order approximation to measuring von Neuann's law we obtain a sensible result. In Fig. 66 we plot Molho *et al.*'s measurement for the average total area of n-sided bubbles as a function of applied external field. This measurement is not equivalent to von Neumann's law because bubbles can change their number of sides. If we note that $< A_n >= \lambda_n < a >$ we obtain simply:

$$\frac{d < A_n >}{d\mathrm{H}} = \lambda_n \frac{d < a >}{d\mathrm{H}} + < a > \frac{d\lambda_n}{d\mathrm{H}}. \qquad \text{(X.4)}$$

In a scaling state soap froth it would show that all bubbles grow with a rate $\frac{d<A_n>}{dt} = \kappa\lambda_n$. For the magnetic bubbles the result is rather different. Average bubble areas, $< A_n >$, do depend linearly on applied magnetic field (which we might not have predicted looking at the nonlinear dependence of total area), but five- and six-sided bubbles shrink and seven- and eight-sided bubbles grow, showing that the distributions continue to evolve. This gives us a relation between $< a >$ and λ_n:

$$\frac{d \ln < a >}{d\mathrm{H}} + \frac{d \ln \lambda_n}{d\mathrm{H}} = \frac{\kappa}{\lambda_n < a >}, \qquad \text{(X.5)}$$

but tells us nothing about the evolution of individual bubbles. Whether this relation will prove useful in developing a theory for magnetic bubble growth remains to be seen. It may prove more helpful as a way to test theories than to create them.

Magnasco has written an interaction model mean field theory for the rapid equilibration of a bubble pattern after a field change and during nucleation at the Néel temperature, taking into account both separations and

radii of the form and assuming nearly circular bubbles.[154] He defined the mean field distance between the surfaces of two bubbles to be

$$d_{ij} \equiv |\vec{x}_i - \vec{x}_j| - r_i - r_j, \tag{X.6}$$

where $\vec{x}_i$ is the position of the center of the ith bubble and r_i its radius. Then he took the movement of the centers of the bubbles to be the effect of the dipole repulsion by the remaining bubbles,

$$\frac{d\vec{x}_i}{t} = \kappa_1 \sum_{j \neq i} \frac{\vec{x}_i - \vec{x}_j}{d_{ij}^3}, \tag{X.7}$$

and the change in radius to be pressure driven by the same dipole force,

$$\frac{dr_i}{dt} = \kappa_2 \sum_{j \neq i} (1 - \frac{1}{d_{ij}^3}), \tag{X.8}$$

where κ_2 controls the equilibrium width of the area distribution, small κ_2 resulting in broad distributions and large κ_2 in narrow distributions. Note the nonlinearity in both terms of the equation. He obtained good agreement with experiment for the qualitative equilibration but has not yet measured the distribution functions. In principle κ_2 should be a decreasing function of the applied magnetic field, and Magnasco is currently developing a model for the field evolution of magnetic bubble patterns using an extended model of this type. The difficulty is in understanding why a model that should work well for Bragg's bubble rafts should also be appropriate in a case where wall breakage and patch rearrangement are important mechanisms.

We could also write a boundary dynamic model along the lines of Frost and Thompson, adding either an exact integrated form for the local magnetization or the mean field version given in equation X.7. It should be possible

to include wall breakage and the stabilization of five-sided bubbles with an auxiliary field. The collapse of finite size bubbles can also be included by increasing the length scale for bubble removal to a larger value. While the Potts model seems like the natural type of model for a magnetic system, the calculation of the local magnetization seems guaranteed to be computationally prohibitive. Perhaps, it would be possible to used a mixed model like that of Weaire and Kermode with Potts model calculations layered on top of a mean field calculation of the local magnetization.

CHAPTER XI
CONCLUSION

After our long ramble among various two dimensional coarsening phenomena it would be nice to be able to write something definitive. We are a long way from that achievement. We do understand a great deal about two dimensional coarsening in soap froths and pure metals. We understand how we go from an ordered pattern to a disordered scaling state and we have developed several methods to measure pattern disorder all of which give compatible results. We have developed a large variety of models, many of which seem accurately to duplicate the evolution of a froth. In the specific points where our models fail, we have some insight into why: anisotropy in the Potts model, failure to consider side shedding anticorrelations in our mean field theories, etc. Having identified the source of our difficulties we still need to study in detail how calculated distributions depend on anisotropy and correlations. We understand, at least qualitatively, the physical reasons why different systems (biological, geological, etc.) give different sorts of patterns, but we have not made any concerted effort to explain those patterns. Lewis' program for biology is still far from completion. In this sense we understand how the interaction of local energy minimization and topology produces complex patterns.

From an experimental point of view, repeating the soap froth experiment with larger cells and more and better controlled initial conditions would be desirable, but we would not expect any real surprises. Repeating the

basic area versus time measurement in a drained cell with constant plateau border width would be ideal. If a drained cell still came up with a growth exponent different from one we would have to rethink our entire theory from the beginning. We also need to measure the anticorrelation between side shedding and side number. In the area of metal coarsening we need more information on anisotropy and temperature effects.

We have skirted or merely touched on a number of interesting points in two dimensional coarsening. We have discussed in a handwaving fashion how the zone refining of impurities and the presence of macroscopic defects leads to anomalous exponents in metal grain growth. It is a simple matter to drill holes and thread pins through a soap bubble cell to duplicate the effect. Glazier has made some preliminary measurements with a regular lattice of pins and found that coarsening slowed and eventually stopped. However, his observations were purely qualitative. A large cell with randomly placed pins would be a worthwhile experiment. It is less clear how we could duplicate anomalous grain growth experimentally. Several of Glazier *et al.*'s experiments suffered from undesired wall breakage. Perhaps, short duration intense heating could be applied intentionally to mimic random grain coalescence. More careful comparisons between the small-Q Potts model and metal systems exhibiting anomalous grain growth would also be interesting.

Theory and experiment are equally deficient when we come to three dimensional froths. Even the Potts model gives relatively poor results, for reasons that are not entirely clear. That we possess one adequate theory

for two dimensional sections of three dimensional materials is no guarantee that we understand the full three dimensional problem. We are currently investigating the possibility of extending some of the existing models to three dimensions. But it will be some time before we have a developed theory. As a first step it would be nice to have a three dimensional von Neumann's law, or at least to know that it did not exist. The experimental picture is bleak. The best hope would be some sort of optical tomography on a rotating drum of froth. It would be an expensive and elaborate, but not impossible experiment. Data analysis and reduction might well prove to be an even worse problem than data collection. However, the good experimental data in three dimensions would be the most important new result we could obtain.

Finally, we have looked at two systems in which long range forces play a role. In the case of lipid monolayers, certain configurations look startlingly like ideal two dimensional grain growth while others look like mean field theory Ostwald ripening. In both cases we observe classical scaling states and familiar behavior. Indeed in the grain growth limit we expect the lipid monolayers to be closer to the ideal than any other system. We have suggested one way in which the von Neumann's law and Ostwald ripening theories could be combined, but lack the experimental data to test it. Additional experiment seems likely to lead to an understanding as complete as that we have for normal coarsening.

In the case of magnetic bubbles, long range interactions are fundamental. Though we have tried to draw analogies with more familiar patterns of

behavior in metals and biology, many of the phenomena and patterns seem bizarre. Treating these patterns with an interaction mean field theory may work for "ordinary" bubble growth, but seems unlikely to explain behavior under field reversals, and the whole zoology of non-standard coarsening. A combination mean field theory plus boundary dynamic approach or mean field theory plus Potts model approach seems most promising.

Experimentally there is an enormous amount to do. All of the different coarsening scenarios need to be quantified. It seems clear that any future experiments should be done with an alternating bias field to smooth out bubble growth. The hysteretic patch reorganization produced by DC fields adds greatly to the complexity of interpreting a set of data already fearsomely complex. For both the lipid monolayers and the magnetic bubbles the fundamental problem is the lack of a basic dynamical equation. Top priority needs to go to an experimental measurement of von Neumann's law. For the lipids it probably exists. For the magnetic bubbles it may well not exist, in which case magnetic bubbles may prove a classic hard problem, like large aspect ratio Rayleigh-Bénard convection.

Spin-glasses may hold an important lesson. Statistics do not always tell the whole story. We ought to be surprised if magnetic bubble patterns could be described simply. It is nice to know that underneath these frightening non-linear problems, lies a simple linear problem that we have managed to solve.

REFERENCES

[1] (anon.), "The Royal Society's Soirée," *Nature*, vol. 3, pp. 395–396, 1871.

[2] G. Abbruzzese, "Computer simulated grain growth stagnation," *Acta. Met.*, vol. 33, pp. 1329–1337, 1985.

[3] G. Abbruzzese, "Computer simulated stagnation and abnormal grain growth," in *Computer Simulation of Microstructural Evolution*, (The Metallurgical Society: Warrendale, 1986), pp. 61–76.

[4] G. Abbruzzese and K. Lüke, "A theory of texture controlled grain growth–I. Derivation and general discussion of the model," *Acta. Met.*, vol. 34, pp. 905–914, 1986.

[5] G. Abbruzzese and K. Lüke, "A statistical theory of grain growth including texture and drag effects and its application to texture controlled grain growth," *Annealing Processes– Recovery, Recrystallization and Grain Growth, Proceedings of the 7th Risø International Symposium on Metallurgy and Materials Science*, N. Hansen, D. J. Jensen, T. Leffers, and B. Ralph, eds. (Risø National Laboratory: Roskilde, 1986), pp. 1–14.

[6] D. A. Aboav, "The Arrangement of Grains in a Polycrystal," *Metallography*, vol. 3, pp. 383–390, 1970.

[7] D. A. Aboav, "The Stability of Grains in a Polycrystal," *Metallography*, vol. 4, pp. 425–441, 1971.

[8] D. A. Aboav, "The Arrangement of Cells in a Net," *Metallography*, vol. 13, pp. 43–58, 1980.

[9] D. A. Aboav and T. G. Langdon, "The Shape of Grains in a Polycrystal," *Metallography*, vol. 2, pp. 171–178, 1969.

[10] R. M. C. de Almeida and J. R. Iglesias, "Towards Statistical Mechanics of a 2-D Random Cellular Structure," *J. Phys. A*, vol. 21, pp. 3365–3371, 1988.

[11] R. M. C. de Almeida and J. R. Iglesias, "Equilibrium States of 2d Cellular Structures," (preprint) 1988.

[12] M. P. Anderson, "Simulation of grain growth in two and three dimensions," *Annealing Processes– Recovery, Recrystallization and Grain Growth, Proceedings of the 7th Risø International Symposium on Metallurgy and Materials Science*, N. Hansen, D. J. Jensen, T. Leffers, and B. Ralph, eds. (Risø National Laboratory: Roskilde, 1986), pp. 15–34.

[13] M. P. Anderson, G. S. Grest, and D. J. Srolovitz, "Grain Growth in three dimensions: A lattice model," *Scripta. Met.*, vol. 19, pp. 225–230, 1985.

[14] M. P. Anderson, G. S. Grest, and D. J. Srolovitz, "The microstructural dynamics of primary and secondary recrystallization," in *Computer Simulation of Microstructural Evolution*, (The Metallurgical Society: Warrendale, 1986), pp. 77–93.

[15] M. P. Anderson, G. S. Grest, and D. J. Srolovitz, "Computer simulation of normal grain growth in three dimensions," *Philos. Mag.*, vol. B 59, pp. 293–329, 1989.

[16] M. P. Anderson, D. J. Srolovitz, G. S. Grest, and P. S. Sahni, "Computer simulation of grain growth–I. Kinetics," *Acta. Met.*, vol. 32, pp. 783–791, 1984.

[17] E. N. da C. Andrade and D. A. Aboav, "Grain growth in metals of close-packed hexagonal structure," *Proc. Roy. Soc. London*, vol. 291A, pp. 18–40, 1966.

[18] A. S. Argon and L. T. Shi, "Analysis of plastic flow in an amorphous soap bubble raft by the use of an inter-bubble potential," *Philos. Mag.*, vol. A 46, pp. 275–294, 1982.

[19] M. F. Ashby and R. A. Verrall, "Diffusion-accommodated flow and superplasticity," *Acta. Met.*, vol. 21, pp. 149–163, 1973.

[20] H. V. Atkinson, "Theories of Normal Grain Growth in Pure Single Phase Systems," *Acta. Met.*, vol. 36, pp. 469–491, 1988.

[21] J. H. Aubert, A. M. Kraynik, P. B. Rand, "Aqueous Foams," *Sci. Am.*, vol. 254 May, pp. 74–82, 1986.

[22] K. L. Babcock and R. M. Westervelt, "Elements of Cellular Domain patterns in Magnetic Garnet Films," (preprint) 1989. In which the authors shamelessly steal results from U. of C. without so much as an acknowledgement.

[23] B. Bay and N. Hansen, "Deformed and recovered microstructures in pure aluminum," *Annealing Processes– Recovery, Recrystallization and Grain Growth, Proceedings of the 7th Risø International Symposium on Metallurgy and Materials Science*, N. Hansen, D. J. Jensen, T. Leffers, and B. Ralph, eds. (Risø National Laboratory: Roskilde, 1986), pp. 215–220.

[24] P. A. Beck, "Annealing of Cold Worked Metals," *Advances in Phys.*, vol. 3, pp. 245–324, 1954.

[25] C. W. J. Beenakker, "Evolution of Two-Dimensional Soap-Film Networks," *Phys. Rev. Lett.*, vol. 57, pp. 2454–2457, 1986.

[26] C. W. J. Beenakker, "Two-Dimensional Soap Froths and polycrystalline networks: Why are large cells many-sided?," *Physica*, vol. 147A, pp. 256–267, 1987.

[27] C. W. J. Beenakker, "Numerical Simulation of Grain Growth in a Two-Dimensional Network," (preprint) 1988.

[28] C. W. J. Beenakker, "Evolution of Two-Dimensional Soap-Film Networks," *Phys. Rev. A*, vol. 37, pp. 1697–1704, 1988.

[29] B. Berge, private communication.

[30] M. Blanc and A. Mocellin, "Grain coordination in plane sections of polycrystals," *Acta. Met.*, vol. 27, pp. 1231–1237, 1979.

[31] A. H. Bobeck, "Properties and Device Applications of Magnetic Domains in Orthoferrites," *Bell Tech. J.*, vol. 46, pp. 1901–1925, 1967.

[32] G. F. Bolling and W. C. Winegard, "Grain growth in zone-refined lead," *Acta. Met.*, vol. 6, pp. 283–287, 1958.

[33] G. F. Bolling and W. C. Winegard, "Some effects of impurities on grain growth in zone-refined lead," *Acta. Met.*, vol. 6, pp. 288–292, 1958.

[34] B. N. Boots, "The Arrangements of Cells in "Random" Networks," *Metallography*, vol. 15, pp. 53–62, 1982.

[35] R. Boyle, *New Experiments, Physico-Mechanical, Touching the Spring of Air* (Oxford: Oxford, 1660).

[36] C. V. Boys, *Soap Bubbles: Their Colours and the Forces which Mold Them*, (Dover Press: New York, 1959). Reissue of 1911 edition.

[37] Sir Lawrence Bragg, "A Model illustrating Intercrystalline Boundaries and Plastic Flow in Metals," *J. Sci. Instr.*, vol. 19, pp. 148–150, 1942.

[38] Sir Lawrence Bragg and J. F. Nye, "A dynamical model of crystal structure," *Proc. Roy. Soc. London*, vol. A 190, pp. 474–481, 1947.

[39] R. J. Brook, "Controlled Grain Growth," in *Ceramic Fabrication Processes, Treaties on Materials Science and Technology*, vol. 9, F. F. Y. Wang, ed. (Academic Press: New York, 1976), pp. 331–364.

[40] Sir. R. Bulkley, "Concerning the Giant's Causeway, . . ." *Phil. Trans. Roy. Soc. London*, vol. 17, pp. 708–711, 1693.

[41] H. J. Bunge and E. Dahlem, "Texture changes and growth anomalies during continuous grain growth," *Annealing Processes- Recovery, Recrystallization and Grain Growth, Proceedings of the 7th Risø International Symposium on Metallurgy and Materials Science*, N. Hansen, D. J. Jensen, T. Leffers, and B. Ralph, eds. (Risø National Laboratory: Roskilde, 1986), pp. 255–260.

[42] J. E. Burke and D. Turnbull, "Recrystallization and grain growth," *Prog. Met. Phys.*, vol. 3, pp. 220–292, 1952.

[43] J. W. Cahn "On Hillert's grain growth catalyst," *Acta. Met.*, vol. 13, pp. 1091–1092, 1965.

[44] R. W. Cahn, "Topology of crystal grains," *Nature*, vol. 250, pp. 702–703, 1974.

[45] J. A. Cape and G. W. Lehman, "Magnetic Domain Structures in Thin Uniaxial Plates with Perpendicular Easy Axis," *J. Appl. Phys.*, vol. 43, pp. 5732–5756, 1971.

[46] E. Carnal and A. Mocellin, "A topological model for plane sections of polycrystals," *Acta. Met.*, vol. 29, pp. 135–143, 1981.

[47] E. A. Ceppi and O. B. Nasello, "Computer simulation of bidimensional grain growth," *Scripta. Met.*, vol. 18, pp. 1221–1225, 1984.

[48] E. A. Ceppi and O. B. Nasello, "Computer Simulation of grain boundary migration (I): The algorithm," in *Computer Simulation of Microstructural Evolution*, (The Metallurgical Society: Warrendale, 1986), pp. 1–11.

[49] C. H. Chen, J. C. Phillips, K. L. Tai, and P. M. Bridenbaugh, "Domain microscopy in chalcogenide alloy glass thin films," *Sol. State Comm.*, vol. 38, pp. 657–661, 1981.

[50] R. Collins and A. Wragg, "Maximum Entropy Histograms," *J. Phys. A*, vol. 10, pp. 1441–1464, 1977.

[51] H. S. M. Coxeter, *Introduction to Geometry* (John Wiley and Sons: New York, 1969).

[52] I. K. Crain, "The Monte-Carlo Generation of Random Polygons," *Comp. and Geosci.*, vol. 4, pp. 131–141, 1978.

[53] J. Cwajna, A. Maciejny, and M. Malinski, "Stereological criteria of grain size homogeneity," *Annealing Processes– Recovery, Recrystallization and Grain Growth, Proceedings of the 7th Risø International Symposium on Metallurgy and Materials Science*, N. Hansen, D. J. Jensen, T. Leffers, and B. Ralph, eds. (Risø National Laboratory: Roskilde, 1986), pp. 273–278.

[54] C. H. Desch, "The Solidification of Metals from the Liquid State," *J. Inst. Metals*, vol. 22, pp. 241–263, 1919.

[55] M. Desmarest, "Mémoire Sur l'origine & la nature du Basalte á grandes colonnes polygones, déterminèes par l'Histiore Naturelle de cette pierre. Observée en Auvergne," *Mem. Acad. Roy. Sci. (Paris)*, vol. 87, pp. 705–774, 1771.

[56] J. Dewar, "Soap Bubbles of Long Duration," *Proc. Roy. Inst. Gt. Brit.*, vol. 22, pp. 179–185, 1917.

[57] J. Dewar, "Soap Films as Detectors: Stream Lines and Sound," *Proc. Roy. Inst. (London)*, vol. 24, pp. 197–204, 1923.

[58] R. D. Doherty, "Discussion of "Mechanism of Steady-State Grain Growth in Aluminum,"" *Met. Trans.*, vol. 6A, pp. 588–589, 1975.

[59] J. P. Drolet and A. Galbois, "The impurity-drag effect on grain growth," *Acta. Met.*, vol. 16, pp. 1387–1399, 1968.

[60] W. F. Druyvesteyn and J. W. F. Dorleijn, "Calculations on some periodic magnetic domain structures; Consequences for bubble devices," *Philips Res. Repts.*, vol. 26, pp. 11–28, 1971.

[61] H. Eichelkraut, K. Lücke, G. Abbruzzese, "Texture controlled grain growth in Cu-Zn and Al-Mg alloys," *Annealing Processes- Recovery, Recrystallization and Grain Growth, Proceedings of the 7th Risø International Symposium on Metallurgy and Materials Science*, N. Hansen, D. J. Jensen, T. Leffers, and B. Ralph, eds. (Risø National Laboratory: Roskilde, 1986), pp. 303–308.

[62] Y. Enomoto, K. Kawasaki, and T. Nagai, "Two-Dimensional Vertex Model with Local Friction Coefficient," *Int. J. of Mod. Phys.*, vol. B 3, pp. 163–169, 1989.

[63] A. H. Eschenfelder, *Magnetic Bubble Technology* (Springer Verlag: Berlin, 1980).

[64] F. Feltham, "Grain growth in metals," *Acta. Met.*, vol. 5, pp. 97–105, 1957.

[65] Samuel Foley, "An Account of the Giants Causway in the North of Ireland," *Phil. Trans. Roy. Soc. London*, vol. 18, pp. 169–182, 1694.

[66] E. Fukushima and A. Ookawa, "The Transition Structure of the Grain Boundary observed in Soap Bubble Raft," *J. Phys. Soc. Japan.*, vol. 8, pp. 129–130, 1953.

[67] E. Fukushima and A. Ookawa, "On the Dynamical Behaviour of the Grain Boundary in Soap Bubble Raft under Shear Stress," *J. Phys. Soc. Japan.*, vol. 8, pp. 280–282, 1953.

[68] E. Fukushima and A. Ookawa, "Observation of the Grain Boundary in Soap Bubble Raft Part I. Static Feature of the Grain Boundary," *J. Phys. Soc. Japan.*, vol. 8, pp. 609–614, 1953.

[69] E. Fukushima and A. Ookawa, "Observation of the Grain Boundary in Soap Bubble Raft Part II. Dynamical behaviour of the Grain Boundary," *J. Phys. Soc. Japan.*, vol. 9, pp. 44–51, 1954.

[70] E. Fukushima and A. Ookawa, "Some Characters of the Soap Bubble Raft in a Vibrating State," *J. Phys. Soc. Japan.*, vol. 10, pp. 970–981, 1955.

[71] E. Fukushima and A. Ookawa, "Observation of the Grain Boundary in Soap Bubble Raft Part III. The Grain Boundary in Vibrating State," *J. Phys. Soc. Japan.*, vol. 10, pp. 139–146, 1957.

[72] M. A. Fortes and A. C. Ferro, "Trivalent polyhedra: Properties, representation and enumeration," *Acta. Met.*, vol. 33, pp. 1683–1696, 1985.

[73] M. A. Fortes and A. C. Ferro, "Topology and transformation in cellular structures," *Acta. Met.*, vol. 33, pp. 1697–1708, 1985.

[74] V. E. Fradkov, "A theoretical investigation of two-dimensional grain growth in the 'gas' approximation," (preprint) 1988.

[75] V. E. Fradkov, A. S. Kravchenko, and L. S. Shvindlerman, "Experimental investigation of normal grain growth in terms of area and topological class," *Scripta. Met.*, vol. 19, pp. 1291–1296, 1985.

[76] V. E. Fradkov, L. S. Shvindlerman, and D. G. Udler, "Computer simulation of grain growth in two dimensions," *Scripta. Met.*, vol. 19, pp. 1285–1290, 1985.

[77] V. E. Fradkov, L. S. Shvindlerman, and D. G. Udler, "Short-range order in the arrangement of grains in two-dimensional polycrystals," *Philos. Mag. Letters*, vol. 55, pp. 289–294, 1987.

[78] V. E. Fradkov, D. G. Udler, and R. E. Kris, "Computer simulation of two-dimensional normal grain growth (the 'gas' approximation)," *Philos. Mag. Letters*, vol. 58, pp. 670–674, 1988.

[79] H. J. Frost and C. V. Thompson, "Microstructural Evolution in thin films," in *Computer Simulation of Microstructural Evolution*, (The Metallurgical Society, Warrendale: 1986), pp. 33–47.

[80] H. J. Frost and C. V. Thompson, "The Effect of Nucleation Conditions on the Topology and Geometry of Two-Dimensional Grain Structures," *Acta. Met.*, vol. 35, pp. 529–540, 1987.

[81] H. J. Frost and C. V. Thompson, "Development of Microstructure in Thin Films," *S.P.I.E.*, vol. 821, pp. 77–87, 1987.

[82] H. J. Frost and C. V. Thompson, "Computer Simulation of Microstructural Evolution in Thin Films," (preprint) 1988.

[83] H. J. Frost, C. V. Thompson, C. L. Howe, and J. Whang, "A two-dimensional computer simulation of capillarity-driven grain growth: Preliminary results," *Scripta. Met.*, vol. 22, pp. 65–70, 1988.

[84] H. J. Frost, J. Whang, and C. V. Thompson, "Modeling of grain growth in thin films," *Annealing Processes– Recovery, Recrystallization and Grain Growth, Proceedings of the 7th Risø International Symposium on Metallurgy and Materials Science*, N. Hansen, D. J. Jensen, T. Leffers, and B. Ralph, eds. (Risø National Laboratory: Roskilde, 1986), pp. 315–320.

[85] Fu Tingliang, "A Study of Two-Dimensional Soap Froths," unpublished M.S. thesis, Trinity College, Dublin, 1986.

[86] R. L. Fullman, "Boundary Migration During Grain Growth," in *Metal Interfaces*, (American Society for Metals, Cleveland, 1952), pp. 179–207.

[87] M. Gardner, "Mathematical Games," *Sci. Am.*, vol. 254 June, pp. 16–23, 1986.

[88] L. Gaultier, "Mémoire Sur les Moyens généraux de construire graphiquement un Cercle déterminé par trois conditions, et une Sphère déterminée par quatre conditions," *Journal de l'Ecole Polytechnique*, vol. 16, pp. 124–214, 1813.

[89] A. Getis and B. Boots, *Models of Spatial Processes: An Approach to the Study of Point, Line and Area Patterns* (Cambridge University Press, Cambridge: 1978).

[90] E. N. Gilbert, "Random Subdivisions of Space into Crystals," *Ann. Math. Stat.*, vol. 33, pp. 958–972, 1962.

[91] Gladstone, "Notes on Froth," *Philos. Mag.*, vol. 14, pp. 314–315, 1857.

[92] J. A. Glazier, from data supplied by B. Berge.

[93] J. A. Glazier, M. P. Anderson, G. S. Grest and J. Stavans, "The Two Dimensional Soap Froth and the Q-state Potts Model: A detailed Comparison," (preprint) 1989.

[94] J. A. Glazier, S. P. Gross, and J. Stavans, "Dynamics of two-dimensional soap froths," *Phys. Rev. A*, vol. 36, pp. 306–312, 1987.

[95] J. A. Glazier, and J. Stavans, unpublished.

[96] M. E. Glicksman and S. P. Marsh, "Microstructural coarsening in 2- and 3-dimensions–Applications of multiparticle diffusion algorithms," in *Computer Simulation of Microstructural Evolution*, (The Metallurgical Society: Warrendale, 1986), pp. 109–124.

[97] J. Gollub, private communication.

[98] W. C. Graustein, "On the Average Number of Sides of Polygons of a Net," *Ann. of Math.*, vol. 32, pp. 149–153, 1931.

[99] G. S. Grest, M. P. Anderson, and D. J. Srolovitz, "Computer simulation of microstructural dynamics," in *Computer Simulation of Microstructural Evolution*, (The Metallurgical Society: Warrendale, 1986), pp. 21–32.

[100] G. S. Grest, D. J. Srolovitz, and M. P. Anderson, "Computer simulation of grain growth–IV. Anisotropic grain boundary energies," *Acta. Met.*, vol. 33, pp. 509–520, 1985.

[101] G. S. Grest, D. J. Srolovitz, and M. P. Anderson, " Domain-growth kinetics for the $Q-$state Potts model in two and three dimensions," *Phys. Rev. B*, vol. 38, pp. 4752–4760, 1988.

[102] E. A. Grey and G. T. Higgins, "A velocity independent drag during grain boundary migration," *Scripta. Met.*, vol. 6, pp. 253–258, 1972.

[103] E. A. Grey and G. T. Higgins, "Solute limited grain boundary migration: A rationalization of grain growth," *Acta. Met.*, vol. 21, pp. 309–321, 1973.

[104] E. Guazzelli, "Deux Etudes Experimentales du Desordre en Hydrodynamique Physique," Unpublished Doctoral Thesis, L'Universite de Provence (1986), pp. 193–195.

[105] M. Hasegawa and M. Tanemura, "On the Pattern of Space division by territories," *Ann. Inst. Statist. Math.*, vol. 28, pp. 509–519, 1976.

[106] M. Hillert, "On the theory of normal and abnormal grain growth," *Acta. Met.*, vol. 13, pp. 227–238, 1965.

[107] E. L. Holmes and W. C. Winegard, "Grain growth in zone-refined tin," *Acta. Met.*, vol. 7, pp. 411–414, 1959.

[108] R. Hooke, *Micrographia*, (London: 1665).

[109] C. L. Howe, *Computer Simulation of Grain growth in two Dimensions*, unpublished M.E. thesis, Dartmouth College, 1987.

[110] H. Hsu and B. B. Rath, "On the Time Exponent in Isothermal Grain Growth," *Met. Trans.*, vol. 1, pp. 3181–3184, 1970.

[111] O. Hunderi, "Steady state grain growth: A note on the kinetics," *Acta. Met.*, vol. 27, pp. 167–169, 1979.

[112] O. Hunderi, N. Ryum, and H. Westengen, "Computer simulation of grain growth," *Acta. Met.*, vol. 27, pp. 161–165, 1979.

[113] O. Hunderi and N. Ryum, "The kinetics of normal grain growth," *J. Mater. Sci.*, vol. 15, pp. 1104–1108, 1980.

[114] O. Hunderi and N. Ryum, "Computer simulation of stagnation in grain growth," *Acta. Met.*, vol. 29, pp. 1737–1745, 1981.

[115] E. T. Jaynes, "Information Theory and Statistical Mechanics," *Phys. Rev.*, vol. 106, pp. 620–630, 1957.

[116] E. T. Jaynes, "Information Theory and Statistical Mechanics. II," *Phys. Rev.*, vol. 108, pp. 171–190, 1957.

[117] K. Kawasaki and Y. Enomoto, "Statistical Theory of Ostwald ripening with elastic field interaction," *Physica*, vol. A 150, pp. 462–498, 1988.

[118] K. Kawasaki, T. Nagai, and K. Nakashima, "Vertex Models of Two-Dimensional Grain Growth," (preprint) 1988.

[119] K. Kawasaki, T. Nagai, and K. Nakashima, "Statistical Physics of Domain Walls and Grain Boundaries in Ordering Kinetics," (preprint) 1988.

[120] Lord Kelvin, "On the Division of Space with Minimum Partitional Area," *Philos. Mag.*, vol. 24, pp. 503–515, 1887.

[121] R. Kikuchi, "Shape Distribution of Two Dimensional Soap Froths," *J. Chem. Phys.*, vol. 24, pp. 861–867, 1956.

[122] H. O. K. Kirchner, "Coarsening of Grain-Boundary Precipitates," *Met. Trans.*, vol. 2, pp. 2861–2864, 1971.

[123] G. Konig and W. Blum, "Comparison Between the Cell Structures Produced in Aluminum by Cycling and by Monotonic Creep," *Acta. Met.*, vol. 28, pp. 519–537, 1980.

[124] C. Kooy and U. Enz, "Experimental and theoretical study of the domain configuration in thin layers of $BaFe_{12}O_{19}$," *Philips Res. Repts.*, vol. 15, pp. 7–29, 1960.

[125] A. M. Kraynik, "Foam Rheology: The Linear Viscoelastic Respones of a Spatially Periodic Model," (preprint) 1987.

[126] A. M. Kraynik, "Foam Flows," *Ann. Rev. Fluid. Mech.*, vol. 20, pp. 325–357, 1988.

[127] A. M. Kraynik, Movie available from A. M. Kraynik, Fluid and Thermal Sciences Department 1510, Sandia National Laboratories, P.O. Box 5800, Albequerque, NM 87185.

[128] W. B. Krantz, K. J. Gleason, and N. Caine, "Patterned Ground," *Sci. Am.*, vol. 259 December, pp. 68–76, 1988.

[129] A. M. Kraynik and M. G. Hansen, "Foam and Emulsion Rheology: A Quasistatic Model for Large Deformations of Spatially-Periodic Cells," *J. Rheology*, vol. 30, pp. 409–439, 1986.

[130] A. M. Kraynik and M. G. Hansen, "Foam Rheology: A Model of Viscous Phenomena," (preprint) 1987.

[131] A. I. Kreines and V. E. Fradkov, "Automatizirsvannie Analiz Iotcheistech Struktur," *Experimental Problems and Techniques*, vol. 5, pp. 62–64, 1986.

[132] S. K. Kurtz and F. M. A. Carpay, "Microstructure and normal grain growth in metals and ceramics. Part I. Theory," *J. Appl. Phys.*, vol. 51, pp. 5725–5744, 1980.

[133] S. K. Kurtz and F. M. A. Carpay, "Microstructure and normal grain growth in metals and ceramics. Part II. Experiment," *J. Appl. Phys.*, vol. 51, pp. 5745–5754, 1980.

[134] C. J. Lambert and D. Weaire, "Theory of the Arrangement of Cells in a Network," *Metallography*, vol. 14, pp. 307–318, 1981.

[135] C. J. Lambert and D. Weaire, "Order and disorder in two-dimensional random networks," *Philos. Mag.*, vol. B 47, pp. 445–450, 1983.

[136] J. S. Langer, "Pattern formation during crystal growth: Theory," in *Nonlinear Phenomena at Phase Transitions and Instabilities*, T. Riste, ed. (New York: Plenum Press, 1981), pp. 309–336.

[137] C. Lantuejoul, "Computation of the histograms of the number of edges and neighbours of cells in a tessellation," in *Geometrical Probability and Biological Structures: Buffon's 200th Anniversary*, R. E. Miles and J. Serra, eds. (Springer-Verlag: Berlin, 1978), pp. 323–329.

[138] A. van Leeuwenhoek, "On the Formation of Rushes," in *Arcana Naturae*, Epistola 74, 1692.

[139] R. D. Levine and M. Tribus, *The Maximum Entropy Formalism* (M.I.T. Press: Cambridge, 1979).

[140] F. T. Lewis, "A further study of the polyhedral shapes of cells," *Proc. A.A.A.S.*, vol. 61, pp. 1–34, 1925.

[141] F. T. Lewis, "The correlation between cell division and the shapes and sizes of prismatic cells in the epidermis of cucumis," *Anat. Rec.*, vol. 38, pp. 341–362, 1928.

[142] F. T. Lewis, "A comparison between the mosaic of polygons in a film of artificial emulsion and the pattern of simple epithelium in surface view (cucumber epidermis and human amnion)," *Anat. Rec.*, vol. 50, pp. 235–265, 1931.

[143] F. T. Lewis, "Mathematically precise features of epithelial mosaics: observations on the endothelium of capillaries," *Anat. Rec.*, vol. 55, pp. 323–341, 1928.

[144] F. T. Lewis, "A geometric accounting for diverse shapes of 14-hedral cells: the transition from dodecahedra to tetrakaidekahedra," *Am. J. Bot.*, vol. 30, pp. 74–81, 1943.

[145] F. T. Lewis, "The geometry of growth and cell division in columnar parenchyma," *Am. J. Bot.*, vol. 31, pp. 619–629, 1944.

[146] F. T. Lewis, "The geometry of growth and cell division in epithelial mosaics," *Am. J. Bot.*, vol. 30, pp. 766–776, 1944.

[147] F. T. Lewis, "The Analogous Shapes of Cells and Bubbles," *Proc. A.A.A.S.*, vol. 77, pp. 147–186, 1948.

[148] I. M. Lifschitz and V. V. Slezov, "Kinetics of diffusive decomposition of supersaturated solid solutions," *Soviet J.E.T.P.*, vol. 35, pp. 331–339, 1959.

[149] I. M. Lifschitz and V. V. Slyozov, "The kinetics of precipitation from supersaturated solid solutions," *J. Phys. Chem. Solids*, vol. 19, pp. 35–50, 1961.

[150] M. Lösche and H. Möhwald, "Fluorescence microscope to observe dynamical processes in monomolecular layers at the air/water interface," *Rev. Sci. Instrum.*, vol. 55, pp. 1968–1972, 1984.

[151] H. W. Lotwick, "Simulation of Some Spatial Hard Core Models, and the Complete Packing Problem," *J. Statist. Comput. Simul.*, vol. 15, pp. 295–314, 1982.

[152] N. P. Louat, "On the Theory of Normal Grain Growth," *Acta. Met.*, vol. 22, pp. 721–724, 1974.

[153] J. Maddox, "Soap bubbles make serious physics," *Nature*, vol. 338, pp. 293–293, 1989.

[154] M. Magnasco, private communication, 1989.

[155] R. Mallet, "On the Origin and Mechanism of production of the Prismatic (or columnar) Structure of Basalt," *Philos. Mag.*, vol. 50, pp. 122–135, and 201–227, 1875.

[156] A. P. Malozemoff and J. C. Slonczewski, *Magnetic Domain Walls in Bubble Materials* (Academic Press: New York, 1979).

[157] M. Marder, "Soap-bubble growth," *Phys. Rev. A*, vol. 36, pp. 438–440, 1987.

[158] J. W. Marvin, "The Shape of Compressed Lead Shot and Its Relation to Cell Shape," *Am. J. Bot.*, vol. , pp. 280–288, 1939.

[159] J. W. Martin and R. D. Doherty, *Stability of Microstructure in Metallic Systems* (Cambridge University Press: Cambridge, 1976), pp. 221–244.

[160] E. B. Matzke, "Volume-shape relationships in lead shot and their bearing on cell shapes," *Am. J. Bot.*, vol. 26, pp. 288–293, 1939.

[161] E. B. Matzke, "The three dimensional shape of bubbles in foam–an analysis of the rôle of surface forces in three dimensional cell shape determination," *Am. J. Bot.*, vol. 33, pp. 58–80, 1946.

[162] E. B. Matzke and J. Nestler, "Volume-shape relationships in variant foams. A further study of the rôle of surface forces in three dimensioanl cell shape determination," *Am. J. Bot.*, vol. 33, pp. 130–144, 1946.

[163] H. M. McConnell, L. K. Tamm, and R. M. Weis, "Periodic structures in lipid monolayer phase transitions," *Proc. Natl. Acad. Sci. USA*, vol. 81, pp. 3249–3253, 1984.

[164] J. L. Meijering, "Interface area, edge length, and number of vertices in crystal aggregates with random nucleation," *Philips Res. Repts.*, vol. 8, pp. 270–290, 1953.

[165] R. Messier and R. C. Ross, "Evolution of microstructure in amorphous hydrogenated silicon," *J. Appl. Phys.*, vol. 53, pp. 6220–6225, 1982.

[166] R. E. Miles, *Stochastic Geometry*, D. G. Kendall and E. F. Harding, eds. (John Wiley: New York, 1974).

[167] P. Molho, private communication.

[168] P. Molho, J. Gouzerh, J. C. S. Levy, and J. L. Porteseil, "Topological hysteresis in stripe domain structures," *J. Mag. & Mag. Materials*, vol. 54-57, pp. 857–858, 1986.

[169] B. Moore, C. M. Knobler, D. Broseta, and F. Rondelez, "Studies in Phase transitions in Langmuir Monolayers by Fluorescence Microscopy," *J. Chem. Soc. Faraday. Trans.*, vol. 2 82, pp. 1753–1761, 1986.

[170] O. G. Mouritsen, "Universal aspects of domain-growth kinetics," *Annealing Processes- Recovery, Recrystallization and Grain Growth, Proceedings of the 7th Risø International Symposium on Metallurgy and Materials Science*, N. Hansen, D. J. Jensen, T. Leffers, and B. Ralph, eds. (Risø National Laboratory: Roskilde, 1986), pp. 457–462.

[171] J. E. Morral and M. F. Ashby, "Dislocated cellular structures," *Acta. Met.*, vol. 22, pp. 567–575, 1974.

[172] W. W. Mullins, "Two-Dimensional Motion of Idealized Grain Boundaries," *J. Appl. Phys.*, vol. 27, pp. 900–904, 1956.

[173] W. W. Mullins, "The statistical self-similarity hypothesis in grain growth and particle coarsening," *J. Appl. Phys.*, vol. 59, pp. 1341–1349, 1986.

[174] W. W. Mullins, "On Idealized Two Dimensional Grain Growth," *Scripta. Met.*, vol. 22, pp. 1441–1451, 1988

[175] W. W. Mullins and R. F. Sekerka, "Morphological Stability of a Particle Growing by Diffusion or Heat Flow," *J. Appl. Phys.*, vol. 34, pp. 323–329, 1963.

[176] K. J. Mysels, K. Shinoda, and S. Frankel, *Soap Films: Studies of their Thinning and a Bibliography*, (Pergamon Press: New York, 1959).

[177] F. R. N. Nabarro, *Theory of Crystal Dislocations*, (Oxford: London, 1967).

[178] T. Nagai, K. Kawasaki, and K. Nakamura, "Dynamics of two dimensional cell patterns," *Nihon Butsuri Gakkaishi*, vol. 43, pp. 437–444, 1988 (in Japanese).

[179] K. Nakashima, T. Nagai, and K. Kawasaki, "Scaling Behavior of Two-dimensional Domain Growth: Computer Simulation of Vertex Models," (preprint) 1988.

[180] O. B. Nasello and E. A. Ceppi, "Computer simulation of bidimensional grain boundary migration (II): An application to grain growth," in *Computer Simulation of Microstructural Evolution*, (The Metallurgical Society: Warrendale, 1986), pp. 13–20.

[181] J. von Neumann, "Discussion," in *Metal Interfaces*, (American Society for Metals: Cleveland, 1952), pp. 108–110.

[182] I. Newton, "Answers to Some Considerations Upon His Doctrine of Light and Colours," *Phil. Trans. Roy. Soc. London*, vol. 7, pp. 5084–5103, 1672.

[183] V. Yu. Novikov, "Computer simulation of normal grain growth," *Acta. Met.*, vol. 26, pp. 1739–1744, 1978.

[184] V. Yu. Novikov, "On computer simulation of texture development in grain growth," *Acta. Met.*, vol. 27, pp. 1461–1466, 1979.

[185] R. Occelli, E. Guazzelli, and J. Pantaloni, "Order in convective structures," *J. Phys. Lett. (Paris)*, vol. 44, pp. L567–L580, 1983.

[186] T. H. O'Dell, "Magnetic bubble domain devices," *Rep. Prog. Phys.*, vol. 49 , pp. 589–620, 1986.

[187] T. H. O'Dell, "The Dynamics of Magnetic Bubble Domain Arrays," *Philos. Mag.*, vol. 27, pp. 595–606, 1973.

[188] R. Peters and K. Beck, "Translational diffusion in phospholipid monolayers measured by fluorescence microphotolysis," *Proc. Natl. Acad. Sci. USA*, vol. 80, pp. 7183–7187, 1983.

[189] J. Plateau, "Memoir on the Phenomena Presented by a Mass of Liquid Free and Removed from the Action of Gravity," *Mem. Acad. Roy. Belg.*, vol. 16, 1843, continuing in subsequent issues through 1872 (in French).

[190] J. Plateau, *Statique Experimentale et Theorique des Liquides Soumis aux Seulles Forces Moleculaires* (Gauthier-Villars, Paris: 1873).

[191] D. C. Pieri, "Lineament and polygon patterns on Europa," *Nature*, vol. 289, pp. 17–21, 1981.

[192] V. Randle, D. Ralph, and N. Hansen, "Grain growth in crystalline materials," *Annealing Processes- Recovery, Recrystallization and Grain Growth, Proceedings of the 7th Risø International Symposium on Metallurgy and Materials Science*, N. Hansen, D. J. Jensen, T. Leffers, and B. Ralph, eds. (Risø National Laboratory: Roskilde, 1986), pp. 123–142.

[193] Lord Rayleigh, "On the Theory of Surface Forces," *Philos. Mag.*, vol. 30, pp. 285–299 and 456–475, 1890.

[194] F. N. Rhines, K. R. Craig, and R. T. DeHoff, "Mechanism of Steady-State Grain Growth in Aluminum," *Met. Trans.*, vol. 5, pp. 413–425, 1974.

[195] F. N. Rhines and K. R. Craig, "Author's Reply," *Met. Trans.*, vol. 6A, pp. 590–591, 1975. Reply to comment of Doherty.[58]

[196] F. N. Rhines and B. R. Patterson, "Effect of the Degree of Prior Cold Work on the Grain Volume Distribution and the Rate of Grain Growth of Recrystallized Aluminum," *Met. Trans.*, vol. 13A, pp. 985–993, 1982.

[197] N. Rivier, "Disclination Lines in Glasses," *Philos. Mag.*, vol. A 40, pp. 859–868, 1979.

[198] N. Rivier, "On the structure of random tissues or froths, and their evolution," *Philos. Mag.*, vol. B 47, pp. L45–L49, 1983.

[199] N. Rivier, "Statistical crystallography: Structure of random cellular networks," *Philos. Mag.*, vol. B 52, pp. 795–819, 1985.

[200] N. Rivier, private communication.

[201] N. Rivier and A. Lissowski, "On the correlation between sizes and shapes of cells in epithelial mosaics," *J. Phys. A*, vol. 15, pp. L143–L148, 1982.

[202] P. S. Sahni, G. S. Grest, M. P. Anderson, and D. J. Srolovitz, "Kinetics of the Q-State Potts Model in Two Dimensions," *Phys. Rev. Lett.*, vol. 50, pp. 263–266, 1983.

[203] T. Senuma and H. Yada, "Microstructural evolution of plain carbon steels in multiple hot working," *Annealing Processes– Recovery, Recrystallization and Grain Growth, Proceedings of the 7th Risø International Symposium on Metallurgy and Materials Science*, N. Hansen, D. J. Jensen, T. Leffers, and B. Ralph, eds. (Risø National Laboratory: Roskilde, 1986), pp. 547–552.

[204] J. F. Shackelford, "Triangle Rafts–Extended Zachariasen schematics for structure modeling," *J. non-Cryst. Sol.*, vol. 49, pp. 19–28, 1982.

[205] C. J. Simpson, K. T. Aust, and W. C. Winegard, "Activation Energies for Normal Grain Growth in Lead and Cadmium Base Alloy," *Met. Trans.*, vol. 2, pp. 993–997, 1971.

[206] C. S. Smith, "Grain shapes and other metallurgical applications of topology," in *Metal Interfaces*, (American Society for Metals: Cleveland, 1952), pp. 65–108.

[207] C. S. Smith, "The Shape of Things," *Sci. Am.*, vol. 190, pp. 58–64, 1954.

[208] C. S. Smith, "Structure, Substructure, and Superstructure," *Rev. Mod. Phys.*, vol. 36, pp. 524–532, 1964.

[209] C. S. Smith, "Some elementary principles of polycrystalline microstructure," *Met. Rev.*, vol. 9, pp. 1–48, 1964.

[210] A. Soares, A. C. Ferro, and M. A. Fortes, "Computer simulation of grain growth in a bidimensional polycrystal," *Scripta. Met.*, vol. 19, pp. 1491–1496, 1985.

[211] S. E. Soliman, N. Hansen, I. Misfeldt, J. G. Rasmussen, and O. T. Sørensen, "Isothermal grain-growth kinetics in UO_2," *Annealing Processes- Recovery, Recrystallization and Grain Growth, Proceedings of the 7th Risø International Symposium on Metallurgy and Materials Science*, N. Hansen, D. J. Jensen, T. Leffers, and B. Ralph, eds. (Risø National Laboratory: Roskilde, 1986), pp. 553–560.

[212] D. Sornette, "Undulation instability in stripe domain structures of 'bubble' material," *J. Phys. (Paris)*, vol. 48, pp. 151–165, 1987.

[213] R. Souèges, "Embyogénie des Géraniacées. Developpement de l'embryon chez le Geranium molle L.," *C. R. Acad. Sci.*, vol. 177, pp. 556–558, 1923.

[214] A. Spry, "The origin of columnar jointing, particularly in basalt flows," *J. Geol. Soc. Australia*, vol. 8, pp. 191–216, 1961.

[215] D. J. Srolovitz, "Grain growth phenomena in films: A Monte Carlo approach," *J. Vac. Sci. Technol.*, vol. A4, pp. 2925–2931, 1986.

[216] D. J. Srolovitz, M. P. Anderson, G. S. Grest, and P. S. Sahni, "Grain growth in two dimensions," *Scripta. Met.*, vol. 17, pp. 241–246, 1983.

[217] D. J. Srolovitz, M. P. Anderson, P. S. Sahni, and G. S. Grest, "Computer simulation of grain growth–II. Grain size distribution, topology, and local dynamics," *Acta. Met.*, vol. 32, pp. 793–802, 1984.

[218] D. J. Srolovitz, M. P. Anderson, G. S. Grest, and P. S. Sahni, "Computer simulation of grain growth–III. Influence of a particle dispersion," *Acta. Met.*, vol. 32, pp. 1429–1438, 1984.

[219] D. J. Srolovitz, G. S. Grest, and M. P. Anderson, "Computer simulation of grain growth–V. Abnormal grain growth." *Acta. Met.*, vol. 33, pp. 2233–2247, 1985.

[220] J. Stavans and J. A. Glazier, "Soap Froth Revisited: Dynamic Scaling in the Two-Dimensional Froth," *Phys. Rev. Lett.*, vol. 62, pp. 1318–1321, 1989.

[221] P. S. Stevens, *Patterns in Nature*, (Atlantic Monthly Press: Boston, 1974).

[222] C. J. Talbot and M. D. A. Jackson, "Salt Tectonics," *Sci. Am.*, vol. 257 August, pp. 70–79, 1987.

[223] H. Telley, T. M. Lieblimg, and A. Mocellin, "Simulation of grain growth in 2-dimensions: Influence of the energy expression for the grain boundary network," *Annealing Processes– Recovery, Recrystallization and Grain Growth, Proceedings of the 7th Risø International Symposium on Metallurgy and Materials Science*, N. Hansen, D. J. Jensen, T. Leffers, and B. Ralph, eds. (Risø National Laboratory: Roskilde, 1986), pp. 573–578.

[224] A. A. Thiele, "The Theory of Cylindrical Magnetic Domains," *Bell Tech. J.*, vol. 48, pp. 3287–3335, 1969.

[225] A. A. Thiele, "Device Implications of the Theory of Cylindrical Magnetic Domains," *Bell Tech. J.*, vol. 50, pp. 725–773, 1971.

[226] A. A. Thiele, A. H. Bobeck, E. Della Torre, and U. F. Gianola, "The energy and general translation force of cylindrical magnetic domains," *Bell Tech. J.*, vol. 50, pp. 711–724, 1971.

[227] C. V. Thompson, "Secondary grain growth in thin films of semiconductors: Theoretical aspects," *J. Appl. Phys.*, vol. 58, pp. 763–772, 1985.

[228] Sir W. Thomson, "On the Division of Space with Minimum Partitional Area," *Philos. Mag.*, vol. 24, pp. 503–514, 1887.

[229] C. V. Thompson, H. J. Frost, and F. Speapen, "The Relative Rates of Secondary and Normal Grain Growth," *Acta. Met.*, vol. 35, pp. 887–890, 1987.

[230] Sir D. Thompson, *On Growth and Form*, 2nd edition, (Cambridge University Press: Cambridge, 1942).

[231] P. W. Voorhees, "The Theory of Ostwald Ripening," *J. Stat. Phys.*, vol. 38, pp. 231–252, 1985.

[232] N. v. Raschevsky, "Zur Theorie der spontanen Teilung von mikroskopischen Tropfen," *Z. Phys.*, vol. 46, pp. 587–593, 1928.

[233] N. v. Raschevsky, "Zur Theorie der spontanen Teilung von mikroskopischen Tropfen. II," *Z. Phys.*, vol. 48, pp. 513–529, 1928.

[234] N. v. Raschevsky, "Über eine für die Biophysik interessante Art von Hysterese," *Z. Phys.*, vol. 63, pp. 666–671, 1936.

[235] M. Warner and R. M. Hornreich, "The stability of quasi 2D lattices of magnetic holes," *J. Phys. A*, vol. 18, pp. 2325–2341, 1985.

[236] D. Weaire, "Some Remarks on the Arrangement of Grains in a Polycrystal," *Metallography*, vol. 7, pp. 157–160, 1974.

[237] D. Weaire, "On the Ultimate Form of Cells in a Two-dimensional Soap Froth," (preprint) 1986.

[238] D. Weaire, "Fizz and froth: how the bubbles take the strain," *New Scientist*, vol. 116, 7 October, p. 33, 1987.

[239] D. Weaire, "A Note on the Elastic Behavior of Ordered Hexagonal Froth," (preprint) 1989.

[240] D. Weaire and T-L Fu, "The Mechanical Behavior of Foams and Emulsions," (preprint) 1988.

[241] D. Weaire, T-L Fu, and J. P. Kermode, "On the Shear Elastic Constant of a Two-Dimensional Froth," (preprint) 1988.

[242] D. Weaire and J. P. Kermode, "The evolution of the structure of a two-dimensional soap froth," *Philos. Mag.*, vol. B 47, pp. L29–L31, 1983.

[243] D. Weaire and J. P. Kermode, "Computer Simulation of a two-dimensional soap froth: I. Method and motivation," *Philos. Mag.*, vol. B 48, pp. 245–259, 1983.

[244] D. Weaire and J. P. Kermode, "Computer simulation of a two-dimensional soap froth, II. Analysis of results," *Philos. Mag.*, vol. B 50, pp. 379–388, 1984.

[245] D. Weaire and J. P. Kermode, "On the distribution of cell areas in a Voronoi network," *Philos. Mag.*, vol. B 53, pp. L101–L105, 1986.

[246] D. Weaire and C. O'Carroll, "A new model for the Giant's Causeway," *Nature*, vol. 302, pp. 240–241, 1983.

[247] D. Weaire and N. Rivier, "Soap, Cells and Statistics–Random patterns in Two Dimensions," *Contemp. Phys.*, vol. 25, pp. 59–99, 1984.

[248] D. Weaire and J. Wejchert, *Computer Simulation of Microstructural Evolution*, (The Metallurgical Society: Warrendale, 1986), pp. 49–60.

[249] J. Wejchert, D. Weaire, and J. P. Kermode, "Monte Carlo simulation of the evolution of a two-dimensional soap froth," *Philos. Mag.*, vol. B 53, pp. 15–24, 1986.

[250] P. L. White and L. H. Van Vlack, "A Comparison of Two- and Three-Dimensional Size Distributions in a Cellular material," *Metallography*, vol. 3, pp. 241–258, 1970.

[251] J. A. Whitehead, Jr., "A survey of hydrodynamic instabilities," in *Fluctuations, Instabilities and Phase Transitions, Proceedings of the NATO Advanced Study Institute, Geilo, Norway, 1975*, T. Riste, ed. (Plenum Press: New York, 1975), pp. 153–180.

[252] W. M. Williams and C. S. Smith, "A Study of Grain Shape in an Aluminum Alloy And Other Applications of Stereographic Microradiography," *Journal of Metals*, vol. 194, pp. 755–765, 1952.

[253] G. R. Woolhouse and P. Chaudhari, "Two-dimensional lattice simulation by magnetic bubbles," *Philos. Mag.*, vol. 28, pp. 161–172, 1974.

[254] P. J. Wray, O. Richmond, and H. I. Morrison, "Use of the Dirichlet Tesselation for Characterizing and Modeling Nonregular Dispersions of Second-Phase Particles," *Metallography*, vol. 16, pp. 39–58, 1983.

[255] A. C. Wright, G. A. N. Connell and J. W. Allen, "Amorphography and the modeling of amorphous solid structures by geometric transformations," *J. non-Cryst. Sol.*, vol. 42, pp. 69–86, 1980.

[256] A. C. Wright, "Basic amorphography," in *Coherence and Energy Transfer in Glasses*, P. A. Fleury and B. Golding, eds. (Plenum Press: New York, 1982), pp. 1–38.

[257] J. I. Yellott, Jr., "Spectral Consequences of Photoreceptor Sampling in the Rhesus Retina," *Science*, vol. 221, pp. 382–385, 1983.

[258] W. H. Zachariasen, "The atomic arrangement in glass," *J. Am. Chem. Soc.*, vol. 54, pp. 3841–3851, 1932.